

**A Rayleigh Quotient Fixed Point Method for
Criticality Eigenvalue Problems in Neutron Transport**

by

Mario Ortega

A dissertation submitted in partial satisfaction of the

requirements for the degree of

Doctor of Philosophy

in

Nuclear Engineering

and the Designated Emphasis

in

Computational Science and Engineering

in the

Graduate Division

of the

University of California, Berkeley

Committee in charge:

Professor Rachel N. Slaybaugh, Chair

Professor Jasmina Vujic

Professor Per-Olof Persson

Dr. Peter N. Brown

Summer 2019

The dissertation of Mario Ortega, titled A Rayleigh Quotient Fixed Point Method for Criticality Eigenvalue Problems in Neutron Transport, is approved:

Chair _____

Date _____

Date _____

Date _____

Date _____

University of California, Berkeley

**A Rayleigh Quotient Fixed Point Method for
Criticality Eigenvalue Problems in Neutron Transport**

Copyright 2019
by
Mario Ortega

Abstract

A Rayleigh Quotient Fixed Point Method for
Criticality Eigenvalue Problems in Neutron Transport

by

Mario Ortega

Doctor of Philosophy in Nuclear Engineering
and the Designated Emphasis in
Computational Science and Engineering

University of California, Berkeley

Professor Rachel N. Slaybaugh, Chair

The alpha- and k-effective eigenproblems describe the criticality and fundamental neutron flux mode of a nuclear system. Traditionally, the alpha-eigenvalue problem has been solved using methods that focus on supercritical systems with large, positive eigenvalues. These methods, however, struggle for very subcritical problems where the negative eigenvalue can lead to negative absorption, potentially causing the methods to diverge. The k-effective eigenvalue problem has generally been solved using power iteration. For problems with dominance ratios close to one, however, power iteration is slow to converge and requires acceleration. We present the Rayleigh Quotient Fixed Point methods, nonlinear fixed-point methods, that are applied to the primitive discretizations of the neutron transport eigenvalue equations. We prove that the discretized eigenvalue equations form a primitive linear system for one-dimensional slab geometry where the unique, positive angular flux eigenvectors are guaranteed to exist from the Frobenius-Perron Theorem for primitive matrices. These methods are capable of solving subcritical and supercritical alpha- and k-effective eigenvalue problems. The derived eigenvalue updates are proven to be optimal in the least squares sense and positive eigenvector updates are guaranteed from the properties of primitive matrices. We consider infinite-medium, one-dimensional slabs and spheres, two-dimensional cylinders, and three-dimensional quarter core benchmark problems and show the ability of the Rayleigh Quotient Fixed Point method to obtain the fundamental eigenvalue and eigenvector of these systems, even when the discretized eigenvalue equations no longer form a primitive system. We also consider the use of Anderson acceleration to accelerate the convergence of the Rayleigh Quotient Fixed Point methods.

A mis papás, Mario y Claudia, a mis hermanos, Daniel y Alan, y a Laura

Contents

Contents	ii
List of Figures	v
List of Tables	vii
1 Introduction	1
2 Background	4
2.1 Neutron Transport	4
2.2 The Criticality Problem of Neutron Transport	6
2.2.1 The α -Eigenvalue Problem	6
2.2.2 The k -Eigenvalue	17
2.3 Review of Linear Algebra Fundamentals	21
2.3.1 Nonnegativity, Positivity, and the Spectral Radius of a Matrix	22
2.3.2 Irreducible and Reducible Matrices	22
2.3.3 Primitive and Cyclic Matrices	22
2.3.4 Perron-Frobenius Theorem for Irreducible Matrices	22
2.3.5 Perron-Frobenius Theorem for Primitive Matrices	23
2.3.6 Kronecker (Tensor) Product	23
2.4 Review of Fixed-Point Iteration	24
2.5 Conclusion	26
3 Discretization and Primitivity of the Neutron Transport Criticality Eigenvalue Problems	27
3.1 Discretization of the Alpha-Eigenvalue and k -Effective Eigenvalue Equations	28
3.1.1 The Multigroup in Energy Discretization and Surface Harmonics Expansion of the Angular Flux	28
3.1.2 Step Differencing and Discrete Ordinates in Angle	31
3.2 Primitivity of the Discretized Alpha-Eigenvalue and k -Effective Eigenvalue Equations	39
3.3 Conclusion	47

4 The Rayleigh Quotient Fixed Point Method	48
4.1 Derivation of the Rayleigh Quotient Fixed Point Method for Alpha-Eigenvalue Problems	48
4.2 Derivation of the Rayleigh Quotient Fixed Point Method for k -Effective Problems	51
4.3 Jacobian of the Rayleigh Quotient Fixed Point Method for Alpha-Eigenvalue Problems	55
4.4 Jacobian of the Rayleigh Quotient Fixed Point Method for k -Effective Eigenvalue Problems	56
4.5 Conclusion	56
5 Eigenvalues for Infinite Medium Problems	58
5.1 Criticality Benchmark One-Speed Verification for Various Critical and Supercritical Problems	58
5.2 Infinite Medium Multigroup Problems	63
5.2.1 Analytical Subcritical & Critical Problems	63
5.2.2 Analytical Infinite Medium Supercritical Problems	65
5.3 Conclusion	71
6 Eigenvalues of Slabs and Spheres	72
6.1 One-Speed Verification for Slab Geometry	73
6.1.1 A Set of Non-Multiplying Purely-Scattering Slabs	74
6.1.2 A Set of Multiplying Homogeneous Slabs	75
6.1.3 Heterogeneous Slabs	79
6.1.4 Multiplying Homogeneous Slabs with Anisotropic Scattering	86
6.2 Multigroup Verification for Slab Geometry	88
6.2.1 Multigroup Multiplying Homogeneous Slabs	88
6.2.2 Multigroup Reflected Slabs	96
6.3 One-Speed Verification for Spherical Geometry	99
6.3.1 Non-Multiplying Homogeneous Spheres	99
6.3.2 Multiplying Homogeneous Spheres	99
6.3.3 Multiplying Homogeneous Spheres with Anisotropic Scattering	103
6.3.4 A Spherical Shell Problem	105
6.4 Multigroup Verification for Spherical Geometry	106
6.4.1 A Plutonium-Nitrate Solution Critical Sphere	106
6.4.2 A Plutonium/Highly Enriched Uranium Mixture Critical Sphere	110
6.4.3 A Uranium-233 Critical Sphere	112
6.5 Conclusion	113
7 Higher Dimensional Eigenvalues	114
7.1 Critical Cylinder Benchmark Problems	116
7.1.1 Homogeneous Critical Cylinder Problems	117

7.2	Two- and Three-Dimensional Cartesian Benchmark Problems	119
7.2.1	Two-Dimensional MOX Fuel Core with Coarse Spatial Discretization	129
7.2.2	Two-Dimensional MOX Fuel Core with Fine Spatial Discretization	134
7.2.3	Three-Dimensional MOX Fuel Core with Coarse Spatial Discretization	138
7.3	Conclusion	142
8	Acceleration of the Alpha-Eigenvalue Rayleigh Quotient Fixed Point Method by Anderson Acceleration	143
8.1	Anderson Acceleration	143
8.2	Anderson Acceleration of Slowly Converging Alpha-Eigenvalue Rayleigh Quotient Fixed Point Problems	145
8.2.1	Uranium-Heavy Water Critical Slab (Sood Criticality Benchmark Problem 68)	146
8.2.2	Uranium-Heavy Water Critical Slab (Sood Criticality Benchmark Problem 73)	151
8.3	Conclusion	156
9	Conclusion	157
A	Discretization of the Alpha-Eigenvalue Problem For Slab Geometry	160
A.1	Discretization of the One-Dimensional Slab Geometry Problem	161
B	Implementation of Anderson Acceleration in Matlab for the Alpha-Eigenvalue Rayleigh Quotient Fixed Point Method	166
B.1	Alpha-Eigenvalue Rayleigh Quotient Fixed Point Method Matlab Implementation	166
B.2	Anderson Acceleration Matlab Implementation	168
	Bibliography	171

List of Figures

2.1	Neutron Direction Angle Space	5
2.2	Contour Integration in Complex Plane of the Operator A	8
2.3	Example Spectrum of the Transport Operator for the One-Speed Slab Geometry Problem	12
2.4	Discretized Alpha-Eigenvalue Spectrum for a Subcritical System	17
2.5	Example Spectrum for k -Effective Eigenvalue	19
3.1	Structure of \mathbf{H}_z^{-1}	41
3.2	Structure of Σ_f for Two Energy Groups, Five Spatial Cells, and Fission in All Energy Groups	42
3.3	Structure of Σ_s for Two Energy Groups, Five Spatial Cells, and Downscattering Only	43
3.4	Structure of \mathbf{V}_z^{-1} for Five Spatial Cells	44
3.5	Structure of $\mathbf{H}_z^{-1}\Sigma_f$ For Two Energy Group Example	45
5.1	Convergence Behavior for the Rayleigh Quotient Fixed Point Methods for Selected Infinite Medium Problems	62
5.2	Alpha-Eigenvalue Spectrum for Problem 5.2.2.1	66
5.3	Alpha-Eigenvalue Spectrum for Problem 5.2.2.2	68
5.4	Alpha-Eigenvalue Spectrum for Problem 5.2.2.3	70
6.1	Heterogeneous Slab Benchmark Problem Domain	79
6.2	Scalar Flux Results for Alternating Slabs Grain Size Problems	81
6.3	Heterogeneous Multiplying Slab Benchmark Problem Domain [43]	82
6.4	Alpha-Eigenvalue Scalar Flux Results for Two-Region Multiplying Slab	82
6.5	Five Region Heterogeneous Slab Benchmark Problem Domain	83
6.6	Case One and Two Scalar Flux Results for Five-Region Multiplying Slab-Two Cases	85
6.7	Critical Width of Slab	86
6.8	Five Region Fuel Pin Spherical Equivalent [10]	105
6.9	Absolute Error Between RQFP Method and Reference Solution for the Alpha-Eigenvalue Energy Spectrum	109

7.1	Cylindrical Space-Angle Coordinate System in Three Dimensions	115
7.2	Critical Radius of Infinite Cylinder	116
7.3	Assembly Layout for MOX Fuel Assembly Benchmark	120
7.4	Fuel Pin Layout for MOX Fuel Assembly Benchmark From [45]	120
7.5	Coarse Spatial Homogenization of MOX Fuel Assembly Benchmark Problem	129
7.6	Alpha-Eigenvalue Group Scalar Fluxes for 2D MOX Fuel Assembly Benchmark Problem - Coarse Spatial Discretization	133
7.7	Absolute Difference between Alpha- and k -Effective Eigenvalue Group Six Scalar Fluxes (Coarse Homogenization)	133
7.8	Fine Spatial Homogenization of MOX Fuel Assembly Benchmark Problem .	134
7.9	Alpha-Eigenvalue Group Scalar Flux for 2D MOX Fuel Assembly Benchmark Problem - Fine Spatial Discretization	137
7.10	Absolute Difference between Alpha- and k -Effective Eigenvalue Group Six Scalar Fluxes (Fine Homogenization)	137
7.11	Coarse Spatial Homogenization of Three-Dimensional MOX Fuel Assembly Benchmark Problem	138
7.12	Alpha-Eigenvalue Group Scalar Flux for 3D MOX Fuel Assembly Benchmark Problem - Coarse Spatial Discretization	141
8.1	Anderson Acceleration Convergence for Sood Criticality Problem 68 ($\beta_n = 1$)	150
8.2	Anderson Acceleration Convergence for Sood Criticality Problem 68 ($\beta_n = 0.5$)	150
8.3	Anderson Acceleration Convergence for Sood Criticality Problem 73 ($\beta_n = 1$)	155
8.4	Anderson Acceleration Convergence for Sood Criticality Problem 73 ($\beta_n = 0.5$)	155

List of Tables

5.1	Sood Criticality Benchmark Infinite Medium Problem Cross Sections (cm^{-1}) in [40]	59
5.2	Reference Eigenvalues and Transport Sweep Comparisons for Sood Criticality Benchmark Infinite Medium Problems in [40]	61
5.3	Infinite Medium Subcritical Problem Cross Sections (cm^{-1}) for Problem 5.2.1.1	64
5.4	Reference Eigenvalues/Transport Sweeps for Convergence for Problem 5.2.1.1	64
5.5	Infinite Medium 81-Group Problem Cross Sections (cm^{-1})	66
5.6	Transport Sweep Comparisons for Problem 5.2.2.1	67
5.7	Infinite Medium 81-Group Problem Cross Sections (cm^{-1}), Velocity Modification	68
5.8	Transport Sweep Comparisons for Problem 5.2.2.2	69
5.9	Transport Sweep Comparisons for Problem 5.2.2.3	70
6.1	Non-Multiplying Purely-Scattering Material Cross Sections (cm^{-1}) from [10]	74
6.2	Comparison of RQFP- and GFM-calculated Alpha-Eigenvalues for a Homogeneous Scattering Slab	75
6.3	Multiplying Homogeneous Material Cross Sections (cm^{-1}) from [10]	75
6.4	Comparison of RQFP- and GFM-calculated Alpha-Eigenvalues for a Homogeneous Scattering Multiplying Slab	77
6.5	Transport Sweep Comparisons for Homogeneous Multiplying Slabs	78
6.6	Non-Multiplying Heterogeneous Material Cross Sections (cm^{-1}) from [10]	79
6.7	Comparison of RQFP-calculated eigenvalues to various methods for multi-region scattering slab ($M = 500$, $L = 64$, Tolerance = 10^{-12})	80
6.8	Multiplying Heterogeneous Slab Material Cross Sections (cm^{-1})	81
6.9	Five Region Slab Material Cross Sections (cm^{-1})	83
6.10	Comparison of RQFP- and GFM-calculated Alpha-Eigenvalues for Multiplying Five-Region Fuel-Pin	84
6.11	Sood Criticality Benchmark Problems 32-35 Cross Sections (cm^{-1}) in [40]	87
6.12	Calculated Eigenvalues and Transport Sweep Comparisons for Sood Criticality Benchmark Problems 32-35 in [40]	87
6.13	Sood Criticality Benchmark Problem 45 Cross Sections (cm^{-1}) in [40]	89
6.14	Calculated Eigenvalues and Transport Sweep Comparisons for Sood Criticality Benchmark Problem 45 in [40]	89

6.15 Sood Criticality Benchmark Problem 48 Cross Sections (cm^{-1})	90
6.16 Calculated Eigenvalues and Transport Sweep Comparisons for Sood Criticality Benchmark Problem 48 in [40]	91
6.17 Sood Criticality Benchmark Problem 51 Cross Sections (cm^{-1}) in [40]	92
6.18 Calculated Eigenvalues and Transport Sweep Comparisons for Sood Criticality Benchmark Problem 51 in [40]	92
6.19 Sood Criticality Benchmark Problem 54 Cross Sections (cm^{-1}) in [40]	93
6.20 Calculated Eigenvalues and Transport Sweep Comparisons for Sood Criticality Benchmark Problem 54 in [40]	94
6.21 Sood Criticality Benchmark Problem 68 Cross Sections (cm^{-1}) in [40]	95
6.22 Calculated Eigenvalues and Transport Sweep Comparisons for Sood Criticality Benchmark Problem 68 in [40]	95
6.23 Sood Criticality Benchmark Problem 58 Cross Sections (cm^{-1}) in [40]	97
6.24 Sood Criticality Benchmark Problem 60 Cross Sections (cm^{-1}) in [40]	98
6.25 Calculated Eigenvalues and Transport Sweep Comparisons for Sood Criticality Benchmark Problem 60 in [40]	98
6.26 Comparison of RQFP- and GFM-Calculated Alpha-Eigenvalues for a Homogeneous Scattering Sphere	100
6.27 Comparison of RQFP- and GFM-Calculated Alpha-Eigenvalues for a Homogeneous Scattering Multiplying Sphere	101
6.28 Transport Sweep Comparisons for Homogeneous Multiplying Spheres	102
6.29 Sood Criticality Benchmark Problems 39, 41, and 43 Cross Sections (cm^{-1}) in [40]	103
6.30 Calculated Eigenvalues and Transport Sweep Comparisons for Sood Criticality Benchmark Problems 39, 41, and 43 in [40]	104
6.31 Comparison of RQFP- and GFM-calculated Alpha-Eigenvalues for a Three Region Multiplying Sphere	106
6.32 Fissile Material Radius and Shell Thicknesses for Plutonium-Nitrate Solution Benchmark	107
6.33 Material Composition for Plutonium-Nitrate Solution System	108
6.34 Calculated Eigenvalues and Transport Sweep Comparisons for Plutonium-Nitrate Solution System	109
6.35 Fissile Material Radius and Shell Thicknesses for PU/HEU Mixture Benchmark	110
6.36 Material Composition for PU/HEU System	111
6.37 Calculated Eigenvalues and Transport Sweep Comparisons for PU/HEU System	111
6.38 Fissile Material Radius and Shell Thicknesses for Uranium-233 Benchmark .	112
6.39 Material Composition for Uranium-233 System	112
6.40 Calculated Eigenvalues and Transport Sweep Comparisons for a Uranium-233 System	113
7.1 One-Group Cross Sections for Infinite Cylinder Critical Problems (cm^{-1}) in [40]	118

7.2	Calculated Eigenvalues and Transport Sweep Comparisons for Critical Infinite Cylinder Problems in [40]	118
7.3	C5G7MOX Energy Group Boundaries (MeV) and Speeds (cm/s)	121
7.4	C5G7MOX Cross Sections - UO ₂ Fuel-Clad	122
7.5	C5G7MOX Cross Sections - 4.3% MOX Fuel	123
7.6	C5G7MOX Cross Sections - 7.0% MOX Fuel	124
7.7	C5G7MOX Cross Sections - 8.7% MOX Fuel	125
7.8	C5G7MOX Cross Sections - Fission Chamber	126
7.9	C5G7MOX Cross Sections - Guide Tube	127
7.10	C5G7MOX Cross Sections - Moderator	128
7.11	Calculated Eigenvalues and Transport Sweep Comparisons for 2D MOX Fuel Core with Coarse Spatial Discretization	131
7.12	Calculated Eigenvalues and Transport Sweep Comparisons for 2D MOX Fuel Core with Fine Spatial Discretization	135
7.13	Calculated Eigenvalues and Transport Sweep Comparisons for 3D MOX Fuel Core with Coarse Spatial Discretization	139
8.1	Sood Criticality Problem 68 Critical Width and Reference Alpha-Eigenvalue [40]	146
8.2	Anderson Acceleration for Sood Criticality Problem 68 ($\beta_n = 1, M = 100, L = 16$)	148
8.3	Two-Group U-D ₂ O Problem Cross Sections (cm ⁻¹)	152
8.4	Sood Criticality Problem 73 Critical Width and Reference Alpha-Eigenvalue [40]	152
8.5	Anderson Acceleration for Sood Criticality Problem 73 ($\beta_n = 1, M = 100, L = 16$)	153

Acknowledgments

To Professor Rachel N. Slaybaugh, my advisor, for her support, friendship, and patience,

To Dr. Peter N. Brown, for his time, conversations, support, guidance, and patience, even when I had no idea what I was doing,

To Dr. Britton Chang, for his wisdom, perspective, friendship, illuminating conversations, and for letting me figure out things for myself,

To Dr. Teresa S. Bailey, for her active interest in my development as a student, researcher, and for hearing me out even when my ideas were not fully developed,

To Professor Jasmina Vujic and Professor Per-Olof Persson for graciously agreeing to serve on my qualifying examination and dissertation committee,

A mis papás, Mario y Claudia, a mis hermanos, Daniel y Alan, y a mi sobrino, Javier, por su amor, apoyo, y por ser mi razón para seguir adelante,

And to Laura, for her unwavering support, love, homemade baked goods, and constant reminders to not take myself too seriously, for making Berkeley home, and giving me a reason to look up from my books,

thank you! None of this would have been possible without all of you.

This research was supported by the Department of Energy Computational Science Graduate Fellowship, provided under grant number DE-FG02-97ER-25308.

Chapter 1

Introduction

The discovery of nuclear fission in 1939 by Otto Hahn precipitated a revolution in science and politics. The construction of the first experimental nuclear reactor and the detonation of the world's first nuclear weapon forced societies throughout the world to grapple with this newfound energy source, whose use could power societies for centuries or bring ruin to its cities within hours. As countries throughout the world built nuclear reactors for energy, the nuclear weapon states built up nuclear arsenals of unfathomable destructive power. With the ever looming threat of nuclear warfare and nuclear reactor accidents in the latter half of the twentieth century, nuclear energy became feared, despite its utility in medicine and electric power production. Nuclear energy and nuclear technologies remain controversial to this day. Fear of radiation (perhaps irrational in certain circumstances), nuclear weapon proliferation (a valid concern given the proliferation of nuclear weapons in the past three decades), and the open question of what to do with nuclear waste (a question of both engineering and policy), have slowed the spread of peaceful nuclear technologies. However, as the demand for clean, sustainable energy increases throughout the world and global climate change threatens societies, nuclear energy is once again poised to deliver the answer to an energy hungry world. Soothing the fears of nuclear energy requires forward thinking, where science and engineering come together with policy to create a culture of safety, risk management, and certainty.

To this end, advances in nuclear engineering technologies have given scientists and engineers the tools necessary to solve the problems of nuclear energy and design even safer, more sustainable nuclear technologies. Whereas seventy years ago the design of nuclear systems required much approximation due to the limited knowledge of neutron transport and the nature of computation, today, designers take advantage of larger computing power and memory to model increasingly complex designs and problems with less approximation. No longer limited by memory, the complex nature of neutron interactions as modeled by material cross sections can be more fully captured. No longer limited by computation, high-fidelity models taking into account complex geometric designs and complex nuclear cross section data can be solved for large numbers of unknowns, giving insight into the time-behavior of materials, reaction rates, and energy production. Continued advances in the mathematical field of neutron transport have allowed for the design of efficient solution algorithms, taking

complete advantage of computing power.

However, despite the progress made in the last few decades in the modeling and design of nuclear systems, much remains to be done. With increasingly complex reactor and accelerator designs, the modeling and numerical techniques of before may no longer work the best or work at all. With increasing computational resources, the problems designers seek to solve have scaled along with them. Once again, we find ourselves stretching the ability of our computational knowledge and our methods. Now, algorithms are required that efficiently scale and make use of the computational resources available. Mathematical methods are required whose properties are known and understood for systems consisting of thousand of materials and irregular and unique geometries. The problems that must be solved are only limited by the imagination. That same sort of imagination is now required for the design of efficient solution algorithms capable of taking complete advantage of our newfound computing power. It is here that this dissertation seeks to make a new contribution to the field.

This dissertation presents a new method, the Rayleigh Quotient Fixed Point (RQFP) method, to solve the the alpha- and k -effective eigenproblems of neutron transport. These eigenproblems describe the criticality and fundamental neutron flux mode of nuclear systems. Using a Rayleigh quotient minimization principle that is applied to demonstrably primitive discretizations of the neutron transport eigenvalue problems and the properties of primitive matrices, a new iterative method is derived. The derived eigenvalue updates are optimal in the least squares sense and positive eigenvector updates are guaranteed from the Frobenius-Perron Theorem for primitive matrices [1]. For alpha-eigenvalue problems, whereas traditional techniques have focused on supercritical problems and were limited in subcritical cases [2], this method allows for the solution of both subcritical and supercritical systems. For k -effective eigenvalue problems, traditionally the update for the eigenvalue has been taken to be some norm of the angular flux. In particular, the total fission rate over the domain is often used to update k . It has been observed that using the Rayleigh quotient can improve the efficiency of the power method [3]. We show this is due to the eigenvalue update being optimal in the least squares sense. We discuss the development, applicability, strengths and weaknesses of the method in this dissertation. The dissertation proceeds as follows

- Chapter 2 discusses neutron transport, the criticality eigenvalue problems of neutron transport, the methods used to solve these problems, as well as reviewing linear algebra and fixed-point concepts.
- Chapter 3 discusses the discretization of the continuous criticality eigenvalue problems into matrix equations. These matrix equations are shown to be primitive matrices.
- Chapter 4 derives the Rayleigh Quotient Fixed Point method for alpha- and k -effective eigenvalue problems. Using the properties of primitive matrices, a fixed-point method is derived to determine the eigenvalue and eigenvector of the system. The Jacobians of the non-linear fixed-point methods are derived and their implication regarding the convergence of the methods discussed.

- Chapter 5 discusses the performance of the Rayleigh Quotient Fixed Point method for infinite medium problems. Both one-speed and multigroup benchmarks and analytical test problems are used to demonstrate the correctness of the method and benchmark its performance as compared to other standard eigenproblem methods used in the field. The chapter also discusses in which circumstances the method might fail to converge.
- Chapter 6 discusses the performance of the method for one-dimensional slab and spherical geometries. Benchmark and analytical test problems are used to show the wide applicability of the method for various realistic cross section sets, one-speed and multigroup-in-energy problems, and heterogenous media.
- Chapter 7 discusses the performance of the Rayleigh Quotient Fixed Point method for two- and three-dimensional Cartesian geometry and two-dimensional cylindrical geometry. Two- and three-dimensional fuel pin and fuel assembly problems are considered and the method compared to standard nuclear engineering eigenproblem methods.
- Chapter 8 discusses the use of Anderson Acceleration to accelerate the Rayleigh Quotient Fixed Point method for alpha-eigenvalue problems. We discuss the benefits and costs for using acceleration in the context of neutron transport.
- Chapter 9 summarizes and reviews the Rayleigh Quotient Fixed Point method for criticality eigenvalue problems and discusses future work.
- Appendix A discusses the discretization of the one-dimensional slab alpha-eigenvalue neutron transport equation.
- Appendix B contains the MATLAB implementation of Anderson Acceleration discussed in Chapter 8.

We find that the Rayleigh Quotient Fixed Point method allows for the solution of subcritical, critical, and supercritical alpha-eigenvalue problems for all types of nuclear systems of interest. The RQFP method solves problems where traditional method fail to converge, specifically subcritical systems and systems without fissile material. The RQFP method also drastically reduces the number of iterations required to converge the solution when compared to traditional alpha-eigenvalue methods. The RQFP method applied to k -effective eigenvalue gives designers another solution method. In specific circumstances, like infinite-medium problems, the RQFP method for k -effective eigenvalue problems improves upon the performance of traditional eigensolvers used in nuclear engineering. We find that in specific circumstances, the alpha- and k -effective eigenvalue problems form primitive linear systems. By using the properties of primitive linear systems, the RQFP method provides a robust and easily implementable method for the solution of alpha- and k -effective eigenvalue problems of interest to the nuclear engineering community.

Chapter 2

Background

2.1 Neutron Transport

Neutron transport is the study of the motion and interactions of neutrons in matter. Neutrons interact with the nuclei of matter and can be absorbed or scattered, depending on the properties of the matter. Neutrons can also leak through a boundary, having passed through matter without being absorbed. Absorption of a neutron leads to one less neutron in the system. The scattering of a neutron does not remove the neutron from the system but rather changes its energy and direction. If a neutron causes fission, it is lost. However, the fission of nuclei lead to the production of neutrons in the system. This accounting of the number of neutrons present in a system at a specific time leads to the fundamental equation of neutron transport, the linear Boltzmann transport equation:

$$\begin{aligned} & \left[\frac{1}{v(E)} \frac{\partial}{\partial t} + \hat{\Omega} \cdot \nabla + \sigma(\vec{r}, E) \right] \psi(\vec{r}, \hat{\Omega}, E, t) \\ &= \int_0^\infty dE' \int_{4\pi} d\hat{\Omega}' \sigma_s(\vec{r}, E' \rightarrow E, \hat{\Omega}' \cdot \hat{\Omega}) \psi(\vec{r}, \hat{\Omega}', E', t) \\ &+ \int_0^\infty dE' \nu(E') \chi(E' \rightarrow E) \sigma_f(\vec{r}, E') \int_{4\pi} d\hat{\Omega}' \psi(\vec{r}, \hat{\Omega}', E', t), \quad (2.1) \end{aligned}$$

where the quantities are located at position \vec{r} , traveling in direction $\hat{\Omega}$, and at energy E , and σ , σ_s , σ_f , and v are the total, scattering, fission macroscopic cross sections, and neutron velocity, respectively. $\chi(E' \rightarrow E)$ is the fission spectrum and specifies the energy distribution of neutrons born from fission and $\nu(E)$ is the average number of neutrons emitted in fission when the neutron causing fission has energy E . The angular flux, denoted by $\psi(\vec{r}, \hat{\Omega}, E, t)$, gives the number of neutrons per unit length squared per steradian per energy per unit time and is the unknown distribution we are looking to solve for. The streaming term of Eq. 2.1 can be rewritten using the angle space shown in Figure 2.1. If the direction vector $\hat{\Omega}$ is given by

$$\hat{\Omega} = \mu \hat{x} + \eta \hat{y} + \xi \hat{z}, \quad (2.2)$$

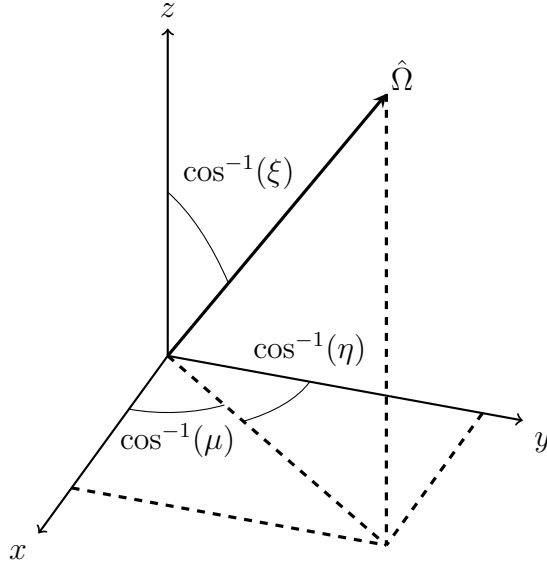


Figure 2.1: Neutron Direction Angle Space

where \hat{x} , \hat{y} , and \hat{z} are unit vectors, then it follows that the streaming term is given by

$$\hat{\Omega} \cdot \nabla \psi(\vec{r}, \hat{\Omega}, E, t) = \mu \frac{\partial \psi}{\partial x} + \eta \frac{\partial \psi}{\partial y} + \xi \frac{\partial \psi}{\partial z}. \quad (2.3)$$

The linear Boltzmann transport equation is used in solving many problems in nuclear engineering [4]. We refer to the linear Boltzmann transport equation as the neutron transport equation for the rest of this dissertation. The neutron transport equation is an integro-differential equation for the neutron angular flux and is a function of seven independent variables: three spatial variables, two direction variables, energy, and time.

Solving the neutron transport equation with appropriate initial conditions and boundary conditions yields the expected number of neutrons within a geometry as a function of space, direction, energy, and time. However, the neutron transport equation for neutrons is an integro-differential equation and in general, few analytic solutions exist [5]. For this reason, it is necessary to use numerical methods to solve practical problems. For neutron transport, there are two classes of computational methods: deterministic and Monte Carlo. In deterministic methods, the position, direction, energy, and time phase space of the transport equation is discretized and a system of equations solved iteratively. Approaches such as the discrete ordinates method where the neutron transport equation is solved along ordinates and quadrature is used to approximate integrals in angle and diamond differencing in space are used to approximate derivative and integral quantities. This discretization process introduces truncation errors and the discretization of irregular geometries can be problematic. In addition, deterministic methods require appropriately homogenized in space and energy nuclear cross sections for system materials which introduces another source of error due to the averaging process. Monte Carlo methods treat the phase space as continuous, allowing

for the detailed modeling of geometry and use of continuous cross section data. The Monte Carlo method does not solve the transport equation directly, instead it stochastically simulates the transport of a finite number of neutrons through the problem geometry [6]. After obtaining a large number of particle interaction histories, averages of particle interactions are extracted, giving the number of neutrons in some part of the phase space, the number of reactions occurring, and other important physical values, within some uncertainty. Monte Carlo methods introduce stochastic uncertainty and can require large number of particle simulations to achieve acceptable uncertainties on calculated parameters.

2.2 The Criticality Problem of Neutron Transport

The ability to fission certain nuclei with neutrons to produce additional neutrons leads to the criticality problem. Given a system with a certain material composition and geometry, is it possible to have a self-sustaining chain reaction? If a system is capable of a self-sustaining chain reaction, we call this system critical, where the loss and production of neutrons are perfectly in balance, allowing the neutron population to be constant in time. If the system is unable to sustain a chain reaction, the system is said to be subcritical. If the neutron population in the system grows without bound, the system is said to be supercritical [7]. It is rare to immediately find a system geometry or material composition that is critical. Instead, some parameter is introduced into the transport equation that forces the system to be critical. Given the sign or magnitude of this parameter, we can judge how far a system is from critical and whether or not the system is subcritical or supercritical. This parameter is the eigenvalue for which we solve numerically. There is no unique way to form an eigenvalue problem [8], and depending on the application, one eigenvalue formulation may be more useful than others. In this dissertation we focus on the α - and k -eigenvalue problems due to their widespread use in nuclear engineering applications.

2.2.1 The α -Eigenvalue Problem

If we are interested in the time asymptotic behavior of neutron flux in a system, the α -eigenvalue problem gives the exponential time-dependent flux behavior and criticality eigenpair of the system [7]. The time asymptotic behavior of the neutron flux is given by the sign of the eigenvalue, which determines whether or not the neutron flux decays to zero, remains constant in time, or grows without bound. We derive the alpha-eigenvalue problem by attempting to solve Eq. 2.1 for some initial condition $\psi_0(\vec{r}, E, \hat{\Omega}, t = 0)$ and vacuum boundary conditions [5]. Defining the operator A as

$$A \equiv v(E) \left[\frac{\chi(E)}{4\pi} \int_{4\pi} d\hat{\Omega}' \int_0^\infty dE' \nu(E) \sigma_f(\vec{r}, E', t) + \int_{4\pi} d\hat{\Omega}' \int_0^\infty dE' \sigma_s(\vec{r}, E' \rightarrow E, \hat{\Omega}' \rightarrow \hat{\Omega}, t) - \hat{\Omega} \cdot \nabla - \sigma(\vec{r}, E, t) \right], \quad (2.4)$$

we can write the initial value problem as

$$\frac{\partial \psi}{\partial t} = A\psi. \quad (2.5)$$

We expect the previous equation to have solutions in the form of

$$\psi = \psi_0 e^{\alpha t}, \quad (2.6)$$

where we obtain the eigenvalues α from the equation

$$\alpha\psi = A\psi. \quad (2.7)$$

Obtaining the solution of the time-dependent neutron transport equation becomes a matter of determining the eigenvalues (spectrum) of A [7]. Taking the Laplace transform of Eq. 2.5, we define

$$\psi_\alpha \equiv \int_0^\infty dt e^{\alpha t} \psi(\vec{r}, E, \hat{\Omega}, t), \quad (2.8)$$

and obtain

$$\alpha\psi_\alpha - \psi_0 = A\psi_\alpha \rightarrow (\alpha - A)\psi_\alpha = \psi_0. \quad (2.9)$$

To solve this equation we invert the left-hand side of the previous equation (resolvent operator) and obtain

$$\psi_\alpha = (\alpha - A)^{-1}\psi_0. \quad (2.10)$$

Applying the inverse Laplace transform, we obtain the solution to the initial value problem

$$\psi = \frac{1}{2\pi i} \int_{b-i\infty}^{b+i\infty} d\alpha (\alpha - A)^{-1} \psi_0 e^{\alpha t}. \quad (2.11)$$

Equation 2.11 is the formal solution of Eq. 2.5. However, this solution still requires that we perform a complex contour integral. To integrate the solution, we must know where the singularities of the integrand operator are located. Assume the operator has a discrete number of poles, then the integral can be performed by extending and closing the contour path to pick up all residue contributions as can be seen in Figure 2.2.

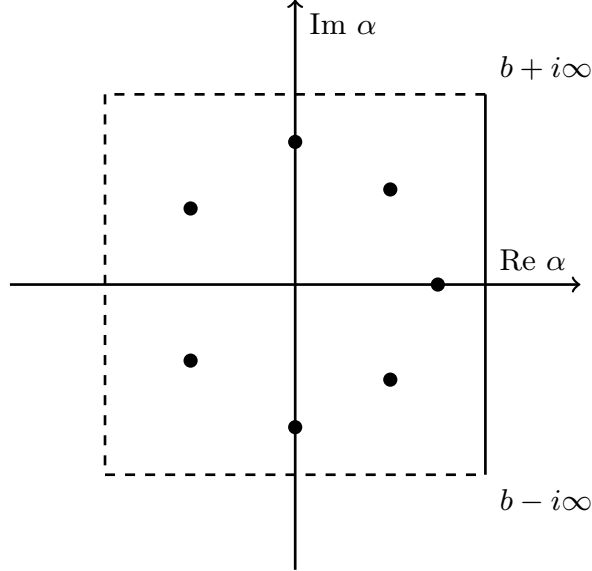
Defining

$$f(\alpha) = (\alpha - A)^{-1}\psi_0 e^{\alpha t}, \quad (2.12)$$

the solution to the initial value problem can be expressed as

$$\psi = \frac{1}{2\pi i} \int_{b-i\infty}^{b+i\infty} d\alpha f(\alpha) = \oint_C d\alpha f(\alpha) = 2\pi i \sum_{k=1}^n \text{Res}(f(\alpha), \alpha_k). \quad (2.13)$$

where α_k are the eigenvalues from Eqn. 2.7. While Eq. 2.13 is the general solution for the initial value problem, usually we are only interested in the asymptotic time solution since at long times it is expected that only the dominant eigenvalue and fundamental mode will

Figure 2.2: Contour Integration in Complex Plane of the Operator A

remain. Rather than taking the Laplace Transform of Eq. 2.5, the α -eigenvalue problem is formed by assuming the angular flux solution is separable in time, giving the asymptotic solution

$$\psi(\vec{r}, \hat{\Omega}, E, t) = \psi(\vec{r}, \hat{\Omega}, E) \exp(\alpha t). \quad (2.14)$$

Substituting the asymptotic solution into the neutron transport equation (Equation 2.1) yields the α -eigenvalue neutron transport equation:

$$\begin{aligned} & \left[\frac{\alpha}{v(E)} + \hat{\Omega} \cdot \nabla + \sigma(\vec{r}, E) \right] \psi(\vec{r}, \hat{\Omega}, E) \\ &= \int dE' \int d\hat{\Omega}' \sigma_s(\vec{r}, E' \rightarrow E, \hat{\Omega}' \cdot \hat{\Omega}) \psi(\vec{r}, \hat{\Omega}', E') \\ & \quad + \int dE' \nu(E') \chi(E' \rightarrow E) \sigma_f(\vec{r}, E') \int d\hat{\Omega}' \psi(\vec{r}, \hat{\Omega}', E'). \end{aligned} \quad (2.15)$$

We define the operator form of Eq. 2.15 as

$$(\mathcal{H} + \alpha \mathcal{V}^{-1})\psi = (\mathcal{S} + \mathcal{F})\psi, \quad (2.16)$$

where the operators are continuous and given by

$$\begin{aligned}\mathcal{H} &= \hat{\Omega} \cdot \nabla + \sigma(\vec{r}, E), \\ \mathcal{V}^{-1} &= \frac{1}{v(E)}, \\ \mathcal{S} &= \int dE' \int d\hat{\Omega} \sigma_s(\vec{r}, E' \rightarrow E, \hat{\Omega}' \cdot \hat{\Omega}) \psi(\vec{r}, \hat{\Omega}', E'), \\ \mathcal{F} &= \int dE' \nu(E') \chi(E' \rightarrow E) \sigma_f(\vec{r}, E') \int d\hat{\Omega}' \psi(\vec{r}, \hat{\Omega}', E').\end{aligned}\tag{2.17}$$

In general, there will be a spectrum of eigenvalues for which there are solutions to Equation 2.15 but at long times, only a unique, positive eigenvector, ψ_0 , corresponding to the algebraically largest eigenvalue, α_0 , remains. The asymptotic solution can be written as [9]

$$\psi_{\text{asym}}(\vec{r}, \hat{\Omega}, E, t) \propto \psi_0(\vec{r}, \hat{\Omega}, E) \exp(\alpha_0 t).\tag{2.18}$$

The criticality of the system can be defined by the sign of α_0

$$\alpha_0 \begin{cases} > 0, & \text{supercritical,} \\ = 0, & \text{critical,} \\ < 0, & \text{subcritical.} \end{cases}$$

The fundamental eigenvalue and eigenvector are real ($\alpha_0 \in \mathbb{R}, \psi_0 \in \mathbb{R}^N$) but any of the higher eigenvalues and eigenvectors may be negative and complex. The α -eigenvalues are ordered by their real part

$$\alpha_0 > Re(\alpha_1) \geq Re(\alpha_2) \geq \dots \geq Re(\alpha_n).\tag{2.19}$$

Let \mathcal{T} be the transport operator defined as

$$\mathcal{T} = \mathcal{V}(\mathcal{S} + \mathcal{F} - \mathcal{H}),\tag{2.20}$$

then it follows that the eigenvalue problem can be written as

$$\alpha\psi = \mathcal{T}\psi.\tag{2.21}$$

Since complex eigenvalues are possible in the spectrum for the real transport operator \mathcal{T} , it follows that the complex conjugate of these eigenvalues are also in the spectrum. We prove this as follows:

Theorem 2.1. *If there exists a complex eigenvalue in the spectrum, then its complex conjugate is also in the spectrum.*

Proof. Consider the linear transport operator $\mathcal{T} \in \mathbb{R}$. If $\lambda \in \mathbb{C}$ is a complex eigenvalue of \mathcal{T}

and $v \in \mathbb{C}^n$ is a non-zero eigenfunction of \mathcal{T} , then by definition

$$\mathcal{T}v = \lambda v. \quad (2.22)$$

Taking the complex conjugate of Equation 2.22 yields

$$\bar{\mathcal{T}}\bar{v} = \mathcal{T}\bar{v} = \bar{\lambda}\bar{v}, \quad (2.23)$$

since \mathcal{T} is real and linear. \square

In addition, given the entire set of eigenvalue and eigenvectors for this eigenvalue problem, any initial condition angular flux can be expressed as a combination of the eigenvectors and eigenvalues. These eigenvalues α exist for systems without fissile material and have units of inverse time as they give a characteristic time of the slowest neutron to leak or be absorbed in the system. In the literature, these eigenvalues are also known as natural, time [2], or λ [4] eigenvalues. For simple problems such as one-speed slabs and multigroup-in energy slab and spherical problems, various features of the α -eigenvalue spectrum have been identified. We discuss these results in Section 2.2.1. It must be noted that the existence of a fundamental eigenvalue is not guaranteed for all problems. In particular, optically thin slabs have been shown to have no fundamental eigenvalue [10]. In contrast to incredibly subcritical problems, for incredibly supercritical systems, two real, positive eigenvalues have been observed [10]. In general, the existence of a sole dominant eigenvalue has also yet to be proven for all cases of interest.

The α -Eigenvalue Spectrum

In this section we examine previous work on the α -eigenvalue spectrum. Initial examination of the spectrum by Lehner and Wing [11] for the linear transport operator \mathcal{T} assumed the one-speed, slab geometry form

$$\mathcal{T}(x, \mu) = -\mu \frac{\partial}{\partial x} + \frac{c}{2} \int_{-1}^1 d\mu'. \quad (2.24)$$

where

$$c = \frac{\bar{\nu}\sigma_f + \sigma_s}{\sigma}. \quad (2.25)$$

Additional studies by Jörgens extended the spectral analysis to multi-energy media [12]. Larsen extended the spectral analysis to more general geometries [13]. Larsen found that the spectrum of \mathcal{T} for more general problems consists of points, line, and in some cases, a continuum of eigenvalues. An example of the spectrum of \mathcal{T} can be seen in Figure 2.3. The spectrum of \mathcal{T} includes more scalars than just the α -eigenvalues. The α -eigenvalues are the point and line spectrum of \mathcal{T} [14]. The point spectrum is finite, all-real set lying in the positive half-plane $\lambda > -\lambda^*$, where λ^* is the minimum value of $v\sigma(v)$. The features of the spectrum of \mathcal{T} are highly dependent on the type of problem being examined. For example,

for slab geometry problems, the continuum of eigenvalue occurs due to the possibility a neutron can travel parallel to one of the faces indefinitely before scattering or leaving the slab [15]. The continuous spectrum is contained in the negative half-plane $\text{Re } \lambda \leq -\lambda^*$. The dividing limit, $-\lambda^*$, called the Corngold limit, marks the minimum physically-possible α -eigenvalue.

Theorem 2.2. *The Corngold limit, $-\lambda^* = -v\sigma(v)$, is the minimum physically possible α -eigenvalue.*

Proof. We use the facts that the α - and k -eigenvalue problems are equal for an exactly critical system and the eigenfunctions corresponding to these eigenvalues are equal [16]. Consider the infinite medium, one energy group eigenvalue problems:

$$\sigma\phi = \sigma_s\phi + \frac{\bar{\nu}\sigma_f}{k_\infty}\phi, \quad (2.26)$$

$$\frac{\alpha_\infty}{v}\phi = \sigma_s\phi + \bar{\nu}\sigma_f\phi - \sigma\phi, \quad (2.27)$$

where $\bar{\nu}$ is the average number of neutrons emitted in fission and k_∞ and α_∞ are the infinite-medium k -effective and alpha-eigenvalues, respectively. Dividing out the fluxes and combining the two equations yields a relationship for the two eigenvalues for the infinite-medium, one-group problem [10]

$$\frac{\alpha_\infty}{v\sigma} = (k_\infty - 1)\left(1 - \frac{\sigma_s}{\sigma}\right). \quad (2.28)$$

The minimum possible α -eigenvalue occurs when there is no fissile material ($k_\infty = 0$) or scattering ($\sigma_s = 0$) present. Substitution of these values into Equation 2.28 yields

$$\alpha_\infty = -v\sigma = -\lambda^*, \quad (2.29)$$

which is the Corngold limit. \square

The minimum velocity, v_{\min} , has interesting impacts on the spectrum of the operator \mathcal{T} . Studies on finite media problems where the minimum velocity is greater than zero ($v_{\min} > 0$) show that the continuous part of the spectrum disappears [12]. Instead of a continuous spectrum, point and line spectra fill the half-space. If the minimum neutron velocity is allowed to approach small speeds, $v_{\min} = 0$, the continuous part of the spectrum reappears. The presence of line spectra results from considering the continuous dependence of the α -eigenvalues on neutron velocity. As the velocity varies from some v to v_{\min} , some eigenvalues trace out curves in the complex plane or remain stationary [13].

Studies suggest that the case where the minimum neutron velocity is bounded away from zero is the more physically valid representation. As the neutron velocity minimum is allowed to go to zero, the neutron wavelength is comparable to the mean free path, thus rendering the neutron transport equation invalid [4]. In this dissertation, the neutron transport equation is discretized and energy-dependent cross sections are bounded away from zero. α -eigenvalue spectra will then contain only point spectra.

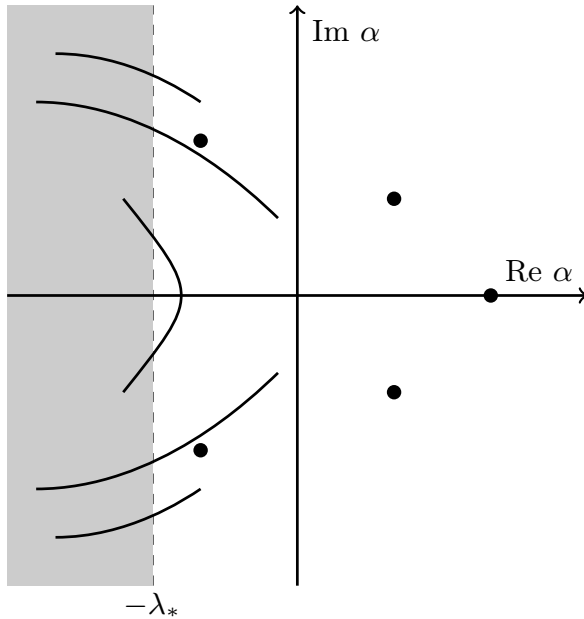


Figure 2.3: Example Spectrum of the Transport Operator for the One-Speed Slab Geometry Problem

Applications of the α -Eigenvalue

The alpha-eigenvalue and its corresponding eigenvector give the time-dependence of the neutron flux in a nuclear system of interest. For subcritical problems, given some external source, the alpha-eigenvalue measures the length of time necessary for all neutrons to leave the system. One type of system of interest is accelerator-driven subcritical (ADS) systems. ADS systems are subcritical configurations containing multiplying material that are pulsed with a large number of neutrons. These neutrons are generated by an accelerator colliding protons or ions onto a spallation target creating large amounts of neutrons [17]. ADS systems have received renewed interest because of their ability to address nuclear reactor waste disposal concerns. These systems are able to transmute radioactive isotopes to stable or shorter half-life isotopes by fissioning the radioactive nuclei of concern using high-energy spallation neutrons. The transmutation of long-lived actinides and fission products provide an alternative to geological disposal. Also, the fissioning of nuclei in the system can provide enough power to supply the accelerator, making ADS systems self-sustainable.

The alpha-eigenvalue and eigenvector are necessary to characterize the neutron flux time and spatial variation when the ADS system is in a subcritical state. With the addition of spallation neutrons into the system, the alpha-eigenvalue describes the length of time necessary for the neutron flux to decay. Knowledge of the spatial and time variations in the neutron flux also allows designers to determine the efficient placement of actinides and other fission products in the system for optimal consumption.

Another application of the alpha-eigenvalue is for nuclear systems that are supercriti-

cal for short periods of time like fast-burst nuclear reactors. Fast-burst reactors generate high-flux neutron pulses that are used in materials radiation testing, electronic hardware hardening testing, and other applications. These supercritical systems return to a subcritical state through some sort of feedback, either geometric or thermal. Since the neutron flux is a time-dependent function, the alpha-eigenvalue gives a measure of the growth rate of the neutron flux. For purely supercritical systems, the neutron flux increases without bound in time and the alpha-eigenvalue measures the e -folding time, the time required by the exponentially growing neutron population to increase by a factor of e [4]. To see this, consider Eq. 2.28

$$\frac{\alpha_\infty}{v\sigma} = (k_\infty - 1) \left(1 - \frac{\sigma_s}{\sigma}\right).$$

Multiplying by $v\sigma$ and using the relation $\sigma_a = \sigma - \sigma_s$, we can write

$$\alpha_\infty = v(\nu\sigma_f - \sigma_a). \quad (2.30)$$

Noting that $k_\infty = \bar{\nu}\sigma_f/\sigma_a$ and the neutron lifetime is given by $\ell = 1/v\sigma_a$, we obtain

$$\alpha_\infty = \frac{k_\infty - 1}{\ell}. \quad (2.31)$$

The time rate change of the number of neutrons $N(t)$ in an infinite medium is given by the ordinary differential equation

$$\frac{dN}{dt} = \frac{(k_\infty - 1)}{\ell} N(t), \quad (2.32)$$

with solution

$$N(t) = N_0 \exp \left[\frac{k_\infty - 1}{\ell} t \right]. \quad (2.33)$$

Comparing the relationship for α_∞ and Eq. 2.33, we see that we can write

$$N(t) = N_0 \exp(\alpha_\infty t). \quad (2.34)$$

Relating α_∞ to the reactor period T (e -folding time), we see that

$$T = \frac{1}{\alpha_\infty}. \quad (2.35)$$

We also note that Eq. 2.31 gives the maximum time eigenvalue for a homogeneous system [10]. Higher alpha-eigenvalues are used in reactor kinetics to determine neutron flux responses to reactivity insertions and feedback mechanisms [18]. We only focus on the dominant eigenvalue in this dissertation, however, since we are interested in the criticality of nuclear systems.

Calculating the α -Eigenvalue

In this section we describe various numerical methods used to determine the alpha-eigenvalue and eigenvector in discrete ordinates neutron transport codes. Methods other than those described in this section exist and this by no means is a full review of all methods. However, the methods presented here are those used predominantly in neutron transport codes or methods used to determine analytical eigenvalues and eigenvectors for benchmarking.

The Critical Search Method: The workhorse method in neutron transport codes for the numerical solution of the the alpha-eigenvalue problem is the critical search method [2]. The critical search method is the primary alpha-eigenvalue solver for supercritical problems in codes such as ARDRA [19] and PARTISN [20]. For Eq. 2.36, the critical search performs multiple k -effective calculations for various values of α :

$$\begin{aligned} & \left[\frac{\alpha^\ell}{v(E)} + \hat{\Omega} \cdot \nabla + \sigma(\vec{r}, E) \right] \psi(\vec{r}, \hat{\Omega}, E, t) \\ &= \int dE' \int d\hat{\Omega}' \sigma_s(\vec{r}, E' \rightarrow E, \hat{\Omega}' \cdot \hat{\Omega}) \psi(\vec{r}, \hat{\Omega}', E', t) \\ &+ \frac{1}{k^\ell} \int dE' \nu(E') \chi(E' \rightarrow E) \sigma_f(\vec{r}, E') \int d\hat{\Omega}' \psi(\vec{r}, \hat{\Omega}', E', t), \quad (2.36) \end{aligned}$$

where α^ℓ and k^ℓ are the alpha- and k -effective eigenvalues at iteration ℓ . The critical search method is described in Algorithm 2.1. Using various guessed values for the alpha-eigenvalue, intermediate k -effective eigenvalue calculations are done. The true alpha-eigenvalue is then found by extrapolation using the (α, k) pairs to find the alpha-eigenvalue such that the system is exactly critical. This extrapolation might require multiple iterations to bracket the eigenvalue.

In this method, the alpha-eigenvalue introduces artificial absorption into the problem. For sufficiently subcritical systems, negative absorption is possible, potentially causing solution methods to diverge [2]. For systems close to critical, many interpolations/extrapolations of alpha-eigenvalue iterates are required and the critical search method might become unacceptably slow. In addition, for systems close to critical, the intermediate k -effective calculation convergence might become slow, increasing the cost of the method in the intermediate stage. The question of how converged the k -effective eigenvalue calculations must be remains open. Using unconverged k -effective eigenvalues in the estimation of the alpha-eigenvalue may slow down or prevent the convergence to the true alpha-eigenvalue. For an eigenvalue that is too tightly converged, iterations are wasted and the method becomes inefficient.

Algorithm 2.1 Critical Search Method [2]

- 1: Make an initial guess for α^0 .
 - 2: Solve Eq. 2.36 for k^0 .
 - 3: Obtain a second guess α^1 by adjusting α^0 by some eigenvalue modifier value: $\alpha^1 = \alpha^0 + \text{EMV}$.
 - 4: Solve Eq. 2.36 for k^1 .
 - 5: **while** $|k^\ell - 1|/k^\ell > \text{tolerance}$ **do**
 - 6: Using (α^ℓ, k^ℓ) and $(\alpha^{\ell-1}, k^{\ell-1})$, perform a linear extrapolation of $k(\alpha)$ to find $\alpha^{\ell+1}$ such that $k^{\ell+1}(\alpha^{\ell+1}) = 1$.
 - 7: Solve Eq. 2.36 for $k^{\ell+1}$.
 - 8: **end while**
-

Green's Function Method (GFM): Green's Function Method [10] uses Green's functions to model one-speed, multiplying, multi-region slabs and obtain boundary flux values for an eigenvalue search. The one-group neutron transport equation for a homogeneous material with isotropic scattering is

$$\left[\mu \frac{\partial}{\partial x} + \sigma + \frac{\alpha}{v} \right] \psi(x, \mu) = \frac{\nu \sigma_f + \sigma_s}{2} \int_{-1}^{-1} d\mu' \psi(x, \mu'). \quad (2.37)$$

Dividing by the total cross section we obtain

$$\left[\frac{\mu}{\sigma} \frac{\partial}{\partial x} + \alpha' \right] \psi(x, \mu) = \frac{c}{2} \int_{-1}^{1} d\mu' \psi(x, \mu'), \quad (2.38)$$

where

$$\alpha' = 1 + \frac{\alpha}{v\sigma} \quad \text{and} \quad c = \frac{\nu \sigma_f + \sigma_s}{\sigma}. \quad (2.39)$$

Eq. 2.38 is measured in mean free paths. For infinite medium problems, $\alpha' \geq 0$. This can be seen by allowing α to be the Corngold limit, the smallest possible alpha-eigenvalue, and evaluating for α' .

The GFM is useful for multi-region systems because of Placzek's lemma [21]. Placzek's lemma states that the angular flux solution in a finite slab can be expressed in terms of a solution in an infinite medium by converting boundary angular flux sources into equivalent volumetric sources. Using the lemma, each slab region can be treated as an infinite homogeneous medium with a specified source based on the angular flux boundary conditions. For an infinite medium, the angular flux can be expressed by the Green's function

$$\psi(x, \mu) = \int_{-\infty}^{\infty} dx' \int_{-1}^{1} d\mu' [\mu' \psi(0, \mu') \delta(x') - \mu' \psi(\Delta, \mu') \delta(x' - \Delta, \mu')] G(x - x', \mu | \mu'), \quad (2.40)$$

where the Green's function satisfies the integro-differential equation

$$\left[\mu \frac{\partial}{\partial x} + \alpha' \right] G(x, \mu | \mu') = \frac{c}{2} \int_{-1}^{1} d\mu'' G(x, \mu'' | \mu') + \delta(x) \delta(\mu - \mu'), \quad (2.41)$$

and Δ is the width of the finite slab in mean free paths.

The solution, $G(x, \mu | \mu')$, to Eq. 2.41 is in the form of the solution to the anisotropic plane source emitting particles in direction μ' for an infinite homogeneous medium problem with scattering parameter c . Taking a Fourier transform of Eq. 2.41, integrating over the scattering angle μ , inverting the transform, and using Placzek's lemma to connect individual slab regions through boundary angular fluxes, an integral equation for the angular flux in the multi-region medium is found:

$$\begin{aligned} & \psi_i(0^+, -\mu) + \int_0^1 d\mu' \mu' \psi_i(0^+, -\mu') [G_c(0^-, \mu | \mu') \pm G_c(-\Delta_i, -\mu' | \mu')] \\ & \pm \psi_i(\Delta_i^-, \mu) \pm \int_0^1 d\mu' \mu' \psi_i(\Delta_i^-, \mu') [G_c(0^-, \mu | \mu') \pm G_c(-\Delta_i, -\mu | \mu')] \\ & \mp \psi_{i-1}(\Delta_{i-1}^-, \mu) \exp\left(\frac{-\alpha' \Delta_i}{\mu}\right) - \int_0^1 d\mu' \mu' \psi_{i-1}(\Delta_{i-1}^-, \mu') [G_c(0^+, -\mu | \mu') \\ & \pm G_c(\Delta_i^-, \mu | \mu')] - \psi_{i+1}(0^+, -\mu) \exp\left(\frac{-\alpha' \Delta_i}{\mu}\right) \\ & \mp \int_0^1 d\mu' \mu' \psi_{i+1}(0^+, -\mu') [G_c(0^+, -\mu | \mu') \pm G_c(\Delta_i^-, \mu | \mu')] = 0, \end{aligned} \quad (2.42)$$

where

$$G_c(x, \mu | \mu') = \frac{c}{2\alpha'} \frac{1}{\mu' - \mu} [h(x, \mu') - h(x, \mu)], \quad (2.43)$$

$$h(x, \mu) = \frac{\mu}{2\pi} \int_{-\infty}^{\infty} dk \frac{e^{ikx}}{\alpha' + ik\mu} \frac{1}{1 - \frac{c}{\alpha'} L\left(\frac{k}{\alpha'}\right)}, \quad (2.44)$$

and

$$L(z) = \frac{1}{2} \int_{-1}^1 d\mu \frac{1}{1 + iz\mu} = \frac{\tan^{-1} z}{z}. \quad (2.45)$$

The eigenvalue problem is formulated by construction of a matrix of the interactions of slab boundary angular fluxes for each region as given by Eq. 2.42. The matrix consists of sub-matrices for each region where the integrals are approximated using numerical quadrature. Eigenvalues are then determined using a brute force search routine where all possible values for the eigenvalue within some search space are tested until a value is found such that the real and imaginary parts of the matrix determinant are zero. This value is then the eigenvalue of the system. GFM allows for the calculation of higher eigenvalues and eigenmodes. GFM provides benchmark-quality calculations for the alpha-eigenvalues in heterogeneous media slab problems.

The increase of computational difficulty increases with the number of regions present in the system. In addition, the search space might become large, especially if there is no estimate of the eigenvalue. The numerical quadrature of the integrals also present another cost, as improper integrals must be approximated in each region of the problem to some

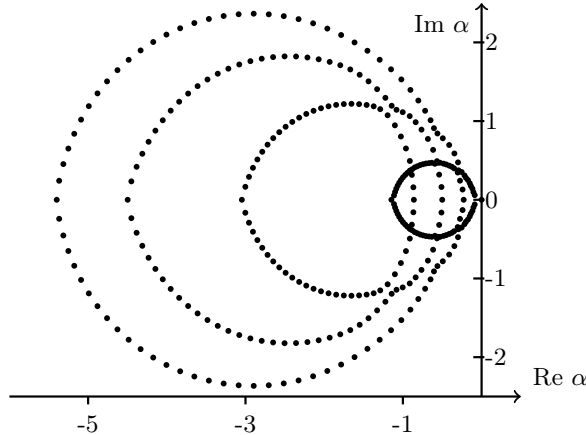


Figure 2.4: Discretized Alpha-Eigenvalue Spectrum for a Subcritical System

tolerance. Determination of the matrix determinant requires a complex LU decomposition routine. Further, the scope of GFM is limited to slab geometry, though by using the slab-spherical equivalence [21] the eigenvalues of one-dimensional spherical systems can be determined by solving an equivalent slab geometry problem when certain conditions are met.

Direct Evaluation: Another numerical method capable of obtaining the alpha-eigenvalue and higher eigenvalues involves forming the matrix problem from the discretized form of the one-speed, one-dimensional transport equation [22] using discrete ordinates in angle and diamond differencing in space. Using a process similar to the one described in Chapter 3 with M directions in angle and N cells in space yields a generalized eigenvalue problem of the form

$$\mathbf{A}\psi = \alpha\mathbf{B}\psi. \quad (2.46)$$

Using standard eigenvalue solvers, the method gives NM eigenpairs. Given the discretization of the problem, the method gives far more eigenvalues than expected from theory as the discretization process introduces additional eigenvalues that are artifacts from the discretization process. The spectrum is composed of the real eigenvalue spectrum and additional eigenvalues which are a product of the discretization of the problem. An example spectrum can be seen in Figure 2.4. If only the dominant eigenvalue and vector are required, the formation of the matrices and the eigenvalue solver could be too costly. Direct evaluation works well for homogeneous and multi-region slabs with isotropic scattering. However, the method quickly becomes complicated and expensive for problems involving complex geometries, anisotropic scattering, and multiple energy groups.

2.2.2 The k -Eigenvalue

In the k -effective eigenvalue problem, the time-dependence of the problem is eliminated and it is assumed there is no external source present [7]. Instead, a time-independent solution is obtained by weighting ν by a parameter k , which expresses the deviation from critical.

Substituting ν/k for ν yields the k-eigenvalue problem:

$$\begin{aligned} \left[\hat{\Omega} \cdot \nabla + \sigma(\vec{r}, E) \right] \psi(\vec{r}, \hat{\Omega}, E) \\ = \int dE' \int d\hat{\Omega} \sigma_s(\vec{r}, E' \rightarrow E, \hat{\Omega}' \cdot \hat{\Omega}) \psi(\vec{r}, \hat{\Omega}', E') \\ + \frac{1}{k} \int dE' \nu(E') \chi(E' \rightarrow E) \sigma_f(\vec{r}, E') \int d\hat{\Omega}' \psi(\vec{r}, \hat{\Omega}', E'). \end{aligned} \quad (2.47)$$

We define the operator form of Eq. 2.47 as

$$\mathcal{H}\psi = \left(\mathcal{S} + \frac{1}{k} \mathcal{F} \right) \psi. \quad (2.48)$$

For Eq 2.48, there are multiple eigenvalues and eigenvectors, but the only positive eigenvector corresponds to the largest real eigenvalue, k_0 . The k -effective eigenvalue exists for any system containing fissile material and corresponding to the eigenvalue is a non-negative eigenvector. For a system containing no fissile material, the k -effective eigenvalue is undefined. The criticality of a system can be defined by the value of k :

$$k \begin{cases} > 1, & \text{supercritical,} \\ = 1, & \text{critical,} \\ < 1, & \text{subcritical.} \end{cases}$$

The spectrum of eigenvalues for the k -effective eigenvalue problem is real and positive. The spectrum is ordered

$$k_0 > k_1 > k_2 > \dots k_N, \quad (2.49)$$

where $k_0 = k$ is the dominant eigenvalue and N is the total number of eigenvalues. An example of a k -effective eigenvalue spectrum can be seen in Figure 2.5. The full set of k -eigenvalues and eigenvectors have applications in perturbation theory and provide a measure of numerical convergence for methods like the power method [5]. The dominance ratio, the ratio k_1/k_0 , provides a measure of convergence for the power method, the standard eigensolver for k -effective eigenvalue problem in nuclear engineering applications [5]. If a designer is interested in how far a system is from a critical configuration, the k -effective eigenvalue is a good measure as it represents the ratio between the fission source and losses due to leakage and absorption. For an exactly critical system, the eigenvector corresponding to k is the flux shape within the reactor. For systems close to critical, the eigenvector is a good approximation of the flux shape. The k -effective eigenvalue has another simple physical interpretation: it is the ratio of neutrons in the next generation to those in the current generation [8].

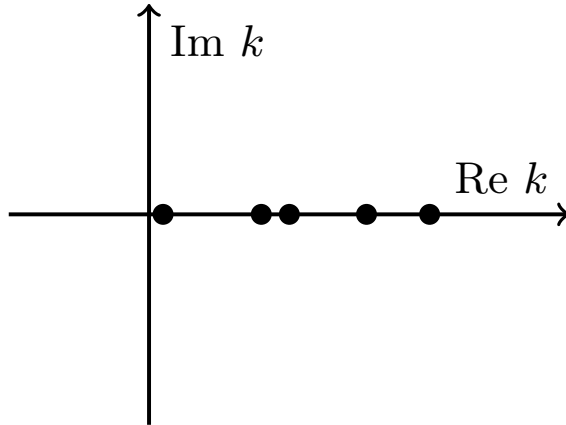


Figure 2.5: Example Spectrum for k -Effective Eigenvalue

Iterative Methods for the k -Effective Eigenvalue

In this section we describe two standard iterative methods used to calculate the k -effective eigenvalue of a nuclear system, the power method and shifted inverse iteration. As discussed in Section 2.2.2, the criticality of the nuclear system is given by the largest real k -effective eigenvalue and corresponding to this eigenvalue is the only positive eigenvector. This positive eigenvector is the neutron angular flux of the nuclear system. Discretization of Eq. 2.47 leads to large sparse linear systems, which makes the use of *direct* eigenvalue solvers (such as the QR method) too expensive or unfeasible. In addition, most transport codes apply the discretized operators of Eq. 2.47 through matrix-vector multiplication or *transport sweeps*, defined as inversions of the operator \mathcal{H} [23], to invert operators and do not construct the large sparse matrices [5]. Given that determining the criticality and fundamental flux mode only requires the dominant eigenvalue, it is instead preferably to use iterative eigenvalue methods.

Power Method with Fission Norm Update: The most basic method for solving for the k -effective eigenvalue is the power method [5]. To apply the method, we write the k -effective criticality problem as the standard eigenvalue problem

$$k\psi = (\mathcal{H} - \mathcal{S})^{-1}\mathcal{F}\psi. \quad (2.50)$$

The power method, described in Algorithm 2.2, consists of iteratively applying the operator on the right of Eq. 2.50 to some eigenfunction approximation at iteration i , ψ^{i+1} . The eigenfunction is then usually normalized by some norm of the angular flux.

Algorithm 2.2 Power Method [5]

-
- 1: Make initial guess $\psi^{(0)}, k^{(0)}$.
 - 2: **for** $i = 0, 1, 2, \dots$, **do**
 - 3: Compute $\psi^{(i+1)} = \frac{1}{k^{(i)}}(\mathcal{H} - \mathcal{S})^{-1}\mathcal{F}\psi^{(i)}$.
 - 4: Normalize $\psi^{(i+1)}$ by some norm, compute $k^{(i+1)}$.
 - 5: Check for convergence: $|k^{(i+1)} - k^{(i)}|/k^{(i+1)} < \text{tolerance}$
 - 6: **end for**
-

There are various ways to compute the eigenvalue iterate. One simple estimate of the eigenvalue is given by the expression

$$k^{(i+1)} = k^{(i)} \frac{\|\psi^{(i+1)}\|}{\|\psi^{(i)}\|}, \quad (2.51)$$

where $\|\psi\|$ is some discrete norm taken over the problem domain. However, only a normalization is necessary and a norm is not required. In many implementations the norm takes into account only the isotropic scalar flux component as this is usually the required unknown [24]. However, there is no mathematical justification for this norm and any consistent norm can be used. Traditionally, in neutron transport codes, the eigenvalue is estimated using the total fission rate in the problem [24] which is given by

$$\|\phi\| \equiv \|\phi\|_F = \sum_{g=1}^G \sum_{s \in \mathcal{D}} \nu \sigma_{f,g,s} \phi_{0,g,s} \quad (2.52)$$

where the summation is over all energy group and over all spatial cells in the problem domain, \mathcal{D} . Another possible eigenvalue update is the Rayleigh quotient, where the Rayleigh quotient is defined as

$$R(M, x) = \frac{x^T M x}{x^T x}, \quad (2.53)$$

where $M \in \mathbb{R}^{N \times N}$ and $x \in \mathbb{R}^{N \times 1}$ [25]. It has been observed that using the Rayleigh quotient can at times improve the efficiency of the power iteration by providing a better estimate of the eigenvalue earlier in the iterative process [24].

The power method converges to the eigenvector corresponding to the largest eigenvalue in modulus provided that the eigenvalue is simple and the initial eigenvector guess contains a component in the eigendirection [26]. It has been shown that k is the largest eigenvalue in modulus for various types of problems in nuclear engineering [27]. However, it is possible the power iteration will not converge. For instance, for multigroup energy problems, it is not known if the dominant eigenvalue is always real and given an all real initial eigenvector guess, it is possible the method will not converge. In addition, the power method converges with rate equal to the dominance ratio, k_1/k_0 , and for problems with dominance ratios close to one, convergence can be unacceptably slow. Problems with dominance ratios close to one

include highly scattering nuclear reactor problems such as heavy water reactors and boiling water reactors. Despite these limitations, the simplicity of the power method makes it the default eigenvalue solver method of choice in neutron transport codes [4].

The Wielandt Method: Another method to calculate the k -effective eigenvalue is the Wielandt method or Wielandt acceleration (Algorithm 2.3) [28]. The Wielandt method, as it is known in the neutron transport community, is a shifted inverse iteration method [29] applied to the k -effective eigenvalue problem. In the shifted inverse iteration method, the power method is applied to the shifted problem of the form

$$(\mathcal{H} - \mathcal{S} - \beta\mathcal{F})\psi = (\lambda - \beta)\mathcal{F}\psi, \quad (2.54)$$

where $\lambda = 1/k$ and the shift β is selected such that $0 < |\lambda_1 - \beta| < |\lambda_2 - \beta| \leq |\lambda_j - \beta|$, $j > 2$. It can be shown that this yields a method with speed of convergence determined by $|\lambda_1 - \beta|/|\lambda_2 - \beta|$ [29]. For an appropriately selected shift β , the method can be faster than the power method. For criticality problems in nuclear engineering, the systems are expected to be close to critical and the shift can be selected to be $\beta = 1$. The power method can be considered a special case of the shifted inverse iteration method with no shift. Despite its improved theoretical convergence rate, the shifted inverse iteration shift requires *a priori* knowledge of the dominant eigenvalue magnitude. Given a poor shift, convergence of the method may be delayed.

Algorithm 2.3 Shifted Inverse Iteration [29]

- 1: Make initial guess $\psi^{(0)}$.
 - 2: **for** $i = 0, 1, 2, \dots$, **do**
 - 3: Define shift $\beta^{(i)}$.
 - 4: Compute $\psi^{(i+1)}$ such that $(\mathcal{H} - \mathcal{S} - \beta^{(i)}\mathcal{F})\psi^{(i+1)} = \mathcal{F}\psi^{(i)}$.
 - 5: Normalize $\psi^{(i+1)}$ by some norm.
 - 6: Check for Convergence
 - 7: **end for**
-

2.3 Review of Linear Algebra Fundamentals

We review and introduce some definitions of linear algebra concepts used in this dissertation. Of particular interest are the concepts of positivity and primitivity, which guide the derivation of the method later in this dissertation. Definitions and theorems are from [25], [30], [31]. The theory of Perron-Frobenius for positive, irreducible, and primitive matrices is discussed and its results are used heavily throughout this dissertation.

2.3.1 Nonnegativity, Positivity, and the Spectral Radius of a Matrix

Definition 2.3. A real matrix \mathbf{A} is nonnegative (or positive) if all entries of \mathbf{A} are nonnegative (or positive). We write $\mathbf{A} \geq \mathbf{0}$ or $\mathbf{A} > \mathbf{0}$.

Definition 2.4. Let $\mathbf{A} = (a_{i,j})$ be an $n \times n$ matrix with eigenvalues $\lambda_i, 1 \leq i \leq n$. Then

$$\rho(\mathbf{A}) \equiv \max_{1 \leq i \leq n} |\lambda_i|$$

is called the *spectral radius* of the matrix \mathbf{A} .

2.3.2 Irreducible and Reducible Matrices

Definition 2.5. For $n \geq 2$, an $n \times n$ real matrix \mathbf{A} is *reducible* if there exists an $n \times n$ permutation matrix \mathbf{P} such that

$$\mathbf{P}\mathbf{A}\mathbf{P}^T = \begin{bmatrix} \mathbf{A}_{1,1} & \mathbf{A}_{1,2} \\ \mathbf{0} & \mathbf{A}_{2,2} \end{bmatrix}$$

Definition 2.6. A matrix \mathbf{A} that is not *reducible* is said to be *irreducible*.

2.3.3 Primitive and Cyclic Matrices

Definition 2.7. Let $\mathbf{A} \geq \mathbf{0}$ be an irreducible $n \times n$ matrix, and let k be the number of eigenvalues of \mathbf{A} with modulus $\rho(\mathbf{A})$. If $k = 1$, then \mathbf{A} is *primitive*.

Definition 2.8. Let $\mathbf{A} \geq \mathbf{0}$, \mathbf{A} is *primitive* if there is some n such that $\mathbf{A}^n > \mathbf{0}$ [25].

Definition 2.9. Let $\mathbf{A} \geq \mathbf{0}$ be an irreducible $n \times n$ matrix, and let k be the number of eigenvalues of \mathbf{A} with modulus $\rho(\mathbf{A})$. If $k > 1$, then \mathbf{A} is *cyclic of index k*.

From the previous definitions, the following can be shown:

Lemma 2.1. Let $\mathbf{A} \geq \mathbf{0}$ be a primitive $n \times n$ matrix. Then \mathbf{A} is irreducible.

2.3.4 Perron-Frobenius Theorem for Irreducible Matrices

Theorem 2.10. Let $\mathbf{A} \geq \mathbf{0}$ be an irreducible $n \times n$ matrix. Then,

1. \mathbf{A} has a positive real eigenvalue, λ_1 , equal to its spectral radius, and which is greater than or equal to (in absolute value) all other eigenvalues.
2. For $\rho(\mathbf{A})$ there is a corresponding eigenvector $x > 0$.
3. $\rho(\mathbf{A})$ is a simple eigenvalue of \mathbf{A} .

2.3.5 Perron-Frobenius Theorem for Primitive Matrices

Theorem 2.11. Let $\mathbf{A} \geq \mathbf{0}$ be a primitive $n \times n$ matrix. Then,

1. \mathbf{A} has a positive real eigenvalue, λ_1 , equal to its spectral radius, and which is greater than (in absolute value) all other eigenvalues.
2. For $\rho(\mathbf{A})$ there is a corresponding eigenvector $x > 0$.
3. $\rho(\mathbf{A})$ is a simple eigenvalue of \mathbf{A} .

2.3.6 Kronecker (Tensor) Product

Throughout this dissertation we use the *Kronecker (tensor) product* to simplify various matrix operations and forms required to discretize the neutron transport eigenvalue equations. We review some of the properties [32] of this product in this section.

For matrices $\mathbf{A} \in \mathbb{R}^{m \times n}$ and $\mathbf{B} \in \mathbb{R}^{k \times l}$, the Kronecker product of \mathbf{A} and \mathbf{B} is the $mk \times nl$ matrix denoted by

$$\mathbf{A} \otimes \mathbf{B} \equiv \begin{pmatrix} a_{11}\mathbf{B} & \dots & a_{1n}\mathbf{B} \\ \vdots & \ddots & \vdots \\ a_{m1}\mathbf{B} & \dots & a_{mn}\mathbf{B} \end{pmatrix}, \quad (2.55)$$

where $\mathbf{A} = (a_{ij})$. More explicitly:

$$\mathbf{A} \otimes \mathbf{B} = \begin{pmatrix} a_{11}b_{11} & a_{11}b_{12} & \dots & a_{11}b_{1l} & \dots & \dots & a_{1n}b_{11} & a_{1n}b_{12} & \dots & a_{1n}b_{1l} \\ a_{11}b_{21} & a_{11}b_{22} & \dots & a_{11}b_{2l} & \dots & \dots & a_{1n}b_{21} & a_{1n}b_{22} & \dots & a_{1n}b_{2l} \\ \vdots & \vdots & \ddots & \vdots & & & \vdots & \vdots & \ddots & \vdots \\ a_{11}b_{k1} & a_{11}b_{k2} & \dots & a_{11}b_{kl} & \dots & \dots & a_{1n}b_{k1} & a_{1n}b_{k2} & \dots & a_{1n}b_{kl} \\ \vdots & \vdots & & \vdots & \ddots & & \vdots & \vdots & & \vdots \\ \vdots & \vdots & & \vdots & & \ddots & \vdots & \vdots & & \vdots \\ a_{m1}b_{11} & a_{m1}b_{12} & \dots & a_{m1}b_{1l} & \dots & \dots & a_{mn}b_{11} & a_{mn}b_{12} & \dots & a_{mn}b_{1l} \\ a_{m1}b_{21} & a_{m1}b_{22} & \dots & a_{m1}b_{2l} & \dots & \dots & a_{mn}b_{21} & a_{mn}b_{22} & \dots & a_{mn}b_{2l} \\ \vdots & \vdots & \ddots & \vdots & & & \vdots & \vdots & \ddots & \vdots \\ a_{m1}b_{k1} & a_{m1}b_{k2} & \dots & a_{m1}b_{kl} & \dots & \dots & a_{mn}b_{k1} & a_{mn}b_{k2} & \dots & a_{mn}b_{kl} \end{pmatrix}. \quad (2.56)$$

Kronecker products have various interesting properties. We list the ones relevant to this dissertation:

- If \mathbf{A} and \mathbf{B} are nonsingular, then $\mathbf{A} \otimes \mathbf{B}$ is nonsingular with $(\mathbf{A} \otimes \mathbf{B})^{-1} = \mathbf{A}^{-1} \otimes \mathbf{B}^{-1}$,
- $(\mathbf{A} \otimes \mathbf{B})^T = \mathbf{A}^T \otimes \mathbf{B}^T$,

- Given matrices \mathbf{A} , \mathbf{B} , \mathbf{C} , and \mathbf{D} , $(\mathbf{A} \otimes \mathbf{B}) \cdot (\mathbf{C} \otimes \mathbf{D}) = \mathbf{AC} \otimes \mathbf{BD}$, as long as both sides of the equation make sense,
- $(\mathbf{A} + \mathbf{B}) \otimes \mathbf{C} = \mathbf{A} \otimes \mathbf{C} + \mathbf{B} \otimes \mathbf{C}$, and
- $\mathbf{A} \otimes (\mathbf{B} + \mathbf{C}) = \mathbf{A} \otimes \mathbf{B} + \mathbf{A} \otimes \mathbf{C}$.

2.4 Review of Fixed-Point Iteration

In this section we review fixed-point iteration methods. Definitions and theorems are from [33]. Many nonlinear equations can be naturally formulated as a fixed-point problem

$$x = g(x) \quad (2.57)$$

where g , called the fixed-point map, may be nonlinear. We begin by defining a *fixed point* of some equation $g(x)$:

Definition 2.12. A point x_0 is called a fixed point of $g(x)$ if it satisfies

$$x_0 = g(x_0). \quad (2.58)$$

Next, we define an *attractive fixed point* of a function $g(x)$:

Definition 2.13. A point x_0 is an attractive fixed point of $g(x)$ if for any value of x in the domain that is sufficiently close to x_0 , the iterated function sequence

$$x, g(x), g(g(x)), g(g(g(x))), \dots \quad (2.59)$$

converges to x_0 .

Given these two definitions, we can define an iterative method to find the fixed point of some function $g(x)$ as

$$x_{n+1} = g(x_n). \quad (2.60)$$

The convergence of this fixed-point iteration method depends on the existence and uniqueness of the fixed point in the domain of the function $g(x)$. We introduce and prove the following theorem

Theorem 2.14. Existence and Uniqueness of Fixed Point

1. *Existence:* If $g \in C[a, b]$ and $g(x) \in [a, b]$ for all $x \in [a, b]$, then g has a fixed point in $[a, b]$.
2. *Uniqueness:* If, in addition, $g'(x)$ exists on (a, b) and a positive constant $k < 1$ exists with

$$|g'(x)| \leq k, \quad \text{for all } x \in (a, b),$$

then there is exactly one fixed point in $[a, b]$.

Proof. We note the following:

- $g \in C[a, b] - g$ is continuous in $[a, b]$.
- $g(x) \in [a, b] - g$ takes values in $[a, b]$.

1. Existence: If $g(a) = a$ or $g(b) = b$, then g has a fixed point at that endpoint. Otherwise, $g(a) > a$ and $g(b) < b$. We define a new function $h(x) = g(x) - x$ such that $h(a) = g(a) - a > 0$, $h(b) = g(b) - b < 0$, and $h(x)$ is continuous. By the intermediate value theorem, there exists $p \in (a, b)$ for which $h(p) = 0$ which implies $g(p) = p$.
2. Uniqueness: Assume $|g'(x)| \leq k < 1$. Suppose there are two fixed points p and q . By the mean value theorem, there is a number ξ between p and q such that

$$g'(\xi) = \frac{g(p) - g(q)}{p - q}. \quad (2.61)$$

This implies

$$|p - q| = |g(p) - g(q)| = |g'(\xi)||p - q| \leq k|p - q| < |p - q|, \quad (2.62)$$

which is a contradiction. This implies there is only one fixed point and it is unique. \square

The previous concepts extend to vector valued functions. Consider the general iteration

$$x_{n+1} = F(x_n), \quad (2.63)$$

where $F : \mathbb{R}^n \rightarrow \mathbb{R}^n$ is a vector valued function. A solution of the equation $x = F(x)$ is called a *fixed point* of F . Unlike iterative methods for linear equations, it is usually only possible to analyze the convergence of Eq. 2.63 in a neighborhood about a fixed point. For any initial guess x_0 in that neighborhood, the general iteration in Eq. 2.63 will converge to the fixed point if the fixed point is a *point of attraction*. More precisely, we define a fixed point as a *point of attraction* as follows:

Definition 2.15. A fixed point x_* of $F : \mathbb{R}^n \rightarrow \mathbb{R}^n$ is a point of attraction of the iteration given in Eq. 2.63 if there is an open neighborhood S of x_* such that when $x_0 \in S$, the iterates are well defined and converge to x_* .

Before we give the basic local convergence theorem for Eq. 2.63, we discuss the *Jacobian matrix* of the vector valued function F . The *Jacobian matrix* of the vector valued function F is denoted by $J(x)$ and is defined as follows:

Definition 2.16. The Jacobian matrix of the vector valued function F is defined as

$$J(x) = \begin{pmatrix} \frac{\partial F_1(x)}{\partial x_1} & \dots & \frac{\partial F_1(x)}{\partial x_n} \\ \vdots & & \vdots \\ \frac{\partial F_n(x)}{\partial x_1} & \dots & \frac{\partial F_n(x)}{\partial x_n} \end{pmatrix}. \quad (2.64)$$

It is assumed that the Jacobian matrix is at least continuous at the fixed point x_* . It can be shown that if the Jacobian matrix is continuous at x_* , then F is differentiable at x_* [33].

We now introduce Ostrowski's Theorem [34], the local convergence theorem for the iteration given by Eq. 2.63.

Theorem 2.17. Ostrowski's Theorem: *Assume that $F : \mathbb{R}^n \rightarrow \mathbb{R}^n$ is differentiable at the fixed point x_* and that $\rho(J(x_*)) < 1$. Then x_* is a point of attraction for the general iteration given by Eq. 2.63.*

It is important to note that the previous theorem is a sufficient but not necessary condition for the convergence of the non-linear fixed-point iteration.

2.5 Conclusion

Starting from the time-dependent neutron transport equation, the alpha- and k -effective eigenvalue problems of neutron transport were derived and their properties discussed. We discussed the physical interpretations of the eigenvalues along with their mathematical properties. For the two eigenvalue problems, we examined various methods used in practice to determine the eigenpairs and discussed their strengths and weaknesses. Finally, we reviewed linear algebra concepts and fixed-point iteration concepts that are used heavily throughout the dissertation. We now move on to the linear algebraic development of the criticality eigenvalue problems of neutron transport and the derivation of a new method, the Rayleigh Quotient Fixed Point method.

Chapter 3

Discretization and Primitivity of the Neutron Transport Criticality Eigenvalue Problems

In this section we describe the discretization of the neutron transport criticality eigenvalue equations for three-dimensional Cartesian geometry. The discretization follows a similar approach to that of Brown [35] [36] [37]. First, we derive semi-discretized forms of the eigenvalue equations by applying the *multigroup* in energy approximation and a spherical harmonics expansion for the scattering integral. We then discretize the spatial and angular variables using step differencing and the discrete ordinates approach. Finally, we write down the discretized matrix forms of the criticality eigenvalue equations for three-dimensional Cartesian geometry. For the one-dimensional slab geometry discretized alpha-eigenvalue problem, we prove that the discretized transport equation matrix is primitive. A similar result can be shown for the two-dimensional and three-dimensional Cartesian discretized eigenvalue equations.

We begin with the linear alpha-eigenvalue neutron transport equation in a three-dimensional box geometry. For a description of the discretization process for the one-dimensional slab neutron transport eigenvalue equations see Appendix A. The spatial domain is the box $\mathcal{D} \equiv \{\vec{r} = (x, y, z) \mid a_x \leq x \leq b_x, a_y \leq y \leq b_y, \text{ and } a_z \leq z \leq b_z\}$, the direction variable is $\hat{\Omega} \in \mathcal{S}^2$, the unit sphere in \mathbb{R}^3 , the energy variable is $E \in (0, \infty)$, and the equation for the angular flux $\psi(\vec{r}, \hat{\Omega}, E)$ is given by

$$\begin{aligned} & \left[\frac{\alpha}{v(E)} + \hat{\Omega} \cdot \nabla + \sigma(\vec{r}, E) \right] \psi(\vec{r}, \hat{\Omega}, E) \\ &= \int_0^\infty dE' \int_{4\pi} d\hat{\Omega}' \sigma_s(\vec{r}, E' \rightarrow E, \hat{\Omega}' \cdot \hat{\Omega}) \psi(\vec{r}, \hat{\Omega}', E') \\ &+ \int_0^\infty dE' \nu(E') \chi(E' \rightarrow E) \sigma_f(\vec{r}, E') \int_{4\pi} d\hat{\Omega}' \psi(\vec{r}, \hat{\Omega}', E'), \quad (3.1) \end{aligned}$$

where

$$\nabla\psi \equiv \left(\frac{\partial\psi}{\partial x}, \frac{\partial\psi}{\partial y}, \frac{\partial\psi}{\partial z} \right), \quad (3.2)$$

and

$$\int_{4\pi} d\hat{\Omega} = 1. \quad (3.3)$$

Boundary conditions must be specified to make Eq. 3.1 well-posed. Various boundary conditions can be specified such as a reflecting condition on a face or a Dirichlet condition where an incident flux is specified on a face. We consider vacuum boundary conditions in this dissertation, a special case of the Dirichlet boundary condition where no incident flux is imposed:

$$\psi(\vec{r}, \hat{\Omega}, E) = 0 \text{ for all } \vec{r} \in \partial\mathcal{D} \text{ and } \hat{\Omega} \in \mathcal{S}^2 \text{ with } \vec{n}(\vec{r}) \cdot \hat{\Omega} < 0, \quad (3.4)$$

where $\vec{n}(\vec{r})$ is the outward pointing unit normal at $\vec{r} \in \partial\mathcal{D}$.

3.1 Discretization of the Alpha-Eigenvalue and k -Effective Eigenvalue Equations

In this section, we discuss the discretization of the alpha- and k -effective eigenvalue neutron transport equations. We begin by approximating the energy dependence of the neutron transport equations using the multigroup in energy approximation. We then discretize the angular flux and scattering cross sections using a surface harmonics expansion. Finally, the spatial and angular dependences of the eigenvalue equations are then approximated using step differencing in space and the discrete ordinates approach in angle.

3.1.1 The Multigroup in Energy Discretization and Surface Harmonics Expansion of the Angular Flux

The Multigroup in Energy Approximation

We begin by discretizing Eq. 3.1 in energy using the *multigroup* approximation [4]. We restrict the energy E to a finite interval and partition the interval into groups:

$$E_{max} = E_0 > E_1 > \dots > E_G = E_{min}.$$

The eigenvalue equation is then integrated over each group $E_g < E < E_{g-1}$ and the cross sections are approximated by a flux-weighted average over each energy group to yield the

following semi-discretization of Eq. 3.1:

$$\left[\frac{\alpha}{v_g} + \hat{\Omega} \cdot \nabla + \sigma_g(\vec{r}) \right] \psi_g(\vec{r}, \hat{\Omega}) = \sum_{g'=1}^G \int_{4\pi} d\hat{\Omega}' \sigma_{s,g,g'}(\vec{r}, \hat{\Omega}' \cdot \hat{\Omega}) \psi_{g'}(\vec{r}, \hat{\Omega}') \\ + \chi_g \sum_{g'=1}^G \nu \sigma_{f,g'}(\vec{r}) \int_{4\pi} d\hat{\Omega}' \psi_{g'}(\vec{r}, \hat{\Omega}'), \quad (3.5)$$

for $g = 1, \dots, G$, where

$$\psi_g(\vec{r}, \hat{\Omega}) \equiv \int_g dE \psi(\vec{r}, \hat{\Omega}, E), \quad (3.6)$$

$$\sigma_g(\vec{r}) \equiv \frac{1}{\Delta E_g} \int_g dE \sigma(\vec{r}, E), \quad (3.7)$$

$$\sigma_{s,g,g'}(\vec{r}, \hat{\Omega}' \cdot \hat{\Omega}) \equiv \frac{1}{\Delta E_{g'}} \int_g \int_{g'} dE' dE \sigma_s(\vec{r}, E' \rightarrow E, \hat{\Omega}' \cdot \hat{\Omega}), \quad (3.8)$$

$$\nu \sigma_{f,g}(\vec{r}) \equiv \frac{1}{\Delta E_g} \int_g dE \nu(E) \sigma_f(E), \quad (3.9)$$

$$\chi_g \equiv \int_g dE \chi(E), \quad (3.10)$$

with

$$\int_g dE = \int_{E_g}^{E_{g-1}} dE. \quad (3.11)$$

We note that

$$\sum_{g=1}^G \chi_g = 1 \quad (3.12)$$

in the multigroup formulation since

$$\int_0^\infty dE \chi(E) = 1. \quad (3.13)$$

The Surface Harmonics Expansion of the Angular Flux

For each flux $\psi_g(\vec{r}, \hat{\Omega})$, the flux is expanded in surface harmonics according to

$$\psi_g(\vec{r}, \hat{\Omega}) = \sum_{n=0}^{\infty} \sum_{m=-n}^n \phi_{g,n,m}(\vec{r}) Y_n^m(\hat{\Omega}), \quad (3.14)$$

where $Y_n^m(\hat{\Omega})$ is a surface harmonic defined as

$$Y_n^m(\hat{\Omega}) = a_n^m P_n^{|m|}(\xi) \tau_m(\varphi), \quad (3.15)$$

$$\hat{\Omega} = (\sin \theta \cos \varphi, \sin \theta \sin \varphi, \cos \theta), \quad (3.16)$$

$$\tau_m(\varphi) = \begin{cases} \cos m\varphi, & \text{if } m \geq 0, \\ \sin|m|\varphi & \text{if } m < 0, \end{cases} \quad (3.17)$$

and $P_n^{|m|}$ is an *associated Legendre polynomial* [4]. The constants a_n^m are defined by

$$a_n^m = \left[\frac{2(2n+1)(n-|m|)!}{(1+\delta_{m0})(n+|m|)!} \right]^{1/2}. \quad (3.18)$$

where $\delta_{n,n'}$ is the *Kronecker delta*. The $(n, m)^{\text{th}}$ moment of $\psi(\vec{r}, \hat{\Omega})$, $\phi_{n,m}$ is given by

$$\phi_{n,m}(\vec{r}) = \int_{4\pi} d\hat{\Omega} \psi(\vec{r}, \hat{\Omega}) Y_n^m(\hat{\Omega}). \quad (3.19)$$

From the properties of the surface harmonics, we have

$$\int_{4\pi} d\hat{\Omega} Y_n^m(\hat{\Omega}) Y_{n'}^{m'}(\hat{\Omega}) = \delta_{n,n'} \delta_{m,m'}, \text{ for all } n, n' = 0, 1, \dots, |m| \leq |n|, |m'| \leq |n'|. \quad (3.20)$$

The scattering integral can be then be written in the form

$$\int_{4\pi} d\hat{\Omega} \sigma_{s,g,g'}(\vec{r}, \hat{\Omega}' \cdot \hat{\Omega}) \psi_{g'}(\vec{r}, \hat{\Omega}') = \sum_{n=0}^{\infty} \sigma_{s,g,g',n}(\vec{r}) \sum_{m=-n}^n \phi_{g',n,m}(\vec{r}) Y_n^m(\hat{\Omega}), \quad (3.21)$$

where

$$\sigma_{s,g,g',n}(\vec{r}) \equiv \frac{1}{2} \int_{-1}^1 d\mu_0 \sigma_{s,g,g'}(\vec{r}, \mu_0) P_n(\mu_0), \quad (3.22)$$

and μ_0 is the cosine of the scattering angle. The infinite series in Eq. 3.21 is truncated to a finite number of terms N_s , where N_s is the maximum value for n . The fission integral can be written similarly with the infinite series truncated after N_f terms. The multigroup equations can then be written as

$$\begin{aligned} \left[\frac{\alpha}{v_g} + \hat{\Omega} \cdot \nabla + \sigma_g(\vec{r}) \right] \psi_g(\vec{r}, \hat{\Omega}) &= \sum_{g'=1}^G \sum_{n=0}^{N_s} \sigma_{s,g,g',n}(\vec{r}) \sum_{m=-n}^n \phi_{g',n,m}(\vec{r}) Y_n^m(\hat{\Omega}) \\ &\quad + \chi_g \sum_{g'=1}^G \sum_{n=0}^{N_f} \nu \sigma_{f,g',n}(\vec{r}) \sum_{m=-n}^n \phi_{g',n,m}(\vec{r}) Y_n^m(\hat{\Omega}), \end{aligned} \quad (3.23)$$

for $g = 1, \dots, G$.

3.1.2 Step Differencing and Discrete Ordinates in Angle

Step Differencing

We continue the discretization of Eq. 3.23 by using a Step differencing method [5] for the spatial variable \vec{r} . We start with the three-dimensional mono-energetic alpha-eigenvalue equation for group g with scattering and fission source f :

$$\begin{cases} \frac{\alpha}{v}\psi + \hat{\Omega} \cdot \nabla\psi + \sigma\psi = f \text{ in } \mathcal{D} \\ \psi(\vec{r}) = 0 \text{ for all } \vec{r} \in \partial\mathcal{D} \text{ with } \vec{n}(\vec{r}) \cdot \hat{\Omega} < 0. \end{cases} \quad (3.24)$$

We discretize the domain \mathcal{D} into zones and define

$$\Delta x_i = x_i - x_{i-1}, \text{ for } i = 1, \dots, M, \quad (3.25)$$

$$\Delta y_j = y_j - y_{j-1}, \text{ for } j = 1, \dots, J, \quad (3.26)$$

$$\Delta z_k = z_k - z_{k-1}, \text{ for } k = 1, \dots, K. \quad (3.27)$$

We define the nodes $r_{ijk} = (x_i, y_j, z_k)$ and the zone volume $\Delta r_{ijk} = \Delta x_i \Delta y_j \Delta z_k$. The function values at the set of nodes, $\{r_{ijk}\}$ are called *nodal values*. We assume that σ and f have constant values, denoted as σ_{ijk} and f_{ijk} respectively, on each *zone* defined as

$$\mathcal{Z}_{ijk} \equiv \{r | x_{i-1} < x < x_i, y_{j-1} < y < y_j, z_{k-1} < z < z_k\}. \quad (3.28)$$

We define ψ_{ijk} to denote the approximation to $\psi(r_{ijk})$, the true solution at the point r_{ijk} .

For a direction in the positive orthant, $\hat{\Omega} = (\mu, \eta, \xi) > 0$, the Step differencing equation for the zone \mathcal{Z}_{ijk} is

$$\frac{\alpha}{v}\psi_{ijk} + \mu \frac{\psi_{ijk} - \psi_{i-1,jk}}{\Delta x_i} + \eta \frac{\psi_{ijk} - \psi_{i,j-1,k}}{\Delta y_j} + \xi \frac{\psi_{ijk} - \psi_{ij,k-1}}{\Delta z_k} + \sigma_{ijk}\psi_{ijk} = f_{ijk}. \quad (3.29)$$

For Eq. 3.29, we have $(M+1)(J+1)(K+1)$ unknowns ψ_{ijk} . There are MJK zonal equations with $JM + JK + M + J + K + 1$ boundary equations.

To write the discretized system in matrix form, we define the discrete angular flux vector

$$\Psi \in \mathbb{R}^{(M+1)(J+1)(K+1)}, \quad (3.30)$$

defined for all nodes ordered by i first, then j , and finally k . We define the diagonal matrices

$$\Delta x \equiv \text{diag}(\Delta x_1, \dots, \Delta x_M), \quad (3.31)$$

$$\Delta y \equiv \text{diag}(\Delta y_1, \dots, \Delta y_J), \quad (3.32)$$

$$\Delta z \equiv \text{diag}(\Delta z_1, \dots, \Delta z_K), \quad (3.33)$$

and the matrices expressing the discretized spatial derivatives

$$D_M \in \mathbb{R}^{M \times (M+1)} \equiv \begin{pmatrix} -1 & 1 & & \\ & \ddots & \ddots & \\ & & -1 & 1 \end{pmatrix}, S_{M,+} \in \mathbb{R}^{M \times (M+1)} \equiv \begin{pmatrix} 0 & 1 & & \\ & \ddots & \ddots & \\ & & 0 & 1 \end{pmatrix}, \quad (3.34)$$

$$D_J \in \mathbb{R}^{J \times (J+1)} \equiv \begin{pmatrix} -1 & 1 & & \\ & \ddots & \ddots & \\ & & -1 & 1 \end{pmatrix}, S_{J,+} \in \mathbb{R}^{J \times (J+1)} \equiv \begin{pmatrix} 0 & 1 & & \\ & \ddots & \ddots & \\ & & 0 & 1 \end{pmatrix}, \quad (3.35)$$

$$D_K \in \mathbb{R}^{K \times (K+1)} \equiv \begin{pmatrix} -1 & 1 & & \\ & \ddots & \ddots & \\ & & -1 & 1 \end{pmatrix}, S_{K,+} \in \mathbb{R}^{K \times (K+1)} \equiv \begin{pmatrix} 0 & 1 & & \\ & \ddots & \ddots & \\ & & 0 & 1 \end{pmatrix}. \quad (3.36)$$

We define the total cross section matrix as

$$\Sigma \equiv \text{diag}(\sigma_{111}, \dots, \sigma_{MJK}), \quad (3.37)$$

and the inverse neutron velocity matrix as

$$V^{-1} \equiv \text{diag}(1/v_{111}, \dots, 1/v_{MJK}). \quad (3.38)$$

The matrices describing the spatial derivatives with respect to a spatial variable C_x , C_y , and C_z are defined by

$$C_x \equiv S_{K,+} \otimes S_{J,+} \otimes \Delta x^{-1} D_M, \quad (3.39)$$

$$C_y \equiv S_{K,+} \otimes \Delta y^{-1} D_J \otimes S_{M,+}, \quad (3.40)$$

$$C_z \equiv \Delta z^{-1} D_K \otimes S_{J,+} \otimes S_{M,+}, \quad (3.41)$$

while the matrix associating the correct total cross section to each cell is defined as

$$S \equiv S_{K,+} \otimes S_{J,+} \otimes S_{M,+}. \quad (3.42)$$

With these matrices defined, we can write the MJK zone-centered equations for the unknown vector Ψ as

$$(\alpha V^{-1} + C + \Sigma S) \Psi = F, \quad (3.43)$$

where

$$C \equiv \mu C_x + \eta C_y + \xi C_z, \quad (3.44)$$

and

$$F \equiv (f_{ijk}) \in \mathbb{R}^{MJK}. \quad (3.45)$$

We note that if the quadrature point $\hat{\Omega}$ is not in the positive octant, then the definitions of the corresponding C_x , etc., matrices would instead use the matrices $S_{M,-}$, $S_{J,-}$ and $S_{K,-}$ depending on the signs of (μ, η, ξ) . The matrix $S_{M,-}$ is defined as

$$S_{M,-} \in \mathbb{R}^{M \times (M+1)} \equiv \begin{pmatrix} 1 & 0 & & \\ & \ddots & \ddots & \\ & & 1 & 0 \end{pmatrix}, \quad (3.46)$$

where $S_{J,-}$ and $S_{K,-}$ are defined similarly.

Boundary values are isolated by noting that for a positive direction vector $\hat{\Omega}$, ψ satisfies the Dirichlet condition for all $\vec{r} = r_{0jk}, r_{i0k}$, or r_{ij0} . These locations correspond to one of the three faces with coordinate $x = x_0, y_0$, or z_0 of the box. For a positive direction vector $\hat{\Omega}$, we define the vector Ψ_B with length equal to the length of Ψ . The vector Ψ_B is nonzero at all indices corresponding to boundary points where there is some incoming angular flux. The discrete boundary conditions can be written

$$E_{000}(\Psi - \Psi_B) = 0, \quad (3.47)$$

where we define E_{000} as

$$E_{000} = \begin{pmatrix} e_{0K}^T \otimes I_{J+1} \otimes I_{M+1} \\ (0, I_K) \otimes e_{0J}^T \otimes I_{M+1} \\ (0, I_K) \otimes (0, I_J) \otimes e_{0M}^T \end{pmatrix}, \quad (3.48)$$

where the vectors e_{0J} and e_{0K} are the standard unit vectors and I is the identity matrix of size given by the subscript. There are different E matrices for other directions. For three-dimensional Cartesian geometry, there are eight different matrices, E_{ijk} , corresponding to boundary points $i = 0, M$, $j = 0, L$, and $k = 0, K$.

Equation 3.43 is the discretized equation for quadrature point $\hat{\Omega}$ and energy group g . We generalize for multiple quadrature points and energy groups by introducing the indices ℓ and g , where ℓ is the index of quadrature point $\hat{\Omega} = \hat{\Omega}_\ell$ and g is the energy group index. The vectors Ψ and Ψ_B and matrix C of Eq. 3.43 become $\Psi_{g,\ell}$, $\Psi_{B,g,\ell}$, and C_ℓ .

We define the matrices Z and Z_b by

$$Z \equiv \begin{pmatrix} I_{MJK} \\ 0 \end{pmatrix} \in \mathbb{R}^{(M+1)(J+1)(K+1) \times MJK} \quad (3.49)$$

and

$$Z_b \equiv \begin{pmatrix} 0 \\ I_{(M+1)(J+1)(K+1)-MJK} \end{pmatrix} \in \mathbb{R}^{(M+1)(J+1)(K+1) \times (M+1)(J+1)(K+1)-MJK}. \quad (3.50)$$

The matrices Z and Z_b inject zone-centered vectors into the nodal vector space. We note the following properties:

$$Z^T Z = I_{MJK}, \quad (3.51)$$

$$Z_b^T Z_b = I_{(M+1)(J+1)(K+1)-MJK}, \quad (3.52)$$

and

$$Z^T Z_b = 0. \quad (3.53)$$

Then the matrix representation of Eq. 3.24 for energy group g and direction ℓ can be written as

$$(\alpha V_{g,\ell}^{-1} + H_{g,\ell})\Psi_{g,\ell} = ZF_{g,\ell} + Z_bB_\ell\Psi_{B,g,\ell}, \quad (3.54)$$

where

$$H_{g,\ell} \equiv Z(C_\ell + \Sigma_g S) + Z_bB_\ell, \quad (3.55)$$

and

$$V_{g,\ell}^{-1} \equiv ZV_g^{-1}S, \quad (3.56)$$

with $B_\ell = E_{ijk}$ for the appropriate choice of i, j , and k and C_ℓ is defined as

$$C_\ell \equiv \mu_\ell C_x + \eta_\ell C_y + \xi_\ell C_z. \quad (3.57)$$

The matrix $H_{g,\ell}$ operates on nodal vectors. We define the angular quadrature scheme in the next section.

The Discrete Ordinates Method

To integrate functions on the unit sphere, we consider symmetric quadrature rules of the form [38]:

$$\int_{4\pi} d\hat{\Omega} \psi(\hat{\Omega}) \approx \sum_{\ell=1}^L w_\ell \psi(\hat{\Omega}_\ell), \quad (3.58)$$

where $\hat{\Omega} \equiv (\mu_\ell, \eta_\ell, \xi_\ell)$, for all $\ell = 1, \dots, L$, with $L = \nu(\nu+2)$ and ν is the number of direction cosines ($\nu = 2, 4, 6, \dots$). It is assumed that $w_\ell > 0$ for all ℓ . We note that

$$\sum_{\ell=1}^L w_\ell = 1, \quad (3.59)$$

since

$$\int_{4\pi} d\hat{\Omega} = 1. \quad (3.60)$$

The symmetry requirement is met using symmetry through the origin. Namely, if $\hat{\Omega}_\ell$ is a quadrature point with corresponding weight, w_ℓ , then $-\hat{\Omega}_\ell$ is also a quadrature point. Letting ℓ^- denote the index, we can write $\hat{\Omega}_{\ell^-} = -\hat{\Omega}_\ell$. It is also true that $w_{-\ell} = w_\ell$ [38].

We define discretized representations of the angular flux moment operators in Eq. 3.24. These operators operate on zone-centered vectors and are easily seen to be given by $MJK \times LMJK$ size matrices

$$L_{n,m} \equiv (l_{n,m}W) \otimes I_{MJK}, \quad (3.61)$$

where

$$l_{n,m} \equiv (Y_n^m(\hat{\Omega}_1), Y_n^m(\hat{\Omega}_2), \dots, Y_n^m(\hat{\Omega}_L)), \quad (3.62)$$

and

$$W \equiv \text{diag}(w_1, w_2, \dots, w_L). \quad (3.63)$$

If the vector Ψ_g approximates $\psi_g(\vec{r}, \hat{\Omega})$, then $L_{n,m}\Psi_g$ approximates the $(n,m)^{\text{th}}$ moment of $\psi_g(\vec{r}, \hat{\Omega})$, $\phi_{g,n,m}(\vec{r})$. Similarly, we define $LMJK \times MJK$ size matrices

$$L_{n,m}^+ \equiv l_{n,m}^T \otimes I_{MJK}. \quad (3.64)$$

If a vector Φ approximates $\phi(\vec{r})$, then $L_{n,m}^+\Phi$ approximates $Y_n^m(\hat{\Omega})\phi(\vec{r})$. We define the grouped matrices L_n and L_n^+ , where

$$L_n = \begin{pmatrix} L_{n,-n} \\ \vdots \\ L_{n,n} \end{pmatrix} \text{ and } L_n^+ = (L_{n,-n}^+, \dots, L_{n,n}^+) \quad (3.65)$$

and the further grouped block matrices

$$L^N = \begin{pmatrix} L_0 \\ \vdots \\ L_N \end{pmatrix} \text{ and } L^{N,+} = (L_0^+, \dots, L_N^+). \quad (3.66)$$

Given $N = N_s$, the number of terms in the scattering kernel, it is assumed that the symmetric quadrature rule is such that the spherical harmonics of order N_s and less satisfy

$$\sum_{\ell=1}^L Y_n^m(\hat{\Omega}_\ell) Y_{n'}^{m'}(\hat{\Omega}_\ell) = \delta_{n,n'} \delta_{m,m'}, \text{ for all } 0 \leq n, n' \leq N_s, |m| \leq n, |m'| \leq n'. \quad (3.67)$$

In matrix form, this can be written more compactly as

$$L^{N_s} L^{N_s,+} = I_{(N_s+1)^2} \otimes I_{MJK}. \quad (3.68)$$

For boundary terms, we define the block diagonal matrices B and C by

$$B \equiv \text{diag}(B_1, B_2, \dots, B_L) \quad (3.69)$$

and

$$C \equiv \text{diag}(C_1, C_2, \dots, C_L). \quad (3.70)$$

The scattering kernel matrix is defined by letting

$$\Sigma_{s,g,g',n} \equiv I_{2n+1} \otimes \hat{\Sigma}_{s,g,g',n}, \quad (3.71)$$

where

$$\hat{\Sigma}_{s,g,g',n} \equiv \text{diag}(\sigma_{s,g,g',n,111}, \dots, \sigma_{s,g,g',n,MJK}), \quad n = 0, 1, \dots \quad (3.72)$$

The fission matrix is defined by letting

$$\Sigma_{f,g,g',n} \equiv I_{2n+1} \otimes \hat{\Sigma}_{f,g,g',n}, \quad (3.73)$$

where

$$\hat{\Sigma}_{f,g,g',n} \equiv \text{diag}(\chi_g \nu \sigma_{f,g',n,111}, \dots, \chi_g \nu \sigma_{f,g',n,MJK}), \quad n = 0, 1, \dots \quad (3.74)$$

We define the matrix \bar{Z} , which injects zone-centered vectors into the nodal vector space, as

$$\bar{Z} \equiv I_L \otimes Z, \quad (3.75)$$

along with the matrix \bar{Z}_B

$$\bar{Z}_B \equiv I_L \otimes Z_b. \quad (3.76)$$

We note that properties of Z and Z_b remain true for the matrices \bar{Z} and \bar{Z}_B . We define the matrix \bar{S} , which averages nodal vectors to obtain zone-centered vectors, as

$$\bar{S} \equiv I_L \otimes S. \quad (3.77)$$

Finally, we define the total cross section matrix for all quadrature points $\bar{\Sigma}_g$ as

$$\bar{\Sigma}_g \equiv I_L \otimes \Sigma_g, \quad (3.78)$$

and the inverse velocity matrix \bar{V}^{-1} as

$$\bar{V}^{-1} \equiv I_L \otimes V^{-1}. \quad (3.79)$$

Using the previously defined matrices, we can define the matrix H_g , the leakage and total cross section matrix for energy group g as

$$H_g \equiv \text{diag}(H_{g,1}, H_{g,2}, \dots, H_{g,L}) = \bar{Z}(C + \bar{\Sigma}_g \bar{S}) + \bar{Z}_B B, \quad (3.80)$$

along with the matrix V_g^{-1}

$$V_g^{-1} \equiv \text{diag}(V_{g,1}^{-1}, V_{g,2}^{-1}, \dots, V_{g,L}^{-1}) = \bar{Z} \bar{V}^{-1} \bar{S}. \quad (3.81)$$

The matrices \bar{Z} and \bar{Z}_B are necessary since H_g operates on nodal vectors while the matrices $\Sigma_{s,g,g',n}$ and $\Sigma_{f,g,g',n}$ operate on zone-centered vectors. Assuming only $N_s + 1$ terms in the scattering operator, then the complete discretization of Eq. 3.24 can be written as

$$\begin{aligned} (\alpha V_g^{-1} + H_g) \Psi_g &= \bar{Z} \sum_{g'=1}^G \sum_{n=0}^{N_s} L_n^+ \Sigma_{s,g,g',n} L_n \bar{S} \Psi_{g'} \\ &\quad + \bar{Z} \sum_{g'=1}^G \sum_{n=0}^{N_s} L_n^+ \Sigma_{f,g,g',n} L_n \bar{S} \Psi_{g'}, g = 1, \dots, G. \end{aligned} \quad (3.82)$$

Finally, we can write the fully discretized in space, angle, and energy matrix equation analog of Eq. 3.1. We first define the complex multigroup scattering and fission matrices

$$\Sigma_s \equiv \begin{pmatrix} \Sigma_{s,11}^{N_s} & \dots & \Sigma_{s,1G}^{N_s} \\ \vdots & \ddots & \vdots \\ \Sigma_{s,G1}^{N_s} & \dots & \Sigma_{s,GG}^{N_s} \end{pmatrix}, \quad (3.83)$$

where

$$\Sigma_{s,gg'}^{N_s} \equiv \text{diag}(\Sigma_{s,g,g',0}, \dots, \Sigma_{s,g,g',N_s}), \quad (3.84)$$

and

$$\Sigma_f \equiv \begin{pmatrix} \Sigma_{f,11}^{N_s} & \dots & \Sigma_{f,1G}^{N_s} \\ \vdots & \ddots & \vdots \\ \Sigma_{f,G1}^{N_s} & \dots & \Sigma_{f,GG}^{N_s} \end{pmatrix}, \quad (3.85)$$

where

$$\Sigma_{f,gg'}^{N_s} \equiv \text{diag}(\Sigma_{f,g,g',0}, \dots, \Sigma_{f,g,g',N_s}). \quad (3.86)$$

We define the following matrices

$$\mathbf{S} \equiv I_G \otimes \bar{S}, \quad (3.87)$$

$$\mathbf{Z} \equiv I_G \otimes \bar{Z}, \quad (3.88)$$

$$\mathbf{Z}_B \equiv I_G \otimes \bar{Z}_B, \quad (3.89)$$

$$\mathbf{L}^+ \equiv I_G \otimes L^{N_s,+}, \quad (3.90)$$

$$\mathbf{L} \equiv I_G \otimes L^{N_s}, \quad (3.91)$$

and

$$\mathbf{B} \equiv I_G \otimes B. \quad (3.92)$$

Finally, we define the matrices \mathbf{H} and \mathbf{V}^{-1} as

$$\mathbf{H} \equiv \text{diag}(H_1, H_2, \dots, H_G), \quad (3.93)$$

and

$$\mathbf{V}^{-1} \equiv \text{diag}(V_1^{-1}, V_2^{-1}, \dots, V_G^{-1}). \quad (3.94)$$

With these matrices defined, we can write Eq. 3.1 as the matrix equation

$$(\alpha \mathbf{V}^{-1} + \mathbf{H}) \Psi = \mathbf{Z} \mathbf{L}^+ (\Sigma_s + \Sigma_f) \mathbf{L} \mathbf{S} \Psi, \quad (3.95)$$

where the angular flux vector, Ψ , is defined as

$$\Psi \equiv \begin{pmatrix} \Psi_1 \\ \Psi_2 \\ \vdots \\ \Psi_G \end{pmatrix}. \quad (3.96)$$

Equation 3.95 is the discretized alpha-eigenvalue neutron transport problem in matrix form for the node-centered angular flux. Similarly, the k -effective eigenvalue problem can be written as

$$\mathbf{H} \Psi = \mathbf{Z} \mathbf{L}^+ \left(\Sigma_s + \frac{1}{k} \Sigma_f \right) \mathbf{L} \mathbf{S} \Psi. \quad (3.97)$$

Equations 3.95 and 3.97 are eigenvalue equations for the criticality eigenvalue and the node-centered angular flux eigenvector. In the derivation of the Rayleigh Quotient Fixed Point method, we require an inner product. However, the inner product is defined for zone-centered vectors, whereas the unknown angular flux eigenvectors in Eqns. 3.95 and 3.97 are node-centered. To satisfy this requirement, we write Eqns. 3.95 and 3.97 using zone-centered angular flux eigenvectors. We denote Ψ_z as the zone-centered unknown and \mathbf{H}_z as the zone-centered version of \mathbf{H} . To write Eqns. 3.95 and 3.97, we use the following lemma.

Lemma 3.1. *For all $\ell = 1, 2, \dots, L$,*

$$B_\ell(ZS + Z_b B_\ell)^{-1}Z = 0 \cdot I_{MJK} \text{ and } S(ZS + Z_b B_\ell)^{-1}Z = I_{MJK}. \quad (3.98)$$

Proof. The matrix $ZS + Z_b B_\ell$ is nonsingular for all $\ell = 1, 2, \dots, L$. [35]. Therefore,

$$I_{MJK} = ZS(ZS + Z_b B_\ell)^{-1} + Z_b B_\ell(ZS + Z_b B_\ell)^{-1}. \quad (3.99)$$

Multiplying by Z_b^T and using the fact $Z^T Z_b = 0$ gives

$$Z_b^T = B_\ell(ZS + Z_b B_\ell)^{-1}. \quad (3.100)$$

Multiplying on the right by Z gives the first assertion in Eq. 3.98. Using the fact $Z^T Z = I_{MJK}$ and $Z^T Z_b = 0$, multiplying Eq. 3.99 on the left by Z^T gives

$$Z^T = S(ZS + Z_b B_\ell)^{-1}. \quad (3.101)$$

Multiplying on the right by Z gives the second assertion in Eq. 3.98. \square

Given a zone-centered angular flux vector Ψ_z , the nodal angular flux vector Ψ defined by

$$\Psi_{g,\ell} \equiv (ZS + Z_b B_\ell)^{-1}Z\Psi_{z,g,\ell} \text{ for all } g = 1, 2, \dots, G \text{ and } \ell = 1, 2, \dots, L, \quad (3.102)$$

satisfies $B_\ell \Psi_{g,\ell} = 0$ and $S \Psi_{g,\ell} = \Psi_{z,g,\ell}$ for all g and ℓ . Defining the matrices

$$\mathbf{C} \equiv I_G \otimes C, \quad (3.103)$$

$$\mathbf{B} \equiv I_G \otimes B, \quad (3.104)$$

$$\mathbf{Z}_B \equiv I_G \otimes \bar{Z}_B, \quad (3.105)$$

and

$$\boldsymbol{\Sigma} \equiv \text{diag}(\bar{\Sigma}_1, \bar{\Sigma}_2, \dots, \bar{\Sigma}_G), \quad (3.106)$$

then \mathbf{H} and \mathbf{V}^{-1} can be rewritten as

$$\mathbf{H} = \mathbf{Z}(\mathbf{C} + \boldsymbol{\Sigma}\mathbf{S}) + \mathbf{Z}_B\mathbf{B}, \quad (3.107)$$

and

$$\mathbf{V}^{-1} = \mathbf{Z}\mathbf{V}^{-1}\mathbf{S}. \quad (3.108)$$

For the nodal-centered angular flux Ψ , we have from Lemma 3.1 that

$$\Psi = (\mathbf{Z}\mathbf{S} + \mathbf{Z}_B\mathbf{B})^{-1}\mathbf{Z}\Psi_z. \quad (3.109)$$

Substituting Eq. 3.109 into Eq. 3.95 and 3.97 and multiplying on the left by \mathbf{Z}^T gives

$$(\alpha\mathbf{V}_z^{-1} + \mathbf{H}_z)\Psi_z = \mathbf{L}^+(\Sigma_s + \Sigma_f)\mathbf{L}\Psi_z, \quad (3.110)$$

where

$$\mathbf{H}_z \equiv \mathbf{C}(\mathbf{Z}\mathbf{S} + \mathbf{Z}_B\mathbf{B})^{-1}\mathbf{Z} + \Sigma, \quad (3.111)$$

and

$$\mathbf{V}_z^{-1} \equiv \mathbf{V}^{-1}\mathbf{S}(\mathbf{Z}\mathbf{S} + \mathbf{Z}_B\mathbf{B})^{-1}\mathbf{Z}. \quad (3.112)$$

Following the same procedure for the k -effective eigenvalue neutron transport equation yields the discretized equation:

$$\mathbf{H}_z\Psi_z = \mathbf{L}^+\left(\Sigma_s + \frac{1}{k}\Sigma_f\right)\mathbf{L}\Psi_z. \quad (3.113)$$

We consider Eqns. 3.110 and 3.113 in the derivation of the Rayleigh Quotient Fixed Point method.

3.2 Primitivity of the Discretized Alpha-Eigenvalue and k -Effective Eigenvalue Equations

In this section we show that the matrices

$$\mathbf{A}(\alpha) = \mathbf{H}_z^{-1}\left(-\alpha\mathbf{V}_z^{-1} + \Sigma_s + \Sigma_f\right) \quad (3.114)$$

and

$$\mathbf{T}(k) = \mathbf{H}_z^{-1}\left(\Sigma_s + \frac{1}{k}\Sigma_f\right) \quad (3.115)$$

are primitive for the one-dimensional slab geometry problem. The discretization of the one-dimensional slab geometry alpha-eigenvalue can be seen in Appendix A. Though there are various definitions of a primitive matrix (see Section 2.3.3), it suffices to show that for some nonnegative matrix \mathbf{A} , if there is some n such that $\mathbf{A}^n > \mathbf{0}$, then \mathbf{A} is primitive.

It is assumed that there is fissile material in all spatial cells and spatial cell widths are small enough to guarantee the positivity of \mathbf{H}_z^{-1} for diamond differencing [39]. Step differencing also guarantees this condition is met. In practice, the requirement for fissile

material in all cells can be relaxed as long as sum of the fission and scattering matrices couple all energy and direction groups. It also assumed that a symmetric about the origin angular quadrature is used.

Given these assumptions, we begin with matrix $\mathbf{A}(\alpha)$. To prove the primitivity of $\mathbf{A}(\alpha)$, we first specify the location of positive elements in each of the matrices \mathbf{H}_z^{-1} , \mathbf{V}^{-1} , Σ_s , and Σ_f .

The matrix \mathbf{H}_z^{-1} can be partitioned into G block matrices corresponding to the total number of energy groups in the following manner

$$\mathbf{H}_z^{-1} = \begin{pmatrix} H_1^{-1} & & \\ & \ddots & \\ & & H_G^{-1} \end{pmatrix}. \quad (3.116)$$

Each energy block matrix can be further partitioned into L block matrices, with each block matrix corresponding to one angular ordinate:

$$H_g^{-1} = \begin{pmatrix} H_{g,-L/2}^{-1} & & \\ & \ddots & \\ & & H_{g,L/2}^{-1} \end{pmatrix}. \quad (3.117)$$

Let $g = 1, 2, \dots, G$ and $\ell = -L/2, -L/2 + 1, \dots, L/2$, then the block matrix corresponding to energy group g and direction ℓ is given by $H_{g,\ell}^{-1}$.

The block matrices $H_{g,\ell}^{-1}$ are of size M where M is the number of spatial cells in the x -direction. The block matrices are either nonnegative lower or upper triangular matrices:

$$H_{g,\ell,ij}^{-1} = \begin{cases} > 0 & \text{if } \mu_\ell > 0 \text{ and } i \leq j \\ > 0 & \text{if } \mu_\ell < 0 \text{ and } i \geq j. \end{cases} \quad (3.118)$$

Given that the angular quadrature is symmetric about the origin, we have

$$\mu_{-\ell} = -\mu_\ell, \quad \ell = 1, 2, \dots, L/2. \quad (3.119)$$

Using this fact, we have the following

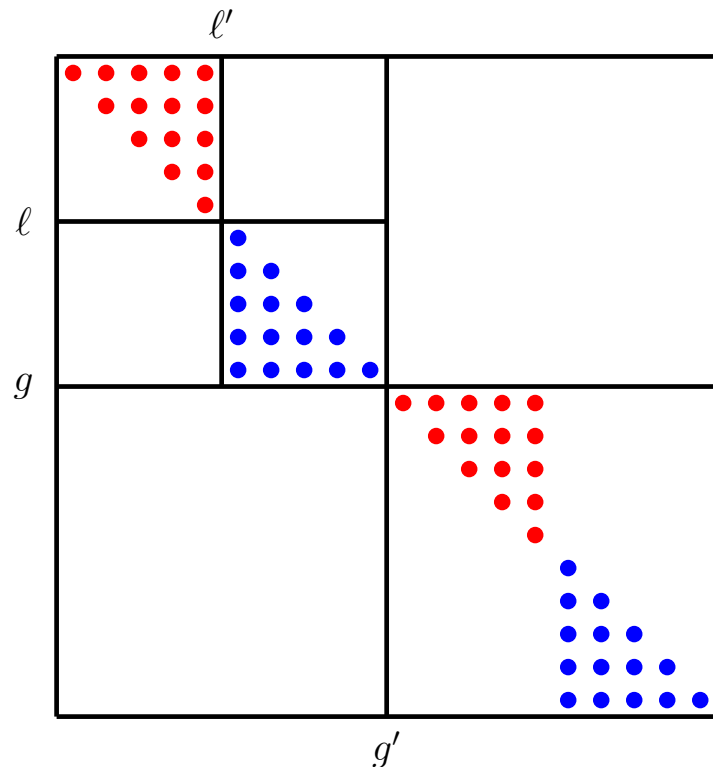
Lemma 3.2.

$$H_{g,\ell}^{-1} + H_{g,-\ell}^{-1} > 0. \quad (3.120)$$

From the previous fact, we have the following for the elements of the matrix \mathbf{H}_z^{-1}

$$(\mathbf{H}_z^{-1})_{g,\ell,ij} \begin{cases} = 0, & \text{if } \mu_\ell > 0, \text{ and } i > j, \\ = 0, & \text{if } \mu_\ell < 0, \text{ and } i < j, \\ > 0, & \text{otherwise.} \end{cases} \quad (3.121)$$

An example of the \mathbf{H}_z^{-1} for five spatial cells ($M = 5$), S_2 discrete ordinates angular quadrature ($L = 2$), and two energy groups ($G = 2$) can be seen in Figure 3.1.

Figure 3.1: Structure of \mathbf{H}_z^{-1}

The structure of \mathbf{H}_z^{-1} . The matrix is blocked into block matrices corresponding to energy groups. The block energy are indexed using $g, g' = 1, 2, \dots, G$. There are a total of $(GL)^2$ block matrices each of size M . Each energy block matrix can be blocked into direction matrices with indices $\ell, \ell' = 1, 2, \dots, L$. The block lower and upper triangular matrices correspond to positive (blue) and negative (red) directions, respectively.

For the fission matrix Σ_f , if the problem domain of interest has fissile material throughout the domain and fission is possible in any energy group, we have the following for the elements of the matrix

$$(\Sigma_f)_{gg',\ell\ell',ij} \begin{cases} = 0, & \text{if } i \neq j, \\ > 0, & \text{otherwise,} \end{cases} \quad (3.122)$$

for all $g, g' = 1, 2, \dots, G$ and $\ell, \ell' = -L/2, -L/2 + 1, \dots, L/2$. We assume fission is isotropic. The fission matrix Σ_f is a block matrix with square block matrices size of M that are only nonzero on the diagonal (see Figure 3.2). For isotropic fission, we have the following for the block matrices of Σ_f

Lemma 3.3.

$$(\Sigma_f)_{gg',\ell\ell'} = (\Sigma_f)_{gg',-\ell-\ell'}. \quad (3.123)$$

An example of the matrix Σ_f for five spatial cells and fission possible in all energy groups is seen in Figure 3.2

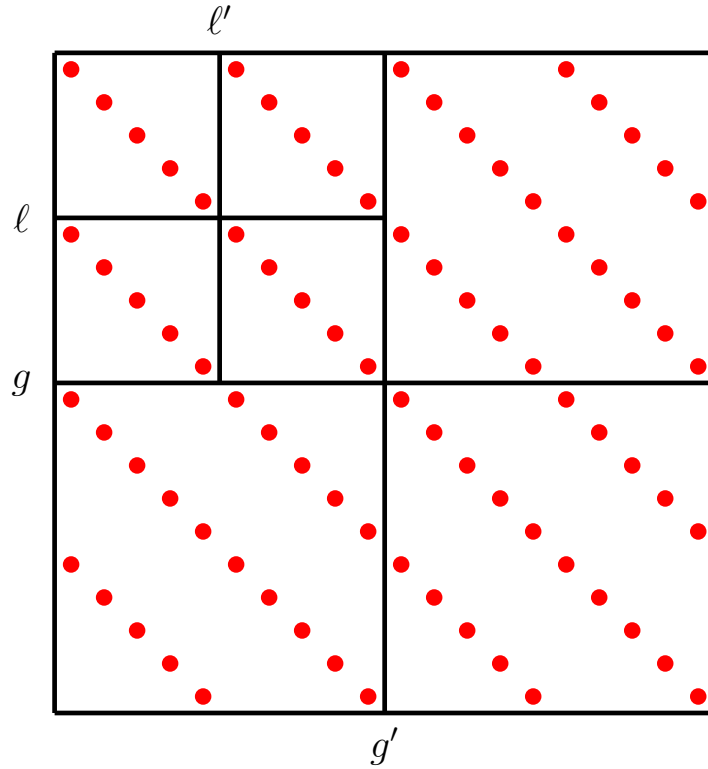


Figure 3.2: Structure of Σ_f for Two Energy Groups, Five Spatial Cells, and Fission in All Energy Groups

For a positive scattering kernel in the entire problem domain where only downscattering is allowed, we have the following for the elements of the matrix Σ_s

$$(\Sigma_s)_{gg',\ell\ell',ij} \begin{cases} = 0, & \text{if } g < g', \\ = 0, & \text{if } i \neq j, \\ > 0, & \text{otherwise,} \end{cases} \quad (3.124)$$

for $\ell, \ell' = -L/2, -L/2+1, \dots, L/2$. Σ_s is composed of block diagonal matrices on and under the diagonal each with size M that are only nonzero on the diagonal of that block matrix.

An example of the matrix Σ_s for five spatial cells and only downscattering is possible is seen in Figure 3.3.

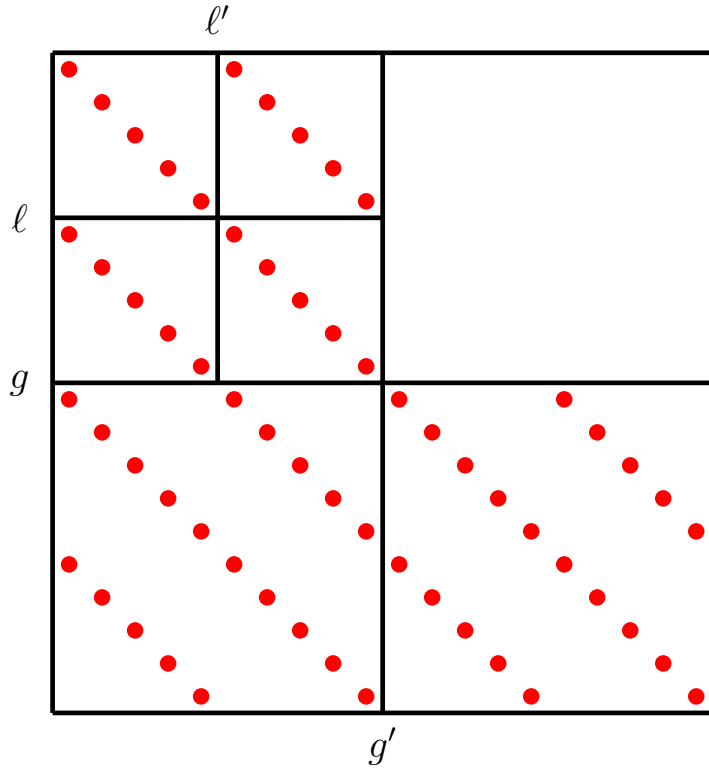
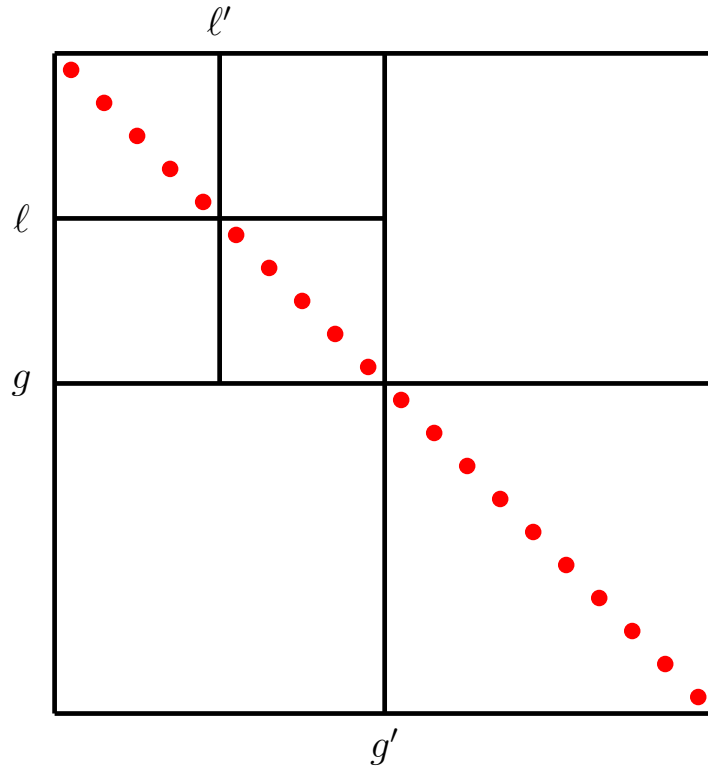


Figure 3.3: Structure of Σ_s for Two Energy Groups, Five Spatial Cells, and Downscattering Only

For all energy groups, the inverse velocity matrix is a diagonal matrix. For the matrix \mathbf{V}_z^{-1} we have the following

$$(\mathbf{V}_z^{-1})_{gg',\ell\ell',ij} \begin{cases} = 0, & \text{if } g \neq g', \ell \neq \ell', i \neq j \\ > 0, & \text{otherwise} \end{cases}, \quad (3.125)$$

An example of the matrix \mathbf{V}_z^{-1} is seen in Figure 3.4.

Figure 3.4: Structure of \mathbf{V}_z^{-1} for Five Spatial Cells

Given the location of nonzero elements in the transport, fission, scattering, and inverse velocity matrices, we set out to prove the primitivity of the matrix $\mathbf{H}_z^{-1}\Sigma_f$. The block matrix of size M of the matrix $\mathbf{H}_z^{-1}\Sigma_f$ is given by the product of the block matrices of \mathbf{H}_z^{-1} and Σ_f

$$(\mathbf{H}_z^{-1}\Sigma_f)_{gg',\ell\ell'} = \sum_{g'',\ell''} (\mathbf{H}_z^{-1})_{gg'',\ell\ell''} (\Sigma_f)_{g''g',\ell''\ell'} = (\mathbf{H}_z^{-1})_{g,\ell} (\Sigma_f)_{gg',\ell\ell'} \quad (3.126)$$

The matrices are either lower or upper triangular block matrices depending on the sign of μ_ℓ :

$$(\mathbf{H}_z^{-1}\Sigma_f)_{gg',\ell\ell'} \begin{cases} = a_{ij} > 0, & \text{if } \mu_\ell < 0 \text{ and } i \geq j \\ = a_{ij} > 0, & \text{if } \mu_\ell > 0 \text{ and } i \leq j \end{cases} \quad (3.127)$$

for all $g, g' = 1, 2, \dots, G$ and $\ell, \ell' = -L/2, -L/2 + 1, \dots, L/2$ (see Figure 3.5).

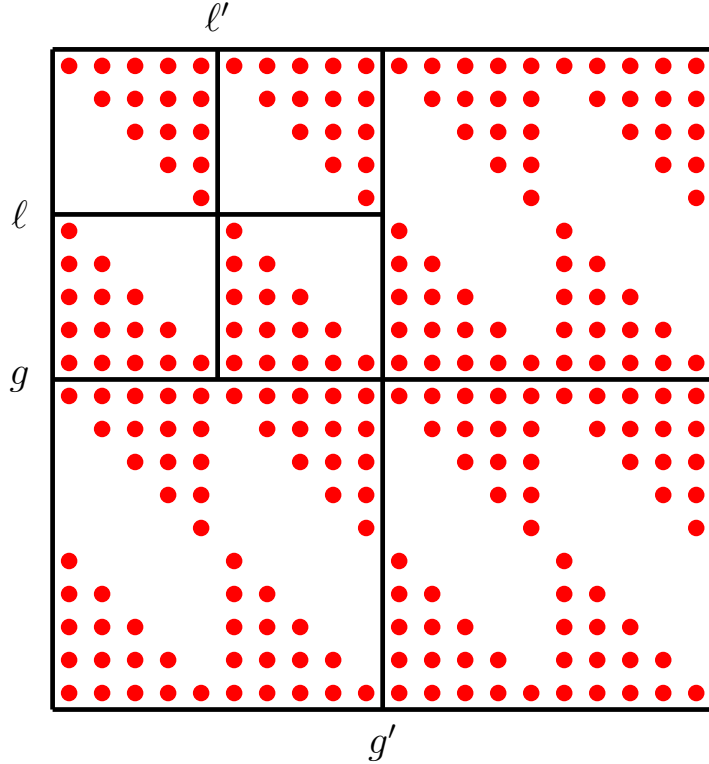


Figure 3.5: Structure of $\mathbf{H}_z^{-1}\boldsymbol{\Sigma}_f$ For Two Energy Group Example

With these facts, we prove the following lemma:

Lemma 3.4. *The matrix $\boldsymbol{\Sigma}_f \mathbf{H}_z^{-1} \boldsymbol{\Sigma}_f$ is positive.*

Proof. The block matrix of size M , $\boldsymbol{\Sigma}_f \mathbf{H}^{-1} \boldsymbol{\Sigma}_f$, is given by

$$(\boldsymbol{\Sigma}_f \mathbf{H}^{-1} \boldsymbol{\Sigma}_f)_{gg',\ell\ell'} = \sum_{g'',\ell''} (\boldsymbol{\Sigma}_f)_{gg'',\ell\ell''} (\mathbf{H}^{-1} \boldsymbol{\Sigma}_f)_{g''g',\ell''\ell'}. \quad (3.128)$$

We can further simplify the previous expression to

$$(\boldsymbol{\Sigma}_f \mathbf{H}^{-1} \boldsymbol{\Sigma}_f)_{gg',\ell\ell'} = \sum_{g'',\ell''} (\boldsymbol{\Sigma}_f)_{gg'',\ell\ell''} (\mathbf{H}_z^{-1})_{g'',\ell''} (\boldsymbol{\Sigma}_f)_{g''g',\ell''\ell'}. \quad (3.129)$$

We can rearrange the sum into opposite-signed direction and write

$$\sum_{g''} \sum_{\ell''=-L/2}^{L/2} (\boldsymbol{\Sigma}_f)_{gg'',\ell\ell''} \left[(\mathbf{H}_z^{-1})_{g'',-\ell''} + (\mathbf{H}_z^{-1})_{g'',\ell''} \right] (\boldsymbol{\Sigma}_f)_{g'',g',\ell'',\ell'}, \quad (3.130)$$

where we have used Lemma 3.3. Using Lemma 3.2, we have

$$\left[(\mathbf{H}_z^{-1})_{g'',-\ell''} + (\mathbf{H}_z^{-1})_{g'',\ell''} \right] > 0. \quad (3.131)$$

Since the matrices $(\Sigma_f)_{gg'', \ell\ell''}$ and $(\Sigma_f)_{g'', g', \ell'', \ell'}$ are nonnegative block diagonal matrices with positive entries on the main diagonal, then the product of the positive matrix times the nonnegative matrices is entirely positive. Therefore $\Sigma_f H_z^{-1} \Sigma_f$ is positive. \square

Using Lemma 3.4, we prove the following lemma:

Lemma 3.5. *The nonnegative matrix $H_z^{-1} \Sigma_f$ is primitive with index of primitivity of two.*

Proof. Multiplying, we obtain

$$(H_z^{-1} \Sigma_f H_z^{-1} \Sigma_f)_{gg', \ell\ell'} = \sum_{g'', \ell''} (H_z^{-1})_{g'', \ell''} (\Sigma_f H_z^{-1} \Sigma_f)_{g'', g', \ell'', \ell'}. \quad (3.132)$$

Since every element of $\Sigma_f H_z^{-1} \Sigma_f$ is positive, a zero element in $H_z^{-1} \Sigma_f H_z^{-1} \Sigma_f$ is possible only if the elements of $(H_z^{-1})_{g'', \ell'', ij} = 0 \forall i = 1, 2, \dots, M$ which is not possible since the elements on row i of $(H_z^{-1})_{gg', \ell\ell', ij'}$ are not all zero. Therefore, $(H_z^{-1} \Sigma_f H_z^{-1} \Sigma_f)_{gg', \ell\ell'} > 0 \forall (g, g', \ell, \ell')$, which implies the matrix $H_z^{-1} \Sigma_f$ is primitive with index of primitivity of two. \square

Using the previous results, we prove the primitivity of the matrix $H_z^{-1}(\Sigma_s + \Sigma_f)$:

Theorem 3.1. *If $(H_z^{-1} \Sigma_f)^2 > \mathbf{0}$ and $\Sigma_s \geq \mathbf{0}$, then $H_z^{-1}(\Sigma_s + \Sigma_f)$ is primitive.*

Proof. By multiplication

$$\begin{aligned} [H_z^{-1}(\Sigma_s + \Sigma_f)]^2 &= (H_z^{-1} \Sigma_s)^2 + (H_z^{-1} \Sigma_f)(H_z^{-1} \Sigma_s) \\ &\quad + (H_z^{-1} \Sigma_s)(H_z^{-1} \Sigma_f) + (H_z^{-1} \Sigma_f)^2 > \mathbf{0}, \end{aligned} \quad (3.133)$$

since $(H_z^{-1} \Sigma_f)^2 > \mathbf{0}$ and the matrices $(H_z^{-1} \Sigma_f)$ and $(H_z^{-1} \Sigma_s)$ are nonnegative. \square

We now show that for $\alpha < \alpha_{\max}$, where α_{\max} is defined as

$$\alpha_{\max} = \max\{\alpha \mid -\alpha V_z^{-1} + \Sigma_s + \Sigma_f \geq \mathbf{0}, \alpha \in \mathbb{R}\}, \quad (3.134)$$

the matrix $A(\alpha) = H_z^{-1}(-\alpha V_z^{-1} + \Sigma_s + \Sigma_f)$ is primitive with index of primitivity of two.

Theorem 3.2. *If $H_z^{-1}(\Sigma_s + \Sigma_f)$ is primitive, then $H_z^{-1}(-\alpha V_z^{-1} + \Sigma_s + \Sigma_f)$ is primitive with index of primitivity equal to two.*

Proof. Let $M = -\alpha H_z^{-1} V_z^{-1}$ and $N = H_z^{-1}(\Sigma_s + \Sigma_f)$. By multiplication,

$$\left[H_z^{-1}(-\alpha V_z^{-1} + \Sigma_s + \Sigma_f) \right]^2 = \left[M + N \right]^2 = M^2 + MN + NM + N^2 > \mathbf{0}, \quad (3.135)$$

since $N^2 = [H_z^{-1}(\Sigma_s + \Sigma_f)]^2 > \mathbf{0}$ and the matrices M^2 , MN , and NM are nonnegative since $\alpha \leq \alpha_{\max}$. \square

Now we prove that the matrix $\mathbf{T}(k) = \mathbf{H}_z^{-1}(\Sigma_s + (1/k)\Sigma_f)$ is primitive.

Theorem 3.3. *If $(\mathbf{H}_z^{-1}\Sigma_f)^2$ is primitive, then $\mathbf{H}_z^{-1}(\Sigma_s + (1/k)\Sigma_f)$ is primitive with index of primitivity equal to two.*

Proof. By multiplication

$$\begin{aligned} \left[\mathbf{H}_z^{-1} \left(\Sigma_s + \frac{1}{k} \Sigma_f \right) \right]^2 &= (\mathbf{H}_z^{-1}\Sigma_s)^2 + (1/k)(\mathbf{H}_z^{-1}\Sigma_f)(\mathbf{H}_z^{-1}\Sigma_s) \\ &\quad + (1/k)(\mathbf{H}_z^{-1}\Sigma_s)(\mathbf{H}_z^{-1}\Sigma_f) + (1/k)^2(\mathbf{H}_z^{-1}\Sigma_f)^2 > \mathbf{0}, \end{aligned} \quad (3.136)$$

since $(\mathbf{H}_z^{-1}\Sigma_f)^2 > \mathbf{0}$, the matrices $(\mathbf{H}_z^{-1}\Sigma_f)$ and $(\mathbf{H}_z^{-1}\Sigma_s)$ are nonnegative, and $k > 0$. \square

3.3 Conclusion

Starting with a three-dimensional Cartesian geometry, the continuous neutron transport criticality eigenvalue equations were discretized using step differencing in space, discrete ordinates angular quadrature, and the multigroup-in-energy approximation. The matrix forms of the alpha- and k -effective eigenvalue equations were derived and the structure and properties of the transport, scattering, fission, and velocity matrices were described. Finally, the primitivity of the discretized one-dimensional slab alpha-eigenvalue equation was proven.

Chapter 4

The Rayleigh Quotient Fixed Point Method

In this chapter we derive the Rayleigh Quotient Fixed Point method for alpha- and k -effective eigenvalue problems. We begin with the matrix form of the eigenvalue equations and proceed to develop a fixed point method for the angular flux eigenvector. Since the eigenvector corresponds to the alpha- or k -effective eigenvalue, we require an update for the eigenvalue at each iteration. We derive an eigenvalue update that is optimal in the least squares sense by relating the alpha- or k -effective eigenvalue to the dominant eigenvalue of a primitive matrix (see Section 2.3). This primitive matrix serves as the fixed point function to determine the solution of the eigenvalue problem. Since the dominant eigenvalue of a primitive matrix corresponds to the only positive eigenvector of the matrix, this eigenvector also solves the discretized criticality eigenvalue neutron transport problem. We end this chapter with a discussion of the primitivity of the discretized alpha- and k -effective eigenvalue matrix equations.

4.1 Derivation of the Rayleigh Quotient Fixed Point Method for Alpha-Eigenvalue Problems

We begin with the discretized alpha-eigenvalue matrix equation:

$$(\alpha \mathbf{V}_z^{-1} + \mathbf{H}_z) \Psi_z = \mathbf{L}^+ (\Sigma_s + \Sigma_f) \mathbf{L} \Psi_z. \quad (4.1)$$

Solution of Eq. 4.1 consists of finding the eigenpair (α, Ψ) that satisfies the equation with α a real number and the vector Ψ positive. We write a fixed point equation for Eq. 4.1 in the form

$$\Psi_z = \mathbf{H}_z^{-1} (-\alpha(\Psi_z) \mathbf{V}_z^{-1} + \mathbf{L}^+ (\Sigma_s + \Sigma_f) \mathbf{L}) \Psi_z \equiv \mathbf{A}(\alpha(\Psi_z)) \Psi_z. \quad (4.2)$$

where the alpha-eigenvalue is function of the eigenvector, $\alpha(\Psi_z)$. For all subcritical and critical systems, the righthand side of Eq. 4.2 is nonnegative since for isotropic scattering

the scattering matrix is nonnegative. For supercritical systems, there is an α_{\max} such that the righthand side is still nonnegative. Various fixed-point equations can be written for the angular flux eigenvector Ψ_z . However, this form was selected as it only requires the inversion of the matrix H_z . In standard neutron transport codes [19] [20], the matrix H_z is inverted without being formed by sweeping across the domain in space and angle. The updated eigenvector iterate is obtained by the action of the inverted operator on the source. By writing the fixed point in this way, the Rayleigh Quotient Fixed Point method can be implemented easily without needing to form the matrices. Instead, all that is required is the action of the matrix H_z^{-1} on the source vector, adjusted by the alpha-eigenvalue inverse velocity vector. This matrix-free form of the algorithm can be easily implemented easily in production neutron transport codes.

We define an iterative method to find the fixed point (see Section 2.4) of Eq. 4.2 as

$$\Psi_z^{(i+1)} = \mathbf{A}(\alpha_{(i)})\Psi_z^{(i)}. \quad (4.3)$$

From some initial positive starting vector $\Psi_z^{(0)}$, the subsequent eigenvector iterate is determined by the action of inversion of the matrix H_z on the scattering and fission source adjusted by the alpha-eigenvalue. At each iteration, an update for the eigenvalue is required. A natural choice of update is that the eigenvalue be a function of the eigenvector iterate. Given an eigenpair, (α_*, Ψ_z^*) to Eq. 4.1, it follows that

$$\Psi_z^* = \mathbf{A}(\alpha_*)\Psi_z^* \quad (4.4)$$

is also an eigenvalue problem for the fixed matrix $\mathbf{A}(\alpha_*)$ with eigenpair $(1, \Psi_z^*)$.

If the matrix $\mathbf{A}(\alpha)$ is a primitive matrix, it follows from the Perron-Frobenius Theorem for Primitive Matrices that there is only one unique positive eigenvector of $\mathbf{A}(\alpha)$ corresponding to the dominant eigenvalue. This fact allows us to derive an update for the alpha-eigenvalue at each iteration.

If (Ψ_z^*, λ) is an eigenpair of the matrix $\mathbf{A}(\alpha_*)$, then

$$\|\mathbf{A}(\alpha_*)\Psi_z^* - \lambda\Psi_z^*\|_2^2 = 0. \quad (4.5)$$

However, suppose $\Psi_{(i)}$ is an approximate eigenvector and we seek to find the best approximate eigenvalue $\hat{\lambda}$ such that

$$\hat{\lambda} = \arg \min_{\mu} \|\mathbf{A}(\alpha_{(i)})\Psi_{(i)} - \mu\Psi_{(i)}\|_2^2. \quad (4.6)$$

This is a linear least squares problem in the variable μ . It is found that [25]

$$\hat{\lambda} = \frac{\Psi_{(i)}^T \mathbf{A}(\alpha_{(i)}) \Psi_{(i)}}{\Psi_{(i)}^T \Psi_{(i)}}, \quad (4.7)$$

the Rayleigh quotient, minimizes the residual in the least squares sense. Setting the Rayleigh quotient to one, the eigenvalue corresponding to the unique positive eigenvector, and solving

Algorithm 4.1 Rayleigh Quotient Fixed Point Method for the Alpha-Eigenvalue Problem

while residual > tolerance **do**

$$\alpha_{(i)} = \frac{\Psi_{(i)}^T \mathbf{H}_z^{-1} \mathbf{L}^+ (\Sigma_s + \Sigma_f) \mathbf{L} \Psi_{(i)} - \Psi_{(i)}^T \Psi_{(i)}}{\Psi_{(i)}^T \mathbf{H}_z^{-1} \mathbf{V}_z^{-1} \Psi_{(i)}}$$

$$\Psi_{(i+1)} = \mathbf{H}_z^{-1} \left(-\alpha_{(i)} \mathbf{V}_z^{-1} + \mathbf{L}^+ (\Sigma_s + \Sigma_f) \mathbf{L} \right) \Psi_{(i)}$$

$$\text{residual} = \frac{\|\Psi_{(i+1)} - \Psi_{(i)}\|_2}{\|\Psi_{(i+1)}\|_2}$$

end while

for the approximate alpha-eigenvalue $\alpha_{(i)}$, we obtain the alpha-eigenvalue update for an approximate eigenvector $\Psi_{(i)}$

$$\alpha_{(i)} = \frac{\Psi_{(i)}^T \mathbf{H}_z^{-1} \mathbf{L}^+ (\Sigma_s + \Sigma_f) \mathbf{L} \Psi_{(i)} - \Psi_{(i)}^T \Psi_{(i)}}{\Psi_{(i)}^T \mathbf{H}_z^{-1} \mathbf{V}_z^{-1} \Psi_{(i)}}. \quad (4.8)$$

Given Eq. 4.8, we introduce Algorithm 4.1, an iterative scheme to determine the alpha-eigenvalue and its corresponding eigenvector. The eigenvalue update is optimal in the least squares sense. For alpha-eigenvalue problems, whereas traditional techniques have focused on supercritical problems and were limited in subcritical cases [2], this method allows for the solution of both subcritical and supercritical systems.

For each iteration in Algorithm 4.1 two transport sweeps (inversions of \mathbf{H}_z) and three vectors of size $GLMJK$ are necessary to calculate the alpha-eigenvalue and angular flux iterates. To reduce the number of transport sweeps and vectors required, we note that Eq. 4.8 can be written as

$$\alpha_{(i)} = \frac{\Psi_{(i)}^T \mathbf{L}^+ (\Sigma_s + \Sigma_f) \mathbf{L} \Psi_{(i)} - \Psi_{(i)}^T \mathbf{H}_z \Psi_{(i)}}{\Psi_{(i)}^T \mathbf{V}_z^{-1} \Psi_{(i)}}. \quad (4.9)$$

Using the fact that

$$\mathbf{H}_z \Psi_{(i)} = \left(-\alpha_{(i-1)} \mathbf{V}_z^{-1} + \mathbf{L}^+ (\Sigma_s + \Sigma_f) \mathbf{L} \right) \Psi_{(i-1)} \equiv \mathbf{q}_{(i-1)}, \quad (4.10)$$

where \mathbf{q} is the scattering and fission source vector, we can write Eq. 4.9 as

$$\alpha_{(i)} = \frac{\Psi_{(i)}^T \mathbf{L}^+ (\Sigma_s + \Sigma_f) \mathbf{L} \Psi_{(i)} - \Psi_{(i)}^T \mathbf{q}_{(i-1)}}{\Psi_{(i)}^T \mathbf{V}_z^{-1} \Psi_{(i)}}. \quad (4.11)$$

We introduce a one-sweep variant of Algorithm 4.1 in Algorithm 4.2. For the first iteration ($i = 0$), $\alpha_{(0)} = 0$. Algorithm 4.2 requires only one transport sweep per iteration of the method. However, the method still requires two vectors per iteration, one to store the angular flux vector and another to store the previous fission and scattering source vector.

Algorithm 4.2 One-Sweep Rayleigh Quotient Fixed Point Method for the Alpha-Eigenvalue Problem

while residual > tolerance **do**

if $i = 0$ **then**

$$\mathbf{q}_{(0)} = \left(\mathbf{L}^+ (\Sigma_s + \Sigma_f) \mathbf{L} \right) \Psi_{(0)}$$

$$\Psi_{(1)} = \mathbf{H}_z^{-1} \mathbf{q}_{(0)}$$

else

$$\alpha_{(i)} = \frac{\Psi_{(i)}^T \mathbf{L}^+ (\Sigma_s + \Sigma_f) \mathbf{L} \Psi_{(i)} - \Psi_{(i)}^T \mathbf{q}_{(i-1)}}{\Psi_{(i)}^T \mathbf{V}_z^{-1} \Psi_{(i)}}.$$

$$\mathbf{q}_{(i)} = \left(-\alpha_{(i)} \mathbf{V}_z^{-1} + \mathbf{L}^+ (\Sigma_s + \Sigma_f) \mathbf{L} \right) \Psi_{(i)}$$

$$\Psi_{(i+1)} = \mathbf{H}_z^{-1} \mathbf{q}_{(i)}$$

end if

$$\text{residual} = \frac{\|\Psi_{(i+1)} - \Psi_{(i)}\|_2}{\|\Psi_{(i+1)}\|_2}$$

end while

4.2 Derivation of the Rayleigh Quotient Fixed Point Method for k -Effective Problems

Derivation of the k -effective RQFP method follows a similar procedure as the alpha-eigenvalue RQFP method. We begin with the discretized k -effective eigenvalue matrix equation:

$$\mathbf{H}_z \Psi_z = \mathbf{L}^+ \left(\Sigma_s + \frac{1}{k} \Sigma_f \right) \mathbf{L} \Psi_z, \quad (4.12)$$

Once again, we search for the eigenpair (k, Ψ) that satisfies Eq. 4.12. We write Eq. 4.12 in the fixed-point form

$$\Psi_z = H_z^{-1} \left[L^+ \left(\Sigma_s + \frac{1}{k(\Psi_z)} \Sigma_f \right) L \right] \Psi \equiv T(k(\Psi_z)) \Psi_z, \quad (4.13)$$

where the k -effective eigenvalue is a function of the eigenvector, $k(\Psi_z)$. For all systems, the righthand side of Eq. 4.13 is nonnegative for isotropic scattering and nonnegative k [24]. The fixed-point form is selected to only require the inversion of the matrix H_z . We define an iterative method to find the fixed point of Eq. 4.13 as

$$\Psi_z^{(i+1)} = T(k_{(i)}) \Psi_z^{(i)}. \quad (4.14)$$

From some initial positive starting vector $\Psi_z^{(0)}$, the subsequent eigenvector iterate is determined by the action of inversion of the matrix H_z on the scattering and fission source, where the fission source is adjusted by the k -effective eigenvalue as seen in Eq. 4.13. At each iteration, an update for the eigenvalue is required. If (k_*, Ψ_z^*) is an eigenpair of Eq. 4.14, it follows that

$$\Psi_z^* = T(k_*) \Psi_z^* \quad (4.15)$$

is also an eigenvalue problem with eigenpair $(1, \Psi_z^*)$.

Similar to the alpha-eigenvalue matrix $A(\alpha)$, if the matrix $T(k)$ is a primitive matrix, it follows from the Perron-Frobenius Theorem for Primitive Matrices that there is only one unique positive eigenvector of $T(k)$ corresponding to the dominant eigenvalue. This fact allows us to derive an update for the k -effective eigenvalue at each iteration.

Suppose $\Psi_{(i)}$ is an approximate eigenvector and we seek to find the best approximate eigenvalue $\hat{\lambda}$ such that

$$\hat{\lambda} = \arg \min_{\mu} \|T(k_{(i)}) \Psi_{(i)} - \mu \Psi_{(i)}\|_2^2. \quad (4.16)$$

This is, once again, a linear least squares problem in the variable μ . From before, it is found that the Rayleigh quotient given by

$$\hat{\lambda} = \frac{\Psi_{(i)}^T T(k_{(i)}) \Psi_{(i)}}{\Psi_{(i)}^T \Psi_{(i)}}, \quad (4.17)$$

minimizes the residual in the least square sense. Setting the Rayleigh quotient to one and solving for the k -effective eigenvalue $k_{(i)}$, we obtain the k -effective eigenvalue update for eigenvector iterate $\Psi_{(i)}$

$$k_{(i)} = \frac{\Psi_{(i)}^T H_z^{-1} L \Sigma_f L^+ \Psi_{(i)}}{\Psi_{(i)}^T \Psi_{(i)} - \Psi_{(i)}^T H_z^{-1} L \Sigma_s L^+ \Psi_{(i)}}. \quad (4.18)$$

Given Eq. 4.18, we introduce Algorithm 4.3, an iterative scheme to determine the k -effective eigenvalue and its corresponding eigenvector. The eigenvalue update is optimal in the least squares sense.

Algorithm 4.3 Rayleigh Quotient Fixed Point Method for the k -Effective Eigenvalue Problem

while residual > tolerance **do**

$$k_{(i)} = \frac{\Psi_{(i)}^T \mathbf{H}_z^{-1} \mathbf{L} \Sigma_f \mathbf{L}^+ \Psi_{(i)}}{\Psi_{(i)}^T \Psi_{(i)} - \Psi_{(i)}^T \mathbf{H}_z^{-1} \mathbf{L} \Sigma_s \mathbf{L}^+ \Psi_{(i)}}$$

$$\Psi_{(i+1)} = \mathbf{H}_z^{-1} \left[\mathbf{L}^+ \left(\Sigma_s + \frac{1}{k_{(i)}} \Sigma_f \right) \mathbf{L} \right] \Psi_{(i)}$$

$$\text{residual} = \frac{\|\Psi_{(i+1)} - \Psi_{(i)}\|_2}{\|\Psi_{(i+1)}\|_2}$$

end while

For each iteration of Algorithm 4.3, two transport sweeps are required to determine the transported fission and scattering terms. To require only one transport sweep, we rewrite Eq. 4.18 as

$$k_{(i)} = \frac{\Psi_{(i)}^T \mathbf{L} \Sigma_f \mathbf{L}^+ \Psi_{(i)}}{\Psi_{(i)}^T \mathbf{H}_z \Psi_{(i)} - \Psi_{(i)}^T \mathbf{L} \Sigma_s \mathbf{L}^+ \Psi_{(i)}}. \quad (4.19)$$

Using the fact that

$$\mathbf{H}_z \Psi_{(i)} = \left[\mathbf{L}^+ \left(\Sigma_s + \frac{1}{k} \Sigma_f \right) \mathbf{L} \right] \Psi_{(i-1)} \equiv \mathbf{q}_{(i-1)}, \quad (4.20)$$

we can write the update, Eq. 4.19 as

$$k_{(i)} = \frac{\Psi_{(i)}^T \mathbf{L} \Sigma_f \mathbf{L}^+ \Psi_{(i)}}{\Psi_{(i)}^T \mathbf{q}_{(i-1)} - \Psi_{(i)}^T \mathbf{L} \Sigma_s \mathbf{L}^+ \Psi_{(i)}}. \quad (4.21)$$

We introduce Algorithm 4.4, a one-sweep variant of Algorithm 4.3. For the initial iteration, $k_{(0)} = 1$. Algorithm 4.4 requires only one transport sweep per iteration of the method. However, it requires three vectors to store the angular flux and fission and scattering sources. For some angular flux iterates, it has been observed that the k -effective eigenvalue iterate can be negative for some iterations. However, in practice, this has not prevented convergence of the method to a positive eigenvalue.

Algorithm 4.4 One-Sweep Rayleigh Quotient Fixed Point Method for the k -Effective Eigenvalue Problem

while residual > tolerance **do**

if $i = 0$ **then**

$$\mathbf{q}_{(0)} = [\mathbf{L}^+ (\boldsymbol{\Sigma}_s + \boldsymbol{\Sigma}_f) \mathbf{L}] \boldsymbol{\Psi}_{(0)}$$

$$\boldsymbol{\Psi}_{(1)} = \mathbf{H}_z^{-1} \mathbf{q}_{(i)}$$

else

$$k_{(i)} = \frac{\boldsymbol{\Psi}_{(i)}^T \mathbf{L} \boldsymbol{\Sigma}_f \mathbf{L}^+ \boldsymbol{\Psi}_{(i)}}{\boldsymbol{\Psi}_{(i)}^T \mathbf{q}_{(i-1)} - \boldsymbol{\Psi}_{(i)}^T \mathbf{L} \boldsymbol{\Sigma}_s \mathbf{L}^+ \boldsymbol{\Psi}_{(i)}}.$$

$$\mathbf{q}_{(i)} = \left[\mathbf{L}^+ \left(\boldsymbol{\Sigma}_s + \frac{1}{k_{(i)}} \boldsymbol{\Sigma}_f \right) \mathbf{L} \right] \boldsymbol{\Psi}_{(i)}$$

$$\boldsymbol{\Psi}_{(i+1)} = \mathbf{H}_z^{-1} \mathbf{q}_{(i)}$$

end if

$$\text{residual} = \frac{\|\boldsymbol{\Psi}_{(i+1)} - \boldsymbol{\Psi}_{(i)}\|_2}{\|\boldsymbol{\Psi}_{(i+1)}\|_2}$$

end while

4.3 Jacobian of the Rayleigh Quotient Fixed Point Method for Alpha-Eigenvalue Problems

The convergence of the non-linear fixed-point method for the alpha-eigenvalue problem is determined by the Jacobian of the fixed-point method evaluated at the fixed point of interest (see Section 2.4). To be more precise, if the spectral radius of the Jacobian matrix at the fixed point is greater than one, the fixed point is a point of repulsion and the fixed-point method may not converge to the fixed point. If the spectral radius of the Jacobian matrix is less than one at the fixed point, the fixed-point method is guaranteed to converge to the fixed point as long as the iterates are within some neighborhood of the fixed point. If the spectral radius is equal to one, then the fixed-point method might or might not converge. To determine the behavior of the fixed-point method at the fixed point of interest, we determine the Jacobian of the non-linear fixed-point iteration.

We begin by defining the matrices \mathbf{U} and \mathbf{W} as

$$\mathbf{U} = \mathbf{H}_z^{-1} \mathbf{L}^+ (\Sigma_s + \Sigma_f) \mathbf{L}, \quad (4.22)$$

$$\mathbf{W} = \mathbf{H}_z^{-1} \mathbf{V}_z^{-1}, \quad (4.23)$$

and writing Eq. 4.2 as

$$\Psi = -\alpha(\Psi) \mathbf{W} \Psi + \mathbf{U} \Psi, \quad (4.24)$$

where Ψ is the zone-centered angular flux vector and the subscript has been dropped for compactness. The alpha-eigenvalue update is then given by

$$\alpha(\Psi) = \frac{\Psi^T \mathbf{U} \Psi - \Psi^T \Psi}{\Psi^T \mathbf{W} \Psi}. \quad (4.25)$$

We obtain the Jacobian of the Rayleigh quotient Fixed Point method for the alpha-eigenvalue problem by differentiating Eq. 4.2 with respect to the vector Ψ :

$$\mathbf{J}_\alpha(\Psi) = -\mathbf{W} \Psi \alpha'(\Psi)^T - \alpha(\Psi) \mathbf{W} + \mathbf{U}. \quad (4.26)$$

The Rayleigh quotient update derivative is given by

$$\alpha'(\Psi) = \frac{[(\mathbf{U} + \mathbf{U}^T) \Psi - 2\Psi](\Psi^T \mathbf{W} \Psi) - (\Psi^T \mathbf{U} \Psi - \Psi^T \Psi)[(\mathbf{W} + \mathbf{W}^T) \Psi]}{(\Psi^T \mathbf{W} \Psi)^2}. \quad (4.27)$$

Using Eq. 4.25, Eq. 4.27 can be written as

$$\alpha'(\Psi) = \frac{[(\mathbf{U} + \mathbf{U}^T) \Psi - 2\Psi] - \alpha(\Psi)[(\mathbf{W} + \mathbf{W}^T) \Psi]}{(\Psi^T \mathbf{W} \Psi)}. \quad (4.28)$$

The Jacobian matrix for the Rayleigh Quotient Fixed Point method can then be written as

$$\mathbf{J}_\alpha(\Psi) = -\mathbf{W} \Psi \left[\frac{[(\mathbf{U} + \mathbf{U}^T) \Psi - 2\Psi] - \alpha(\Psi)[(\mathbf{W} + \mathbf{W}^T) \Psi]}{(\Psi^T \mathbf{W} \Psi)} \right]^T - \alpha(\Psi) \mathbf{W} + \mathbf{U}. \quad (4.29)$$

4.4 Jacobian of the Rayleigh Quotient Fixed Point Method for k -Effective Eigenvalue Problems

Similar to the Rayleigh Quotient Fixed Point method for the alpha-eigenvalue problem, we determine the Jacobian of the fixed-point iteration for the k -effective eigenvalue problem. We define the matrices \mathbf{X} and \mathbf{Y}

$$\mathbf{X} = \mathbf{H}_z^{-1} \mathbf{L}^+ \boldsymbol{\Sigma}_s \mathbf{L}, \quad (4.30)$$

$$\mathbf{Y} = \mathbf{H}_z^{-1} \mathbf{L}^+ \boldsymbol{\Sigma}_f \mathbf{L}. \quad (4.31)$$

Equation 4.13 can then be written as

$$\boldsymbol{\Psi} = \mathbf{X}\boldsymbol{\Psi} + \gamma(\boldsymbol{\Psi})\mathbf{Y}\boldsymbol{\Psi}, \quad (4.32)$$

where the k -effective eigenvalue update (Eq. 4.18) is given by

$$\gamma(\boldsymbol{\Psi}) = \frac{\boldsymbol{\Psi}^T \boldsymbol{\Psi} - \boldsymbol{\Psi}^T \mathbf{X} \boldsymbol{\Psi}}{\boldsymbol{\Psi}^T \mathbf{Y} \boldsymbol{\Psi}} = \frac{1}{k(\boldsymbol{\Psi})}. \quad (4.33)$$

Differentiating Eq. 4.32 with respect to the vector $\boldsymbol{\Psi}$, we obtain the Jacobian of the Rayleigh quotient Fixed Point method for k -effective eigenvalue problems:

$$\mathbf{J}_k(\boldsymbol{\Psi}) = \mathbf{Y}\boldsymbol{\Psi}\gamma'(\boldsymbol{\Psi})^T + \mathbf{X} + \gamma(\boldsymbol{\Psi})\mathbf{Y}. \quad (4.34)$$

The inverse Rayleigh quotient update derivative is given by

$$\gamma'(\boldsymbol{\Psi}) = \frac{[2\boldsymbol{\Psi} - (\mathbf{X} + \mathbf{X}^T)\boldsymbol{\Psi}] (\boldsymbol{\Psi}^T \mathbf{Y} \boldsymbol{\Psi}) - (\boldsymbol{\Psi}^T \boldsymbol{\Psi} - \boldsymbol{\Psi}^T \mathbf{X} \boldsymbol{\Psi}) [(\mathbf{Y} + \mathbf{Y}^T)\boldsymbol{\Psi}]}{(\boldsymbol{\Psi}^T \mathbf{Y} \boldsymbol{\Psi})^2}. \quad (4.35)$$

Simplifying, we obtain

$$\gamma'(\boldsymbol{\Psi}) = \frac{[2\boldsymbol{\Psi} - (\mathbf{X} + \mathbf{X}^T)\boldsymbol{\Psi}] - \gamma(\boldsymbol{\Psi})[(\mathbf{Y} + \mathbf{Y}^T)\boldsymbol{\Psi}]}{(\boldsymbol{\Psi}^T \mathbf{Y} \boldsymbol{\Psi})}. \quad (4.36)$$

The Jacobian matrix for the Rayleigh Quotient Fixed Point method for k -effective eigenvalue problems can then be written as

$$\mathbf{J}_k(\boldsymbol{\Psi}) = \mathbf{Y}\boldsymbol{\Psi} \left[\frac{[2\boldsymbol{\Psi} - (\mathbf{X} + \mathbf{X}^T)\boldsymbol{\Psi}] - \gamma(\boldsymbol{\Psi})[(\mathbf{Y} + \mathbf{Y}^T)\boldsymbol{\Psi}]}{(\boldsymbol{\Psi}^T \mathbf{Y} \boldsymbol{\Psi})} \right]^T + \mathbf{X} + \gamma(\boldsymbol{\Psi})\mathbf{Y} \quad (4.37)$$

4.5 Conclusion

We have derived a Rayleigh quotient fixed point method for alpha- and k -effective eigenvalue problems. From the matrix form of the criticality eigenvalue equations, a fixed-point

iteration that requires only a transport sweep was developed. Using the properties of primitive matrices, an eigenvalue update that is optimal in the least squares sense was obtained. This eigenvalue corresponds to the positive angular flux eigenvector that solves the criticality eigenvalue problems. The Jacobians of the fixed point methods were derived for the alpha- and k -effective Rayleigh Quotient Fixed Point methods to determine if a problem was expected to converge. In the next chapter, we examine various problems where the RQFP method does not converge and we use the spectral radius of the Jacobian to characterize this behavior. In practice, calculating the Jacobian requires forming the matrices. However, for simple problems, the Jacobian is a useful measure of the convergence behavior and rate of the RQFP methods.

Chapter 5

Eigenvalues for Infinite Medium Problems

In this chapter we describe the performance of the Rayleigh quotient methods for various infinite medium problem selected from the *Analytical Benchmark Test Set for Criticality Code Verification* [40] or analytical benchmark solutions. Some problems were selected that did not meet the assumptions used in deriving the RQFP methods to test the general applicability of the methods. For example, problems with anisotropic scattering and fissioning only in specific energy groups were selected to verify whether the RQFP methods would converge when the primitivity condition no longer applied. The Rayleigh quotient method was compared to the critical search method [2] for alpha-eigenvalue problems and to standard power iteration for k -effective eigenvalue problems. The total number of transport sweeps, the action of \mathbf{H}_z^{-1} on the source vector, was compared for each method as they represent the majority of computational expense in standard transport codes. The methods were implemented in ARDRA, a 1D, 2D, and 3D deterministic discrete ordinates neutron and gamma transport code developed and maintained by Lawrence Livermore National Laboratory [19].

5.1 Criticality Benchmark One-Speed Verification for Various Critical and Supercritical Problems

A set of six one-material infinite medium supercritical problems were selected from the *Analytical Benchmark Test Set for Criticality Code Verification* [40] to test the Rayleigh Quotient Fixed Point method for both alpha-eigenvalue and k -effective eigenvalue problems. Each problem was modeled as a slab with reflective boundary conditions on both sides. The slab was discretized using diamond differencing discretization in space ($M = 2$) and S_2 discrete ordinates Legendre quadrature ($L = 2$) in angle [5]. The eigenvector/eigenvalue residual was converged to a tolerance of 10^{-12} . These problems were selected as they contained cross sections of commonly used fissile isotopes in nuclear engineering applications such as plutonium-239 and uranium-235 (Table 5.1). Sood Criticality Benchmark Problems

Table 5.1: Sood Criticality Benchmark Infinite Medium Problem Cross Sections (cm^{-1}) in [40]

Cross Section Set	σ	$\nu\sigma_f$	σ_s	v [cm/s]
Sood Prob. 1	0.32640	0.264384	0.225216	1.0
Sood Prob. 5	0.231744	0.264384	0.225216	1.0
(a) Plutonium-239-like Cross Section Sets				
Cross Section Set	σ	$\nu\sigma_f$	σ_s	v [cm/s]
Sood Prob. 11	0.32640	0.176256	0.248064	1.0
Sood Prob. 15	0.32640	0.18259475328	0.248064	1.0
Sood Prob. 17	0.32640	0.17673306624	0.248064	1.0
Sood Prob. 19	0.32640	0.17489804544	0.248064	1.0
(b) Uranium-235-like Cross Section Sets				

1 and 5 consisted of two sets of plutonium-239-like cross sections, each with a different k_∞ values. Sood Criticality Benchmark Problems 11, 15, 17, and 19 consisted of four uranium-235-like cross section sets used to characterize a system approaching the critical state. The reference eigenvalues for these problems can be seen in Table 5.2. For one-speed problems, the velocity was set to 1 cm/s unless otherwise noted.

For the supercritical one-speed criticality benchmark problems, the alpha-eigenvalue Rayleigh Quotient Fixed Point method performed substantially better than the critical search method, reducing the number of transport sweeps by a factor of 30 (Table 5.2a). Reductions in transport sweeps were achieved by removing the need for intermediate k -effective eigenvalue calculations. In the critical search method, two sets of k -effective eigenvalue calculations are required before the linear interpolation or extrapolation of the alpha-eigenvalue can be done. Subsequent updates of the alpha-eigenvalue are dependent on the bracketing procedure finding the correct alpha-eigenvalue. With each update of the alpha-eigenvalue requiring a converged k -effective eigenvalue calculation, the number of transport sweeps increases rapidly. The computation expense of one iteration of the alpha-eigenvalue RQFP method is the same as one iteration of the k -effective eigenvalue calculation. Since there is no need for any intermediate calculations, the Rayleigh Quotient Fixed Point method can calculate the eigenvalue/eigenvector pair directly, avoiding this drawback of the critical search method and drastically reducing the number of total sweeps necessary. In one particular instance, the bracketing procedure of the critical search method failed and the method did not converge. An example of the convergence behavior of the alpha-eigenvalue RQFP method is shown for the PUa cross section set infinite medium problem in Figure 5.1a.

These plots show that the convergence rate for the RQFP methods is linear in general for all problems. For these very supercritical systems, the Rayleigh Quotient Fixed Point method was able to calculate the supercritical alpha-eigenvalues without issue.

The RQFP for the k -effective eigenvalue reduces the number of sweeps by a factor of three (Table 5.2b) as compared to the power method with the fission source norm update. In these particular problems, all cells contain fissile material and the angular flux is exactly equal to the fission source to some constant. The rapid convergence of the angular flux by the Rayleigh Quotient Fixed Point method as compared to the power method with fission source norm update results in a substantial reduction in the number of transport sweeps necessary to converge the eigenvector/eigenvalue. While the convergence of the method is linear, it appears in practice to have a lower asymptotic constant coefficient than the power method as seen in Figure 5.1b.

Table 5.2: Reference Eigenvalues and Transport Sweep Comparisons for Sood Criticality Benchmark Infinite Medium Problems in [40]

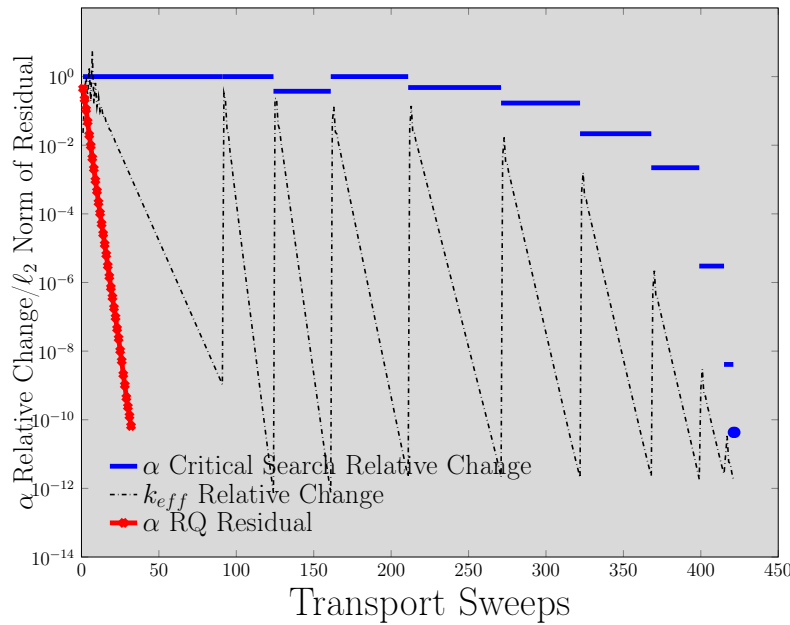
Cross Section Set	Reference α_∞ [s^{-1}]	Transport Sweeps	
		RQFP	Critical Search
Sood Prob. 1	0.1632	29	7,361
Sood Prob. 5	0.257856	40	*
Sood Prob. 11	0.09792	28	6,101
Sood Prob. 15	0.104258753	28	6,426
Sood Prob. 17	0.0983970662	28	6,114
Sood Prob. 19	0.0965620454	28	5,995

*Did Not Converge

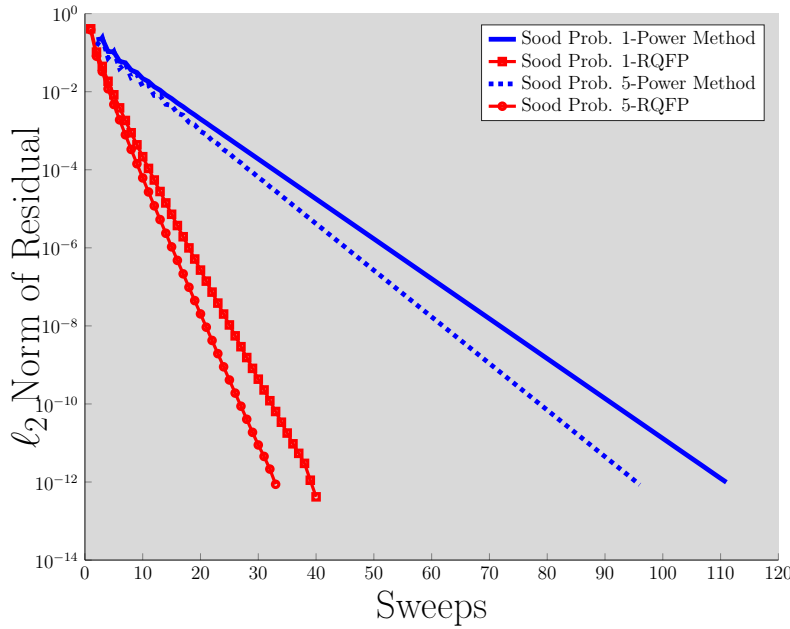
(a) Alpha-Eigenvalue: Comparison of RQFP and Critical Search Transport Sweeps

Cross Section Set	Reference k_∞	Transport Sweeps	
		RQFP	Power Method
Sood Prob. 1	2.612903	41	111
Sood Prob. 5	2.290323	34	96
Sood Prob. 11	2.25	29	130
Sood Prob. 15	2.330917	30	132
Sood Prob. 17	2.256083	27	131
Sood Prob. 19	2.232667	33	131

(b) k -Effective: Comparison of RQFP and Power Method Transport Sweeps



(a) Convergence of Rayleigh Quotient Fixed Point and Critical Search Methods for Sood Prob. 1 Cross Section Set



(b) Eigenvector Residual as a Function of Transport Sweeps for Two Infinite Medium k -Effective Eigenvalue Problems

Figure 5.1: Convergence Behavior for the Rayleigh Quotient Fixed Point Methods for Selected Infinite Medium Problems

5.2 Infinite Medium Multigroup Problems

In this section, we consider various analytical multigroup infinite medium problems with analytic expressions for the alpha- and k -effective eigenvalues. The problems are divided into subcritical, critical, and supercritical problems. The subcritical and critical problems consist of ten variations of a three energy-group problem cross section set. For the supercritical case, we examine three 81 energy-group cross section sets. We discuss the performance of the Rayleigh Quotient Fixed Point method for these problems and discuss various cases where the method fails to converge to the correct eigenvalue. The alpha-eigenvalue spectra of these problems are examined to demonstrate in what cases the method is expected to fail and how violating the assumptions used in deriving the methods affects the performance of the method.

5.2.1 Analytical Subcritical & Critical Problems

Problem 5.2.1.1: We consider a three energy group problem from [41] with cross sections shown in Table 5.3. The problem only has fissions in the fast energy group, $g = 3$, emitting $\bar{\nu}$ neutrons in energy group $g = 1$. There is no upscatter, and downscatter only occurs into the next group. We vary $\bar{\nu}$ from zero neutrons emitted in fission to $\bar{\nu} = 3$ to create various subcritical systems. The analytic k -eigenvalue is given by

$$k = \frac{\bar{\nu}\sigma_{f,1}\sigma_{s12}\sigma_{s23}}{\sigma_1\sigma_2\sigma_3}, \quad (5.1)$$

and the analytical alpha-eigenvalue can be calculated from the system

$$\begin{pmatrix} -v_1\sigma_1 & v_1\sigma_{s12} & 0 \\ 0 & -v_2\sigma_2 & v_2\sigma_{s23} \\ v_1\bar{\nu}\sigma_{f1} & 0 & -v_3\sigma_3 \end{pmatrix} \begin{pmatrix} \phi_1 \\ \phi_2 \\ \phi_3 \end{pmatrix} = \alpha \begin{pmatrix} \phi_1 \\ \phi_2 \\ \phi_3 \end{pmatrix}. \quad (5.2)$$

The reference eigenvalues and the number of transport sweeps needed to converge the eigenvector residuals to a value of 10^{-8} are seen in Table 5.4.

For alpha-eigenvalue problems, the Rayleigh Quotient Fixed Point method is able to converge the various subcritical problems to the correct eigenvalue. The number of sweeps necessary varies, with the most subcritical and closest to critical problems requiring more sweeps to converge the angular flux. The critical search method is unable to converge these problems as the sum of the total cross section and the negative eigenvalue introduces negative absorption into the system (Table 5.4a). This pseudo-absorption term causes instabilities in the transport sweep algorithm and forces the method to terminate before convergence. We see that for even simple, three energy group, subcritical problems, the Rayleigh Quotient Fixed Point method is able to converge very subcritical problems and critical problems without difficulty.

For k -effective eigenvalue problems, the Rayleigh Quotient Fixed Point method requires a similar number of sweeps for all values of k_∞ . It requires approximately 40% more iterations

than the traditional power method (Table 5.4b). One reason for this is that the fission source of Problem 5.1.1 is simple, with fissions only occurring in the highest energy group and neutrons are only born in the lowest energy group. Using the fission distribution as the norm is better in this particular case because it does not require all energy group scalar fluxes to converge.

Table 5.3: Infinite Medium Subcritical Problem Cross Sections (cm^{-1}) for Problem 5.2.1.1

g	σ	σ_f	$\sigma_{sg,g+1}$	χ	v_g [cm/s]
1	6.0	0.0	5.0	1.0	4.0
2	5.0	0.0	4.0	0.0	2.0
3	4.0	2.0	0.0	0.0	1.0

Table 5.4: Reference Eigenvalues/Transport Sweeps for Convergence for Problem 5.2.1.1

Transport Sweeps				Transport Sweeps			
$\bar{\nu}$	α_∞	RQFP	Critical Search	$\bar{\nu}$	α_∞	RQFP	Critical Search
0.30	-3.30687	89	*	1.80	-1.15114	48	*
0.60	-2.75305	48	*	2.10	-0.83485	56	*
0.90	-2.28186	35	*	2.40	-0.53965	66	*
1.20	-1.86682	38	*	2.70	-0.26222	77	*
1.50	-1.49303	43	*	3.00	0.00000	91	*

*Did Not Converge

(a) Alpha-Eigenvalue: Comparison of RQFP and Critical Search Transport Sweeps

Transport Sweeps				Transport Sweeps			
$\bar{\nu}$	k_∞	RQFP	Power Method	$\bar{\nu}$	k_∞	RQFP	Power Method
0.30	0.10	76	53	1.80	0.60	74	50
0.60	0.20	74	49	2.10	0.70	74	51
0.90	0.30	74	40	2.40	0.80	72	51
1.20	0.40	74	48	2.70	0.90	72	51
1.50	0.50	74	50	3.00	1.00	72	52

(b) k -Effective Eigenvalue: Comparison of RQFP and Power Method Transport Sweeps

5.2.2 Analytical Infinite Medium Supercritical Problems

Problem 5.2.2.1: We consider a $G = 81$ energy group medium with cross sections shown in Table 5.5 from [41]. Neutrons can only downscatter to the next energy group ($\sigma_{s,gg} = 0 \forall g$) and prompt fissions in energy group $g = 81$ emit $\bar{\nu} = 2.5$ neutrons per fission into energy group $g = 1$.

The total cross sections σ_g , neutron speeds v_g , and neutron removal cross sections are the same for all groups. With these cross sections, this unphysical problem yields an analytical solution for both k -effective and alpha-eigenvalues. The k -effective eigenvalue is given by

$$k = \frac{\bar{\nu}\sigma_f(\sigma_{sg,g+1})^{G-1}}{(\sigma_g)^G} = 1.11663. \quad (5.3)$$

Using the multigroup equations, the analytical expression for the alpha-eigenvalues is found to be

$$\frac{\alpha_n}{v} = -(\sigma_g - \sigma_f) + \sigma_{sg,g+1} \left[\bar{\nu}^{G-1} \exp\left(\frac{2\pi i n}{G}\right) - 1 \right], \text{ for } n = 0, \dots, G-1. \quad (5.4)$$

The alpha-eigenvalues are located along a circle in the complex plane centered on the real axis at $\text{Re}(\alpha) = -(\sigma_g - \sigma_f)$ with radius $r = \bar{\nu}^{G-1} \sigma_{gs,s+1}$. Using this expression, the fundamental alpha-eigenvalue is found to be $\alpha_0 = 0.13765 \text{ s}^{-1}$.

The number of transport sweep needed to converge to a eigenvalue residual of 10^{-8} for Problem 5.2.2.1 can be seen in Table 5.6. We note that the alpha-eigenvalue Rayleigh Quotient Fixed Point method does not converge for this problem. The failure to converge for this problem can be explained as follows. The alpha-eigenvalue spectrum for Problem 5.2.2.1 can be seen in Figure 5.2 and shows that all eigenvalues lie on a circle. Therefore, there are some eigenvalues that are equal in magnitude to the eigenvalue that corresponds to the positive eigenvector that we are seeking to find. Since the Rayleigh Quotient Fixed Point method is looking for the positive eigenvector corresponding to the dominant eigenvalue, it is unable to find the unique eigenvalue corresponding to the positive eigenvector. The spectral radius of the Jacobian matrix of the Rayleigh Quotient Fixed Point method at the fixed point (Section 4.3) was found to be larger than one, implying the method will not converge. It is interesting to note the method cycles with period 81, indicating that it goes through every single eigenvalue unsuccessfully before failing to converge.

Both the k -effective eigenvalue Rayleigh Quotient Fixed Point method and the power method converge for this particular problem requiring a similar number of iterations. The fact that the k -effective eigenvalue is the dominant eigenvalue with a corresponding positive eigenvector allows the Rayleigh Quotient Fixed Point method to converge to the right eigenvalue and eigenvector. In this particular problem, all other eigenvalues except for the dominant eigenvalue are zero. Both methods require a large number of iterations, reflecting the unphysical nature of the problem cross sections.

Table 5.5: Infinite Medium 81-Group Problem Cross Sections (cm^{-1})

g	σ	σ_f	$\sigma_{sg,g+1}$	χ	v_g [cm/s]
1	101.0	0.0	100.0	1.0	1.0
2-80	101.0	0.0	100.0	0.0	1.0
81	101.0	100.0	0.0	0.0	1.0

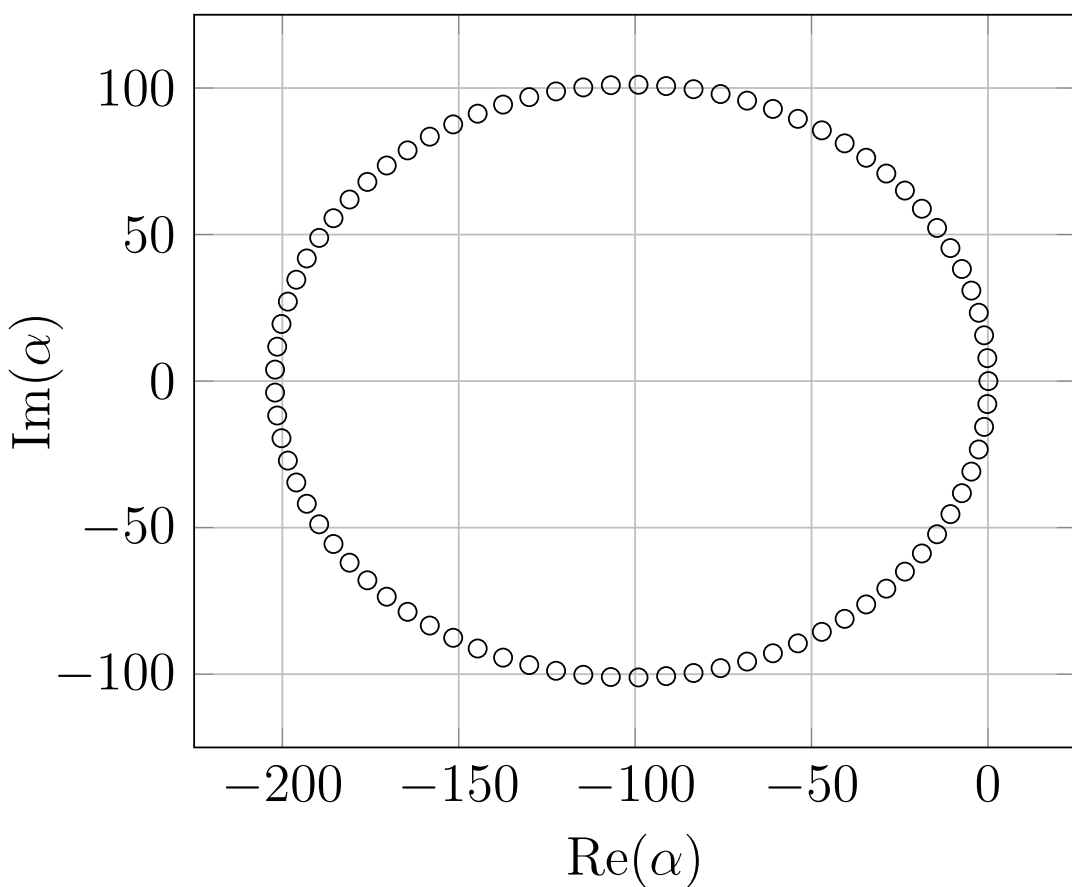


Figure 5.2: Alpha-Eigenvalue Spectrum for Problem 5.2.2.1

Table 5.6: Transport Sweep Comparisons for Problem 5.2.2.1

Transport Sweeps		
α (s ⁻¹)	RQFP	Critical Search
0.13765	*	63,843

*Did Not Converge

(a) Alpha-Eigenvalue: Comparison of RQFP and Critical Search Sweeps

Transport Sweeps		
k_{eff}	RQFP	Power Method
1.11663	6,701	6,707

(b) k -Effective: Comparison of RQFP and Critical Search Sweeps

Problem 5.2.2.2: We consider a problem similar to Problem 5.2.1.1 where the energy group velocities are group-dependent. The velocity of each group is given by $v_g = 82 - g$ and the cross sections are the same as Problem 5.2.1.1 (Table 5.7). The k -effective eigenvalue remains 1.11663 as only the velocity terms have been modified. The problem no longer has an analytical expression for the alpha-eigenvalue spectrum. The dominant alpha-eigenvalue is found to be 2.2464 s⁻¹ from numerical eigenvalue solvers. With the change in the velocity, the alpha-eigenvalue spectrum eigenvalues are no longer on a circle (Figure 5.3). Instead, the eigenvalues are along elliptical shapes with very negative real eigenvalues now existing.

Similar to Problem 5.2.2.1, the alpha-eigenvalue Rayleigh Quotient Fixed Point method does not converge for this method. The spectral radius of the Jacobian matrix for the fixed-point formulation evaluated at the fixed point is found to be larger than one, implying the method will not converge for this problem. The critical search method is able to converge the alpha-eigenvalue. However, it requires a large number of iterations (Table 5.8a).

Also similar to Problem 5.2.2.1, both the Rayleigh Quotient Fixed Point method and power method were able to converge the k -effective eigenvalue. This is expected as the only change from Problem 5.2.2.1 was in the group velocities which do not matter in the k -effective eigenvalue problem. The number of transport sweeps required to converge the problem did not change (Table 5.8b).

Table 5.7: Infinite Medium 81-Group Problem Cross Sections (cm^{-1}), Velocity Modification

g	σ	σ_f	$\sigma_{sg,g+1}$	χ	v_g [cm/s]
1	101.0	0.0	100.0	1.0	1.0
2-80	101.0	0.0	100.0	0.0	2.0-80.0
81	101.0	100.0	0.0	0.0	81.0

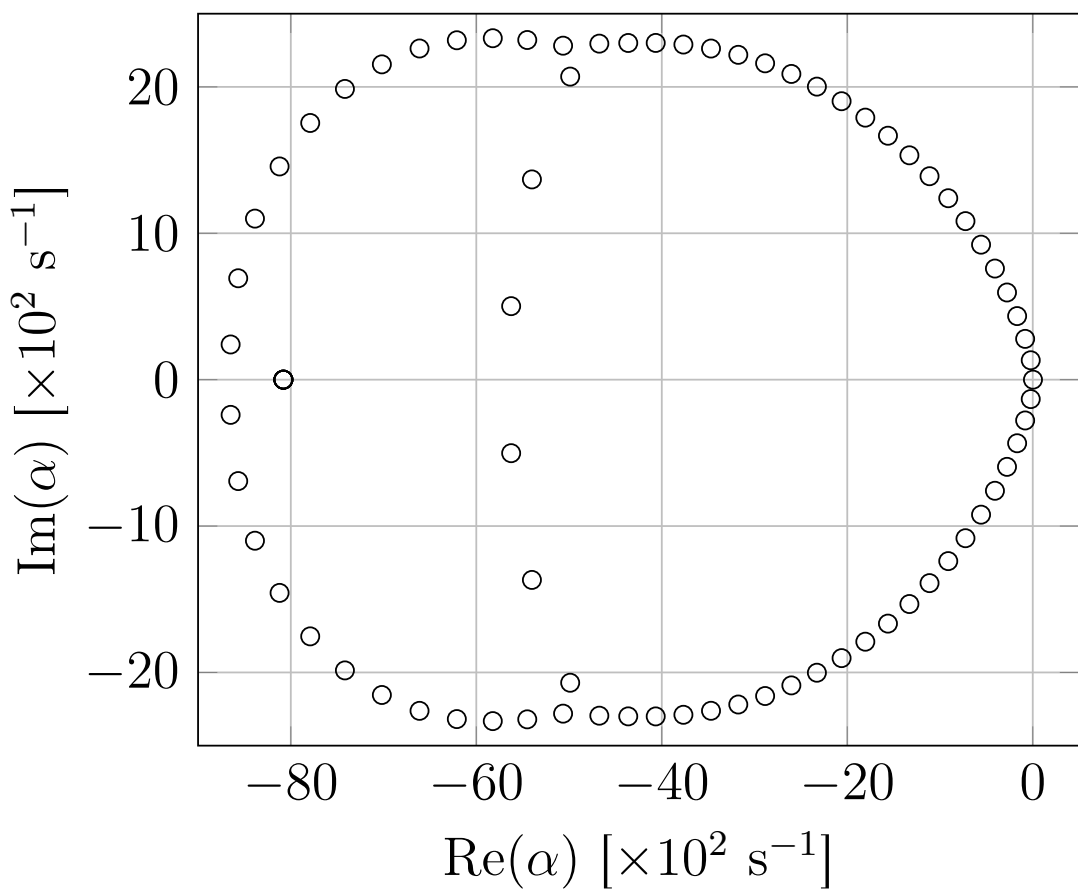


Figure 5.3: Alpha-Eigenvalue Spectrum for Problem 5.2.2.2

Table 5.8: Transport Sweep Comparisons for Problem 5.2.2.2

Transport Sweeps		
α (s^{-1})	RQFP	Critical Search
2.2464	*	50,773

*Did Not Converge

(a) Alpha-Eigenvalue: Comparison of RQFP and Critical Search Sweeps

Transport Sweeps		
k_{eff}	RQFP	Power Method
1.11663	6,701	6,707

(b) k -Effective: Comparison of RQFP and Critical Search Sweeps

Problem 5.2.2.3: We consider another problem similar to Problem 5.2.1.1 where we now allow downscattering from energy group $g \rightarrow g'$ over several energy groups with equal probability where $g + 1 \leq g' \leq g + 5$. For the last five energy groups, the downscattering cross section is equally distributed among the remaining groups where $g + 1 \leq g' \leq G$. The total scattering cross section remains unchanged. The k -effective eigenvalue is 1.8853 and the alpha-eigenvalue is $2.2914\ s^{-1}$.

The alpha-eigenvalue spectrum seen in Figure 5.4 is significantly different to that of Problem 5.2.2.1. The spectrum contains more eigenvalues with large real negative parts. This is due to neutrons being able to downscatter quickly by skipping several energy groups.

The alpha-eigenvalue Rayleigh Quotient Fixed Point method was able to converge on the analytical alpha-eigenvalue. By allowing downscattering to more energy groups, the Jacobian of the fixed-point method at the fixed point is now less than one, allowing the convergence of the method (Section 4.3). In this particular problem, the alpha-eigenvalue RQFP method vastly outperforms the critical search method. The critical search method requires 20 times the number of sweeps the RQFP method does (Table 5.9a). This is caused by the need for multiple k -effective eigenvalue calculations to bracket the alpha-eigenvalue.

Both the Rayleigh Quotient Fixed Point method and power method with fission norm update were able to converge the eigenvalue and eigenvector for the k -effective eigenvalue problem requiring a similar number of iterations (Table 5.9b).

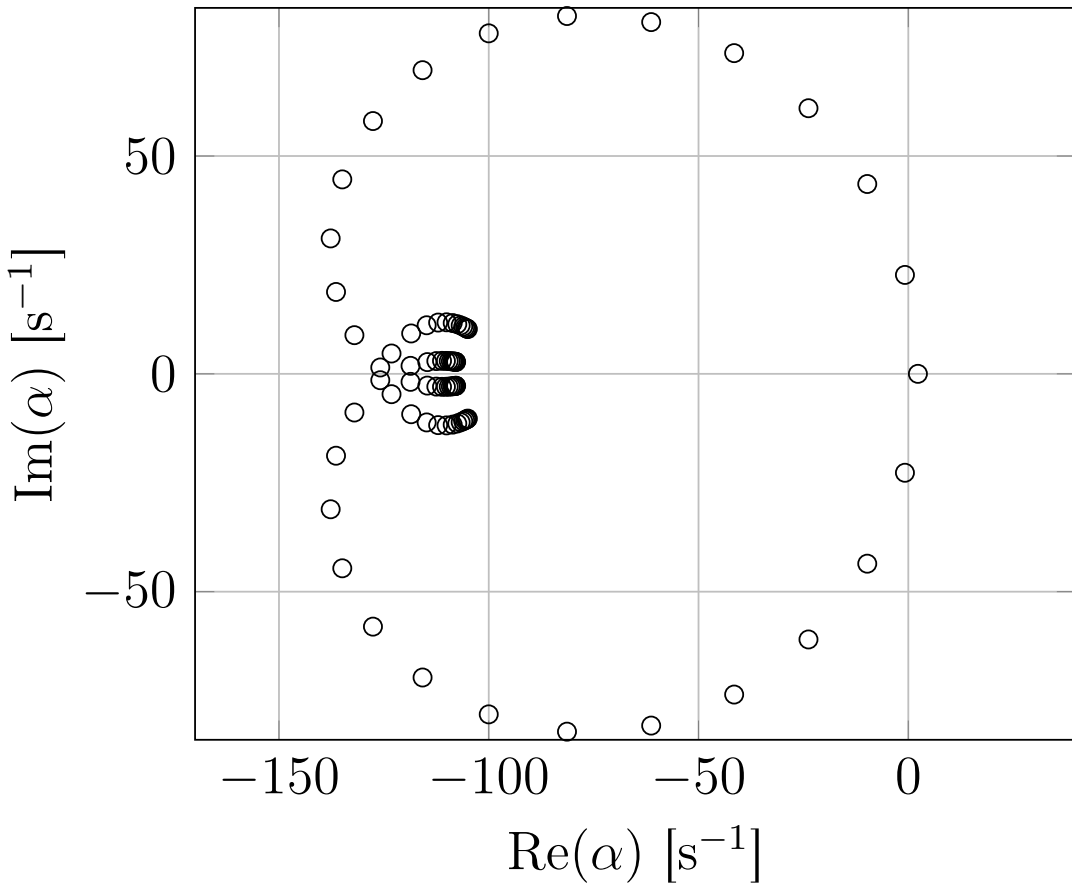


Figure 5.4: Alpha-Eigenvalue Spectrum for Problem 5.2.2.3

Table 5.9: Transport Sweep Comparisons for Problem 5.2.2.3

Transport Sweeps		
α (s^{-1})	RQFP	Critical Search
2.2914	5,516	105,570

(a) Alpha-Eigenvalue: Comparison of RQFP and Critical Search Sweeps

Transport Sweeps		
k_{eff}	RQFP	Power Method
1.8853	5,306	5,080

(b) k -Effective: Comparison of RQFP and Critical Search Sweeps

5.3 Conclusion

The RQFP method for alpha- and k -effective eigenvalues performs well for infinite medium problems, reducing in certain cases the number of iterations up to a factor of twenty. For the alpha-eigenvalue RQFP method, the method is able to converge subcritical systems without issue. For a certain class of problems with unphysical cross sections, the alpha-eigenvalue RQFP method fails to converge. This failure to converge is caused by the structure of the alpha-eigenvalue spectrum. However, these problems are special cases, with unphysical data such as unit velocity in all energy groups. For these particular problems, it is found that the spectral radius of the Jacobian matrix implies convergence is not possible. For this reason, we believe the alpha-eigenvalue RQFP method is robust for all infinite-medium problems of interest. The RQFP method for k -effective eigenvalue calculations performed better or similar to the power method with a fission norm update for the eigenvalue. For problems where only the number of neutrons emitted in fission was varied, the RQFP method took a similar number of iterations to converge for all problems, no matter the criticality of the system. This suggests that the method's convergence is determined by the eigenvector shape rather than the eigenvalue.

Chapter 6

Eigenvalues of Slabs and Spheres

In this chapter we verify the correctness and examine the performance of the Rayleigh Quotient Fixed Point methods for one-dimensional media such as slabs and one-dimensional spheres. In slab geometry, the phase space of the neutron transport equation is simplified with only one position variable x and one angular variable μ defined as the x -direction cosine. For slab geometry, the alpha- and k -effective eigenvalue neutron transport equations are given by Eq. 6.1 and Eq. 6.2, respectively:

$$\begin{aligned} & \left[\mu \frac{\partial}{\partial x} + \frac{\alpha}{v(E)} + \sigma(x, E) \right] \psi(x, \mu, E) \\ &= \frac{\chi(E)}{2} \int_0^\infty dE' \nu(E') \sigma_f(x, E') \int_{-1}^1 d\mu' \psi(x, \mu', E) \\ &+ \frac{1}{2} \int_0^\infty dE' \sigma_s(x, E' \rightarrow E) \int_{-1}^1 d\mu' \psi(x, \mu', E), \quad (6.1) \end{aligned}$$

$$\begin{aligned} & \left[\mu \frac{\partial}{\partial x} + \sigma(x, E) \right] \psi(x, \mu, E) \\ &= \frac{1}{k} \frac{\chi(E)}{2} \int_0^\infty dE' \nu(E') \sigma_f(x, E') \int_{-1}^1 d\mu' \psi(x, \mu', E) \\ &+ \frac{1}{2} \int_0^\infty dE' \sigma_s(x, E' \rightarrow E) \int_{-1}^1 d\mu' \psi(x, \mu', E). \quad (6.2) \end{aligned}$$

Various homogeneous and heterogeneous slab geometry problems with vacuum boundary conditions were modeled in ARDRA. These slab media problems consist of multiplying and non-multiplying materials with thicknesses Δ . Alpha- and k -effective eigenvalues were calculated and the number of transport sweeps compared to various methods such as the critical search method and the power method. To verify the correctness of the Rayleigh Quotient

Fixed Point method, the method was compared to various methods such as Green's Function Method (GFM) and Direct Evaluation (DE) and compared to other discrete ordinate neutron transport codes such as Los Alamos National Laboratory's PARTISN/DANT [20].

In one-dimensional spherical geometry, there is only one position variable r , the radial position from the center of the sphere, and one angular variable μ defined as the direction cosine with respect to the radial direction. For spherical geometry, the alpha- and k -effective eigenvalue neutron transport equations are given by Eq. 6.4 and Eq. 6.3, respectively:

$$\begin{aligned} \frac{\mu}{r^2} \frac{\partial}{\partial r} \left[r^2 \psi(r, \mu, E) \right] + \frac{1}{r} \frac{\partial}{\partial \mu} \left[(1 - \mu^2) \psi(r, \mu, E) \right] + \left[\frac{\alpha}{v(E)} + \sigma(x, E) \right] \psi(r, \mu, E) \\ = \frac{\chi(E)}{2} \int_0^\infty dE' \nu(E') \sigma_f(r, E') \int_{-1}^1 d\mu' \psi(r, \mu', E) \\ + \frac{1}{2} \int_0^\infty dE' \sigma_s(r, E' \rightarrow E) \int_{-1}^1 d\mu' \psi(r, \mu', E). \quad (6.3) \end{aligned}$$

$$\begin{aligned} \frac{\mu}{r^2} \frac{\partial}{\partial r} \left[r^2 \psi(r, \mu, E) \right] + \frac{1}{r} \frac{\partial}{\partial \mu} \left[(1 - \mu^2) \psi(r, \mu, E) \right] + \sigma(x, E) \psi(r, \mu, E) \\ = \frac{1}{k} \frac{\chi(E)}{2} \int_0^\infty dE' \nu(E') \sigma_f(r, E') \int_{-1}^1 d\mu' \psi(r, \mu', E) \\ + \frac{1}{2} \int_0^\infty dE' \sigma_s(r, E' \rightarrow E) \int_{-1}^1 d\mu' \psi(r, \mu', E), \quad (6.4) \end{aligned}$$

For one-dimensional spherical geometry, various homogeneous and heterogeneous spherical problems with vacuum boundary conditions were modeled in ARDRA. Using the same cross-sections for multiplying and non-multiplying materials as the slab media problems, equivalent spherical systems were created using the Davison sphere-equivalence theorem [42] and the alpha-eigenvalue calculated. To verify the correctness of the RQFP for one-dimensional spherical geometry, the method was compared to GFM. Performance of the RQFP for one-dimensional spherical problems was measured by comparing the number of transport sweeps necessary for convergence as compared to the critical search method.

6.1 One-Speed Verification for Slab Geometry

In this section, we verify the correctness of the RQFP method in slab geometry for various one-speed cross section sets. These cross section sets are from [10] and have analytical alpha-eigenvalues determined by the GFM [10], described in Section 2.2.1. These analytical alpha-eigenvalues were used to verify the correctness of the RQFP method. Each cross section set was used in a variety of problems where problem parameters such as slab thickness, the

number of neutrons emitted in fission, and materials were varied to achieve various alpha-eigenvalues. Verification of the RQFP method for alpha-eigenvalue problems was determined by comparing RQFP-calculated alpha-eigenvalues to the analytical values determined by the GFM.

6.1.1 A Set of Non-Multiplying Purely-Scattering Slabs

The first cross section set considered consisted of a non-multiplying purely-scattering material with cross sections given in Table 6.1. The neutron speed was set to $v = 1 \text{ cm/s}$ as in [10] and the total cross section set to unity, $\sigma = 1 \text{ cm}^{-1}$.

Table 6.1: Non-Multiplying Purely-Scattering Material Cross Sections (cm^{-1}) from [10]

σ	$\nu\sigma_f$	σ_s	$v [\text{cm/s}]$
1.0	0.0	1.0	1.0

Five slabs of thicknesses $\Delta = 1, 5, 10, 25$, and 25 mean free paths (mfps) were modeled using diamond difference discretization ($M = 500$ cells) and S_{64} discrete ordinates quadrature ($L = 64$). 500 spatial cells and 64 angular quadrature points were selected to guarantee the positivity of the flux solution for all slab widths.

Compared to the GFM alpha-eigenvalues, the RQFP-calculated alpha-eigenvalues showed good agreement with relative error being less than 0.1% for all five slab thicknesses as shown in Table 6.2. The greatest discrepancy between the two methods was for $\Delta = 1.0$ mfp. In [10], it is noted that the GFM has difficulty obtaining accurate eigenvalue results for thin slabs. This is due to the sensitivity of the alpha-eigenvalue to the discretization process where different discretization parameters can substantially change the calculated alpha-eigenvalue of the system. The RQFP method also shares the same behavior as discretization can change the alpha-eigenvalue of the system. However, as the slab thickness increases, the alpha-eigenvalue becomes less sensitive to discretization and both methods are in closer agreement with the relative error between RQFP and the GFM decreasing. We note that the number of transport sweeps necessary to converge the alpha-eigenvalue to a tolerance of 10^{-12} increases as problem thickness increases. Physically, this can be explained as follows: as the slab thickness increases, neutrons will have to travel longer before leaking from the system. Since the alpha-eigenvalue is determined by the last neutron to leave the system, the increased transit time means a neutron will undergo many more interactions before finally exiting the system, thus increasing the number of iterations required to converge the fundamental angular flux mode. For problems without any multiplication, the k -effective eigenvalue is not defined.

Table 6.2: Comparison of RQFP- and GFM-calculated Alpha-Eigenvalues for a Homogeneous Scattering Slab

Δ	Alpha-Eigenvalue/Percent Relative Error		
	RQFP	GFM	RQFP/GFM % Relative Error
1	-6.08420×10^{-1}	-6.08072×10^{-1}	0.057189
5	-8.10966×10^{-2}	-8.10933×10^{-2}	0.004113
10	-2.53506×10^{-2}	-2.53500×10^{-2}	0.002349
20	-7.18015×10^{-3}	-7.17962×10^{-3}	0.007358
25	-4.71736×10^{-3}	-4.71722×10^{-3}	0.002966

$M = 500$, $L = 64$, Tolerance = 10^{-12}

6.1.2 A Set of Multiplying Homogeneous Slabs

A fissile material cross section set was considered for 22 one-speed slabs of varying thickness Δ . The total cross section was set to unity and the slab neutron multiplication set to $\nu\sigma_f = 0.25$. The scattering cross section was set to $\sigma_s = 0.9 \text{ cm}^{-1}$ as seen in Table 6.3.

Table 6.3: Multiplying Homogeneous Material Cross Sections (cm^{-1}) from [10]

σ	$\nu\sigma_f$	σ_s	$v [\text{cm}/\text{s}]$
1.0	0.25	0.9	1.0

For slabs of thicknesses ranging from $\Delta = 1.0$ to $\Delta = 50.0$ mfp the RQFP-calculated alpha-eigenvalues showed good agreement with the GFM-calculated eigenvalues with the exception of thin slabs. For thin slabs of up to width $\Delta = 1.0$ mfp, percent relative error was substantial with percent relative error as high as 17%. As before, this was caused by the sensitivity of the alpha-eigenvalue to the discretization used by both the GFM and the RQFP method. Similar to the non-multiplying slabs, as the slab thickness increased, agreement was substantially better as shown in Table 6.4, with percent relative error being less than 0.1% for all slabs of thickness greater than one mfp.

With the correctness of the RQFP method verified, the alpha-eigenvalue RQFP method was compared to the critical search method (Table 6.5a). The RQFP method substantially outperformed the critical search method in all cases and was able to converge subcritical alpha-eigenvalues that the critical search method could not determine. As the problem thickness increased, the slab problem became more supercritical and the number of transport sweeps necessary to converge increased for both methods. For the most supercritical slab ($\Delta = 50.0$ mfp), the number of sweeps necessary for the RQFP method to converge was

less than the number of transport sweeps necessary for critical search to converge for the $\Delta = 4.0$ mfp case. Since the RQFP method requires no intermediate k -effective eigenvalue calculations, the method substantially reduced the number of transport sweeps necessary as there was no need to do multiple k -effective eigenvalue calculations to bracket the alpha-eigenvalue.

For the one-speed homogeneous multiplying slabs of varying thickness, the k -effective eigenvalue RQFP method was compared to the power method with the fission norm update. It was seen that the number of transport sweeps for convergence increased as the k -effective eigenvalue increased as shown in Table 6.5b. The RQFP method required far more sweeps than the power method, requiring many more sweeps when the slab became more supercritical. For the largest slab, the RQFP method required five times the transport sweeps as the power method.

Table 6.4: Comparison of RQFP- and GFM-calculated Alpha-Eigenvalues for a Homogeneous Scattering Multiplying Slab

Δ	Alpha-Eigenvalue/Percent Relative Error		
	RQFP	GFM	RQFP/GFM % Relative Error
0.25	-1.15480	-9.90300×10^{-1}	16.611352
0.30	-1.06633	-9.74300×10^{-1}	9.446240
0.35	-9.98584×10^{-1}	-9.49350×10^{-1}	5.186069
0.40	-9.42114×10^{-1}	-9.17000×10^{-1}	2.738758
0.45	-8.91833×10^{-1}	-8.79460×10^{-1}	1.406940
0.50	-8.44920×10^{-1}	-8.38790×10^{-1}	0.730822
0.75	-6.34756×10^{-1}	-6.34060×10^{-1}	0.109818
1	-4.69398×10^{-1}	-4.69160×10^{-1}	0.050762
2	-1.36335×10^{-1}	-1.36310×10^{-1}	0.018335
3	-1.39888×10^{-2}	-1.39790×10^{-2}	0.070397
4	4.36998×10^{-2}	4.37050×10^{-2}	0.011811
5	7.54667×10^{-2}	7.54690×10^{-2}	0.003096
6	9.48296×10^{-2}	9.48310×10^{-2}	0.001470
7	1.07508×10^{-1}	1.07510×10^{-1}	0.002137
8	1.16263×10^{-1}	1.16260×10^{-1}	0.002344
9	1.22563×10^{-1}	1.22560×10^{-1}	0.002390
10	1.27248×10^{-1}	1.27250×10^{-1}	0.001492
15	1.39126×10^{-1}	1.39130×10^{-1}	0.002605
20	1.43649×10^{-1}	1.43650×10^{-1}	0.000663
30	1.47066×10^{-1}	1.47070×10^{-1}	0.002483
40	1.48317×10^{-1}	1.48320×10^{-1}	0.001982
50	1.48910×10^{-1}	1.48910×10^{-1}	0.000004

$M = 500, L = 64, \text{Tolerance} = 10^{-12}$

Table 6.5: Transport Sweep Comparisons for Homogeneous Multiplying Slabs

Δ	Transport Sweeps		Transport Sweeps		
	RQFP	Critical Search	Δ	RQFP	Critical Search
0.25	95	*	5	70	33,036
0.30	98	*	6	85	44,655
0.35	99	*	7	103	55,242
0.40	95	*	8	122	63,851
0.45	91	*	9	143	71,181
0.50	84	*	10	166	78,002
0.75	52	*	15	308	89,627
1	34	*	20	495	97,267
2	32	*	30	1,002	98,087
3	43	*	40	1,682	106,055
4	56	21,044	50	2,530	113,189

$M = 500, L = 64, \text{Tolerance} = 10^{-12}$, *Did Not Converge

(a) Alpha-Eigenvalue: Comparison of RQFP and Critical Search Sweeps

Δ	Transport Sweeps		Transport Sweeps		
	RQFP	Power Method	Δ	RQFP	Power Method
0.25	16	17	5	67	37
0.30	16	17	6	81	40
0.35	17	18	7	97	44
0.40	18	19	8	115	47
0.45	18	19	9	133	51
0.50	19	19	10	154	55
0.75	21	21	15	280	81
1	23	22	20	445	115
2	33	27	30	892	206
3	43	31	40	1,490	238
4	54	34	50	2,235	481

$M = 500, L = 64, \text{Tolerance} = 10^{-12}$

(b) k -Effective: Comparison of RQFP and Power Method Transport Sweeps

6.1.3 Heterogeneous Slabs

Problem 6.1.3.1-Non-multiplying Heterogeneous Slab: Five one-speed heterogeneous slab problems consisting of two materials were examined and the RQFP-calculated alpha-eigenvalues compared to the GFM, direct evaluation (DE) [22], and DANT/PARTISN [20].

For the subcritical heterogeneous medium shown in Figure 6.1, five problems were constructed by varying the grain sizes of alternating slabs consisting of materials with the cross sections shown in Table 6.6 from [10]. With a fixed maximum medium width, material slabs of thickness Δ were alternated until reaching the maximum fixed width. The impact of material widths on the alpha-eigenvalue was examined for this non-multiplying medium.

Table 6.6: Non-Multiplying Heterogeneous Material Cross Sections (cm^{-1}) from [10]

Material	σ	$\nu\sigma_f$	σ_s	v_g [cm/s]
1	10.0	0.0	10.0	1.0
2	10.0	0.0	9.0	1.0
Homogeneous	10.0	0.0	9.5	1.0

The maximum width of the domain was fixed at 10.0 mfp as in [10]. Grain sizes of 0.5, 1, 2.5, and 5 mfp were examined. One case consisting of a homogenized material was considered. In all cases, the RQFP method showed good agreement with DANT/PARTISN (Table 6.7a), Green's Function Method (Table 6.7b), and Direct Evaluation (Table 6.7c) with percent relative error within 0.15%. The number of transport sweeps required to obtain the eigenvalue and eigenvector increased as the problem approached critical and the number of regions increased. The scalar fluxes for the four heterogeneous region problems can be seen in Figure 6.2

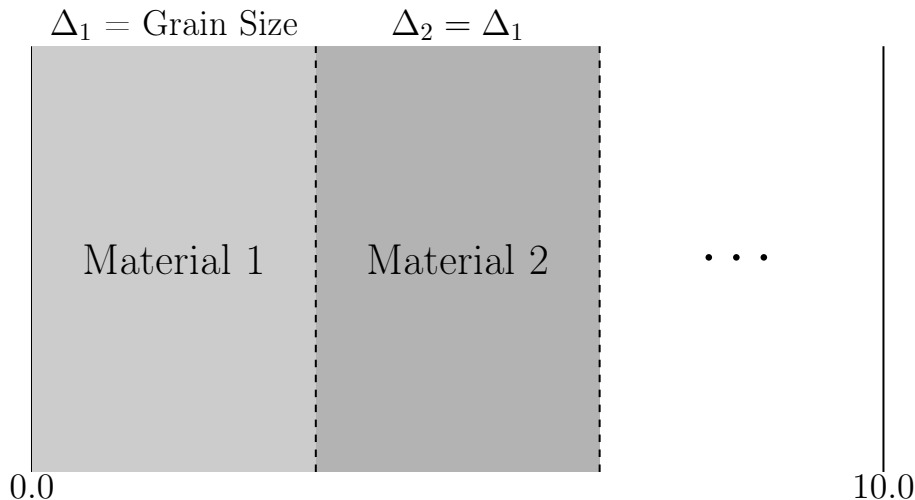


Figure 6.1: Heterogeneous Slab Benchmark Problem Domain

Table 6.7: Comparison of RQFP-calculated eigenvalues to various methods for multi-region scattering slab ($M = 500$, $L = 64$, Tolerance = 10^{-12})

Grain Size	Alpha-Eigenvalue/Percent Relative Error		
	RQFP	DANT/PARTISN	% Relative Error
5 (2 slabs)	-5.51528×10^{-1}	-5.50813×10^{-1}	0.129782
2.5 (4 slabs)	-7.03144×10^{-1}	-7.03134×10^{-1}	0.001470
1 (10 slabs)	-7.48808×10^{-1}	-7.48793×10^{-1}	0.001942
0.5 (20 slabs)	-7.57221×10^{-1}	-7.57199×10^{-1}	0.002882
0 (homogeneous)	-7.63513×10^{-1}	-7.63507×10^{-1}	0.000848

(a) Comparison of RQFP- and DANT/PARTISN-calculated alpha-eigenvalues

Grain Size	Alpha-Eigenvalue/Percent Relative Error		
	RQFP	GFM	% Relative Error
5 (2 slabs)	-5.51528×10^{-1}	-5.50812×10^{-1}	0.129964
2.5 (4 slabs)	-7.03144×10^{-1}	-7.03133×10^{-1}	0.001612
1 (10 slabs)	-7.48808×10^{-1}	-7.48792×10^{-1}	0.002075
0.5 (20 slabs)	-7.57221×10^{-1}	-7.57198×10^{-1}	0.003014
0 (homogeneous)	-7.63513×10^{-1}	-7.63507×10^{-1}	0.000848

(b) Comparison of RQFP- and GFM-calculated alpha-eigenvalues

Grain Size	Alpha-Eigenvalue/Percent Relative Error		
	RQFP	GFM	% Relative Error
5 (2 slabs)	-5.51528×10^{-1}	-5.50812×10^{-1}	0.129964
2.5 (4 slabs)	-7.03144×10^{-1}	-7.03133×10^{-1}	0.001612
1 (10 slabs)	-7.48808×10^{-1}	-7.48792×10^{-1}	0.002075
0.5 (20 slabs)	-7.57221×10^{-1}	-7.57198×10^{-1}	0.003014
0 (homogeneous)	-7.63513×10^{-1}	-7.63507×10^{-1}	0.000848

(c) Comparison of RQFP- and DE-calculated alpha-eigenvalues

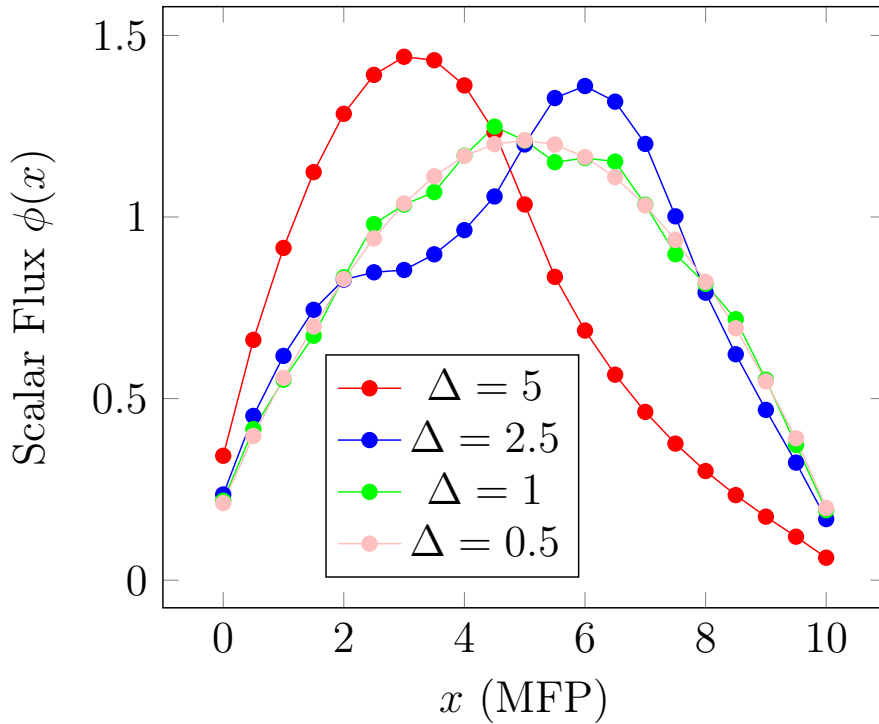


Figure 6.2: Scalar Flux Results for Alternating Slabs Grain Size Problems

Problem 6.1.3.2-Multiplying Two Region Heterogeneous Slab: A two-region multiplying slab was examined with material properties as seen in Table 6.8. The problem consisted of a 1.5 mfp region on the right and a 1.0 mfp region to the left. Both materials were multiplying and the system was supercritical [43].

Table 6.8: Multiplying Heterogeneous Slab Material Cross Sections (cm^{-1})

Material	σ	$\nu\sigma_f$	σ_s	v_g [cm/s]
1	1.0	0.6	0.9	1.0
2	1.0	0.3	0.2	1.0

For the two-region slab problem shown in Figure 6.3), the calculated alpha-eigenvalue and scalar flux were compared to the Green's Function Method. The calculated alpha-eigenvalue $\alpha = 0.142473 \text{ s}^{-1}$ agreed with the GFM eigenvalue. The alpha-eigenvalue RQFP method required 48 iterations to converge the problems to a tolerance of 10^{-12} . The critical search method required 22076 iterations, requiring multiple bracketing attempts. The multiple bracketing attempts were required since the system was close to critical. To verify the correctness of the RQFP alpha-eigenvalue scalar flux, the scalar flux was compared to the GFM scalar flux. The fluxes were found to be in agreement within tolerance (Figure 6.4).

The k -effective eigenvalue of the supercritical two-region medium was found to be 1.28656. The RQFP method was found to require 46 transport sweeps to converge to a tolerance of 10^{-12} . The power method with fission norm update required 36 transport sweeps.

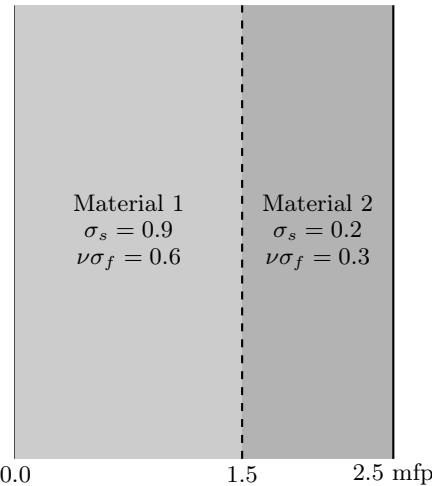


Figure 6.3: Heterogeneous Multiplying Slab Benchmark Problem Domain [43]

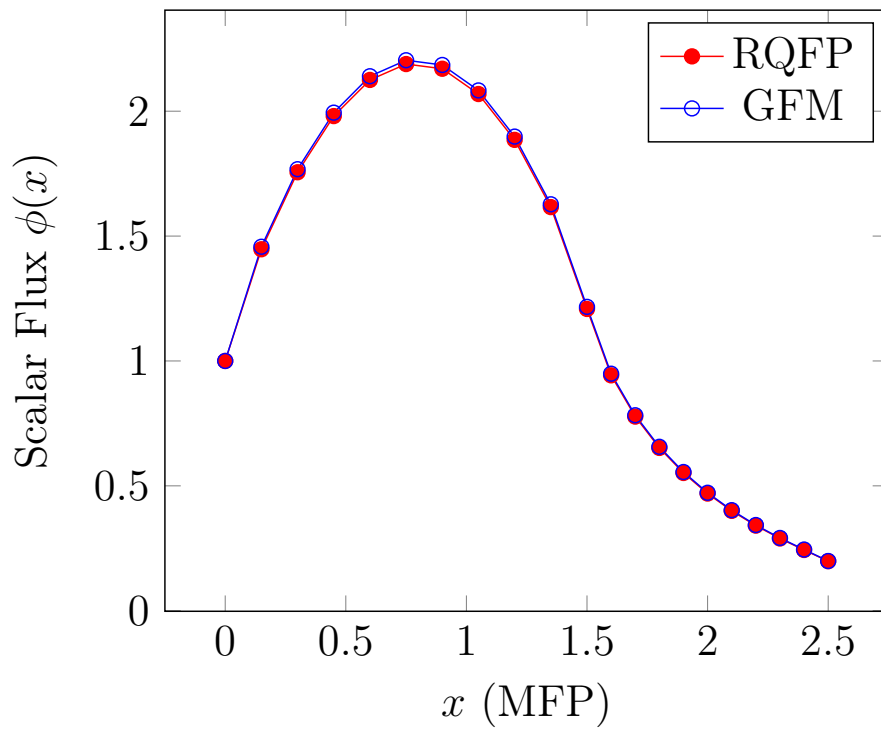


Figure 6.4: Alpha-Eigenvalue Scalar Flux Results for Two-Region Multiplying Slab

Problem 6.1.3.3-Multiplying Five Region Fuel-Pin: Four one-speed five region slab problems consisting of fuel, moderator, and absorber materials were examined and the RQFP method alpha-eigenvalue compared to the GFM. The leftmost fuel pin width was allowed to vary. The alpha-eigenvalue was calculated for different fuel width thicknesses with the fuel having $\nu\sigma_f = 0.3$ or 0.7 . Cross sections for the three materials are seen in Table 6.9.

Table 6.9: Five Region Slab Material Cross Sections (cm^{-1})

Material	σ	$\nu\sigma_f$	σ_s	v_g [cm/s]
Fuel	1.0	0.3/0.7	0.8	1.0
Moderator	1.0	0.0	0.8	1.0
Absorber	1.0	0.0	0.1	1.0

The five region fuel-pin-like domain shown in Figure 6.5 was modeled ($M = 1000$ and $L = 64$) and the alpha-eigenvalues compared to GFM for four cases. For cases one and two, the fuel-pin domain consisted of five regions, fuel, moderator, absorber, moderator, and fuel, with the leftmost fuel pin having a width of one mean free path. For cases three and four, the fuel-pin domain also consisted of five regions. However, the leftmost fuel pin instead had a width of 1.1 mean free paths.

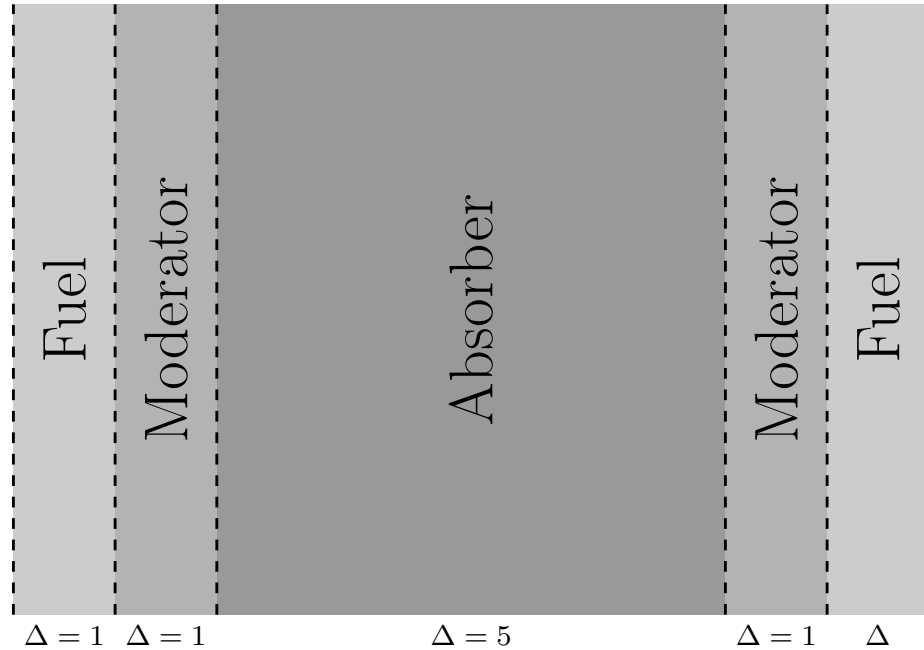


Figure 6.5: Five Region Heterogeneous Slab Benchmark Problem Domain

For case one and two, the fuel fission cross section was set to $\nu\sigma_f = 0.3$ and $\nu\sigma_f = 0.7$, respectively. The alpha-eigenvalues were $\alpha = -0.3197041 \text{ s}^{-1}$ and $\alpha = -0.0062120 \text{ s}^{-1}$ for

the $\nu\sigma_f = 0.3$ and $\nu\sigma_f = 0.7$ cases, respectively. The RQFP method eigenvalues matched the GFM-calculated alpha-eigenvalues within tolerance as shown in Table 6.10. Convergence of the $\nu\sigma_f = 0.3$ and $\nu\sigma_f = 0.7$ cases for the RQFP method required 30 and 27 transport sweeps, respectively. The scalar fluxes for both cases matched GFM within tolerance and are seen in Figure 6.6.

For cases three and four, the leftmost fuel pin width was set to 1.1 mfp. The alpha-eigenvalues for $\nu\sigma_f = 0.3$ and $\nu\sigma_f = 0.7$ were found to be $-0.2932897 \text{ s}^{-1}$ and 0.0375543 s^{-1} , respectively. The RQFP method eigenvalues matched the GFM-calculated alpha-eigenvalues within tolerance (Table 6.10). For the supercritical case, the alpha-eigenvalue RQFP required 502 sweeps as compared to 13,099 sweeps for the critical search method.

For leftmost fuel pin width of one mean free path, the k -effective eigenvalue of the five region fuel-pin-like was determined to be 0.42428 and 0.98998 for the $\nu\sigma_f = 0.3$ and $\nu\sigma_f = 0.7$ cases, respectively. For the $\nu\sigma_f = 0.3$ fuel pin, the RQFP method required 29 transport sweeps while the power method with fission norm update required 22 transport sweeps. For the $\nu\sigma_f = 0.7$ fuel pin, the RQFP method required 28 transport sweeps while the power method with fission norm update required 21 transport sweeps. For leftmost fuel pin width of 1.1 mean free paths, the k -effective was determined to be 0.45554 and 1.06316, respectively, for $\nu\sigma_f = 0.3$ and $\nu\sigma_f = 0.7$. For the $\nu\sigma_f = 0.3$ fuel pin, the RQFP method required 514 transport sweeps while the power method with fission norm update required 355 transport sweeps. For the $\nu\sigma_f = 0.7$ fuel pin, the RQFP method required 513 transport sweeps while the power method with fission norm update required 355 transport sweeps.

Table 6.10: Comparison of RQFP- and GFM-calculated Alpha-Eigenvalues for Multiplying Five-Region Fuel-Pin

Alpha-Eigenvalue/Percent Relative Error					
Δ	$\nu\sigma_f$	RQFP	GFM	RQFP/GFM % Relative Error	
1	0.3	-3.197041×10^{-1}	-3.196537×10^{-2}	1.58×10^{-2}	
1	0.7	-6.212026×10^{-3}	-6.156369×10^{-3}	9.041×10^{-1}	
1.1	0.3	-2.932897×10^{-1}	-2.93247×10^{-1}	1.46×10^{-2}	
1.1	0.7	3.75543×10^{-2}	3.759991×10^{-2}	1.213×10^{-1}	

$$M = 1000, L = 64, \text{Tolerance} = 10^{-12}$$

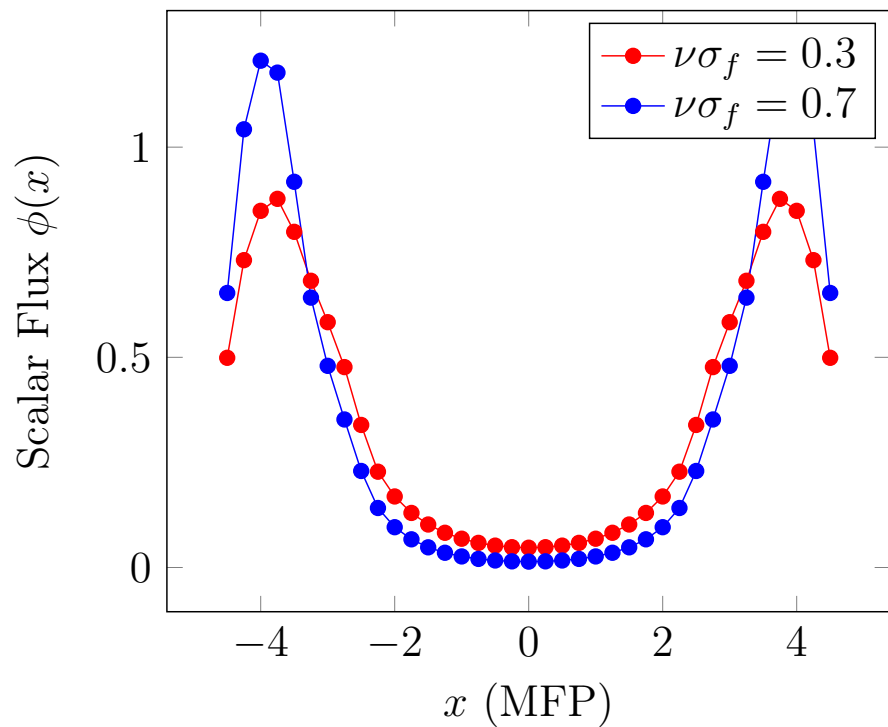


Figure 6.6: Case One and Two Scalar Flux Results for Five-Region Multiplying Slab-Two Cases

6.1.4 Multiplying Homogeneous Slabs with Anisotropic Scattering

Sood Criticality Benchmark Problems 32-35: Four one-group critical slab problems with anisotropic scattering from [40] were examined to demonstrate the performance of the RQFP method for problems with anisotropic scattering. Sood Criticality Benchmark Problem 32 consists of a plutonium-like cross section set with a small anisotropic scattering cross section solved using a P1 scattering expansion. Sood Criticality Benchmark Problem 33 uses the same cross section set but is instead solved using a P2 scattering expansion. Sood Criticality Benchmark Problems 34 and 35 consider another plutonium-like material with a much higher anisotropic scattering cross section. The cross sections for the plutonium-like materials are shown in Table 6.11. In these problems, the scattering kernel is non-negative. All problems were exactly critical with the critical half-width, r_c , defined in Figure 6.7, given in Table 6.12.

For the alpha-eigenvalue problems, the RQFP-calculated alpha-eigenvalues are seen in Table 6.12a. All problems were slightly subcritical but within 10^{-5} of the actual alpha-eigenvalue of zero. The RQFP method took 22-26 transport sweeps to converge the eigenvector ℓ_2 norm residual to 10^{-12} (Table 6.12a). Since the problems were too close to critical and slightly subcritical, the critical search method could not converge the problem.

For k -effective eigenvalue problems, the RQFP-calculated eigenvalues are seen in Table 6.12b. The problems had a calculated k -effective eigenvalue slightly below the true eigenvalue of one. The RQFP method took 22-26 transport sweeps to converge the ℓ_2 norm eigenvector residual to 10^{-12} . The power method with the fission source update required 3-4 transport sweeps less than the RQFP method for all problems.

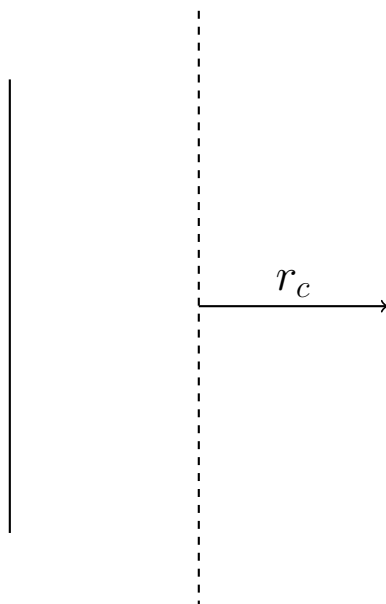


Figure 6.7: Critical Width of Slab

Table 6.11: Sood Criticality Benchmark Problems 32-35 Cross Sections (cm^{-1}) in [40]

Cross Section Set	σ	$\nu\sigma_f$	σ_{s0}	σ_{s1}	v [cm/s]
Sood Prob. 32	0.32640	0.176256	0.248064	0.042432	1
Sood Prob. 34	0.32640	0.176256	0.248064	0.212160	1

Table 6.12: Calculated Eigenvalues and Transport Sweep Comparisons for Sood Criticality Benchmark Problems 32-35 in [40]

Cross Section Set	r_c [cm]	Calculated α [s^{-1}]	Transport Sweeps	
			RQFP	Critical Search
Sood Prob. 32-P1 Scattering	0.77032	-3.50639×10^{-5}	24	*
Sood Prob. 34-P1 Scattering	0.76378	-6.16666×10^{-5}	26	*
Sood Prob. 32-P2 Scattering	0.79606	-5.29475×10^{-5}	24	*
Sood Prob. 34-P2 Scattering	0.78396	-2.72628×10^{-5}	22	*

$M = 500$, $L = 64$, Tolerance = 10^{-12} , *Did Not Converge

(a) Alpha-Eigenvalue: Comparison of RQFP and Critical Search Transport Sweeps

Cross Section Set	r_c [cm]	Calculated k_{eff}	Transport Sweeps	
			RQFP	Power Method
Sood Prob. 32-P1 Scattering	0.77032	0.99995	25	22
Sood Prob. 34-P1 Scattering	0.76378	0.99991	26	24
Sood Prob. 32-P2 Scattering	0.79606	0.99993	22	18
Sood Prob. 34-P2 Scattering	0.78396	0.99996	24	21

$M = 500$, $L = 64$, Tolerance = 10^{-12}

(b) k -Effective: Comparison of RQFP and Power Method Transport Sweeps

6.2 Multigroup Verification for Slab Geometry

In this section, we examine the performance of the RQFP method for various multigroup-in-energy, homogeneous and heterogeneous slab benchmark problems listed in [40]. These problems are exactly critical, though in practice some problems are found to be slightly subcritical or supercritical. Problem cross sections and critical radii are given for all benchmarks. The benchmark problems provide a diverse set of nuclear system physics problems, including fast spectrum plutonium slabs, a uranium-aluminum system, highly-enriched uranium for research reactors system, and uranium-heavy water reactors.

6.2.1 Multigroup Multiplying Homogeneous Slabs

Sood Criticality Benchmark Problem 45: The alpha and k -effective eigenvalues for a two-group plutonium-239 critical slab were calculated and the RQFP method performance compared to the critical search and power methods. The plutonium-239 cross sections, listed in Table 6.13a, allowed for fission in both energy groups. Fission neutrons can be born in both energy groups with more neutrons being born in the highest energy group. The scattering cross sections of the problem do not allow for upscattering (Table 6.13b).

For the critical slab width given in Table 6.14, the alpha-eigenvalue of the system was found to be $\alpha = -4.64633 \times 10^{-5} \text{ s}^{-1}$, requiring 48 transport sweeps to converge the eigenvector residual norm to a tolerance of 10^{-12} (Table 6.14a). As the problem was slightly subcritical because of numerical error, the critical search method did not converge to the correct eigenvalue. The k -effective eigenvalue was determined to be $k = 0.99988$ requiring 48 transport sweeps for the RQFP method as compared to 46 transport sweeps for the power method using the fission source normalization (Table 6.14b). As the system is incredibly close to critical, the number of transport sweeps required by the RQFP method for both eigenvalues is the same. This is due to the fact that the fundamental eigenvectors are equal for both the alpha- and k -effective eigenvalue problems when a nuclear system is exactly critical.

Table 6.13: Sood Criticality Benchmark Problem 45 Cross Sections (cm^{-1}) in [40]

g	σ_g	ν_g	σ_{fg}	χ_g	v_g [cm/s]
1	0.2208	3.10	0.0936	0.575	2.0
2	0.3360	2.93	0.08544	0.425	1.0
(a) Pu-239 Cross Sections					
$g' \rightarrow g$	1	2			
1	0.0792	0.0432			
2	0.0	0.23616			
(b) Pu-239 Scattering Block					

Table 6.14: Calculated Eigenvalues and Transport Sweep Comparisons for Sood Criticality Benchmark Problem 45 in [40]

r_c [cm]	Calculated α [s^{-1}]	Transport Sweeps	
		RQFP	Critical Search
1.795602	-4.64633×10^{-5}	48	*

$M = 500$, $L = 64$, Tolerance = 10^{-12} , *Did Not Converge

(a) Alpha-Eigenvalue: Comparison of RQFP and Critical Search Transport Sweeps

r_c [cm]	Calculated k_{eff}	Transport Sweeps	
		RQFP	Power Method
1.795602	0.99988	48	46

$M = 500$, $L = 64$, Tolerance = 10^{-12}

(b) k -Effective: Comparison of RQFP and Power Method Transport Sweeps

Sood Criticality Benchmark Problem 48: The alpha and k -effective eigenvalues were calculated for a critical slab consisting of a uranium-235-like material. The material cross sections, seen in Table 6.15a, consist of two energy groups, with fission possible in both groups. Fission neutrons can be born in both groups with a preference for the higher energy group. The material scattering cross sections (Table 6.15b) did not allow for upscattering.

The alpha-eigenvalue of the system was calculated to be $\alpha = -1.28364 \times 10^{-5} \text{ s}^{-1}$, requiring 62 transport sweeps to converge to a tolerance of 10^{-12} for the RQFP method. The critical search method was not able to converge (Table 6.16a). The k -effective eigenvalue was determined to be $k = 0.99995$, requiring 62 transport sweeps for the RQFP method to converge the eigenvector. The power method required slightly fewer transport sweeps, requiring 58 transport sweeps. Similar to the plutonium-239 problem, the number of transport sweeps required by the RQFP method for both eigenvalues was the same. This was due to how close the problem was to being exactly critical.

Table 6.15: Sood Criticality Benchmark Problem 48 Cross Sections (cm^{-1})

g	σ_g	ν_g	σ_{fg}	χ_g	v_g [cm/s]
1	0.2160	2.70	0.06192	0.575	2.0
2	0.3456	2.50	0.06912	0.425	1.0

(a) U-235 Cross Sections

$g' \rightarrow g$	1	2
1	0.078240	0.0720
2	0.0	0.26304

(b) U-235 Scattering Block

Table 6.16: Calculated Eigenvalues and Transport Sweep Comparisons for Sood Criticality Benchmark Problem 48 in [40]

Transport Sweeps			
r_c [cm]	Calculated α [s^{-1}]	RQFP	Critical Search
3.006375	-1.28364×10^{-5}	62	*

$M = 500$, $L = 64$, Tolerance = 10^{-12} , *Did Not Converge

(a) Alpha-Eigenvalue: Comparison of RQFP and Critical Search Transport Sweeps

Transport Sweeps			
r_c [cm]	Calculated k_{eff}	RQFP	Power Method
3.006375	0.99995	62	58

$M = 500$, $L = 64$, Tolerance = 10^{-12}

(b) k -Effective: Comparison of RQFP and Power Method Transport Sweeps

Sood Criticality Benchmark Problem 51: The eigenvalues of critical slab consisting of a uranium/aluminum (U/Al) mixture similar to those seen in nuclear reactor applications were calculated. The material cross sections (Table 6.17a) consist of two energy groups with fission occurring in the lower energy (**thermal**) group. All fission neutrons are born in the fast energy group. The material does not allow for upscattering (Table 6.17b) but does have a large self-scattering cross section in the lowest energy group.

The alpha-eigenvalue was calculated to be $-6.39646 \times 10^{-6} s^{-1}$ and required 492 transport sweeps to converge (Table 6.18a). The increase in transport sweeps as compared to the plutonium and uranium problem is due to the increased scattering present in this problem. The increase in scattering, caused by the inclusion of aluminum in the cross sections, increases the number of iterations necessary to suppress higher eigenmodes in the problem. The critical search method was unable to converge the eigenvalue/eigenvector pair. The k -effective eigenvalue was determined to be $k = 0.99985$ for the system. The RQFP method required a substantially larger number of transport sweeps as compared to power method. The RQFP method required 592 iterations as compared to 82 (Table 6.18b). The degradation of the performance of the RQFP method is due to the fact that the method converges the eigenvector as opposed to the fission source. Converging the eigenvector requires many more sweeps due to the increased scattering present in the system causing the spectral radius of the Jacobian to be very close to one.

Table 6.17: Sood Criticality Benchmark Problem 51 Cross Sections (cm^{-1}) in [40]

g	σ_g	ν_g	σ_{fg}	χ_g	v_g [cm/s]
1	0.26817	0.0	0.0	1.0	2.0
2	1.27698	2.83	0.06070636042	0.0	1.0
(a) U/Al Cross Sections					
$g' \rightarrow g$		1	2		
1		0.020432	0.247516		
2		0.0	1.21313		
(b) U/Al Scattering Block					

Table 6.18: Calculated Eigenvalues and Transport Sweep Comparisons for Sood Criticality Benchmark Problem 51 in [40]

r_c [cm]	Calculated α [s^{-1}]	Transport Sweeps	
		RQFP	Critical Search
7.830630	-6.39646×10^{-6}	492	*

$M = 500$, $L = 64$, Tolerance = 10^{-12} , *Did Not Converge

(a) Alpha-Eigenvalue: Comparison of RQFP and Critical Search Transport Sweeps

r_c [cm]	Calculated k_{eff}	Transport Sweeps	
		RQFP	Power Method
7.830630	0.99985	592	82

$M = 500$, $L = 64$, Tolerance = 10^{-12}

(b) k -Effective: Comparison of RQFP and Power Method Transport Sweeps

Sood Criticality Benchmark Problem 54: A highly-enriched uranium slab was modeled and the number of transport sweeps required for convergence compared between the RQFP method and standard methods. The highly-enriched uranium cross sections are similar to those found in research reactors across the world. The cross section set (Table 6.19a) consists of two energy groups. Fission occurs in both energy groups, with most fissions taking place in the lower energy group. However, fission neutron are only born in the highest energy group. The cross section set allows only for downscattering of neutrons through the two energy groups with a much larger within-group scattering cross section in the low energy group (Table 6.19b).

The alpha-eigenvalue of the slab was determined to be $-3.28714 \times 10^{-7} \text{ s}^{-1}$. The RQFP method required 1188 transport sweeps to converge the eigenvector, the increase in sweeps a product of the high amount of scattering in the system. The critical search method was not able to converge the eigenvector. The k -effective eigenvalue was found to be $k = 0.99999$. The RQFP method required 1188 transport sweeps to converge, similar to the alpha-eigenvalue calculation due to how close the system was to critical. The RQFP method for the k -effective eigenvalue required 10 times more iterations than the power method. The degradation of performance is caused by the increased scattering of the system.

Table 6.19: Sood Criticality Benchmark Problem 54 Cross Sections (cm^{-1}) in [40]

g	σ_g	ν_g	σ_{fg}	χ_g	v_g [cm/s]
1	0.65696	2.50	0.0010484	1.0	2.0
2	2.52025	2.50	0.050632	0.0	1.0

(a) 93% Enriched Uranium Cross Sections

$g' \rightarrow g$	1	2
1	0.62568	0.029227
2	0.0	2.44383

(b) 93% Enriched Uranium Scattering Block

Table 6.20: Calculated Eigenvalues and Transport Sweep Comparisons for Sood Criticality Benchmark Problem 54 in [40]

Transport Sweeps			
r_c [cm]	Calculated α [s^{-1}]	RQFP	Critical Search
7.566853	-3.28714×10^{-7}	1188	*

$M = 500$, $L = 64$, Tolerance = 10^{-12} , *Did Not Converge

(a) Alpha-Eigenvalue: Comparison of RQFP and Critical Search Transport Sweeps

Transport Sweeps			
r_c [cm]	Calculated k_{eff}	RQFP	Power Method
7.566853	0.99999	1,188	98

$M = 500$, $L = 64$, Tolerance = 10^{-12}

(b) k -Effective: Comparison of RQFP and Power Method Transport Sweeps

Sood Criticality Benchmark Problem 68: To analyze the performance of the RQFP method for highly scattering systems, a two-energy group uranium/heavy water critical slab problem with cross sections given in Table 6.21 was modeled. Fission occurs in both energy groups with all fission neutrons born in the higher energy group. However, the fission cross sections are substantially smaller than in previous systems. The system allows no upscattering but has large within-group scattering cross sections for both groups (Table 6.21b). The critical width of the slab is much larger than previous problems, due to the small fission cross sections and highly scattering nature of the problem.

For the critical width listed in Table 6.22a, the alpha-eigenvalue was determined to be $-6.93314 \times 10^{-7} s^{-1}$. The RQFP method required 451,136 transport sweeps for convergence, a substantial increase as compared to the previous problems (Table 6.22a). The critical search method was unable to converge the eigenvalue and eigenvector pair. The k -effective eigenvalue was determined to be $k = 0.99887$. The RQFP method required 451,136 transport sweeps, performing far worse than the power method which only required 52,964 transport sweeps to converge (Table 6.22b). The sensitivity of the RQFP method to scattering cross sections caused the Jacobian spectral radius at the fixed point to be very close to one.

Table 6.21: Sood Criticality Benchmark Problem 68 Cross Sections (cm^{-1}) in [40]

g	σ_g	ν_g	σ_{fg}	χ_g	v_g [cm/s]
1	0.33588	2.50	0.002817	1.0	2.0
2	0.54628	2.50	0.097	0.0	1.0
(a) U-D ₂ O Cross Sections					
$g' \rightarrow g$	1	2			
1	0.31980	0.004555			
2	0.0	0.42410			
(b) U-D ₂ O Scattering Block					

Table 6.22: Calculated Eigenvalues and Transport Sweep Comparisons for Sood Criticality Benchmark Problem 68 in [40]

r_c [cm]	Calculated α [s^{-1}]	Transport Sweeps	
		RQFP	Critical Search
846.632726	-6.93314×10^{-7}	451,140	*

$M = 2000$, $L = 64$, Tolerance = 10^{-12} , *Did Not Converge

(a) Alpha-Eigenvalue: Comparison of RQFP and Critical Search Transport Sweeps

r_c [cm]	Calculated k_{eff}	Transport Sweeps	
		RQFP	Power Method
846.632726	0.99887	451,136	52,964

$M = 2000$, $L = 64$, Tolerance = 10^{-12}

(b) k -Effective: Comparison of RQFP and Power Method Transport Sweeps

6.2.2 Multigroup Reflected Slabs

Two water-reflected research reactor-like slab problems, Sood Criticality Benchmark Problem 58 and Sood Criticality Benchmark Problem 60, were considered. For the cross section sets shown in Table 6.23 and Table 6.24, fissile material slabs were reflected by a water reflector on the right side of the slab that made the problem exactly critical. The two-group cross section sets allowed for upscattering. The fissile slab width along with slab and reflector width are listed in Table 6.25.

The reflected slab problems were found to be slightly subcritical (Table 6.25a). Using the Rayleigh Quotient Fixed Point method for the alpha-eigenvalue, the alpha-eigenvalue and eigenvector were determined in 2042 and 3192 transport sweeps, respectively. Due to the large amount of scattering in the reflector, the convergence rate of the method was slowed and required many more transport sweeps compared to problems with less scattering. Attempting to calculate the alpha-eigenvalue with the critical search method was unsuccessful due to the negative alpha-eigenvalue. Despite the problems only being slightly subcritical, the critical search method was unable to converge the problems.

For the k -effective eigenvalue, the Rayleigh Quotient Fixed Point method underperformed the power method with fission source update dramatically (Table 6.25b). The RQFP method required 20-30 times the number of iterations as compared to the default method. Since the reflected slabs were only slightly subcritical, the number of transport sweeps required to converge the alpha- and k -effective eigenvalues were similar. With convergence of the fixed-point methods determined by the scattering present in the problems, the scattering in the water reflector slowed down convergence dramatically. With the fission source update only concerned with fissile regions of the problem, convergence was achieved faster as the water reflector had less of an impact on the convergence rate.

Table 6.23: Sood Criticality Benchmark Problem 58 Cross Sections (cm^{-1}) in [40]

g	σ_g	ν_g	σ_{fg}	χ_g	v_g [cm/s]		
1	0.88721	2.50	0.000836	1.0	2.0		
2	2.9727	2.50	0.029564	0.0	1.0		
(a) Fissile Material Cross Sections							
$g' \rightarrow g$		1	2				
1	0.83892	0.04635					
2	0.000767	2.9183					
(b) Fissile Material Scattering Block							
g	σ_g	ν_g	σ_{fg}	χ_g	v_g [cm/s]		
1	0.88798	0.0	0.0	0.0	2.0		
2	2.9865	0.0	0.0	0.0	1.0		
(c) H_2O Cross Sections							
$g' \rightarrow g$		1	2				
1	0.83975	0.04749					
2	0.000336	2.9676					
(d) H_2O Scattering Block							

Table 6.24: Sood Criticality Benchmark Problem 60 Cross Sections (cm^{-1}) in [40]

g	σ_g	ν_g	σ_{fg}	χ_g	v_g [cm/s]
1	0.88655	2.50	0.001648	1.0	2.0
2	2.9628	2.50	0.057296	0.0	1.0

(a) Fissile Material Cross Sections

$g' \rightarrow g$	1	2
1	0.83807	0.04536
2	0.00116	2.8751

(b) Fissile Material Scattering Block

Table 6.25: Calculated Eigenvalues and Transport Sweep Comparisons for Sood Criticality Benchmark Problem 60 in [40]

Cross Section Set	r_c [cm]	$r_c + r_{\text{refl}}$ [cm]	Calculated α [s^{-1}]	Transport Sweeps	
				RQFP	Critical Search
Sood Prob. 58	6.696802	7.822954	-1.10466×10^{-7}	2,042	*
Sood Prob. 60	4.863392	10.494149	-5.92658×10^{-9}	3,192	*

*Did Not Converge

(a) Alpha-Eigenvalue: Comparison of RQFP and Critical Search Transport Sweeps

Cross Section Set	r_c [cm]	$r_c + r_{\text{refl}}$ [cm]	Calculated k_{eff}	Transport Sweeps	
				RQFP	Power Method
Sood Prob. 58	6.696802	7.822954	0.99999	2,038	112
Sood Prob. 60	4.863392	10.494149	0.99999	3,280	94

$M = 2000$, $L = 64$, Tolerance = 10^{-12}

(b) k -Effective: Comparison of RQFP and Power Method Transport Sweeps

6.3 One-Speed Verification for Spherical Geometry

In certain circumstances, alpha-eigenvalue results for slab geometry also apply to spherical geometry problems. This slab-sphere equivalence holds for isotropically scattering heterogeneous media where the total cross section is equal for all regions [42]. More generally, a convenient property of spherically symmetric systems is that if the mean free path in the system is independent of position and scattering is isotropic, then the determination of the spherically symmetric neutron distribution of these systems is reduced to the determination of these distributions in certain systems with plane symmetries. Thus, for all homogeneous slab and symmetric heterogeneous slab systems where each region has the same total cross section, it follows that there exists a spherical equivalent for the problems studied in the previous sections. Specifically, it can be shown that the second eigenvalue of a slab system is identical to the fundamental eigenvalue for the equivalent sphere. In this section, we examine the performance of the RQFP method for one-dimensional spherical problems which are equivalent to the slab problems from before. We verify the correctness of the method for this subset of problems and compare its performance to the critical search and power methods.

6.3.1 Non-Multiplying Homogeneous Spheres

To verify the correctness of the RQFP method for one-dimensional spherical geometry, four non-multiplying homogeneous slab problems in [43] with a second eigenvalue listed were modeled as equivalent spherical problems with radii of $\Delta/2$ mfp. The dominant alpha-eigenvalue of the equivalent spherical systems is the second eigenvalue of the slab problems. The calculated alpha-eigenvalues were then compared to the GFM-calculated eigenvalues. The purely homogeneous scattering spheres used the cross sections listed in Table 6.1. For all problems, the percent relative error between the RQFP- and GFM-calculated eigenvalues was less than 0.005 % (Table 6.26) for diamond differencing discretization ($M = 500$) and an S_{64} discrete ordinates quadrature in angle ($L = 64$). As the radius of the spheres increases, the system approaches the critical state and the alpha-eigenvalue approaches zero. However, as there is no fissile material, the eigenvalue can never reach zero.

6.3.2 Multiplying Homogeneous Spheres

For homogeneous slab problems with multiplication (Cross sections Table 6.3), the equivalent spherical problems were modeled and the performance and correctness of the RQFP methods for alpha- and k -effective eigenvalue calculations were examined.

To verify the correctness of the RQFP method for alpha-eigenvalue problems, the RQFP-calculated eigenvalues were compared to the GFM-calculated eigenvalues listed in [43]. The problems were modeled using diamond differencing ($M = 500$) and an S_{64} discrete ordinates quadrature in angle ($L = 64$). For spherical problems with diameters ranging from three to 50 mean free paths, it was found that the eigenvalues agreed within 0.02% relative error

Table 6.26: Comparison of RQFP- and GFM-Calculated Alpha-Eigenvalues for a Homogeneous Scattering Sphere

Δ	Alpha-Eigenvalue/Percent Relative Error		
	RQFP	GFM	% Relative Error
5	-3.41177×10^{-1}	-3.41216×10^{-1}	0.0114
10	-1.02973×10^{-1}	-1.02978×10^{-1}	0.0049
20	-2.88443×10^{-2}	-2.88447×10^{-2}	0.0014
25	-1.89226×10^{-2}	-1.89228×10^{-2}	0.0011

$M = 500, L = 64, \text{Tolerance} = 10^{-12}$

(Table 6.27). Alpha-eigenvalue agreement increased as the spherical system became larger. In all cases, the RQFP method was able to correctly determine the criticality of the system, even for systems that were slightly subcritical or supercritical.

The performance of the RQFP method for alpha-eigenvalue problems was compared to the critical search method. The number of transport sweeps required to converge the eigen-vector norm residual to a tolerance of 10^{-12} for various spherical radii is seen in Table 6.28a. For problems that were subcritical ($\Delta = 3 - 7$ mfp), the RQFP method was able to converge to the correct eigenvalue while the critical search method was not able to converge the problem. As problems became increasingly supercritical, the number of transport sweeps required to converge increased for both the RQFP and critical search methods. This is due to the fact that as the systems become larger, neutrons can survive longer before being absorbed or leaking out of the system. These longer lived neutrons cause the increase in the alpha-eigenvalue but more transport sweeps are required before reaching the fundamental mode of the angular flux. For the supercritical cases, the critical search method was able to correctly determine the eigenvalue of the spherical systems. However, in all cases, the number of transport sweeps required by the RQFP method was approximately 20-40 times less than the critical search method.

The RQFP method was compared to the power method with a fission norm update for the k -effective eigenvalue. In all cases, the power method performed better than the RQFP method. The number of transport sweeps necessary to converge was similar to subcritical and slightly supercritical problems for both methods. However, as the problems became more supercritical, the RQFP method's performance deteriorated (Table 6.28b).

Table 6.27: Comparison of RQFP- and GFM-Calculated Alpha-Eigenvalues for a Homogeneous Scattering Multiplying Sphere

Δ	Alpha-Eigenvalue/Percent Relative Error		
	RQFP	GFM	% Relative Error
3	-5.68218×10^{-1}	-5.6833×10^{-1}	0.0197
4	-3.00486×10^{-1}	-3.0054×10^{-1}	0.0180
5	-1.60321×10^{-1}	-1.6035×10^{-1}	0.0181
6	-7.72739×10^{-2}	-7.7292×10^{-2}	0.0234
7	-2.38450×10^{-2}	-2.3857×10^{-2}	0.0503
8	1.26235×10^{-2}	1.2616×10^{-2}	0.0594
9	3.86541×10^{-2}	3.8649×10^{-2}	0.0132
10	5.78980×10^{-2}	5.7894×10^{-2}	0.0069
15	1.06258×10^{-1}	1.0626×10^{-1}	0.0019
20	1.24512×10^{-1}	1.2451×10^{-1}	0.0016
30	1.38248×10^{-1}	1.3825×10^{-1}	0.0014
40	1.43262×10^{-1}	1.4326×10^{-1}	0.0014
50	1.45638×10^{-1}	1.4564×10^{-1}	0.0014

$M = 500, L = 64, \text{Tolerance} = 10^{-12}$

Table 6.28: Transport Sweep Comparisons for Homogeneous Multiplying Spheres

Δ	Transport Sweeps		Δ	Transport Sweeps	
	RQFP	Critical Search		RQFP	Critical Search
3	46	*	10	128	29,645
4	46	*	15	227	61,303
5	52	*	20	357	84,353
6	67	*	30	707	100,433
7	81	*	40	1,176	99,135
8	96	10,865	50	1,761	97,037
9	111	21,555			

*Did Not Converge

(a) Alpha-Eigenvalue: Comparison of RQFP and Critical Search Sweeps

Δ	Transport Sweeps		Δ	Transport Sweeps	
	RQFP	Power Method		RQFP	Power Method
3	49	43	10	127	62
4	57	47	15	214	79
5	66	49	20	329	103
6	76	52	30	636	167
7	87	54	40	1049	253
8	99	56	50	1562	360
9	113	59			

$M = 500, L = 64, \text{Tolerance} = 10^{-12}$

(b) k -Effective: Comparison of RQFP and Power Method Transport Sweeps

6.3.3 Multiplying Homogeneous Spheres with Anisotropic Scattering

Three exactly critical multiplying homogeneous spheres with anisotropic scattering from [40], Sood Criticality Benchmark Problems 39, 41, and 43, were modeled to determine the impacts of higher scattering order cross sections on the performance of the RQFP methods. Three sets of uranium-heavy water cross sections sets (Table 6.29) were examined, each with different anisotropic scattering cross section orders. In particular, cross section set U-D₂O (c) had a negative anisotropic scattering cross section. The critical radii for the three problems are listed in Table 6.30. These problems were modeled using the diamond differencing scheme in space (500 cells), and S₆₄ discrete ordinate angular quadrature.

For alpha-eigenvalue problems, the RQFP method calculated alpha-eigenvalues that were within 10⁻⁷ of the true alpha-eigenvalue of zero. For two cases, Sood Criticality Benchmark Problem 39 and 41, the problems were slightly supercritical, while for Sood Criticality Benchmark Problem 43 the problem was subcritical. For the two supercritical cases, both the RQFP and critical search methods were able to converge to the same eigenvalue. The RQFP method required approximately half the transport sweeps as the critical search method (Table 6.30a). For the subcritical case, the critical search method could not converge to the correct eigenvalue as the problem was slightly subcritical. For the RQFP method, the number of transport sweeps required to converge the case with a negative anisotropic scattering cross section increased by a factor of 1.5 compared to non-negative anisotropic cross sections. This further suggests the negative anisotropic cross section can impact the rate of convergence of the RQFP method.

For k -effective eigenvalue problems, the RQFP method calculated k -effective eigenvalues were within 10⁻⁷ of the true value of $k_{\text{eff}} = 1.00000$. In all three cases, the RQFP method required approximately double the iterations the power method with fission norm update did. (Table 6.30b). Similar to the alpha-eigenvalue problems, the inclusion of a negative anisotropic scattering cross section increased the number of transport sweeps necessary to converge to a tolerance of 10⁻¹².

Table 6.29: Sood Criticality Benchmark Problems 39, 41, and 43 Cross Sections (cm⁻¹) in [40]

Cross Section Set	σ	$\nu\sigma_f$	σ_{s0}	σ_{s1}	v [cm/s]
Sood Prob. 39	0.54628	0.098788237268	0.464338	0.056312624	1
Sood Prob. 41	0.54628	0.100574846008	0.464338	0.112982569	1
Sood Prob. 43	0.54628	0.0926709392	0.464338	-0.27850447	1

Table 6.30: Calculated Eigenvalues and Transport Sweep Comparisons for Sood Criticality Benchmark Problems 39, 41, and 43 in [40]

Cross Section Set	r_c [cm]	Calculated α [s^{-1}]	Transport Sweeps	
			RQFP	Critical Search
Sood Prob. 39	18.30563081	3.165772×10^{-7}	299	513
Sood Prob. 41	18.30563081	3.930857×10^{-7}	270	476
Sood Prob. 43	18.30563081	-6.613381×10^{-7}	456	*

*Did Not Converge

(a) Alpha-Eigenvalue: Comparison of RQFP and Critical Search Transport Sweeps

Cross Section Set	r_c [cm]	Reference k_{eff}	Transport Sweeps	
			RQFP	Power Method
Sood Prob. 39	18.30563081	1.000003	301	118
Sood Prob. 41	18.30563081	1.000003	273	106
Sood Prob. 43	18.30563081	0.999993	456	207

$M = 500$, $L = 64$, Tolerance = 10^{-12}

(b) k -Effective: Comparison of RQFP and Power Method Transport Sweeps

6.3.4 A Spherical Shell Problem

To verify the correctness of the alpha-eigenvalue RQFP method in spherical geometry, two spherical shell problems were modeled and the calculated alpha-eigenvalues compared to the GFM-calculated value in [43]. For any symmetric heterogeneous slab problem, an equivalent spherical shell problem can be modeled. As before, the second eigenvalue of the heterogeneous slab problem is the dominant eigenvalue of the spherical shell problem. Using the five-region fuel pin from Figure 6.5 with the right fuel pin width set to one mean free path, an equivalent spherical problem shown in Figure 6.8 was modeled. For this particular problem, the width of each material section remained the same as in the five region slab case. Cross sections for the three materials were the same as the slab geometry problem (Table 6.9). Similar to the five region slab problem, two cases were examined where $\nu\sigma_f = 0.3$ and 0.7 .

The RQFP- and GFM-calculated alpha-eigenvalues are listed in Table 6.31. For the $\nu\sigma_f = 0.3$ case, the alpha-eigenvalues matched within 0.5%. For the $\nu\sigma_f = 0.7$ case, agreement was within 2.2%. The higher discrepancy in the eigenvalue was most likely due to differences in how ARDRA and the GFM treated the neutron angular redistribution of spherical geometry. The GFM-calculated alpha-eigenvalue uses analytic Green's Functions and then determines the eigenvalues numerically through a search process and does not discretize the underlying integro-differential equation like ARDRA.

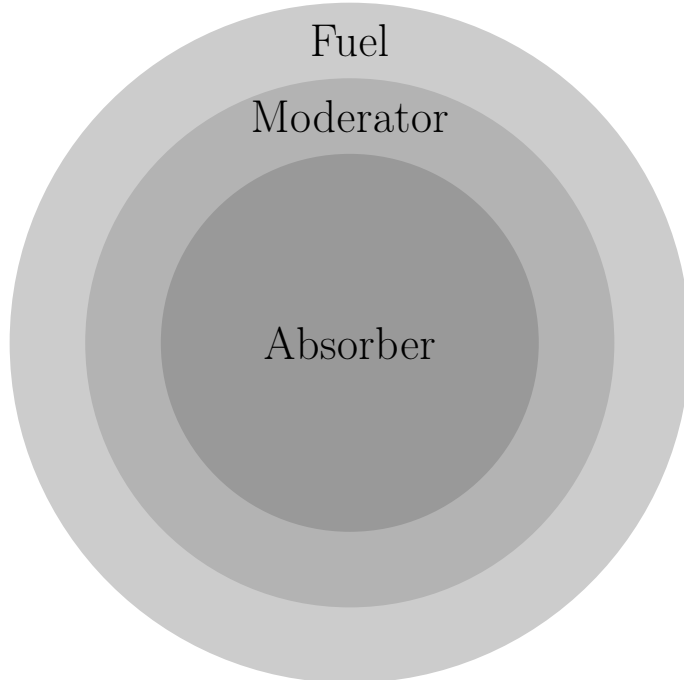


Figure 6.8: Five Region Fuel Pin Spherical Equivalent [10]

Table 6.31: Comparison of RQFP- and GFM-calculated Alpha-Eigenvalues for a Three Region Multiplying Sphere

$\nu\sigma_f$	Alpha-Eigenvalue/Percent Relative Error		
	RQFP	GFM	% Relative Error
0.3	-3.213384×10^{-1}	-3.229855×10^{-1}	5.10×10^{-1}
0.7	-6.300281×10^{-3}	-6.440766×10^{-3}	2.18

$M = 1000, L = 64, \text{Tolerance} = 10^{-12}$

6.4 Multigroup Verification for Spherical Geometry

In this section, we examine the performance of the RQFP method for three multigroup-in-energy, reflected, critical spheres from the International Handbook of Evaluated Criticality Safety Benchmark Experiments [44]. The handbook contains criticality safety benchmark specifications that have been derived from various experiments performed at various facilities throughout the world. These specifications are intended to help researchers validate calculation techniques and methods by providing researchers with integral quantities such as k -effective and energy spectra. The problems examined in this section provide a diverse set of critical systems consisting of a large number of materials, large cross-section libraries, anisotropically scattering materials, and other characteristics intended to test the performance of the RQFP methods for realistic problems.

6.4.1 A Plutonium-Nitrate Solution Critical Sphere

The alpha- and k -effective eigenvalues and eigenvectors of a plutonium-nitrate solution covered with cadmium were calculated and the number of transport sweeps required for convergence compared to standard eigensolver methods. The benchmark problem (Cross Section Evaluation Working Group (CSEWG) ID: T-15 and International Criticality Safety Benchmark Evaluation Project (ICSBEP) ID: PU_SOL_THERM_011) consisted of an 18-inch diameter sphere of a plutonium-nitrate solution with density 22.35 grams/liter covered with stainless steel and cadmium shells. The fissile sphere radius, r_U , and stainless steel and cadmium shell thicknesses, δ_{SS} and δ_{Cd} , respectively, are listed in Table 6.32 and material composition and number fractions in Table 6.33. The problem was modeled using a 230 neutron energy group cross section set with a scattering order of five.

For the alpha-eigenvalue problem, the RQFP method required 106,200 transport sweeps to converge the alpha-eigenvalue and eigenvector to a tolerance of 10^{-6} (Table 6.34a). For the modeled problem, the system was found to be slightly supercritical with an alpha-eigenvalue of $2.287638 \times 10^{-4} \mu s^{-1}$. The critical search method was able to converge the eigenpair, requiring 219,650 transport sweeps to converge to the same tolerance. The group scalar

flux for the alpha-eigenvalue problem was compared to the benchmark reference solution. The absolute difference between the two fluxes is seen in Figure 6.9. The largest differences were located in the fast region of the energy spectrum but were only on the order of 10^{-4} . Overall, the absolute difference was less than 10^{-6} , within the tolerance of the solution method.

For the k -effective eigenvalue problem, the problem was found to have an eigenvalue of $k = 1.012216$. For this particular problem, the RQFP method was unable to converge the k -effective eigenvalue and eigenvector (Table 6.34b). At each iteration step, the eigenvalue iterate was found to be negative. Though this behavior has been seen before with the RQFP method, it is usually found that the eigenvalue eventually becomes positive and converges to a physically possible k -effective eigenvalue. In this particular problem, that did not occur. It was found that a better initial guess for the eigenvector allowed for convergence, but this required using the eigenvector solution from the power method. The power method with the fission source update assures the positivity of the eigenvalue at each iteration. For this particular problem, the power method with fission source update required 58,650 transport sweeps.

Problem Dimensions [cm]			
ICSBEP ID	r_{Pu}	δ_{SS}	δ_{Cd}
PU_SOL_THERM_001	22.6974	0.127	0.0508

Table 6.32: Fissile Material Radius and Shell Thicknesses for Plutonium-Nitrate Solution Benchmark

Table 6.33: Material Composition for Plutonium-Nitrate Solution System

Material Number	Temperature (°C)	Component	Density (g/cm ³)	Number Fraction
1	20.0	1001	1.066	6.484E-01
		7014		7.358E-03
		8016		3.437E-01
		26000		1.280E-05
		94239		5.638E-04
		94240		2.344E-05
2	20.0	24000	7.998	1.921E-01
		26000		6.945E-01
		28000		1.134E-01
3	20.0	48000	11.72	1.000E+00
4	20.0	7014	1.293E-03	7.800E-01
		8016		2.200E-01

Table 6.34: Calculated Eigenvalues and Transport Sweep Comparisons for Plutonium-Nitrate Solution System

ICSBEP ID	Calculated α [μs^{-1}]	Transport Sweeps	
		RQFP	Critical Search
PU_SOL_THERM_011	2.287638×10^{-4}	106,260	219,650

M = 137, L = 128, Tolerance = 10^{-6}

(a) Alpha-Eigenvalue: Comparison of RQFP and Critical Search Transport Sweeps

ICSBEP ID	Calculated k_{eff}	Transport Sweeps	
		RQFP	Power Method
PU_SOL_THERM_001	1.012216	*	58,650

M = 137, L = 128, Tolerance = 10^{-6} , *Did Not Converge

(b) k -Effective: Comparison of RQFP and Critical Search Transport Sweeps

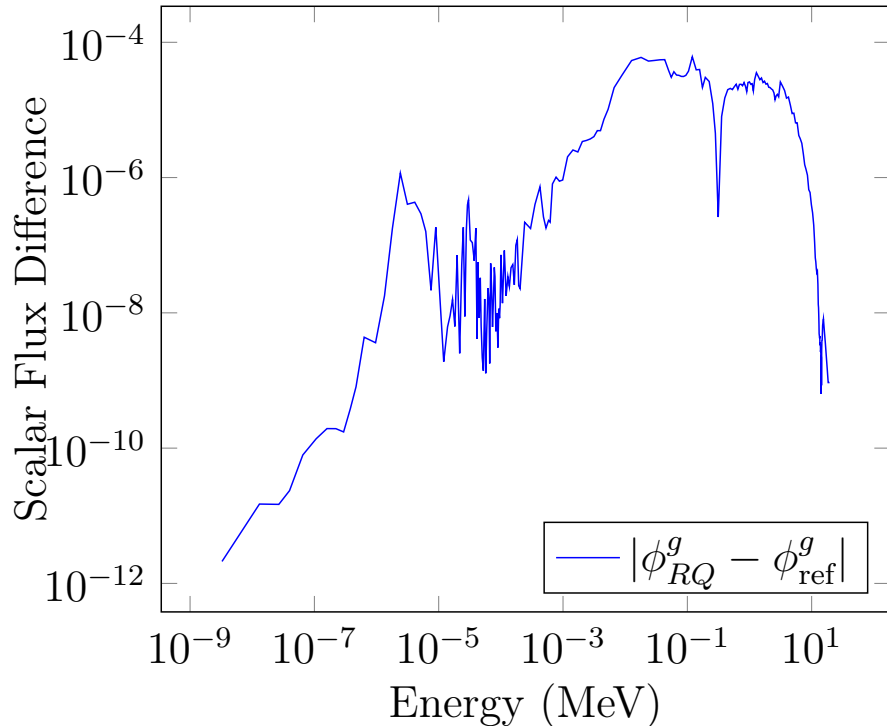


Figure 6.9: Absolute Error Between RQFP Method and Reference Solution for the Alpha-Eigenvalue Energy Spectrum

6.4.2 A Plutonium/Highly Enriched Uranium Mixture Critical Sphere

The alpha- and k -effective eigenvalues and eigenvectors of a plutonium/highly enriched uranium (PU/HEU) mixture spherical assembly were calculated. The number of transport sweeps required by the RQFP method for convergence of the eigenpair was compared to the standard eigenvalue methods for the alpha- and k -effective eigenvalue problems. The benchmark problem (International Criticality Safety Benchmark Evaluation Project (ICSBEP) ID: MIX_MET_FAST_001) consisted of a plutonium metal sphere surrounded by a uranium-235 and uranium-238 shell. The plutonium sphere radius and uranium shell thickness are listed in Table 6.35. Material compositions and number fractions are listed in Table 6.36. The problem was modeled using a 230 neutron energy group cross section set with a scattering order of five.

The problem as modeled in ARDRA was found to be slightly subcritical with alpha-eigenvalue $\alpha = -4.114757 \times 10^{-1} \mu s^{-1}$. The RQFP method required 22,310 transport sweeps to converge the eigenvalue and eigenvector to a tolerance of 10^{-6} (Table 6.37a). The critical search method was unable to converge the eigenpair. Despite the slightly subcritical nature of the system, the alpha-eigenvalue introduced sufficient negative absorption to prevent the critical search method from converging.

The k -effective eigenvalue was determined to be $k = 0.999063$. The RQFP method required 7130 transport sweeps to converge the eigenvalue/eigenvector pair to a tolerance of 10^{-6} . The power method with fission source update only required 4,370 transport sweeps (Table 6.37b). The high amount of scattering in this problem appears to degrade the performance of the RQFP method in comparison to the power method.

Problem Dimensions [cm]		
ICSBEP ID	r_{Pu}	δ_U
MIX_MET_FAST_001	5.0419	1.6637

Table 6.35: Fissile Material Radius and Shell Thicknesses for PU/HEU Mixture Benchmark

Table 6.36: Material Composition for PU/HEU System

Material Number	Temperature (°C)	Component	Density (g/cm³)	Number Fraction
1	20.0	31069	1.578E+01	2.012E-02
		31071		1.336E-02
		94239		9.162E-01
		94240		4.736E-02
		94241		2.996E-03
2	20.0	92235	1.880E+01	9.328E-01
		92238		6.720E-02
3	20.0	7014	1.293E-03	7.800E-01
		8016		2.200E-01

Table 6.37: Calculated Eigenvalues and Transport Sweep Comparisons for PU/HEU System

ICSBEP ID	Calculated α [μs^{-1}]	Transport Sweeps	
		RQFP	Critical Search
MIX_MET_FAST_001	-4.114757×10^{-1}	22,310	*

$M = 1042$, $L = 128$, Tolerance = 10^{-6} , *Did Not Converge

(a) Alpha-Eigenvalue: Comparison of RQFP and Critical Search Transport Sweeps

ICSBEP ID	Calculated k_{eff}	Transport Sweeps	
		RQFP	Power Method
MIX_MET_FAST_001	0.999063	7,130	4,370

$M = 1042$, $L = 128$, Tolerance = 10^{-6}

(b) k -Effective: Comparison of RQFP and Critical Search Transport Sweeps

6.4.3 A Uranium-233 Critical Sphere

The alpha- and k -effective eigenvalue and eigenvectors of a 0.481 inch uranium-233 sphere reflected by an HEU shell were calculated and the number of transport sweeps necessary for converge compared to standard eigenproblem solvers. The uranium-233 system was a fast energy spectrum critical benchmark problem (ICSBEP ID: U233_MET_FAST_002). The critical sphere radius and shell thickness are listed in Table 6.38. Material compositions and number fractions are shown in Table 6.39. This benchmark problem also used a 230 energy group cross section library.

For the alpha-eigenvalue of the uranium-233 system, the eigenvalue was determined to be $-5.158602 \times 10^{-1} \mu\text{s}^{-1}$ as listed in Table 6.40a. For this subcritical system, the RQFP method required 30,590 transport sweeps to converge the alpha eigenpair to a tolerance of 10^{-6} . The critical search method was unable to converge the eigenpair.

The k -effective eigenvalue was determined to be $k = 0.998474$. For this particular benchmark problem, the RQFP method underperformed the power method with fission source update, requiring 15,640 transport sweeps to the power method's 10,580 (Table 6.40b).

Problem Dimensions [cm]		
ICSBEP ID	$r_{\text{U}_{233}}$	δ_{U}
U233_MET_FAST_002	5.0444	6.2661

Table 6.38: Fissile Material Radius and Shell Thicknesses for Uranium-233 Benchmark

Table 6.39: Material Composition for Uranium-233 System

Material Number	Temperature (°C)	Component	Density (g/cm ³)	Number Fraction
1	20.0	92233	1.862E+01	9.822E-01
		92234		1.096E-02
		92238		6.854E-03
2	20.0	92235	1.880E+01	9.328E-01
		92238		6.720E-02
3	20.0	7014	1.293E-03	7.800E-01
		8016		2.200E-01

Table 6.40: Calculated Eigenvalues and Transport Sweep Comparisons for a Uranium-233 System

Transport Sweeps			
ICSBEP ID	Calculated $\alpha [\mu\text{s}^{-1}]$	RQFP	Critical Search
U233_MET_FAST_002	-5.158602×10^{-1}	30,590	*

$M = 1042, L = 128, \text{Tolerance} = 10^{-6}$, *Did Not Converge

(a) Alpha-Eigenvalue: Comparison of RQFP and Critical Search Transport Sweeps

Transport Sweeps			
ICSBEP ID	Calculated k_{eff}	RQFP	Power Method
U233_MET_FAST_002	0.998474	15,640	10,580

$M = 526, L = 128, \text{Tolerance} = 10^{-6}$

(b) k -Effective: Comparison of RQFP and Critical Search Transport Sweeps

6.5 Conclusion

The RQFP method for alpha-eigenvalue performs well for various slab and spherical geometry benchmark problems. Through the various benchmark problems examined in this chapter, the correctness of the method was verified by comparisons to other methods such as Green's Function Method and to other codes such as PARTISN. The RQFP method is able to converge problems which violate the assumptions of slab geometry, isotropic scattering, and fissile regions used in deriving the method. The method, applied to spherical systems, successfully obtained the eigenpair of interest. The RQFP method was able to obtain analytical and measured alpha-eigenvalues of various benchmark problems from the literature and substantially reduced the number of transport sweeps necessary to obtain the alpha-eigenvalue/eigenvector as compared to the traditional critical search method. For various subcritical problems, the RQFP method was able to converge the eigenpair when the critical search failed. This gives evidence that the Rayleigh Quotient Fixed Point method for alpha-eigenvalue problems is robust enough to handle large one-dimensional, multigroup-in-energy problems where the assumptions made in deriving the method might not be true.

The RQFP method for k -effective problems was found to be less successful. The RQFP method for k -effective eigenvalue problems underperforms for most problems considered in this chapter. The method appears to be more sensitive to the violation of assumptions made in its derivation as compared to the RQFP method for alpha-eigenvalue problems. Nevertheless, the RQFP method provides another option to solve k -effective eigenvalue problems.

Chapter 7

Higher Dimensional Eigenvalues

In this chapter we verify the correctness and examine the performance of the Rayleigh Quotient Fixed Point methods for higher-dimensional problems. We consider realistic two- and three-dimensional problems involving fuel rods and fuel assemblies. For higher dimensions, the phase space of the neutron transport equation is a function of two (x, y) or three (x, y, z) spatial variables and two $\hat{\Omega} = (\mu, \eta)$ or three $\hat{\Omega} = (\mu, \eta, \xi)$ angular variables defined as the x -, y -, and z -direction cosines. For higher-dimensional Cartesian geometry, the two-dimensional and three-dimensional alpha-eigenvalue neutron transport equations are given by Eq. 7.1 and Eq. 7.2, respectively:

$$\begin{aligned} & \left[\mu \frac{\partial}{\partial x} + \eta \frac{\partial}{\partial y} + \frac{\alpha}{v(E)} + \sigma(x, y, E) \right] \psi(x, y, \hat{\Omega}, E) \\ &= \frac{\chi(E)}{2} \int_0^\infty dE' \nu(E') \sigma_f(x, y, E') \int_{2\pi} d\hat{\Omega}' \psi(x, y, \hat{\Omega}', E') \\ &+ \frac{1}{2\pi} \int_0^\infty dE' \sigma_s(x, y, E' \rightarrow E) \int_{2\pi} d\hat{\Omega}' \psi(x, y, \hat{\Omega}', E'), \quad (7.1) \end{aligned}$$

$$\begin{aligned} & \left[\mu \frac{\partial}{\partial x} + \eta \frac{\partial}{\partial y} + \xi \frac{\partial}{\partial z} + \frac{\alpha}{v(E)} + \sigma(x, y, z, E) \right] \psi(x, y, z, \hat{\Omega}, E) \\ &= \frac{\chi(E)}{2} \int_0^\infty dE' \nu(E') \sigma_f(x, y, z, E') \int_{4\pi} d\hat{\Omega}' \psi(x, y, z, \hat{\Omega}', E') \\ &+ \frac{1}{4\pi} \int_0^\infty dE' \sigma_s(x, y, z, E' \rightarrow E) \int_{4\pi} d\hat{\Omega}' \psi(x, y, z, \hat{\Omega}', E'). \quad (7.2) \end{aligned}$$

The three-dimensional k -effective eigenvalue neutron transport equation is given by 7.3:

$$\begin{aligned}
& \left[\mu \frac{\partial}{\partial x} + \eta \frac{\partial}{\partial y} + \xi \frac{\partial}{\partial z} + \sigma(x, y, z, E) \right] \psi(x, y, z, \hat{\Omega}, E) \\
&= \frac{1}{k} \frac{\chi(E)}{2} \int_0^\infty dE' \nu(E') \sigma_f(x, y, z, E') \int_{4\pi} d\hat{\Omega}' \psi(x, y, z, \hat{\Omega}', E') \\
&\quad + \frac{1}{4\pi} \int_0^\infty dE' \sigma_s(x, y, z, E' \rightarrow E) \int_{4\pi} d\hat{\Omega}' \psi(x, y, z, \hat{\Omega}', E'). \quad (7.3)
\end{aligned}$$

We also consider two-dimensional cylindrical geometry problems. For cylindrical geometry problems, the complexity is increased due to the fact that for one spatial dimension, two angular variables are required to describe the angular flux. For two-dimensional cylindrical problems, the alpha-eigenvalue neutron transport equation is given by

$$\begin{aligned}
& \frac{\mu}{\rho} \frac{\partial}{\partial \rho} (\rho \psi) + \xi \frac{\partial \psi}{\partial z} - \frac{1}{\rho} \frac{\partial}{\partial \omega} (\eta \psi) + \frac{\alpha}{v(E)} \psi(\rho, \hat{\Omega}, E) + \sigma(\rho, E) \psi(\rho, \hat{\Omega} E) \\
&= \frac{\chi(E)}{2} \int_0^\infty dE' \nu(E') \sigma_f(\rho, E') \int_{4\pi} d\hat{\Omega}' \psi(\rho, \hat{\Omega}', E') \\
&\quad + \frac{1}{4\pi} \int_0^\infty dE' \sigma_s(\rho, E' \rightarrow E) \int_{4\pi} d\hat{\Omega}' \psi(\rho, \hat{\Omega}', E'), \quad (7.4)
\end{aligned}$$

where ρ is the radial distance from the origin and $\mu = (1-\xi^2)^{1/2} \cos \omega$ and $\eta = (1-\xi^2)^{1/2} \sin \omega$ (Figure 7.1).

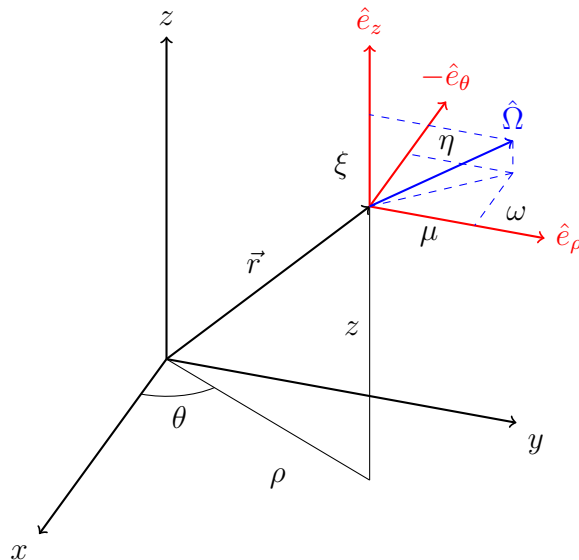


Figure 7.1: Cylindrical Space-Angle Coordinate System in Three Dimensions

Reactor fuel assemblies and fuel pins were modeled in ARDRA. These benchmark problems consisted of detailed heterogeneous domains with many nuclei of interest to reactor design and physics. The higher dimension geometry of the problems along with the many energy-group cross section libraries allowed for analysis of the Rayleigh Quotient Fixed Point method for alpha- and k -effective eigenvalue problems in situations where assumptions of positivity might no longer be valid.

7.1 Critical Cylinder Benchmark Problems

We consider homogeneous and heterogeneous two-dimensional cylindrical problems in this section. In the homogeneous case, a critical *infinite cylinder* domain is modeled with critical radius r_c and height z_c to approximate an infinite cylinder in the z -direction (Figure 7.2). In the heterogeneous case, an infinite cylinder is surrounded by some reflector (such as water). The inclusion of the reflector introduces regions in the problem domain where fission is not possible and only downscattering is allowed. This violates the conditions necessary for primitivity (see Section 3.2). We find that the inclusion of non-fissile reflector material does not impact the ability of the Rayleigh Quotient Fixed Point method for alpha- and k -effective eigenvalue problems to obtain the fundamental eigenpair.

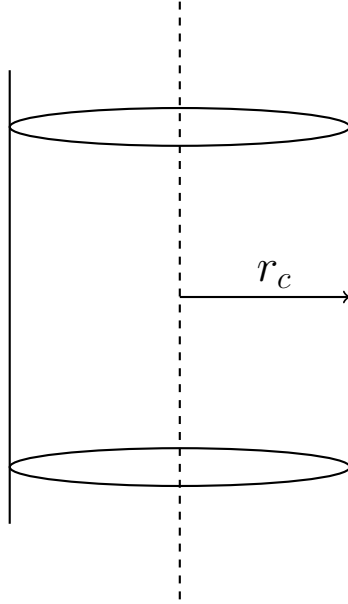


Figure 7.2: Critical Radius of Infinite Cylinder

7.1.1 Homogeneous Critical Cylinder Problems

Five exactly critical homogeneous cylinder problems from Sood [40] were considered with cross sections listed in Table 7.1. These problems consisted of plutonium (Sood Criticality Benchmark Problem 7), uranium-235 (Sood Criticality Benchmark Problems 13, 36, and 37) and heavy-water/uranium mixture (Sood Criticality Problem 23) cylinders with critical radii listed in Table 7.2. All problem cross-sections were one-group and two problems included anisotropic scattering.

The number of transport sweeps necessary for convergence for the RQFP and critical search method can be seen in Table 7.2a. For the plutonium problem (Sood Prob. 7), the RQFP method required 38 sweeps to converge the alpha-eigenvalue and eigenvector. The critical search method required 461 transport sweeps. In this particular problem the RQFP method reduced the number of transport sweeps necessary by a factor of 10. For the uranium-235 with isotropic scattering problem (Sood Prob. 13), the RQFP method required 45 transport sweeps as compared to 455 sweeps for the critical search method, a factor of 10 reduction. For the heavy-water/uranium mixture (Sood Prob. 23), the number of transport sweeps required to converge the eigenpair increased dramatically. For this set of cross section data, 319 transport sweeps were required by the RQFP method to converge the fundamental mode and eigenvalue. The critical search method was not able to converge the alpha-eigenvalue as the system as modeled was slightly subcritical. For the uranium-235 cross sections with anisotropic scattering (Sood Prob. 36 and 37), the RQFP method was found to take 41 and 53 transport sweeps each. The critical search method was unable to converge these methods despite the fact that the systems were slightly supercritical. The critical search method was unable to converge the alpha-eigenvalue and eigenvector due to the fact that the k -effective eigenvalue becomes negative in the interpolation part of the algorithm.

The number of transport sweeps necessary for convergence for the RQFP and power method with fission source update can be seen in Table 7.2b. The RQFP method requires a similar number of sweeps to converge the k -effective eigenvalue problem except for the heavy-water/uranium mixture problem. In this case, the RQFP method requires 320 transport sweeps to only 121 transport sweeps for the power method with fission source update. This implies that the convergence rate of the RQFP method is much more strongly influenced by the amount of scattering in the system than the power method. In all cases, the number of sweeps required by the RQFP method to converge the k -effective eigenvalue was similar to the number of sweeps required to converge the alpha-eigenvalue problem.

Table 7.1: One-Group Cross Sections for Infinite Cylinder Critical Problems (cm^{-1}) in [40]

Cross Section Set	σ	$\nu\sigma_f$	σ_{s0}	σ_{s1}	v [cm/s]
Sood Prob. 7	0.32640	0.231744	0.225216	0.0	1
Sood Prob. 13	0.32640	0.176256	0.248064	0.0	1
Sood Prob. 23	0.54628	0.0928676	0.464338	0.0	1
Sood Prob. 36	0.32640	1.76256	0.248064	0.042432	1
Sood Prob. 37	0.32640	1.76256	0.248064	0.212160	1

Table 7.2: Calculated Eigenvalues and Transport Sweep Comparisons for Critical Infinite Cylinder Problems in [40]

Cross Section Set	r_c [cm]	Calculated α [s^{-1}]	Transport Sweeps	
			RQFP	Critical Search
Sood Prob. 7	4.279960	3.783833×10^{-4}	38	461
Sood Prob. 13	5.284935	1.973082×10^{-4}	45	455
Sood Prob. 23	16.554249	-1.007328×10^{-4}	319	*
Sood Prob. 36	5.514296811	2.012672×10^{-4}	41	*
Sood Prob. 37	6.940205668	1.906997×10^{-4}	53	*

$M = 500$, $L = 10$, Tolerance = 10^{-12} , *Did Not Converge

(a) Alpha-Eigenvalue: Comparison of RQFP and Critical Search Transport Sweeps

Cross Section Set	r_c [cm]	Calculated k_{eff}	Transport Sweeps	
			RQFP	Power Method
Sood Prob. 7	4.279960	1.001419	43	40
Sood Prob. 13	5.284935	1.000989	49	42
Sood Prob. 23	16.554249	0.998935	320	121
Sood Prob. 36	5.514296811	1.000997	48	40
Sood Prob. 37	6.940205668	1.000870	37	43

$M = 500$, $L = 10$, Tolerance = 10^{-12}

(b) k -Effective: Comparison of RQFP and Power Method Transport Sweeps

7.2 Two- and Three-Dimensional Cartesian Benchmark Problems

We consider three versions of the MOX Fuel Assembly 3D Extension Case from the *Benchmark on Deterministic Transport Calculations Without Spatial Homogenisation* [45]. The benchmark geometry is a three-dimensional representation of sixteen assembly (quarter core symmetry) C5G7 MOX fuel assembly problem described in [46]. The benchmark problem is meant to provide a challenging test of the ability of three-dimensional methods to handle spatial heterogeneities.

The benchmark problem materials consist of seven materials: UO₂ fuel-clad, 4.3% MOX fuel, 7.0% MOX fuel, 8.7% MOX fuel, the fission chamber, the guide tube, and the moderator. Each material has a seven-energy cross section set with energy group boundaries and group speeds listed in Table 7.3. The seven-energy-group, isotropic scattering cross sections for the UO₂ fuel-clad are provided in Table 7.4. The seven-energy-group, isotropic scattering cross sections for the three enrichments of MOX are listed in Table 7.5, Table 7.6, and Table 7.7, respectively, while the cross sections for the fission chamber, guide tube, and moderator are listed in Table 7.8, Table 7.9, and Table 7.10, respectively. We note that the material cross sections include a group transport cross section, $\sigma_{g,tr}$, defined as

$$\sigma_{g,tr} = \sigma_g - \bar{\mu} \sum_{g'=0}^6 \sigma_{s,g'g}, \quad (7.5)$$

where $\bar{\mu}$ is the average cosine of the neutron scattering angle. Also included is a group absorption cross section, $\sigma_{g,a}$, defined as the sum of the parasitic absorption cross section, $\sigma_{\gamma,g}$, and the fission cross section, $\sigma_{f,g}$.

The quarter core has dimensions 64.26 cm by 64.26 cm by 214.20 cm. Each fuel pin cell has width 1.26 cm and the radius of the fuel cylinder is 0.54cm. The quarter core model consists to two types of assemblies, UO₂ and MOX surrounded by moderator as seen in Figure 7.3. Each fuel assembly has a pin layout as shown in Figure 7.4. Reflected boundary conditions are imposed on the bottom and right quarter core boundaries. Vacuum boundary conditions are imposed on the top and left edges of the quarter core. The k -effective eigenvalue of the system benchmark problem is $k = 1.186550$.

Three variations of the benchmark problem were considered. Two two-dimensional variants of the benchmark problem were modeled where reflective boundary conditions were placed on the top and bottom of the quarter core. In the first problem, a coarse spatial homogenization was done on a high-fidelity geometric model created for the LLNL Monte Carlo code COG [47] and the problem solved using ARDRA. In the second case, a finer spatial homogenization was done on the high-fidelity geometric model. Finally, a full three-dimensional calculation with coarse spatial homogenization was done. The performance of the RQFP method for alpha- and k -effective eigenvalues was investigated for all problems and compared to traditional eigenvalue solution methods in the field.

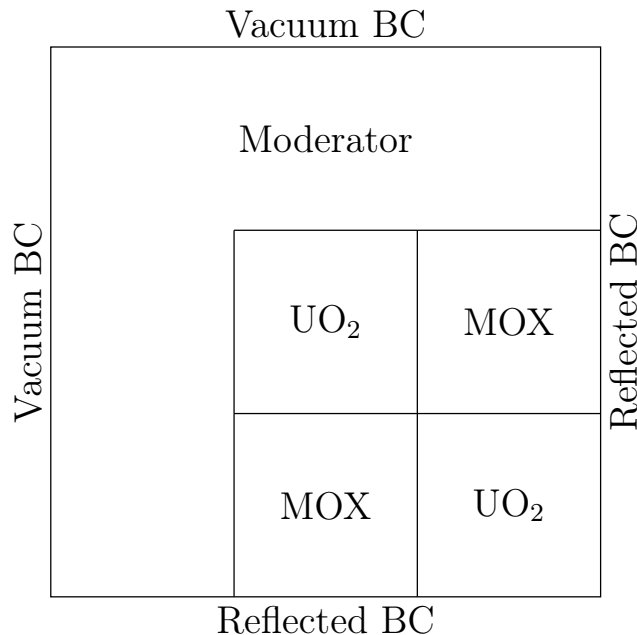


Figure 7.3: Assembly Layout for MOX Fuel Assembly Benchmark

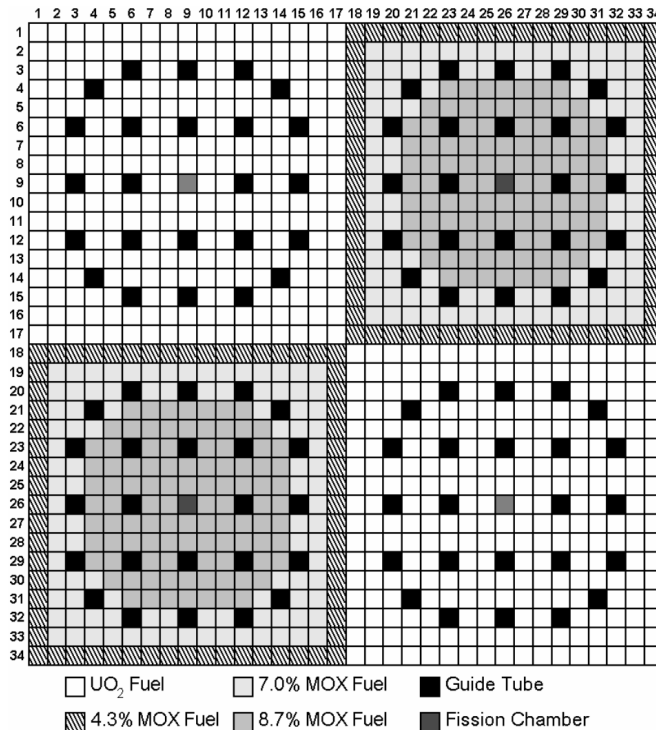


Figure 7.4: Fuel Pin Layout for MOX Fuel Assembly Benchmark From [45]

Table 7.3: C5G7MOX Energy Group Boundaries (MeV) and Speeds (cm/s)

Energy Group g	Upper Energy Boundary	Midpoint Energy	Lower Energy Boundary	Speed
0	2.000000E+01	1.750000E+01	1.500000E+01	5.692375E+03
1	1.500000E+01	1.250000E+01	1.000000E+01	4.817827E+03
2	1.000000E+01	7.500000E+00	5.000000E+00	3.711626E+03
3	5.000000E+00	2.550000E+00	1.000000E-01	1.762394E+03
4	1.000000E-01	5.050000E-02	1.000000E-03	2.405592e+02
5	1.000000E-03	5.050000E-04	1.000000E-05	2.405663E+01
6	1.000000E-05	5.000500e-06	1.000000E-09	2.208836E+00

Table 7.4: C5G7MOX Cross Sections - UO₂ Fuel-Clad

Energy Group g	σ_g	$\sigma_{g,tr}$	$\sigma_{a,g}$	$\sigma_{\gamma,g}$	$\sigma_{f,g}$	ν_g	χ_g
0	2.12450E-01	1.77949E-01	8.02480E-03	8.12740E-04	7.21206E-03	2.78145E+00	5.87910E-01
1	3.55470E-01	3.29805E-01	3.71740E-03	2.89810E-03	8.19301E-04	2.47443E+00	4.11760E-01
2	4.85540E-01	4.80388E-01	2.67690E-02	2.03158E-02	6.45320E-03	2.43383E+00	3.39060E-04
3	5.59400E-01	5.54367E-01	9.62360E-02	7.76712E-02	1.85648E-02	2.43380E+00	1.17610E-07
4	3.18030E-01	3.11801E-01	3.00200E-02	1.22116E-02	1.78084E-02	2.43380E+00	0.00000E+00
5	4.01460E-01	3.95168E-01	1.11260E-01	2.82252E-02	8.30348E-02	2.43380E+00	0.00000E+00
6	5.70610E-01	5.64406E-01	2.82780E-01	6.67760E-02	2.16004E-01	2.43380E+00	0.00000E+00

(a) UO₂ Fuel-Clad Cross Sections – (cm⁻¹)

g', g	1	2	3	4	5	6	7
1	1.27537E-01	4.23780E-02	9.43740E-06	5.51630E-09	0.00000E+00	0.00000E+00	0.00000E+00
2	0.00000E+00	3.24456E-01	1.63140E-03	3.14270E-09	0.00000E+00	0.00000E+00	0.00000E+00
3	0.00000E+00	0.00000E+00	4.50940E-01	2.67920E-03	0.00000E+00	0.00000E+00	0.00000E+00
4	0.00000E+00	0.00000E+00	0.00000E+00	4.52565E-01	5.56640E-03	0.00000E+00	0.00000E+00
5	0.00000E+00	0.00000E+00	0.00000E+00	1.25250E-04	2.71401E-01	1.02550E-02	1.00210E-08
6	0.00000E+00	0.00000E+00	0.00000E+00	0.00000E+00	1.29680E-03	2.65802E-01	1.68090E-02
7	0.00000E+00	0.00000E+00	0.00000E+00	0.00000E+00	0.00000E+00	8.54580E-03	2.73080E-01

(b) UO₂ Fuel-Clad Scattering Block (cm⁻¹)

Table 7.5: C5G7MOX Cross Sections - 4.3% MOX Fuel

Energy Group g	σ_g	$\sigma_{g,tr}$	$\sigma_{a,g}$	$\sigma_{\gamma,g}$	$\sigma_{f,g}$	ν_g	χ_g
0	2.11920E-01	1.78731E-01	8.43390E-03	8.06860E-04	7.62704E-03	2.85209E+00	5.87910E-01
1	3.55810E-01	3.30849E-01	3.75770E-03	2.88080E-03	8.76898E-04	2.89099E+00	4.11760E-01
2	4.88900E-01	4.83772E-01	2.79700E-02	2.22717E-02	5.69835E-03	2.85486E+00	3.39060E-04
3	5.71940E-01	5.66922E-01	1.04210E-01	8.13228E-02	2.28872E-02	2.86073E+00	1.17610E-07
4	4.32390E-01	4.26227E-01	1.39940E-01	1.29177E-01	1.07635E-02	2.85447E+00	0.00000E+00
5	6.84950E-01	6.78997E-01	4.09180E-01	1.76423E-01	2.32757E-01	2.86415E+00	0.00000E+00
6	6.88910E-01	6.82852E-01	4.09350E-01	1.60382E-01	2.48968E-01	2.86780E+00	0.00000E+00

(a) 4.3% MOX Fuel – Clad Cross Sections (cm^{-1})

g', g	1	2	3	4	5	6	7
0	1.28876E-01	4.14130E-02	8.22900E-06	5.04050E-09	0.00000E+00	0.00000E+00	0.00000E+00
1	0.00000E+00	3.25452E-01	1.63950E-03	1.59820E-09	0.00000E+00	0.00000E+00	0.00000E+00
2	0.00000E+00	0.00000E+00	4.53188E-01	2.61420E-03	0.00000E+00	0.00000E+00	0.00000E+00
3	0.00000E+00	0.00000E+00	0.00000E+00	4.57173E-01	5.53940E-03	0.00000E+00	0.00000E+00
4	0.00000E+00	0.00000E+00	0.00000E+00	1.60460E-04	2.76814E-01	9.31270E-03	9.16560E-09
5	0.00000E+00	0.00000E+00	0.00000E+00	0.00000E+00	2.00510E-03	2.52962E-01	1.48500E-02
6	0.00000E+00	0.00000E+00	0.00000E+00	0.00000E+00	0.00000E+00	8.49480E-03	2.65007E-01

(b) 4.3% MOX Fuel Scattering Block (cm^{-1})

Table 7.6: C5G7MOX Cross Sections - 7.0% MOX Fuel

Energy Group g	σ_g	$\sigma_{g,tr}$	$\sigma_{a,g}$	$\sigma_{\gamma,g}$	$\sigma_{f,g}$	ν_g	χ_g
1	2.14540E-01	1.81323E-01	9.06570E-03	8.11240E-04	8.25446E-03	2.88498E+00	5.87910E-01
2	3.59350E-01	3.34368E-01	4.29670E-03	2.97105E-03	1.32565E-03	2.91079E+00	4.11760E-01
3	4.98910E-01	4.93785E-01	3.28810E-02	2.44594E-02	8.42156E-03	2.86574E+00	3.39060E-04
4	5.96220E-01	5.91216E-01	1.22030E-01	8.91570E-02	3.28730E-02	2.87063E+00	1.17610E-07
5	4.80350E-01	4.74198E-01	1.82980E-01	1.67016E-01	1.59636E-02	2.86714E+00	0.00000E+00
6	8.39360E-01	8.33601E-01	5.68460E-01	2.44666E-01	3.23794E-01	2.86658E+00	0.00000E+00
7	8.59480E-01	8.53603E-01	5.85210E-01	2.22407E-01	3.62803E-01	2.87539E+00	0.00000E+00

(a) 7.0% MOX Fuel – Clad Cross Sections (cm^{-1})

g', g	1	2	3	4	5	6	7
0	1.30457E-01	4.17920E-02	8.51050E-06	5.13290E-09	0.00000E+00	0.00000E+00	0.00000E+00
1	0.00000E+00	3.28428E-01	1.64360E-03	2.20170E-09	0.00000E+00	0.00000E+00	0.00000E+00
2	0.00000E+00	0.00000E+00	4.58371E-01	2.53310E-03	0.00000E+00	0.00000E+00	0.00000E+00
3	0.00000E+00	0.00000E+00	0.00000E+00	4.63709E-01	5.47660E-03	0.00000E+00	0.00000E+00
4	0.00000E+00	0.00000E+00	0.00000E+00	1.76190E-04	2.82313E-01	8.72890E-03	9.00160E-09
5	0.00000E+00	0.00000E+00	0.00000E+00	0.00000E+00	2.27600E-03	2.49751E-01	1.31140E-02
6	0.00000E+00	0.00000E+00	0.00000E+00	0.00000E+00	0.00000E+00	8.86450E-03	2.59529E-01

(b) 7.0% MOX Fuel Scattering Block (cm^{-1})

Table 7.7: C5G7MOX Cross Sections - 8.7% MOX Fuel

Energy Group g	σ_g	$\sigma_{g,tr}$	$\sigma_{a,g}$	$\sigma_{\gamma,g}$	$\sigma_{f,g}$	ν_g	χ_g
0	2.16280E-01	1.83045E-01	9.48620E-03	8.14110E-04	8.67209E-03	2.90426E+00	5.87910E-01
1	3.61700E-01	3.36705E-01	4.65560E-03	3.03134E-03	1.62426E-03	2.91795E+00	4.11760E-01
2	5.05630E-01	5.00507E-01	3.62400E-02	2.59684E-02	1.02716E-02	2.86986E+00	3.39060E-04
3	6.11170E-01	6.06174E-01	1.32720E-01	9.36753E-02	3.90447E-02	2.87491E+00	1.17610E-07
4	5.08900E-01	5.02754E-01	2.08400E-01	1.89142E-01	1.92576E-02	2.87175E+00	0.00000E+00
5	9.266670E-01	9.21028E-01	6.58700E-01	2.83812E-01	3.74888E-01	2.86752E+00	0.00000E+00
6	9.60990E-01	9.55231E-01	6.90170E-01	2.59571E-01	4.30599E-01	2.87808E+00	0.00000E+00

(a) 8.7% MOX Fuel – Clad Cross Sections (cm^{-1})

g', g	1	2	3	4	5	6	7
0	1.31504E-01	4.20460E-02	8.69720E-06	5.19380E-09	0.00000E+00	0.00000E+00	0.00000E+00
1	0.00000E+00	3.30403E-01	1.64630E-03	2.60060E-09	0.00000E+00	0.00000E+00	0.00000E+00
2	0.00000E+00	0.00000E+00	4.61792E-01	2.47490E-03	0.00000E+00	0.00000E+00	0.00000E+00
3	0.00000E+00	0.00000E+00	0.00000E+00	4.68021E-01	5.43300E-03	0.00000E+00	0.00000E+00
4	0.00000E+00	0.00000E+00	0.00000E+00	1.85970E-04	2.85771E-01	8.39730E-03	8.92800E-09
5	0.00000E+00	0.00000E+00	0.00000E+00	0.00000E+00	2.39160E-03	2.47614E-01	1.23220E-02
6	0.00000E+00	0.00000E+00	0.00000E+00	0.00000E+00	0.00000E+00	8.96810E-03	2.56093E-01

(b) 8.7% MOX Fuel Scattering Block (cm^{-1})

Table 7.8: C5G7MOX Cross Sections - Fission Chamber

Energy Group g	σ_g	$\sigma_{g,tr}$	$\sigma_{a,g}$	$\sigma_{\gamma,g}$	$\sigma_{f,g}$	ν_g	χ_g
0	1.90730E-01	1.26032E-01	5.11320E-04	5.11315E-04	4.79002E-09	2.76283E+00	5.87910E-01
	4.56520E-01	2.93160E-01	7.58130E-05	7.58072E-05	5.82564E-09	2.46239E+00	4.11760E-01
1	6.40700E-01	2.84250E-01	3.16430E-04	3.15966E-04	4.63719E-07	2.43380E+00	3.39060E-04
	6.49840E-01	2.81020E-01	1.16750E-03	1.16226E-03	5.24406E-06	2.43380E+00	1.17610E-07
2	6.70630E-01	3.34460E-01	3.39770E-03	3.39755E-03	1.45390E-07	2.43380E+00	0.00000E+00
	8.75060E-01	5.65640E-01	9.18860E-03	9.18789E-03	7.14972E-07	2.43380E+00	0.00000E+00
3	1.43450E+00	1.17214E+00	2.32440E-02	2.32419E-02	2.08041E-06	2.43380E+00	0.00000E+00
	6						

(a) Fission Chamber – Cross Sections (cm^{-1})

g', g	1	2	3	4	5	6	7
0	6.61659E-02	5.90700E-02	2.83340E-04	1.46220E-06	2.06420E-08	0.00000E+00	0.00000E+00
1	0.00000E+00	2.40377E-01	5.24350E-02	2.49900E-04	1.92390E-05	2.98750E-06	4.21400E-07
2	0.00000E+00	0.00000E+00	1.83425E-01	9.22880E-02	6.93650E-03	1.07900E-03	2.05430E-04
3	0.00000E+00	0.00000E+00	0.00000E+00	7.90769E-02	1.69990E-01	2.58600E-02	4.92560E-03
4	0.00000E+00	0.00000E+00	0.00000E+00	3.73400E-05	9.97570E-02	2.06790E-01	2.44780E-02
5	0.00000E+00	0.00000E+00	0.00000E+00	0.00000E+00	9.17420E-04	3.16774E-01	2.38760E-01
6	0.00000E+00	0.00000E+00	0.00000E+00	0.00000E+00	0.00000E+00	4.97930E-02	1.09910E+00

(b) Fission Chamber Scattering Block (cm^{-1})

Table 7.9: C5G7MOX Cross Sections - Guide Tube

Energy Group g	σ_g	$\sigma_{g,tr}$	$\sigma_{a,g}$	$\sigma_{\gamma,g}$
0	1.90730E-01	1.26032E-01	5.11320E-04	5.11320E-04
1	4.56520E-01	2.93160E-01	7.58010E-05	7.58010E-05
2	6.40670E-01	2.84240E-01	3.15720E-04	3.15720E-04
3	6.49670E-01	2.80960E-01	1.15820E-03	1.15820E-03
4	6.70580E-01	3.34440E-01	3.39750E-03	3.39750E-03
5	8.75050E-01	5.65640E-01	9.18780E-03	9.18780E-03
6	1.43450E+00	1.17215E+00	2.32420E-02	2.32420E-02

(a) Guide Tube Cross Sections (cm^{-1})						
g', g	1	2	3	4	5	6
0	6.61659E-02	5.90700E-02	2.83340E-04	1.46220E-06	2.06420E-08	0.00000E+00
1	0.00000E+00	2.40377E-01	5.24350E-02	2.49900E-04	1.92390E-05	2.98750E-06
2	0.00000E+00	0.00000E+00	1.83297E-01	9.23970E-02	6.94460E-03	1.08030E-03
3	0.00000E+00	0.00000E+00	0.00000E+00	7.88511E-02	1.70140E-01	2.58810E-02
4	0.00000E+00	0.00000E+00	0.00000E+00	3.73330E-05	9.97372E-02	2.06790E-01
5	0.00000E+00	0.00000E+00	0.00000E+00	0.00000E+00	9.17260E-04	3.16765E-01
6	0.00000E+00	0.00000E+00	0.00000E+00	0.00000E+00	0.00000E+00	4.97920E-02

(b) Guide Tube Scattering Block (cm^{-1})						
g', g	1	2	3	4	5	6

Table 7.10: C5G7MOX Cross Sections - Moderator

Energy Group g	σ_g	$\sigma_{g,tr}$	$\sigma_{a,g}$	$\sigma_{\gamma,g}$
0	2.30070E-01	1.59206E-01	6.01050E-04	6.01050E-04
1	7.76460E-01	4.12970E-01	1.57930E-05	1.57930E-05
2	1.48420E+00	5.90310E-01	3.37160E-04	3.37160E-04
3	1.50520E+00	5.84350E-01	1.94060E-03	1.94060E-03
4	1.55920E+00	7.18000E-01	5.74160E-03	5.74160E-03
5	2.02540E+00	1.25445E+00	1.50010E-02	1.50010E-02
6	3.30570E+00	2.65038E+00	3.72390E-02	3.72390E-02

g', g	1	2	3	4	5	6	7
0	4.44777E-02	1.13400E-01	7.23470E-04	3.74990E-06	5.31840E-08	0.00000E+00	0.00000E+00
1	0.00000E+00	2.82334E-01	1.29940E-01	6.23400E-04	4.80020E-05	7.44860E-06	1.04550E-06
2	0.00000E+00	0.00000E+00	3.45256E-01	2.24570E-01	1.69990E-02	2.64430E-03	5.03440E-04
3	0.00000E+00	0.00000E+00	0.00000E+00	9.10284E-02	4.15510E-01	6.37320E-02	1.21390E-02
4	0.00000E+00	0.00000E+00	0.00000E+00	7.14370E-05	1.39138E-01	5.11820E-01	6.12290E-02
5	0.00000E+00	0.00000E+00	0.00000E+00	0.00000E+00	2.21570E-03	6.99913E-01	5.37320E-01
6	0.00000E+00	0.00000E+00	0.00000E+00	0.00000E+00	0.00000E+00	1.32440E-01	2.48070E+00

(b) Moderator Scattering Block (cm^{-1})

7.2.1 Two-Dimensional MOX Fuel Core with Coarse Spatial Discretization

A coarse spatial homogenization of the benchmark problem led to the assembly geometry shown in Figure 7.5. In particular, the coarse homogenization procedure led to the inclusion of moderator in assembly regions where there was none previously. Spatial discretization was done using diamond differencing with twenty spatial cells in both the x - and y - directions. S_{16} discrete ordinates quadrature was used to model the two-dimensional problem.

Given the coarse spatial homogenization, it was expected the the k -effective eigenvalue of the system would be greater than the reference $k = 1.184977$ due to decreased absorption in the system caused by the coarse discretization. The k -effective eigenvalue of the problem was found to be $k = 1.185404$. The alpha-eigenvalue was found to be $\alpha = 1.492999 \times 10^{-1} \mu s^{-1}$. The RQFP method for both the alpha- and k -effective eigenproblems obtained the same eigenvalue as the critical search method and power iteration.

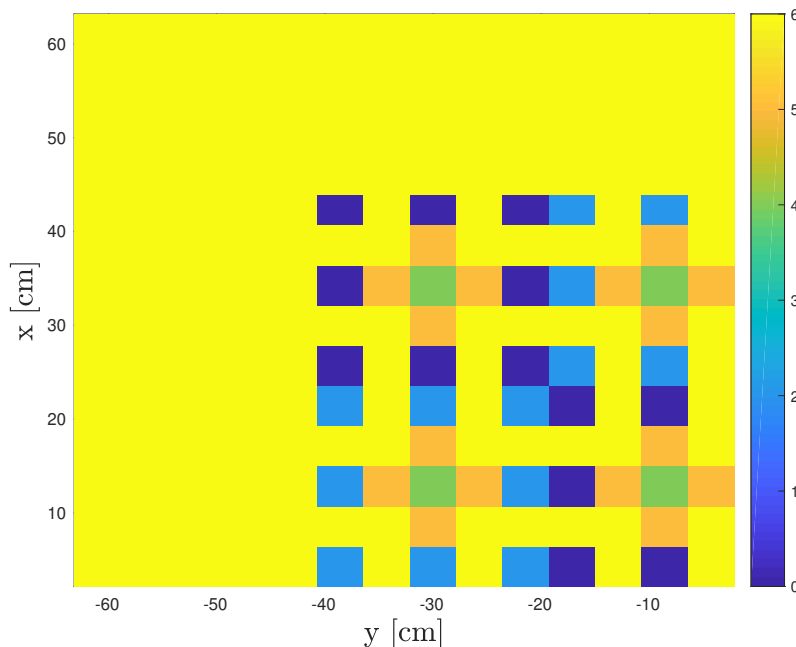


Figure 7.5: Coarse Spatial Homogenization of MOX Fuel Assembly Benchmark Problem
Each material is given a number which corresponds to the color shown in the figure: $UO_2 = 0$, 4.3% MOX Fuel = 1, 7.0% MOX Fuel = 2, 8.7% MOX Fuel = 3, Guide Tube = 4, Fission Chamber = 5, Moderator = 6.

For the alpha-eigenvalue, the RQFP method required 6,776 transport sweeps to converge the eigenvalue/eigenvector residual to a tolerance of 10^{-6} as seen in Table 7.11a. The critical search method required 81,445 transport sweeps after requiring seven intermediate k -effective calculations. The group scalar fluxes for the seven groups can be seen in Figures 7.6a-7.6g. The RQFP method was able to converge the alpha-eigenvalue/eigenvector despite the system being highly supercritical. While not all cells contained fissile material and the moderator contained only downscattering, the violation of the primitivity condition did not affect the ability of the method to converge.

For the k -effective eigenvalue, the RQFP method required 9,064 transport sweeps as compared to 9,681 transport sweeps for the power method with fission source norm update (Table 7.11b). As the problem was substantially supercritical, the performance of the RQFP method was not degraded by the large amounts of scattering in the moderator regions of the problem because of the localization of the group eigenvectors in the fissile regions of the problem. This allowed the RQFP method to converge the solution in fewer iterations than the power method. The k -effective eigenvalue group scalar fluxes were substantially different from the alpha-eigenvalue group scalar fluxes as expected since the problem was not close to critical. This is expected as the fundamental modes are expected to be substantially different as the positive alpha-eigenvalue hardens the neutron energy spectra while the k -effective eigenvalue softens the spectrum. Unlike previous problems that were critical or close to critical, the number of transport sweeps required to converge both eigenvector problems was substantially different, with the k -effective eigenvector requiring approximately 33% more sweeps. This result gives more evidence of the sensitivity of the RQFP method to the shape of the eigenvectors. An example of the difference in the alpha- and k -effective eigenvectors is shown for the thermal group ($g = 6$) in Figure 7.7. The absolute difference between the alpha-eigenvalue and k -effective eigenvectors for energy group six shows major differences in the boundaries of the core where neutron leakage is different for both eigenproblems.

Table 7.11: Calculated Eigenvalues and Transport Sweep Comparisons for 2D MOX Fuel Core with Coarse Spatial Discretization

Benchmark Problem	Calculated α [μs^{-1}]	Transport Sweeps	
		RQFP	Critical Search
2D MOX Coarse Discretization	1.492999×10^{-1}	6,776	81,445

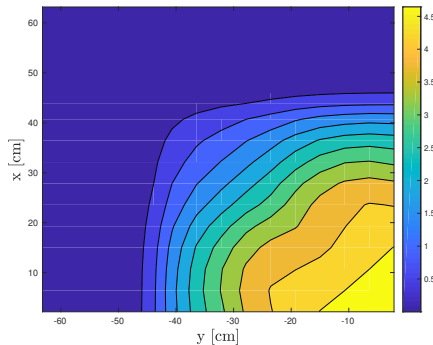
$M = 20 \times 20$, $L = 16$, Tolerance = 10^{-6}

(a) Alpha-Eigenvalue: Comparison of RQFP and Critical Search Transport Sweeps

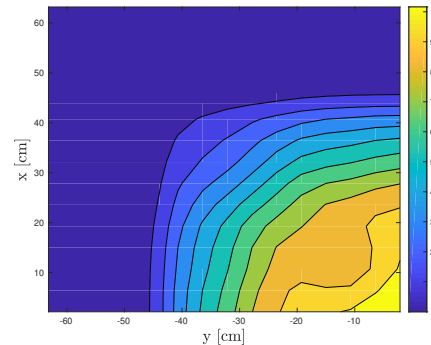
Benchmark Problem	Calculated k_{eff}	Transport Sweeps	
		RQFP	Power Method
2D MOX Coarse Discretization	1.184977	9,064	9,681

$M = 20 \times 20$, $L = 16$, Tolerance = 10^{-6}

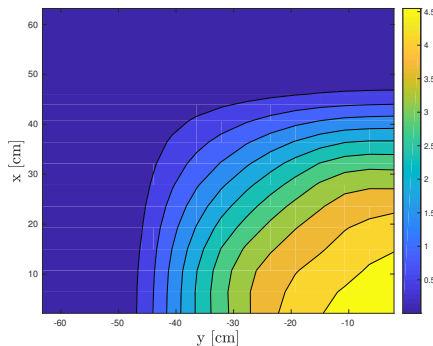
(b) k -Effective: Comparison of RQFP and Power Method Transport Sweeps



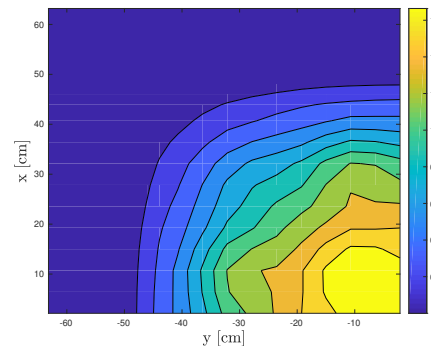
(a) Scalar Flux for Energy Group Zero



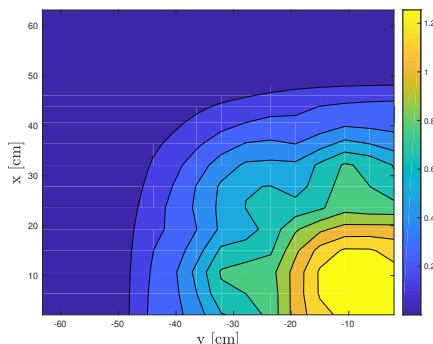
(b) Scalar Flux for Energy Group One



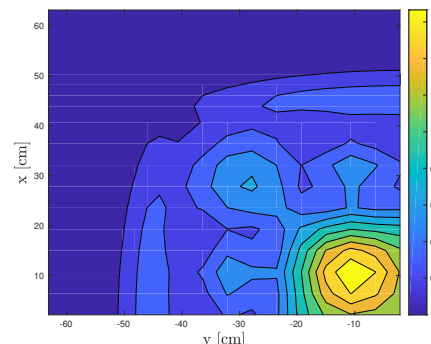
(c) Scalar Flux for Energy Group Two



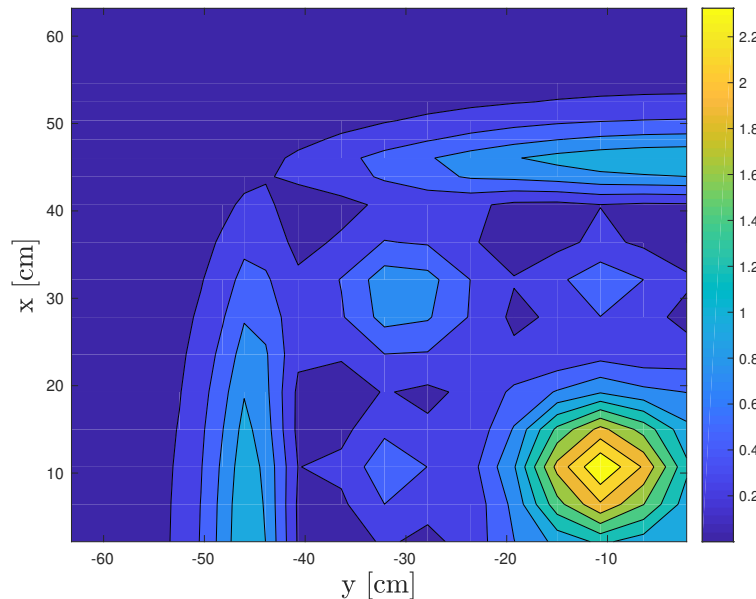
(d) Scalar Flux for Energy Group Three



(e) Scalar Flux for Energy Group Four



(f) Scalar Flux for Energy Group Five



(g) Scalar Flux for Energy Group Six

Figure 7.6: Alpha-Eigenvalue Group Scalar Fluxes for 2D MOX Fuel Assembly Benchmark Problem - Coarse Spatial Discretization

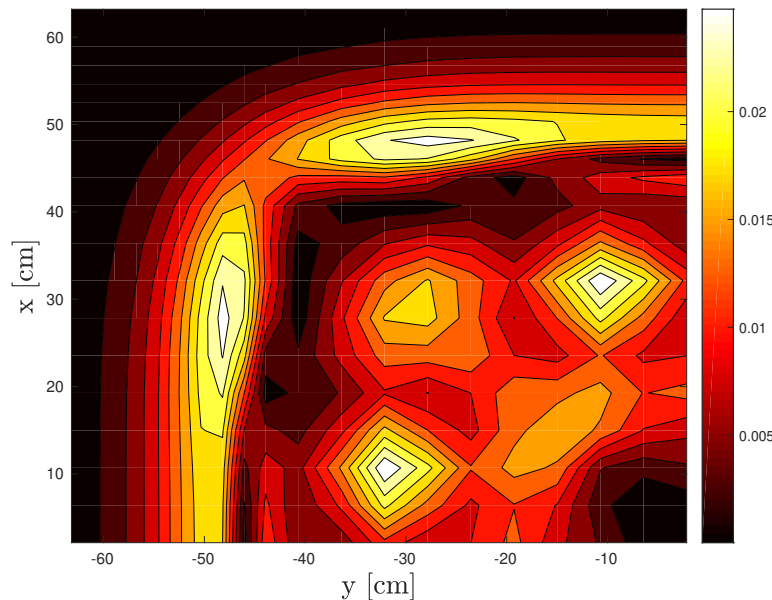


Figure 7.7: Absolute Difference between Alpha- and k -Effective Eigenvalue Group Six Scalar Fluxes (Coarse Homogenization)

7.2.2 Two-Dimensional MOX Fuel Core with Fine Spatial Discretization

A fine spatial homogenization of the benchmark led to the assembly geometry shown in Figure 7.8. The fine spatial homogenization allowed for high-fidelity modeling of the assembly, with individual fuel pins, guide tubes, and fission chambers resolved in the model. For the fine spatial discretization, diamond differencing was used with 340 spatial cells in both the x - and y -direction. The problem used S_{16} discrete ordinates angular quadrature. For the fine spatial homogenization, the k -effective eigenvalue of the problem was found to be $k = 1.185303$. The alpha-eigenvalue was found to be $\alpha = 1.396240 \times 10^{-1} \mu s^{-1}$. The RQFP method for both the alpha- and k -effective eigenproblems obtained the same eigenvalue as the critical search method and power iteration.

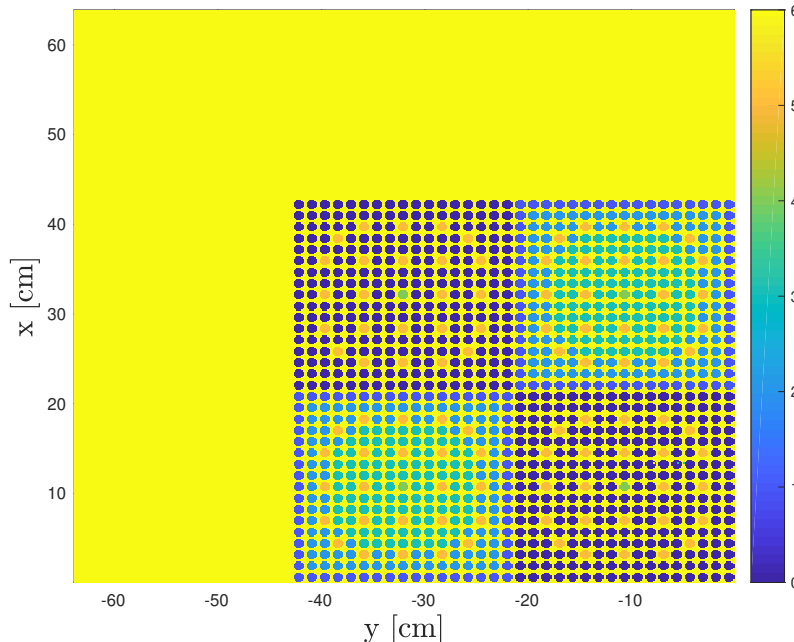


Figure 7.8: Fine Spatial Homogenization of MOX Fuel Assembly Benchmark Problem
The color in each cell corresponds to the material in that cell. Each material is given a number which corresponds to the color shown in the figure: $UO_2 = 0$, 4.3% MOX Fuel = 1, 7.0% MOX Fuel = 2, 8.7% MOX Fuel = 3, Guide Tube = 4, Fission Chamber = 5, Moderator = 6.

Determining the alpha-eigenvalue and eigenvector using the RQFP method required 4,096 transport sweeps while the critical search method required 39,942 transport sweeps as shown in Table 7.12a. The RQFP method reduced the number of transport sweeps necessary to converge the eigenpair to a tolerance of 10^{-6} by approximately a factor of ten. The critical search required 12 intermediate k -effective eigenvalue calculations. The alpha-eigenvalue group scalar fluxes for all seven groups are shown in Figures 7.9a-7.9g. Similar to the coarse spatial homogenization problem, the RQFP method is able to resolve the alpha-eigenvalue and eigenvector despite the presence of cells that violate the assumptions made in deriving the method.

For the k -effective eigenvalue, the RQFP method required 5,579 transport sweeps to converge as compared to 5,523 transport sweep for the power method with fission norm update. Unlike the coarse spatial homogenization, the RQFP method underperformed the power method slightly. Despite this, the RQFP method provides another competitive solution method to the eigenvalue problem. As compared to the alpha-eigenvalue RQFP method, the k -effective RQFP method required approximately 40% more transport sweeps to converge the eigenvalue/eigenvector to the same tolerance. The absolute difference between the thermal energy alpha-eigenvalue scalar flux and the thermal energy k -effective scalar flux is seen in Figure 7.10.

Table 7.12: Calculated Eigenvalues and Transport Sweep Comparisons for 2D MOX Fuel Core with Fine Spatial Discretization

		Transport Sweeps	
Benchmark Problem	Calculated $\alpha [\mu\text{s}^{-1}]$	RQFP	Critical Search
2D MOX Fine Discretization	1.396240×10^{-1}	4,046	39,942

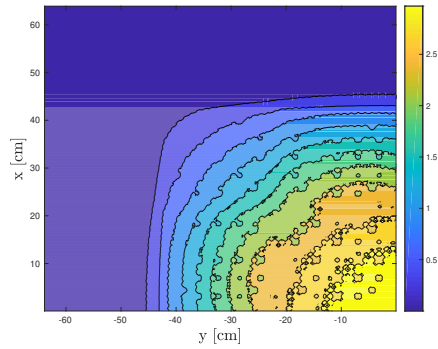
$M = 340 \times 340$, $L = 16$, Tolerance = 10^{-6}

(a) Alpha-Eigenvalue: Comparison of RQFP and Critical Search Transport Sweeps

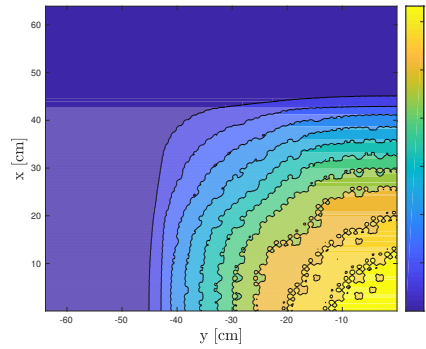
		Transport Sweeps	
Benchmark Problem	Calculated k_{eff}	RQFP	Power Method
2D MOX Fine Discretization	1.185303	5,579	5,523

$M = 340 \times 340$, $L = 16$, Tolerance = 10^{-6}

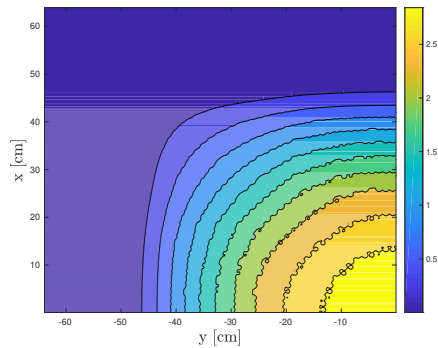
(b) k -Effective: Comparison of RQFP and Power Method Transport Sweeps



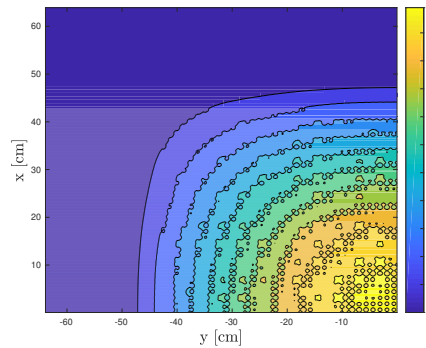
(a) Scalar Flux for Energy Group Zero



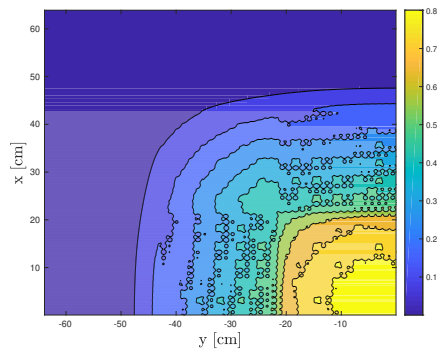
(b) Scalar Flux for Energy Group One



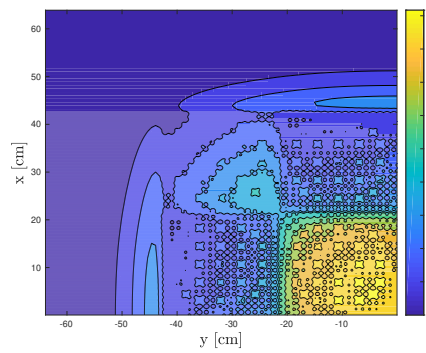
(c) Scalar Flux for Energy Group Two



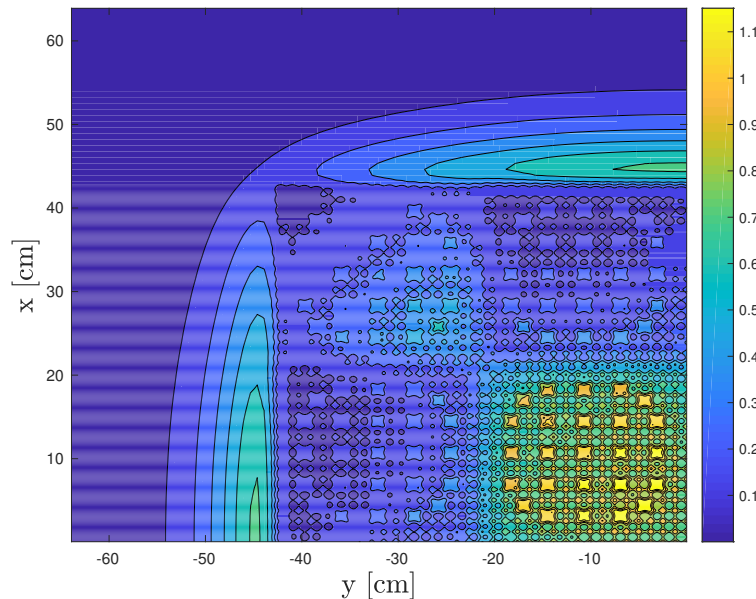
(d) Scalar Flux for Energy Group Three



(e) Scalar Flux for Energy Group Four



(f) Scalar Flux for Energy Group Five



(g) Scalar Flux for Energy Group Six

Figure 7.9: Alpha-Eigenvalue Group Scalar Flux for 2D MOX Fuel Assembly Benchmark Problem - Fine Spatial Discretization

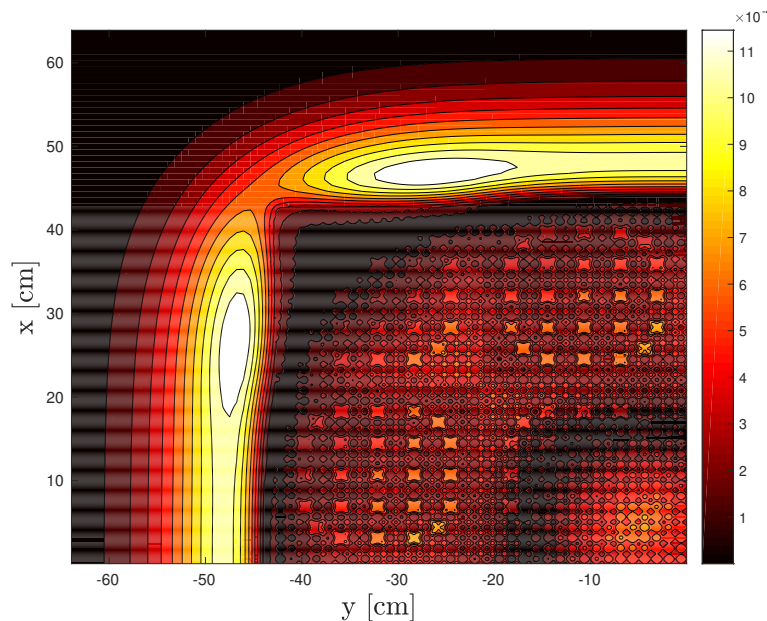


Figure 7.10: Absolute Difference between Alpha- and k -Effective Eigenvalue Group Six Scalar Fluxes (Fine Homogenization)

7.2.3 Three-Dimensional MOX Fuel Core with Coarse Spatial Discretization

A coarse spatial homogenization of the three-dimensional quarter core benchmark led to the assembly geometry shown in Figure 7.11. Spatial discretization was done using the diamond difference method with the coarse spatial homogenization using twenty cells in the x-, y-, and z-directions each. This benchmark problem used S₈ discrete ordinates angular quadrature. A reflective boundary condition was placed on the bottom of the assembly and a vacuum boundary condition was placed on the top of the assembly. The k -effective eigenvalue of this assembly benchmark model was $k = 1.182340$, slightly less supercritical than the benchmark k -effective of $k = 1.186550$. Differences in the k -effective eigenvalue were caused by the spatial homogenization of the benchmark input model. The alpha-eigenvalue of the benchmark was $\alpha = 1.467369 \times 10^{-1} \mu\text{s}^{-1}$. Once again, the RQFP-obtained eigenvalues agreed with those obtained by the critical search method and power iteration.

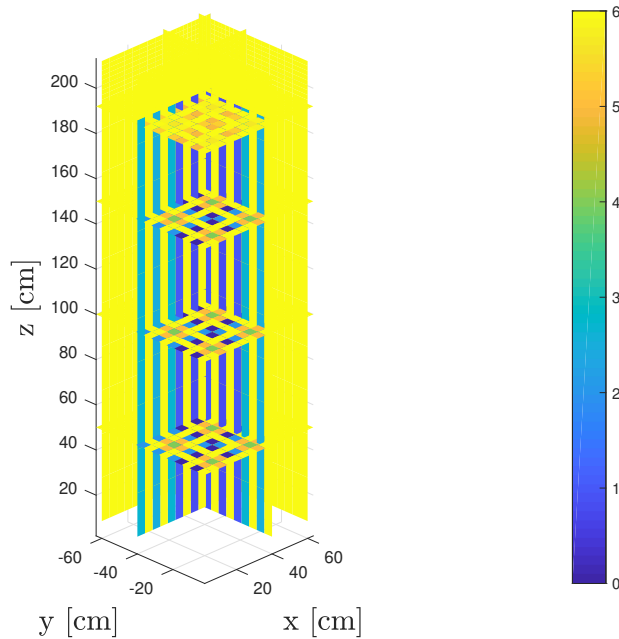


Figure 7.11: Coarse Spatial Homogenization of Three-Dimensional MOX Fuel Assembly Benchmark Problem

The color in each cell corresponds to the material in that cell. Each material is given a number which corresponds to the color shown in the figure: UO₂ = 0, 4.3% MOX Fuel = 1, 7.0% MOX Fuel = 2, 8.7% MOX Fuel = 3, Guide Tube = 4, Fission Chamber = 5, Moderator = 6.

To determine the alpha-eigenvalue and eigenvector of the three-dimensional assembly problem to a tolerance of 10^{-6} , the RQFP method required 38,521 transport sweeps as compared to 286,566 transport sweeps for the critical search method as shown in Table 7.13a. The critical search method required 12 k -effective eigenvalue calculations in order to converge the alpha-eigenvalue and eigenvector, with some individual k -effective calculations requiring a similar number of transport sweeps as the RQFP method. The alpha-eigenvalue group scalar fluxes are seen in Figures 7.12a-7.12g.

The RQFP method required 43,309 transport sweeps to converge the k -effective eigenvalue and eigenvector (Table 7.13b). The power method with fission source update required 43,666 transport sweeps. Both methods were converged to a tolerance of 10^{-6} . The RQFP method performed slightly better than the power method for the three-dimensional fuel assembly benchmark problem. Compared to the alpha-eigenvalue problem, the RQFP method required approximately 12% more transport sweeps to converge the k -effective eigenvalue and eigenvector to the same tolerance.

Table 7.13: Calculated Eigenvalues and Transport Sweep Comparisons for 3D MOX Fuel Core with Coarse Spatial Discretization

Benchmark Problem	Calculated α [μs^{-1}]	Transport Sweeps	
		RQFP	Critical Search
3D MOX Coarse Discretization	1.467369×10^{-1}	38,521	286,566

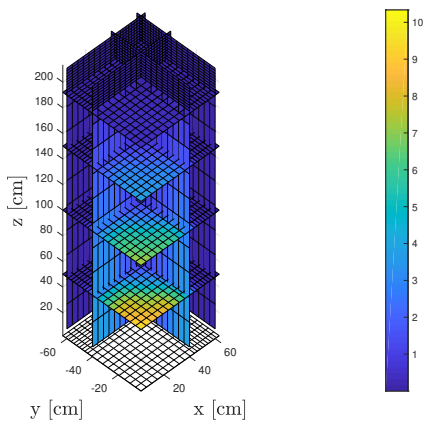
$M = 20 \times 20 \times 20$, $L = 8$, Tolerance = 10^{-6}

(a) Alpha-Eigenvalue: Comparison of RQFP and Critical Search Transport Sweeps

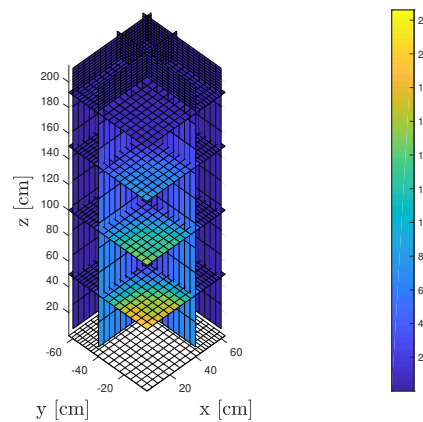
Benchmark Problem	Calculated k_{eff}	Transport Sweeps	
		RQFP	Power Method
3D MOX Coarse Discretization	1.182330	43,309	43,666

$M = 20 \times 20 \times 20$, $L = 8$, Tolerance = 10^{-6}

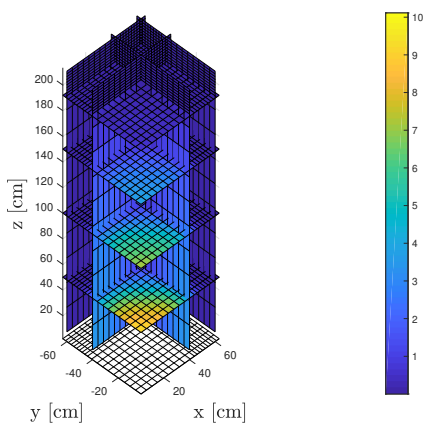
(b) k -Effective: Comparison of RQFP and Power Method Transport Sweeps



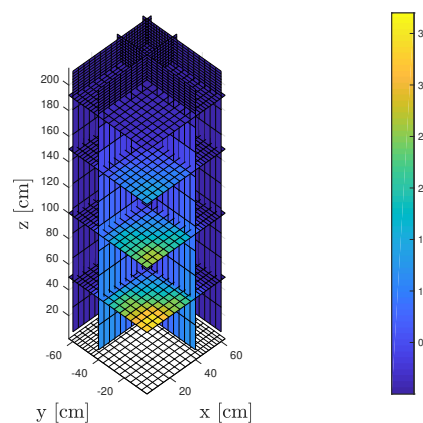
(a) Scalar Flux for Energy Group Zero



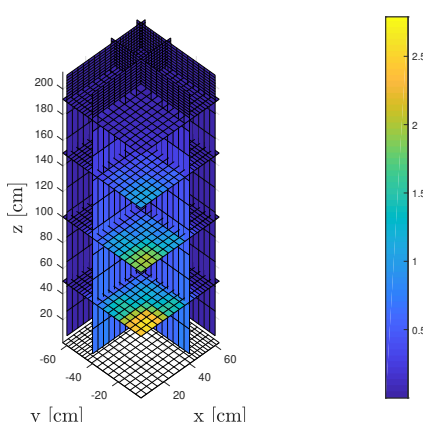
(b) Scalar Flux for Energy Group One



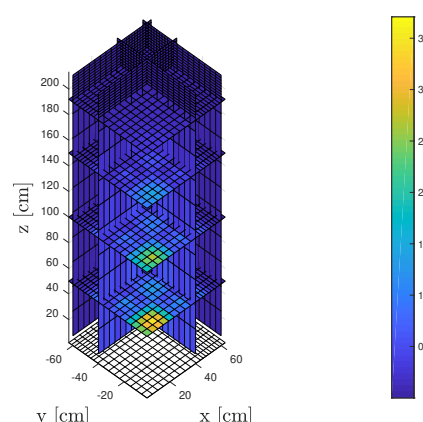
(c) Scalar Flux for Energy Group Two



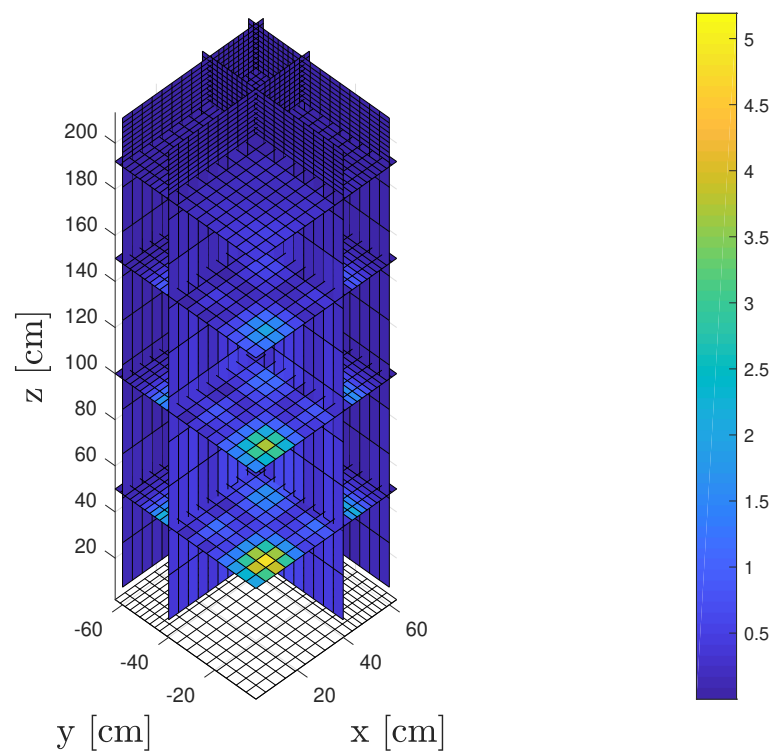
(d) Scalar Flux for Energy Group Three



(e) Scalar Flux for Energy Group Four



(f) Scalar Flux for Energy Group Five



(g) Scalar Flux for Energy Group Six

Figure 7.12: Alpha-Eigenvalue Group Scalar Flux for 3D MOX Fuel Assembly Benchmark Problem - Coarse Spatial Discretization

7.3 Conclusion

The Rayleigh Quotient Fixed Point method was applied to alpha- and k -effective eigenvalue problems for higher dimensional benchmark problems. Homogeneous critical cylinder problems were examined and the performance of the RQFP method compared to traditional eigensolvers. For alpha-eigenvalue problems, the RQFP method required approximately ten times fewer transport sweeps for critical cylinder problems and was able to converge problems that the critical search method failed to converge. It was found that the rate of convergence of the RQFP method was influenced by the size of the critical system and the amount of scattering present. For k -effective eigenvalue problems, the RQFP method required a similar number of transport sweeps as the traditional power method with fission source update. Both the alpha-eigenvalue and k -effective eigenvalue RQFP methods required a similar number of iterations for each benchmark, as expected due to the similarity of the eigenvectors for both eigenvalue problems.

Three quarter-core benchmarks consisting of MOX fuel assemblies were analyzed and the performance of the RQFP method compared to traditional eigensolvers. The criticality eigenvalues of two two-dimensional benchmark problems with coarse and fine spatial homogenizations were determined, and it was found that the alpha-eigenvalue RQFP method required approximately ten times fewer transport sweeps than the critical search method. The RQFP method for k -effective eigenvalues reduced the number of transport sweeps required for convergence by approximately 10%. For a coarse spatial homogenization three-dimensional benchmark problem, the RQFP method for the alpha-eigenvalue required one-tenth of the transport sweeps required by the critical search method. For the k -effective eigenvalue, the RQFP method required fewer iterations than the power method. The RQFP methods were able to determine the fundamental angular flux eigenvector of highly heterogeneous systems. In particular, these systems do not meet all the primitivity requirement made in the derivation of the methods. However, the RQFP method still converges to the eigenvalue and eigenvector of interest and provides substantial reductions in the number of transport sweeps required to converge realistic reactor benchmark problems.

The two- and three-dimensional benchmark problems used to test the RQFP method demonstrate that the RQFP method is robust enough to solve realistic nuclear reactor problems composed of many materials. The transport sweep reductions it provides for alpha-eigenvalue problems greatly reduce the computational cost of determining the alpha-eigenvalue and eigenvector of interest in comparison to the critical search method. For k -effective problems, the RQFP method provides another robust and competitive solution method when compared to the power method. In cases where the primitivity condition is not met by the discretized transport equations, the RQFP method is still able to determine the fundamental eigenvector. For highly supercritical problems, the RQFP method rapidly converges the eigenvector for both the alpha- and k -effective eigenvalue problems. However, for problems exhibiting large amounts of scattering, the RQFP method converges slowly. In these cases, it might be necessary to accelerate the RQFP method in some manner.

Chapter 8

Acceleration of the Alpha-Eigenvalue Rayleigh Quotient Fixed Point Method by Anderson Acceleration

Like all fixed-point methods, the alpha-eigenvalue Rayleigh Quotient Fixed Point method exhibits only linear convergence. In most cases, this rate of convergence is acceptable when other methods are unable to converge the alpha-eigenvalue and eigenvector of interest. However, there exists a set of problems where the alpha-eigenvalue Rayleigh Quotient Fixed Point method converges unacceptably slow. These problems are characterized by large domains where neutrons experience a large amount of scattering before finally being absorbed or leaking out of the domain. For these problems, it might become necessary to use acceleration methods to mitigate slow convergence. In this chapter, we discuss the use of *Anderson acceleration* on the Rayleigh Quotient Fixed Point method for alpha-eigenvalue problems. We examine various slow converging criticality problems of interest and describe the performance of Anderson acceleration. We discuss the reduction in transport sweeps, the associated memory costs of the method, and the practical considerations when using Anderson acceleration.

8.1 Anderson Acceleration

We begin by describing Anderson acceleration. Anderson acceleration originated in the work of Anderson [48] for the solution of nonlinear integral equations. More recently, work by Walker and Ni [49] and Toth and Kelley [50] have focused on the use of Anderson acceleration in other applications such as multiphysics problems.

Consider the fixed-point problem

$$G(u) = u, \quad G : \mathbb{R}^N \rightarrow \mathbb{R}^N.$$

We assume that the iteration converges ($\rho(G'(u^*)) < 1$) [34]. Anderson acceleration maintains a history of residuals

$$f(u) = G(u) - u \quad (8.1)$$

of depth at most $m + 1$, where m is a parameter in the algorithm. An Anderson acceleration iteration that uses m residual histories is referred to as Anderson(m). Anderson(0) is fixed-point iteration by definition. Anderson acceleration for the fixed-point problem, Eq. 8.1, is given by Algorithm 8.1.

Algorithm 8.1 Anderson Acceleration

```

Set  $u_0$  = an initial guess and  $m \geq 1$ 
 $u_1 = G(u_0)$ 
for  $n = 0, 1, 2, \dots$  until convergence do
    Set  $m_n = \min(m, n)$ 
    Set  $F_n = (f_{n-m_n}, \dots, f_n)$ , where  $f_i = G(u_i) - u_i$ 
    Determine  $\alpha^n = (\alpha_0^{(n)}, \dots, \alpha_{m_n}^{(n)})$  that solves  $\min_{\alpha} \|F_n \alpha^T\|_2$  such that  $\sum_{i=0}^{m_n} \alpha_i = 1$ 
    Set  $u_{n+1} = \sum_{i=0}^{m_n} \alpha_i^{(n)} G(u_{n-m_n+i})$ 
    Test for convergence
end for

```

Any norm can be used in the minimization step. However, the ℓ_2 is typically used so that the minimization problem can be formulated as a linear least squares problem [49].

In practice, each m_n may be further modified to maintain acceptable conditioning of F_n . In most applications m_n is small. $m_n = 1$ or $m_n = 2$ is common for large systems due to memory constraints and conditioning requirements.

In the original formulation of Anderson acceleration [48], the formulation of the next iterate can be made more general using the expression

$$u_{n+1} = (1 - \beta_n) \sum_{i=0}^{m_n} \alpha_i^{(n)} u_{n-m_n+i} + \beta_n \sum_{i=0}^{m_n} \alpha_i^{(n)} G(u_{n-m_n+i}) \quad (8.2)$$

$$= \sum_{i=0}^{m_n} \alpha_i^{(n)} u_{n-m_n+i} + \beta_n \left(\sum_{i=0}^{m_n} \alpha_i^{(n)} G(u_{n-m_n+i}) - \sum_{i=0}^{m_n} \alpha_i^{(n)} u_{n-m_n+i} \right), \quad (8.3)$$

where β_n is a relaxation parameter. The relaxation parameters β_n are usually determined heuristically. In practice, β_n is a damping parameter ($0 < \beta_n \leq 1$) and is used to improve convergence by reducing step lengths when iterates are not near the fixed-point solution. Setting $\beta_n = 1$ gives the update in Algorithm 8.1.

Algorithm 8.1 requires solving the constrained linear least-squares problem:

$$\min_{\alpha} \|F_n \alpha^T\|_2 \text{ s.t. } \sum_{i=0}^{m_n} \alpha_i = 1. \quad (8.4)$$

Instead, the least squares problem can be formulated [48] into an equivalent unconstrained problem. This unconstrained Anderson acceleration algorithm is shown in Algorithm 8.2.

Algorithm 8.2 Unconstrained Anderson Acceleration

```

Set  $u_0$  = an initial guess and  $m \geq 1$ 
 $u_1 = G(u_0)$ 
for  $n = 0, 1, 2, \dots$  until convergence do
    Set  $m_n = \min(m, n)$ 
     $\Delta F_n = (\Delta f_{n-m_n}, \dots, \Delta f_{n-1})$  where  $\Delta f_i = f_{i+1} - f_i$  and  $f_i = G(u_i) - u_i$ 
    Determine  $\gamma^{(n)} = (\gamma_0^{(n)}, \dots, \gamma_{m_n-1}^{(n)})$  that solves  $\min_{\gamma} \|f_n - \Delta F_n \gamma^T\|_2$ 
    Set  $u_{n+1} = G(u_n) - \sum_{i=0}^{m_n-1} \gamma_i^{(n)} \Delta g_{n-m_n+i}$  with  $\Delta g_i = G(u_{i+1}) - G(u_i)$ 
    Test for convergence
end for

```

Determining the coefficients $\gamma^{(n)} = (\gamma_0^{(n)}, \dots, \gamma_{m_n-1}^{(n)})$ is done by a QR factorization

$$\Delta F_n = Q_n R_n, \quad (8.5)$$

$$R_n \gamma^{(n)} = Q_n^T f_n. \quad (8.6)$$

The need for a QR factorization increases the computation cost of one iteration of Anderson acceleration. However, various fast and inexpensive QR factorization methods are available. Despite the increased cost per iteration, if Anderson acceleration substantially reduces the number of iterations required for convergence then this cost may be acceptable.

It is usually desirable to do multiple fixed-point iterations before beginning acceleration. Doing fixed-point iterations may allow the vector iterates to get closer to the region of convergence of the fixed point. This is easily implementable in the Anderson acceleration algorithms by prescribing the number of fixed-point iteration evaluations to be done before starting the acceleration.

It is Algorithm 8.2 that is applied to the acceleration of the alpha-eigenvalue Rayleigh Quotient Fixed Point method.

8.2 Anderson Acceleration of Slowly Converging Alpha-Eigenvalue Rayleigh Quotient Fixed Point Problems

In this section we consider various critical slab problems that are slow to converge using the alpha-eigenvalue Rayleigh Quotient Fixed Point method. These problems are characterized by long slab widths and high amounts of scattering. Since the alpha-eigenvalue is related to the time it takes for a neutron to be absorbed or leak out of the system, the wide slabs with many scattering interactions require many transport sweeps to converge. We apply Anderson acceleration to these problems and explore the performance of the acceleration method for various parameters of the method. We look at the effects of the number of

residual vectors used in the calculation of the next iterate, the number of initial fixed-point iterations done before beginning acceleration, and the impacts of the relaxation parameter β_n . All calculations were done in Matlab [51], with reference eigenvalues determined by forming the neutron transport matrices and the Matlab eigenvalue function to determine the dominant alpha-eigenvalue. The implementation of Anderson acceleration used to examine these problems is shown in Appendix B.

8.2.1 Uranium-Heavy Water Critical Slab (Sood Criticality Benchmark Problem 68)

In Section 6.2.1, the uranium-heavy water critical slab problem, Sood Criticality Problem 68, was examined. The problem was characterized by large in-group scattering cross sections and a large critical width. Due to these characteristics, the Rayleigh Quotient Fixed Point method for alpha-eigenvalue problems was slow to converge. Unlike previous problems, Sood Criticality Problem 68 required hundreds of thousands of transport sweeps to converge. We reexamine Sood Criticality Problem 68 and apply Anderson acceleration. The problem cross sections are seen in Chapter 6, Table 6.21 and the problem critical width and reference alpha-eigenvalue for one hundred spatial cells, step-differencing, and S_{16} discrete ordinates angular quadrature are shown in Table 8.1.

The number of iterations required to converge the eigenvalue/eigenvector fixed point is shown in Table 8.2. In this chapter, we define one iteration to equal the transport sweep plus the cost of the Anderson acceleration. It follows that for the alpha-eigenvalue Rayleigh Quotient Fixed Point Method, one iteration is equal to one transport sweep. Zero, five, ten, 20, 50, and 100 fixed point iterations were done before beginning acceleration. Table 8.2 shows results for relaxation parameter $\beta_n = 1$. The Rayleigh Quotient Fixed Point method (Anderson(0)) required 23796 transport sweeps to converge to the fixed point to a ℓ_2 residual tolerance of 10^{-8} . The tolerance for Anderson accelerated calculations was set to 10^{-12} to prevent false convergence as mentioned in [49]. For zero initial fixed-point iterations, it is seen that Anderson(1), the variant of the method which only keeps the most current residual vector, does not converge to the correct eigenvalue. Increasing the number of residual vectors allows the method to converge to the correct eigenvalue and results in substantial reductions in the number of iterations required for convergence. Each additional residual vector is of size GLM and using many residual vectors quickly becomes untenable for large problems.

Table 8.1: Sood Criticality Problem 68 Critical Width and Reference Alpha-Eigenvalue [40]

Cross Section Set	r_c [cm]	Reference α [s^{-1}]
U-D ₂ O(68)	846.632726	-1.508539×10^{-5}
$M = 100, L = 16, \text{Tolerance} = 10^{-12}$		

Figure 8.1 shows the convergence behavior of the Anderson acceleration variants that converge to the correct eigenvalue. Compared to the monotonic decrease in the residual of the Rayleigh Quotient Fixed Point method, the Anderson acceleration variants show significant oscillations. These oscillations make it possible to converge prematurely and for this reason a tighter tolerance is required. The increase of residual vectors used damped out the oscillations faster and allowed the acceleration method to converge with fewer iterations at the cost of additional memory.

Given the tendency of the acceleration method to oscillate, the relaxation parameter β_n can be used to reduce these oscillations. For relaxation parameter $\beta_n = 0.5$, Figure 8.2 shows the convergence behavior of Anderson acceleration. The relaxation parameter increased the number of iterations required to converge the problem but also allowed for the Anderson(1) variant of the problem to converge to the correct eigenvalue though it underperformed Anderson(0) acceleration. This increase in iterations is seen in the shift of the residual to the right in Figure 8.2. The relaxation parameter β_n can be used to force the method to converge to the correct fixed point at the cost of additional iterations.

For an increasing number of initial fixed-point iterations, we see in Table 8.2 that this resulted in the reduction of iterations required to converge to the fixed point. The preliminary fixed-point iterations allowed for the iterates to approach the region of convergence of the fixed point. The additional fixed-point iterations allow other Anderson acceleration variants to converge to the correct eigenvalue/eigenvector that would otherwise not converge to the the correct fixed point.

In most variants of Anderson acceleration, we see that increasing the number of residual vectors improves the performance of the acceleration method. However, in certain circumstances we see that using five vectors degraded the performance of the method. In these cases, it is thought that the condition number of the system has become large. This can be avoid by deleting rows of the system. However, given this fact, for Sood Criticality Benchmark Problem 68, it is recommended that three or four residual vectors be used with any number of initial fixed-point iterations or relaxation parameter β_n . Anderson acceleration provides substantial reductions in the number of iterations required for converge despite it requiring a tighter tolerance and being more expensive than the alpha-eigenvalue Rayleigh Quotient Fixed Point method.

Table 8.2: Anderson Acceleration for Sood Criticality Problem 68 ($\beta_n = 1, M = 100, L = 16$)

Anderson(m_n)	Calculated α [s $^{-1}$]	Iterations
Anderson(0)	-1.508539×10^{-5}	23796
Anderson(1)	-8.790638×10^{-4}	30872
Anderson(2)	-1.508539×10^{-5}	7130
Anderson(3)	-1.508539×10^{-5}	6976
Anderson(4)	-1.508539×10^{-5}	3596
Anderson(5)	-1.508539×10^{-5}	2668
Initial Fixed-Point Iterations = 0		
Anderson(m_n)	Calculated α [s $^{-1}$]	Iterations
Anderson(1)	-8.790638×10^{-4}	19447
Anderson(2)	-1.508539×10^{-5}	8782
Anderson(3)	-1.508539×10^{-5}	3148
Anderson(4)	-1.508539×10^{-5}	1964
Anderson(5)	-1.508539×10^{-5}	2624
Initial Fixed-Point Iterations = 5		
Anderson(m_n)	Calculated α [s $^{-1}$]	Iterations
Anderson(1)	-1.508539×10^{-5}	18514
Anderson(2)	-1.508539×10^{-5}	5813
Anderson(3)	-1.508539×10^{-5}	4664
Anderson(4)	-1.508539×10^{-5}	2806
Anderson(5)	-1.508539×10^{-5}	4669
Initial Fixed-Point Iterations = 10		

Anderson(m_n)	Calculated α [s $^{-1}$]	Iterations
Anderson(1)	-1.508539×10^{-5}	16665
Anderson(2)	-1.508539×10^{-5}	5944
Anderson(3)	-1.508539×10^{-5}	5430
Anderson(4)	-1.508539×10^{-5}	1498
Anderson(5)	-1.508539×10^{-5}	1729

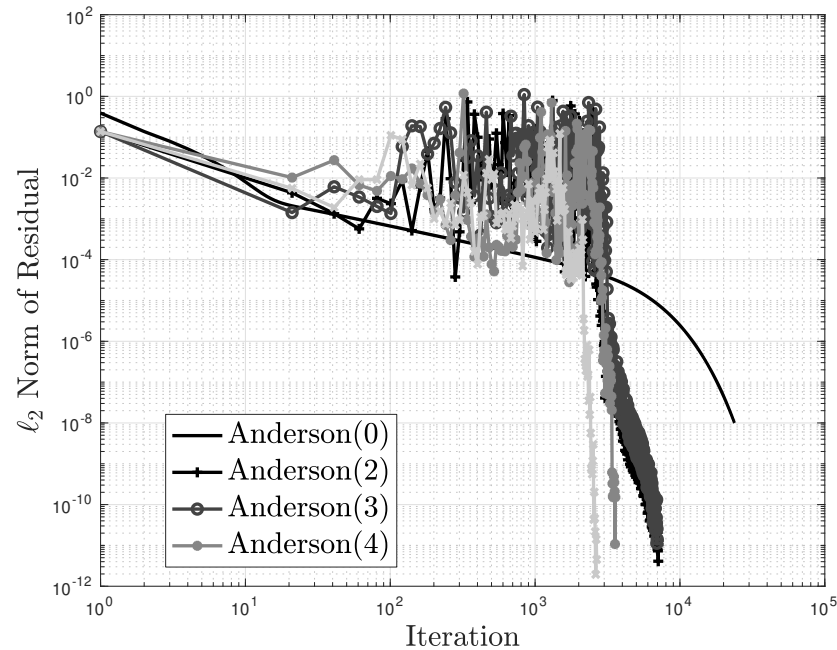
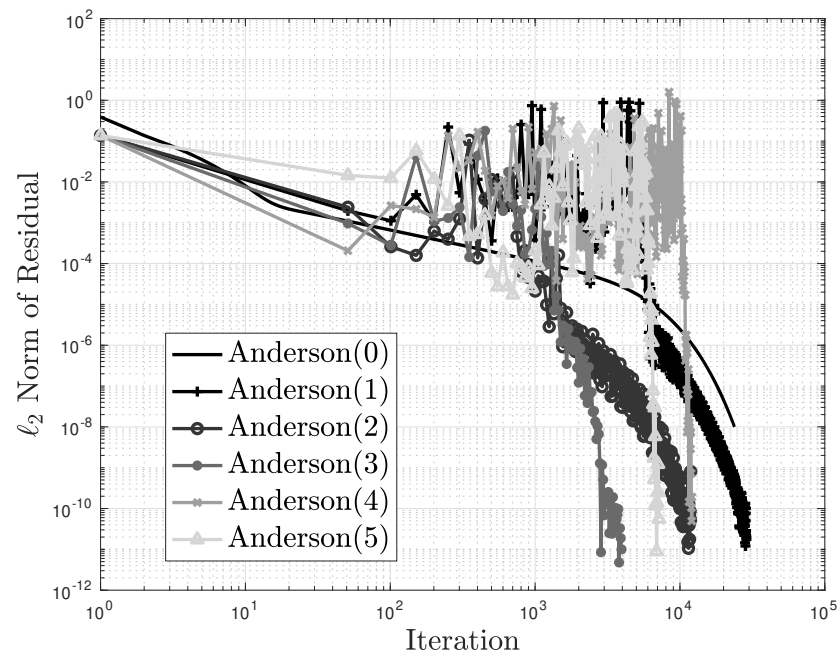
Initial Fixed-Point Iterations = 20

Anderson(m_n)	Calculated α [s $^{-1}$]	Iterations
Anderson(1)	-1.508539×10^{-5}	13396
Anderson(2)	-1.508539×10^{-5}	10641
Anderson(3)	-1.599327×10^{-4}	8375
Anderson(4)	-1.508539×10^{-5}	3441
Anderson(5)	-1.508539×10^{-5}	2416

Initial Fixed-Point Iterations = 50

Anderson(m_n)	Calculated α [s $^{-1}$]	Iterations
Anderson(1)	-1.508539×10^{-5}	11729
Anderson(2)	-1.508539×10^{-5}	7066
Anderson(3)	-1.508539×10^{-5}	4748
Anderson(4)	-1.508539×10^{-5}	1894
Anderson(5)	-1.508539×10^{-5}	3280

Initial Fixed-Point Iterations = 100

Figure 8.1: Anderson Acceleration Convergence for Sood Criticality Problem 68 ($\beta_n = 1$)Figure 8.2: Anderson Acceleration Convergence for Sood Criticality Problem 68 ($\beta_n = 0.5$)

8.2.2 Uranium-Heavy Water Critical Slab (Sood Criticality Benchmark Problem 73)

In this section we examine another uranium-heavy water critical slab problem that is slow to converge when using the Rayleigh Quotient Fixed Point method. Similar to Sood Criticality Benchmark Problem 68, Sood Criticality Benchmark Problem 73 has large amounts of scattering and a large critical width. This problem also contains anisotropic scattering where some of these cross sections are negative. Table 8.3 lists the two-group cross sections and Table 8.4 lists the critical width of the slab and the reference alpha-eigenvalue. The problem was modeled using one hundred spatial cells, step differencing, and S_{16} discrete ordinates angular quadrature.

The number of iterations required to converge the eigenvalue/eigenvector is shown in Table 8.5. Zero, five, ten, 20, 50, and 100 preliminary fixed-point iteration variants were studied with relaxation factor $\beta_n = 1$. The Rayleigh Quotient Fixed Point (Anderson(0)) required 22749 iterations to converge the eigenvalue/eigenvector to an ℓ_2 residual of 10^{-8} . As before, the tolerance of the Anderson acceleration calculations was set to 10^{-12} to prevent false convergence. Unlike Sood Criticality Benchmark Problem 68, it was found that all Anderson acceleration variants converged to the correct eigenvalue. As the number of residual vectors increased, the number of iterations decreased except in the case of five residual vectors. For this number of residual vectors, it was found that the linear system was poorly conditioned.

Figure 8.3 shows the convergence behavior of the different Anderson acceleration variants ($\beta_n = 1$, zero initial fixed-point iterations) and the Rayleigh Quotient Fixed Point method. The Anderson acceleration variants oscillate substantially until converging to the fixed point. While Anderson(1) only reduced the number of iterations required by a factor of 20%, Anderson(3) and Anderson(4) reduced iteration number by up to factor of 10. Using relaxation parameter $\beta_n = 0.5$, the number of iterations increased. We see a shift toward the right of the convergence behavior in Figure 8.4. For this particular problem, the relaxation parameter is not necessary since all Anderson acceleration variants converge onto the right fixed point.

Increasing the number of initial fixed-point iterations before acceleration only reduces the number of total iterations in some cases. As the number of initial fixed-point iterations increases, it was seen that the number of iterations either remained the same or increased (Table 8.5). By allowing for more initial iterations, it is possible that the vector iterates ended up much further from the fixed point. If instead the acceleration were turned on sooner, the iterates would instead end up in the region of convergence much sooner.

For this particular problem, Anderson acceleration provided substantial reductions in iterations. However, for certain combinations of residual vector number, relaxation parameters, and initial fixed-point iterations, it was found that the acceleration method would not perform as well. Similar to the previous problem, using three or four residual vectors with five or ten initial fixed-point iterations was found to give the best results. This problem, however, shows that the various parameters of Anderson acceleration require experimentation in

order to find the best results.

Table 8.3: Two-Group U-D₂O Problem Cross Sections (cm⁻¹)

g	σ_g	ν_g	σ_{fg}	χ_g	v_g [cm/s]
1	0.33588	2.50	0.002817	1.0	2.0
2	0.54628	2.50	0.097	0.0	1.0
(a) U-D ₂ O(73) Cross Sections					
$g' \rightarrow g$	1	2			
1	0.31980	0.004555			
2	0.0	0.42410			
(b) U-D ₂ O(73) Scattering Block- σ_{s0}					
$g' \rightarrow g$	1	2			
1	0.06694	-0.0003972			
2	0.0	0.05439			
(c) U-D ₂ O(73) Scattering Block- σ_{s1}					

Table 8.4: Sood Criticality Problem 73 Critical Width and Reference Alpha-Eigenvalue [40]

Cross Section Set	r_c [cm]	Reference α [s ⁻¹]
U-D ₂ O(73)	1000.506133	-1.221913×10^{-5}
$M = 100, L = 16, \text{Tolerance} = 10^{-12}$		

Table 8.5: Anderson Acceleration for Sood Criticality Problem 73 ($\beta_n = 1, M = 100, L = 16$)

Anderson(m_n)	Calculated α [s $^{-1}$]	Iterations
Anderson(0)	-1.221913×10^{-5}	22749
Anderson(1)	-1.221913×10^{-5}	17620
Anderson(2)	-1.221913×10^{-5}	4814
Anderson(3)	-1.221913×10^{-5}	2777
Anderson(4)	-1.221913×10^{-5}	1854
Anderson(5)	-1.221913×10^{-5}	6008
Initial Fixed-Point Iterations = 0		
Anderson(m_n)	Calculated α [s $^{-1}$]	Iterations
Anderson(1)	-1.221913×10^{-5}	17775
Anderson(2)	-1.221913×10^{-5}	9204
Anderson(3)	-1.221913×10^{-5}	2583
Anderson(4)	-1.221913×10^{-5}	1407
Anderson(5)	-1.221913×10^{-5}	6172
Initial Fixed-Point Iterations = 5		
Anderson(m_n)	Calculated α [s $^{-1}$]	Iterations
Anderson(1)	-1.221913×10^{-5}	12186
Anderson(2)	-1.221913×10^{-5}	11382
Anderson(3)	-1.221913×10^{-5}	4809
Anderson(4)	-1.221913×10^{-5}	2626
Anderson(5)	-1.221913×10^{-5}	3603
Initial Fixed-Point Iterations = 10		

Anderson(m_n)	Calculated α [s ⁻¹]	Iterations
Anderson(1)	-1.221913×10^{-5}	12241
Anderson(2)	-1.221913×10^{-5}	3604
Anderson(3)	-1.221913×10^{-5}	6713
Anderson(4)	-1.221913×10^{-5}	5430
Anderson(5)	-1.221913×10^{-5}	2925

Initial Fixed-Point Iterations = 20

Anderson(m_n)	Calculated α [s ⁻¹]	Iterations
Anderson(1)	-1.221913×10^{-5}	17166
Anderson(2)	-1.221913×10^{-5}	7363
Anderson(3)	-1.221913×10^{-5}	4205
Anderson(4)	-1.221913×10^{-5}	1729
Anderson(5)	-1.221913×10^{-5}	2253

Initial Fixed-Point Iterations = 50

Anderson(m_n)	Calculated α [s ⁻¹]	Iterations
Anderson(1)	-1.221913×10^{-5}	17313
Anderson(2)	-1.221913×10^{-5}	14811
Anderson(3)	-1.221913×10^{-5}	10654
Anderson(4)	-1.221913×10^{-5}	3923
Anderson(5)	-1.221913×10^{-5}	3657

Initial Fixed-Point Iterations = 100

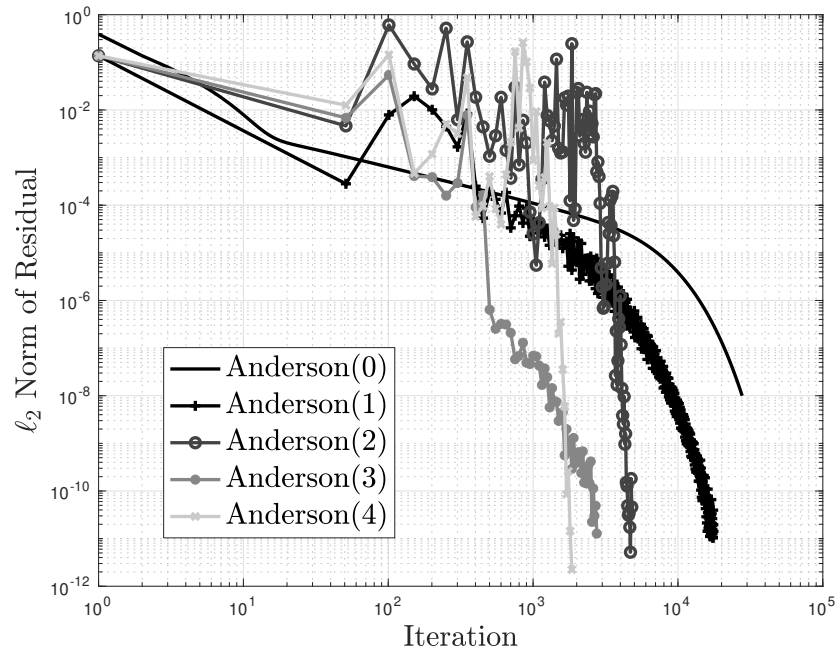


Figure 8.3: Anderson Acceleration Convergence for Sood Criticality Problem 73 ($\beta_n = 1$)

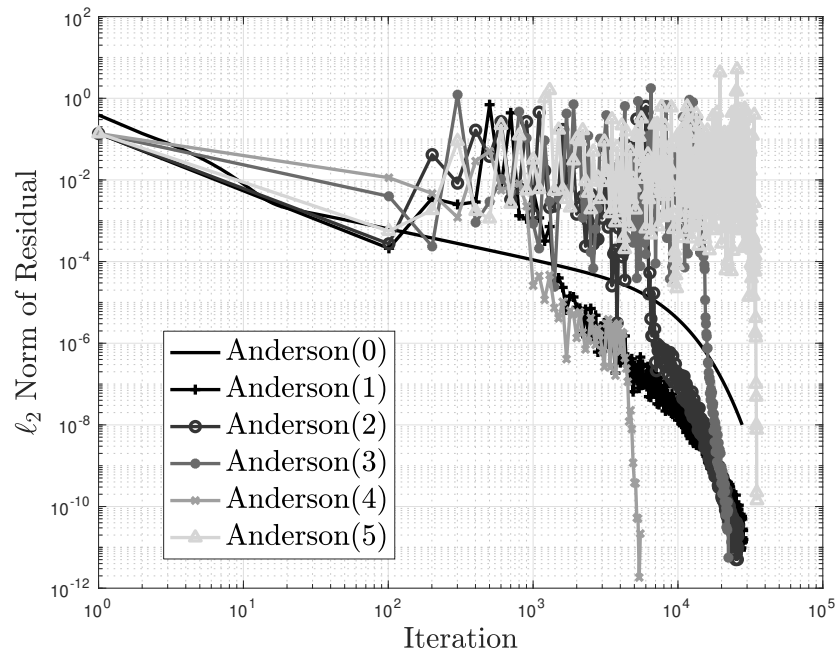


Figure 8.4: Anderson Acceleration Convergence for Sood Criticality Problem 73 ($\beta_n = 0.5$)

8.3 Conclusion

Anderson acceleration was applied to the Rayleigh Quotient Fixed Point method for alpha-eigenvalue problems. Anderson acceleration and its constrained and unconstrained formulations were presented. The unconstrained formulation of Anderson acceleration was implemented in MATLAB and applied to the RQFP method. Two slowly converging one-dimensional slab geometry problems were considered and the number of iterations compared for various variants of the acceleration scheme. The effects of different numbers of residual vectors and initial fixed-point iterations before acceleration were considered and their effects on the ability of the method to converge to the fundamental eigenvector and eigenvalue were discussed. It was found that while larger numbers of residual vectors produced faster convergence, memory limitations quickly became apparent. Instead it was found that by using a combination of initial fixed-point iterations and a lesser number of residual vectors produced substantial speedups. In particular, the initial fixed-point iterations were found to help the method to converge to the correct eigenpair by allowing the vector iterate to enter the region of convergence for the fixed point.

Chapter 9

Conclusion

This dissertation described the derivation and mathematical foundation of the Rayleigh Quotient Fixed Point method and its use to determine the alpha- and k -effective eigenvalue criticality problems in neutron transport. The Rayleigh Quotient Fixed Point method is a non-linear fixed-point method that uses the proven primitivity property of the discretized neutron transport eigenvalue equations to find the positive angular flux eigenvector solution and corresponding eigenvalue. This dissertation discusses the application of the Rayleigh Quotient Fixed Point method to infinite media, one-dimensional slabs and sphere, as well as realistic two- and three-dimensional reactor models using the neutral particle transport code ARDRA [19].

For alpha-eigenvalue problems, previous methods were limited to transport-based matrix method or criticality search iterative schemes. For transport-based matrix methods, the discretized matrices of the alpha-eigenvalue were formed and traditional eigenvalue solution methods were applied. These methods become increasingly expensive in memory and computational effort as problems increase in complexity. For criticality search iterative schemes, the alpha-eigenvalue is determined by relating the eigenvalue to another eigenvalue problem, the k -effective eigenvalue. These methods require multiple k -effective eigenvalue calculations to converge the alpha-eigenvalue, increasing the number of transport sweeps required to converge the alpha-eigenvalue. A substantial amount of iterations are spent determining an eigenvalue not of interest to the problem. Furthermore, there remain open questions as to how converged the proxy eigenvalue calculation must be to allow for convergence of the alpha-eigenvalue problem. These methods also historically have been applied to supercritical nuclear systems, being of limited use for subcritical problems that are become more of interest in the recent years. The Rayleigh Quotient Fixed Point for alpha-eigenvalue problems is an iterative method that uses an eigenvalue update that is optimal in the least squares sense. The Rayleigh Quotient Fixed Point method directly updates the alpha-eigenvalue, not requiring knowledge of any other eigenvalue, substantially reducing the number of iterations required for convergence. Additionally, it is able to solve subcritical, critical, and supercritical systems, providing a more general solution method to alpha-eigenvalue problems.

For k -effective problems, the traditional workhorse method, the power method, tradition-

ally used a fission source update for the eigenvalue at each iteration. By using the Rayleigh Quotient Fixed Point method, the k -effective eigenvalue problem can be viewed as a non-linear fixed-point method where an optimal update for the eigenvalue can be derived. In certain circumstances, this provides a reduction in transport sweeps necessary to converge the eigenvalue and eigenvector of interest.

Throughout the derivation of the Rayleigh Quotient Fixed Point method, the primitivity property of the discretized eigenvalue equations was used to guarantee the existence of a unique positive eigenvector corresponding to the spectral radius as stated in the Perron-Frobenius theory for primitive matrices. It was shown that for a one-dimensional slab geometry eigenvalue problem discretized with diamond differencing in space, discrete ordinates angular quadrature, and the multigroup-in-energy approximation, the discretized linear system is a primitive system with index of primitivity of two. This result is similar to that of Mokhtar-Kharroubi where it was found that the continuous neutron transport equation eigenvalue problem was *positivity-improving* or primitive with index of primitivity of two [52]. The existence of a unique eigenvector and a way to relate it to either the alpha- or k -effective eigenvalue provided a powerful tool to derive a fixed-point method capable of determining the eigenvalue and the physical, positive angular flux eigenvector.

The Rayleigh Quotient Fixed Point method for alpha- and k -effective eigenvalues accurately determined the alpha- and k -effective eigenvalues of various analytic, infinite-medium problems by Betzler [41]. It was also demonstrated the failure of the eigenvalue problem when the conditions of irreducibility and primitivity failed to exist and how these problems were unphysical in most cases. Next, the method was validated for one-dimensional slabs and spheres and compared to the Green's Function Method of Kornreich and Parsons [10]. The number of transport sweeps required by the Rayleigh Quotient Fixed Point method was compared to the standard solvers, showing that the RQFP method provided major reductions in the number of iterations required for convergence and the ability to converge problems where other methods failed. Next, realistic two-dimensional cylindrical problems and two- and three-dimensional fuel assembly benchmark problems were analyzed to show the general applicability of the RQFP method even when some of the assumptions made in deriving the method did not apply. Transport sweep comparisons were used to show the improvement the RQFP method provides over traditional eigenvalue solvers for both alpha- and k -effective eigenvalue problems. For realistic reactor problems with large amounts of materials, energies, and other heterogeneities, the RQFP method outperformed the standard eigensolvers.

Acceleration of the Rayleigh Quotient Fixed Point method was shown to be possible using Anderson acceleration [49]. For slowly converging alpha-eigenvalue problems solved using the RQFP method, Anderson acceleration provided acceleration of the linear fixed-point method convergence by a factor of up to ten. These slowly converging alpha-eigenvalue problems were characterized by large amounts of scattering and long critical widths. Neutrons in these systems would experience a large amount of scattering before finally being absorbed or leaked out of the system, slowing down convergence of the method.

By using a number of residual vectors, Anderson acceleration solves a constrained least

squares problem for a set of weights used to generate a new vector iterate from a combination of residual vectors and the previous vector iterate. However, the acceleration comes at the cost of increased cost and memory. The number of residual vectors used in the acceleration scheme impacts the convergence of the method, with more residual vectors decreasing the number of iterations required for convergence. However, in practice, each additional residual vector requires the same size of memory as the eigenvector of interest, with the memory cost quickly becoming prohibitive for large problems. This increased cost requires a careful balancing of problem acceleration and cost for each alpha-eigenvalue problem of interest. However, Anderson acceleration provides a useful option for the acceleration of the Rayleigh Quotient Fixed Point method.

Future work required involves the proof of primitivity for two- and three-dimensional Cartesian geometry problems. In these problems, approximation of spatial derivatives by diamond differencing using a sufficiently small cell width no longer guarantees positivity of the angular flux solution [39]. Instead, step differencing is required in space. Given this limitation, it is sought to prove that the two- and three-dimensional Cartesian geometry discretized alpha- and k -effective eigenvalue equations form primitive systems. Another avenue for possible future work is the determination of the asymptotic constant coefficient describing the rate of converge of the system. It is thought that the asymptotic constant coefficient is related to the scattering cross section of the system but this has not been determined rigorously. Continued investigation into the use of Anderson acceleration is required to determine the optimal number of residual vectors given memory limitations and calculation costs. Given this acceleration method, slowly converging problems can be solved in fewer iterations allowing for the Rayleigh Quotient Fixed Point method to be widely applicable in all problems of interest.

Appendix A

Discretization of the Alpha-Eigenvalue Problem For Slab Geometry

In Appendix A, we describe the discretization of the alpha-eigenvalue problem for one-dimensional slab geometry using a matrix formalism similar to that of three-dimensional Cartesian geometry. In one dimension, the discretization of the continuous eigenvalue equation is substantially simpler and may be helpful to reader to study this case before analyzing the three-dimensional problem.

We begin with the alpha-eigenvalue transport equation in one-dimensional slab geometry with isotropic scattering. The spatial domain is the interval $[a, b]$ in x , μ is the angle cosine in $[-1, 1]$, the energy variable is $E \in [0, \infty)$, and the equations for the angular flux $\psi(x, \mu, E)$ are given by

$$\begin{aligned} & \left[\mu \frac{\partial}{\partial x} + \frac{\alpha}{v(E)} + \sigma(x, E) \right] \psi(x, \mu, E) \\ &= \frac{\chi(E)}{2} \int_0^\infty dE' \nu(E') \sigma_f(x, E') \int_{-1}^1 d\mu' \psi(x, \mu', E) \\ & \quad + \frac{1}{2} \int_0^\infty dE' \sigma_s(x, E' \rightarrow E) \int_{-1}^1 d\mu' \psi(x, \mu', E). \end{aligned} \quad (\text{A.1})$$

We assume vacuum Dirichlet conditions

$$\psi(a, \mu, E) = 0, \quad 0 < \mu \leq 1, \quad (\text{A.2})$$

$$\psi(b, \mu, E) = 0, \quad -1 \leq \mu < 0. \quad (\text{A.3})$$

The discretization of Eqn A.1 is done using diamond differencing in space, multigroup in energy, and discrete ordinates collocation in angle.

A.1 Discretization of the One-Dimensional Slab Geometry Problem

We begin by discretizing Eq. A.1 in energy using the *multigroup* approximation. We restrict the energy E to a finite interval and partition the interval into groups:

$$E_{max} = E_0 > E_1 > \dots > E_G = E_{min}. \quad (\text{A.4})$$

The eigenvalue equation is then averaged over each group $E_g < E < E_{g-1}$ and the cross sections are approximated by a flux-weighted average over each energy group. In the spatial dimension, we introduce a spatial grid

$$a \equiv x_0 < \dots < x_{i+1} < x_i < \dots < x_M \equiv b, \quad (\text{A.5})$$

and let

$$\Delta x_i = x_i - x_{i-1}. \quad (\text{A.6})$$

We refer to the x_i as nodes and function values at the nodes are called nodal values. We assume that σ_g and $\sigma_{s,g,g'}$, the total and scattering cross sections for energy group g , are constant on the zone $x_{i-1} < x < x_i$ and denote these values by $\sigma_{g,i}$ and $\sigma_{s,g,g',i}$. We use a discrete ordinates collocation of Eq. A.1 at an even number of Gauss points μ_ℓ with

$$-1 < \mu_1 < \dots < \mu_{L/2} < 0 < \mu_{L/2+1} < \dots < \mu_L < 1, \mu_{L+1-\ell} = -\mu_\ell. \quad (\text{A.7})$$

The integrals in angle in Eq. A.1 are then approximated by

$$\frac{1}{2} \int_{-1}^1 d\mu \psi_g(x, \mu) \approx \sum_{\ell=1}^L w_\ell \psi_g(x, \mu_\ell). \quad (\text{A.8})$$

Using diamond differencing in the spatial dimension [5], we obtain the fully discretized set of equations for the eigenvalue problems

$$\begin{aligned} & \mu_\ell \frac{\psi_{g,\ell,i} - \psi_{g,\ell,i-1}}{\Delta x_i} + \frac{\alpha}{v_g} \frac{\psi_{g,\ell,i} + \psi_{g,\ell,i-1}}{2} + \sigma_{g,i} \frac{\psi_{g,\ell,i} + \psi_{g,\ell,i-1}}{2} \\ &= \frac{\chi_g}{2} \sum_{g'=1}^G \frac{\nu_g \sigma_{f,g',i}}{2} \sum_{\ell'=1}^L w_{\ell'} \left(\frac{\psi_{g',\ell',i} + \psi_{g',\ell',i-1}}{2} \right) + \sum_{g'=1}^G \frac{\sigma_{s,g,g',i}}{2} \sum_{\ell'=1}^L w_{\ell'} \left(\frac{\psi_{g',\ell',i} + \psi_{g',\ell',i-1}}{2} \right), \end{aligned} \quad (\text{A.9})$$

for $g = 1, \dots, G$, $i = 1, \dots, M$, and $\ell = 1, \dots, L$. The discretized boundary conditions are given by

$$\psi_{g,\ell,M} = 0 \text{ for } \ell = 1, \dots, L/2, \quad (\text{A.10})$$

$$\psi_{g,\ell,0} = 0 \text{ for } \ell = L/2 + 1, \dots, L. \quad (\text{A.11})$$

Using cell-centered flux values, it follows that Eq. A.9 is a system of $GL(M+1)$ equations for $GL(M+1)$ unknowns.

To write Eq. A.9 in matrix form, we define the angular flux vector for a single energy group g as

$$\Psi_g \equiv \begin{pmatrix} \Psi_{g,1} \\ \vdots \\ \Psi_{g,L} \end{pmatrix} \in \mathbb{R}^{L(M+1)} \quad \text{with} \quad \Psi_{g,\ell} \equiv \begin{pmatrix} \psi_{g,\ell,0} \\ \vdots \\ \psi_{g,L,M} \end{pmatrix} \in \mathbb{R}^{M+1}. \quad (\text{A.12})$$

To write the matrix form of the diamond difference discretized operator $\mu_\ell \partial/\partial x + 1/v_g + \sigma_g$, we define the block diagonal matrix

$$\bar{S} \equiv \text{diag}(S_1, \dots, S_L) \in \mathbb{R}^{LM \times L(M+1)} \quad (\text{A.13})$$

with

$$S_\ell = S = \frac{1}{2} \begin{pmatrix} 1 & 1 & & & \\ & \ddots & \ddots & & \\ & & & \ddots & \\ & & & & 1 & 1 \end{pmatrix} \in \mathbb{R}^{M \times (M+1)}, \quad (\text{A.14})$$

for all ℓ . The matrix S interpolates nodal vectors into zone-centered vectors by averaging the nodal values. Now we define the total cross section and inverse velocity matrices for energy group g as

$$\Sigma_g \equiv \text{diag}(\sigma_{g,1}, \dots, \sigma_{g,M}) \in \mathbb{R}^{M \times M}, \quad (\text{A.15})$$

$$V_g^{-1} \equiv \text{diag}(1/v_{g,1}, \dots, 1/v_{g,M}) \in \mathbb{R}^{M \times M}. \quad (\text{A.16})$$

We define the following matrices to describe the discretized derivative term

$$\Delta x \equiv \text{diag}(\Delta x_1, \dots, \Delta x_M) \in \mathbb{R}^{M \times M} \quad (\text{A.17})$$

and

$$D \equiv \begin{pmatrix} -1 & 1 & & & \\ & \ddots & \ddots & & \\ & & & \ddots & \\ & & & & -1 & 1 \end{pmatrix} \in \mathbb{R}^{M \times (M+1)}. \quad (\text{A.18})$$

Boundary values are isolated by defining the row vector

$$B_\ell \equiv \begin{cases} e_M^T & \text{if } \ell \leq L/2, \\ e_0^T & \text{if } \ell > L/2, \end{cases} \in \mathbb{R}^{M+1}, \quad (\text{A.19})$$

where the indices on the standard basis vectors e_ℓ are from 0 to M . Finally, we define the matrices Z and Z_b as

$$Z \equiv \begin{pmatrix} I_M \\ 0 \end{pmatrix} \in \mathbb{R}^{(M+1) \times M} \quad \text{and} \quad Z_b \equiv e_M. \quad (\text{A.20})$$

We can now define the matrix form of the diamond difference representation of $\mu_\ell \partial/\partial x + \alpha/v_g + \sigma_g$ as

$$H_g + \alpha V_g^{-1} \equiv \text{diag}(H_{g,1}, \dots, H_{g,L}) + \alpha \text{ diag}(V_{g,1}^{-1}, \dots, V_{g,L}^{-1}) \in \mathbb{R}^{L(M+1)}, \quad (\text{A.21})$$

where

$$H_{g,\ell} + \alpha V_{g,\ell}^{-1} \equiv Z(\mu_\ell \Delta x^{-1} D + \Sigma_g S_\ell) + Z_b B_\ell + \alpha Z V_g^{-1} S_\ell. \quad (\text{A.22})$$

It can be shown that $H_g + \alpha V_g^{-1}$ is nonsingular for the diamond difference method if α is not too negative.

We now define discretized representations of angular flux moment operators. The matrices operate on zone-centered vectors and are in $\mathbb{R}^{M \times LM}$. We define the matrix

$$L_n \equiv (l_n W) \otimes I_M, \quad (\text{A.23})$$

where $l_n \equiv (P_n(\mu_1), P_n(\mu_2), \dots, P_n(\mu_L))$ are the Legendre polynomials and the quadrature weights are given by $W \equiv \text{diag}(w_1, \dots, w_L)$. If the vector Ψ_g approximates $\psi_g(x, \mu)$, then $L_n \Psi_g$ approximates taking the n^{th} moment of the angular flux $\phi_{g,n}(x)$. We also define the matrix

$$L_n^+ \equiv (2n+1) l_n^T \otimes I_M \in \mathbb{R}^{LM \times M}. \quad (\text{A.24})$$

If a vector Φ approximates $\phi(x)$, then $L_n^+ \Psi$ will approximate $P_n(\mu) \phi(x)$. We define the grouped matrices for N_s moments as

$$L^N = \begin{pmatrix} L_0 \\ \vdots \\ L_N \end{pmatrix} \quad \text{and} \quad L^{N,+} = (L_0^+, \dots, L_N^+). \quad (\text{A.25})$$

We can define the scattering and fission matrices as

$$\Sigma_{s,g,g',n} \equiv \text{diag}(\sigma_{s,g,g',n,1}, \dots, \sigma_{s,g,g',n,M}) \in \mathbb{R}^{M \times M} \quad (\text{A.26})$$

and

$$\Sigma_{f,g,g',n} \equiv \text{diag}(\chi_g \nu \sigma_{f,g',n,1}, \dots, \chi_g \nu \sigma_{f,g',n,M}) \in \mathbb{R}^{M \times M}. \quad (\text{A.27})$$

We now define matrices that inject zone-centered vectors into nodal vector space and vice versa. We define the matrices

$$\bar{\Sigma}_g \equiv I_L \otimes \Sigma_g \in \mathbb{R}^{LM \times LM}, \quad (\text{A.28})$$

$$\bar{V}^{-1}_g \equiv I_L \otimes V_g^{-1} \in \mathbb{R}^{LM \times LM}, \quad (\text{A.29})$$

$$\bar{Z} = I_L \otimes Z \in \mathbb{R}^{L(M+1) \times LM}, \quad (\text{A.30})$$

$$\bar{Z}_B = I_L \otimes Z_b \in \mathbb{R}^{L(M+1) \times L}, \quad (\text{A.31})$$

$$B = \text{diag}(B_1, \dots, B_L) \in \mathbb{R}^{L \times L(M+1)}, \quad (\text{A.32})$$

and

$$C = \text{diag}(\mu_1 \Delta x^{-1} D, \dots, \mu_L \Delta x^{-1} D) \in \mathbb{R}^{LM \times L(M+1)}. \quad (\text{A.33})$$

Using the above matrices, we can write the matrix $H_g + V_g^{-1}$ as

$$\begin{aligned} H_g + V_g^{-1} &\equiv \text{diag}(H_{g,1}, \dots, H_{g,L}) + \text{diag}(V_{g,1}^{-1}, \dots, V_{g,L}^{-1}) \\ &= \bar{Z}(C + \bar{\Sigma}_g \bar{S}) + \bar{Z}_B B + \bar{Z} \bar{V}^{-1} \bar{S}. \end{aligned} \quad (\text{A.34})$$

The discretized multigroup eigenvalue equations can then be written in the matrix form as

$$H_g \Psi_g + \alpha V_g^{-1} \Psi_g = \bar{Z} \sum_{g'=1}^G \sum_{n=0}^{N_s} L_n^+ \Sigma_{s,g,g',n} L_n \bar{S} \Psi_{g'} + \bar{Z} \sum_{g'=1}^G \sum_{n=0}^{N_s} L_n^+ \Sigma_{f,g,g',n} L_n \bar{S} \Psi_{g'}, \quad (\text{A.35})$$

Finally, we can write the multigroup discretized eigenvalue equations if we define the matrices

$$\Psi \equiv \begin{pmatrix} \Psi_1 \\ \Psi_2 \\ \vdots \\ \Psi_G \end{pmatrix}, \quad \Sigma_s \equiv \begin{pmatrix} \Sigma_{s,11}^{N_s} & \dots & \Sigma_{s,1G}^{N_s} \\ \vdots & \ddots & \vdots \\ \Sigma_{s,G1}^{N_s} & \dots & \Sigma_{s,GG}^{N_s} \end{pmatrix}, \quad \Sigma_f \equiv \begin{pmatrix} \Sigma_{f,11}^{N_s} & \dots & \Sigma_{f,1G}^{N_s} \\ \vdots & \ddots & \vdots \\ \Sigma_{f,G1}^{N_s} & \dots & \Sigma_{f,GG}^{N_s} \end{pmatrix}, \quad (\text{A.36})$$

where

$$\Sigma_{s,gg'}^{N_s} \equiv \text{diag}(\Sigma_{s,g,g',0}, \dots, \Sigma_{s,g,g',N_s}) \quad (\text{A.37})$$

and

$$\Sigma_{f,gg'}^{N_s} \equiv \text{diag}(\Sigma_{f,g,g',0}, \dots, \Sigma_{f,g,g',N_s}). \quad (\text{A.38})$$

Defining the following matrices

$$\mathbf{S} \equiv I_G \otimes \bar{S}, \quad (\text{A.39})$$

$$\mathbf{Z} \equiv I_G \otimes \bar{Z}, \quad (\text{A.40})$$

$$\mathbf{H} + \mathbf{V}^{-1} \equiv \text{diag}(H_1 + V_1^{-1}, H_2 + V_2^{-1}, \dots, H_G + V_G^{-1}), \quad (\text{A.41})$$

$$\mathbf{L}^+ \equiv I_G \otimes L^{N_s,+}, \quad (\text{A.42})$$

$$\mathbf{L} \equiv I_G \otimes L^{N_s}, \quad (\text{A.43})$$

then Eq. A.35 can be written as

$$(\mathbf{H} + \alpha \mathbf{V}^{-1}) \Psi = \mathbf{Z} \mathbf{L}^+ (\Sigma_s + \Sigma_f) \mathbf{L} \mathbf{S} \Psi. \quad (\text{A.44})$$

Similarly, the discretized k -eigenvalue problem can be written as

$$\mathbf{H} \Psi = \mathbf{Z} \mathbf{L}^+ \left(\Sigma_s + \frac{1}{k} \Sigma_f \right) \mathbf{L} \mathbf{S} \Psi. \quad (\text{A.45})$$

Equations A.44 and A.45 are eigenvalue equations for the criticality eigenvalue and the node-centered angular flux eigenvector. In the derivation of the Rayleigh Quotient Fixed

Point method, an inner product is required. However, the inner product is defined for zone-centered vectors, whereas the unknown angular flux vectors in Eqns. A.44 and A.45 are node-centered. To satisfy this requirement, Eqns. A.44 and A.45 are rewritten using zone-centered angular flux eigenvectors. We denote Ψ_z as the zone-centered unknown and \mathbf{H}_z as the zone-centered version of \mathbf{H} .

Given a zone-centered angular flux vector Ψ_z , the nodal angular flux vector Ψ defined by

$$\Psi_{g,\ell} \equiv (ZS + Z_b B_\ell)^{-1} Z \Psi_{z,g,\ell} \text{ for all } g = 1, 2, \dots, G \text{ and } \ell = 1, 2, \dots, L, \quad (\text{A.46})$$

satisfies $B_\ell \Psi_{g,\ell} = 0$ and $S \Psi_{g,\ell} = \Psi_{z,g,\ell}$ for all g and ℓ . Defining the matrices

$$\mathbf{C} \equiv I_G \otimes C, \quad (\text{A.47})$$

$$\mathbf{B} \equiv I_G \otimes B, \quad (\text{A.48})$$

$$\mathbf{Z}_B \equiv I_G \otimes \bar{Z}_B, \quad (\text{A.49})$$

and

$$\boldsymbol{\Sigma} \equiv \text{diag}(\bar{\Sigma}_1, \bar{\Sigma}_2, \dots, \bar{\Sigma}_G), \quad (\text{A.50})$$

then \mathbf{H} and \mathbf{V}^{-1} can be rewritten as

$$\mathbf{H} = \mathbf{Z}(\mathbf{C} + \boldsymbol{\Sigma}\mathbf{S}) + \mathbf{Z}_B\mathbf{B}, \quad (\text{A.51})$$

and

$$\mathbf{V}^{-1} = \mathbf{Z}\mathbf{V}^{-1}\mathbf{S}. \quad (\text{A.52})$$

For the nodal-centered angular flux Ψ , we have from Lemma 3.1 that

$$\Psi = (\mathbf{Z}\mathbf{S} + \mathbf{Z}_B\mathbf{B})^{-1} \mathbf{Z} \Psi_z. \quad (\text{A.53})$$

Substituting Eq. A.53 into Eq. A.44 and A.45 and multiplying on the left by \mathbf{Z}^T gives

$$(\alpha \mathbf{V}_z^{-1} + \mathbf{H}_z) \Psi_z = \mathbf{L}^+ (\boldsymbol{\Sigma}_s + \boldsymbol{\Sigma}_f) \mathbf{L} \Psi_z, \quad (\text{A.54})$$

and

$$\mathbf{H}_z \Psi_z = \mathbf{L}^+ \left(\boldsymbol{\Sigma}_s + \frac{1}{k} \boldsymbol{\Sigma}_f \right) \mathbf{L} \Psi_z, \quad (\text{A.55})$$

where

$$\mathbf{H}_z \equiv \mathbf{C}(\mathbf{Z}\mathbf{S} + \mathbf{Z}_B\mathbf{B})^{-1} \mathbf{Z} + \boldsymbol{\Sigma}, \quad (\text{A.56})$$

and

$$\mathbf{V}_z^{-1} \equiv \mathbf{V}^{-1} \mathbf{S} (\mathbf{Z}\mathbf{S} + \mathbf{Z}_B\mathbf{B})^{-1} \mathbf{Z}. \quad (\text{A.57})$$

Equations A.54 and A.55 are the cell-centered eigenvalue equations for one-dimensional slab geometry.

Appendix B

Implementation of Anderson Acceleration in Matlab for the Alpha-Eigenvalue Rayleigh Quotient Fixed Point Method

In Appendix B we describe the implementation of Anderson acceleration for the Rayleigh Quotient Fixed Point method for alpha-eigenvalue problems. We include the Matlab code for future use. First, we describe the one-sweep alpha-eigenvalue Rayleigh Quotient Fixed Point method implementation and its input and outputs. We then describe the Anderson acceleration implementation of the unconstrained problem and describe the various features of the method. We describe the solution process for the update and the matrix deletion required to maintain acceptable conditioning of the system.

B.1 Alpha-Eigenvalue Rayleigh Quotient Fixed Point Method Matlab Implementation

The Matlab function `AlphaRQSweep` performs one iteration (transport sweep) of the Rayleigh Quotient Fixed Point method for alpha-eigenvalue problems. The function requires the matrices H , S , F , iV , the numerical matrix representations of the matrices H_z , V_z^{-1} , Σ_s , and Σ_f described in Chapter 3. The function also requires input vectors x and q , the previous angular flux vector and previous source, respectively, as described in Chapter 4. The function calculates the alpha-eigenvalue and returns it to `alpha` and determines the next angular flux iterate and source. `AlphaRQSweep` is used as the fixed-point function evaluation in Anderson acceleration. The Matlab code is shown in Listing B.1.

```

function [x, alpha, q] = AlphaRQSweep(H, S, F, iV, x, q)

%[x,alpha,q] = AlphaRQSweep(H,S,F,iV,x,q) is the one-sweep
%alpha-eigenvalue Rayleigh Quotient Fixed Point. The function
%performs one sweep of the system.

%Input: H - Leakage/Transport Matrix
%       S - Scattering Matrix
%       F - Fission Matrix
%       iV - Inverse Velocity Matrix
%       x - Previous Angular Flux Vector Iterate
%       q - Previous Scattering and Fission Source Vector

%Output: x - New Angular Flux Iterate
%       alpha - New Alpha-Eigenvalue Iterate
%       q - New Scattering and Fission Source Vector

%Check if source is nonzero
if ( sum(q) == 0 )
    alpha = 0;
else
    %Alpha-eigenvalue RQ update
    alpha = (x'*(S+F)*x - x'*q)/(x'*iV*x);
end

%Set new source
q = (-alpha*iV + S + F)*x;

%Transport Sweep
x = H\q;

return

```

Listing B.1: AlphaRQSweep-Alpha-Eigenvalue RQFP Matlab Implementation

B.2 Anderson Acceleration Matlab Implementation

The Matlab function `AndersonAcc` performs the Anderson acceleration of the Rayleigh Quotient Fixed Point method for alpha-eigenvalue problems. The function requires the matrices `H`, `S`, `F`, `iV`, the number of maximum iterations, `maxits`, the ℓ_2 norm tolerance, `tol`, the maximum number of residual vectors to be used in the method, `mmax`, the number of initial fixed-point iterations, `fptrers`, and the relaxation parameter, `beta`. These parameters are described in Chapter 8.

The function `AndersonAcc` initializes the initial angular flux guess and source and then performs a fixed number of initial fixed-point function evaluations given by the input argument `fptrers` before beginning the acceleration of the fixed-point method. The fixed-point evaluation is done by calling the function `AlphaRQSweep`, described in Section B.1. The function then performs a maximum number of iterations given by `maxits` or until the residual tolerance is less than the value given by the input argument `tol`. The function then performs one fixed-point function evaluation of `AlphaRQSweep`, calculated the residual and sets the residual vector matrix, deletes old residual vector columns, performs a QR decomposition, and then sets the new angular flux iterate. The function returns the converged alpha-eigenvalue, the converged angular flux vector, and a vector of residuals. The Matlab code is shown in Listing B.2.

```
function [alpha,x,residual] = AndersonAcc(H,S,F,iV,maxits,tol,mmax,fptrers,
    beta)

%[alpha,x,residual] = AnderAccel(H,S,F,iV,maxits,tol,mmax,fptrers,beta) is
%the Anderson acceleration implementation for the alpha-eigenvalue Rayleigh
%Quotient Fixed Point method.

%Input: H - Leakage/Transport Matrix
%       S - Scattering Matrix
%       F - Fission Matrix
%       iV - Inverse Velocity Matrix
%       maxits - Maximum Number of Iterations
%       tol - L2 Norm Residual Tolerance
%       mmax - Maximum Number of Residual Vectors used by Anderson
%              Acceleration
%       fptrers - Initial Fixed-point Iteration Function Evaluations
%       beta - Relaxation Parameter

%Output: alpha - Converged Alpha-Eigenvalue
%        x - Converged Angular Flux Vector
%        residual - Residual vector
```

```
%Initialize initial angular flux guess and source
x = ones(length(H),1);
q = zeros(length(H),1);

fold = 0;

maa = 0;
G = [];

%Initial fixed-point iterations
for i = 1:fpiters
    [x,alpha,q] = AlphaRQSweep(H,S,F,iV,x,q);
end

%Start Anderson acceleration
for k = 0:maxits

    %Fixed-point iteration evaluation
    xold = x;
    [gcur, alpha, q] = AlphaFcn(H,S,F,iV,x,q);
    fcur = gcur - x;

    %Form residual and function matrices
    if ( k > 0 )
        dF = fcur - fold;
        dG = gcur - gold;
        if ( maa < mmax )
            G = [G,dG];
        else
            G = [G(:,2:maa),dG];
        end
        maa = maa + 1;
    end
    fold = fcur;
    gold = gcur;

    %Gram-Schmidt orthogonalization
    if ( maa == 0 )
        x = gcur;
    else
        if ( maa == 1 )
            Q(:,1) = dF/norm(dF); R(1,1) = norm(dF);
        else
            for j = 2:maa
                v = gcur - Q(:,1:j-1)*R(1:j-1,j);
                r = norm(v);
                if ( r < 1e-10 )
                    break;
                else
                    Q(:,j) = v/r;
                    R(j,j) = r;
                end
            end
        end
    end
end
```

```

else
    if ( maa > mmax )
        [Q,R] = qrdelete(Q,R,1); %Delete matrix column
        maa = maa - 1;
    end
    for i = 1:maa - 1
        R(i,maa) = Q(:,i)'*dF;
        dF = dF - R(i,maa)*Q(:,i); %QR decomposition
    end
    Q(:,maa) = dF/norm(dF); R(maa,maa) = norm(dF);
end

gamma = R\Q'*fcur; %Solve for gamma coefficients
x = gcur - G*gamma; %Set next iterate
x = x - (1-beta)*(fcur - Q*R*gamma); %Relaxation Coefficient
end

residual(k+1) = norm(x-xold)/norm(x);

fprintf('Iter: %i alpha = %e residual = %e \n',...
    k+1, alpha, residual(k+1));

%Termination criterion
if ( residual(k+1) < tol )
    break
end

%Break if NaN
if (isnan(alpha) == 1 )
    break
end

end

return

```

Listing B.2: AndersonAcc-Anderson Acceleration Matlab Implementation

Bibliography

- [1] G. Birkhoff and R. S. Varga. “Reactor Criticality and Nonnegative Matrices”. In: *Journal of the Society for Industrial and Applied Mathematics* 6.4 (1958), pp. 354–377.
- [2] T. R. Hill. “Efficient Methods for Time Absorption (a) Eigenvalue Calculations”. In: *Proc. of Top. Meeting*. 1983.
- [3] J. S. Warsa et al. “Krylov Subspace Iterations for Deterministic k-Eigenvalue Calculations”. In: *Nuclear Science and Engineering* 147.1 (2004), pp. 26–42.
- [4] J. J. Duderstadt and L. J. Hamilton. *Nuclear Reactor Analysis*. Wiley, 1976. ISBN: 978-0-471-22363-4.
- [5] E. E. Lewis and W. F. Miller. *Computational Methods of Neutron Transport*. en. Wiley, 1984. ISBN: 978-0-471-09245-2.
- [6] I. Lux and L. Koblinger. *Monte Carlo Particle Transport Methods: Neutron and Photon Calculations*. en. CRC Press, 1991.
- [7] G. I. Bell and S. Glasstone. *Nuclear Reactor Theory*. English. Tech. rep. TID-25606. Division of Technical Information, US Atomic Energy Commission, 1970.
- [8] Y. Ronen, D. Shvarts, and J. J. Wagschal. “A Comparison of Some Eigenvalues in Reactor Theory”. In: *Nuclear Science and Engineering* 60.1 (1976), pp. 97–101.
- [9] M. Nelkin. “Asymptotic solutions of the transport equation for thermal neutrons”. In: *Physica* 29.4 (1963), pp. 261–273.
- [10] D. E. Kornreich and D. K. Parsons. “Time-eigenvalue calculations in multi-region Cartesian geometry using Green’s functions”. In: *Annals of Nuclear Energy* 32.9 (2005), pp. 964–985.
- [11] J. Lehner and G. M. Wing. “On the spectrum of an unsymmetric operator arising in the transport theory of neutrons”. en. In: *Communications on Pure and Applied Mathematics* 8.2 (1955), pp. 217–234.
- [12] K. Jörgens. “An asymptotic expansion in the theory of neutron transport”. en. In: *Communications on Pure and Applied Mathematics* 11.2 (1958), pp. 219–242.
- [13] E. W. Larsen and P. F. Zweifel. “On the spectrum of the linear transport operator”. In: *Journal of Mathematical Physics* 15.11 (1974), pp. 1987–1997.

- [14] J. J. Duderstadt and W. R. Martin. *Transport Theory*. 1979.
- [15] G. M. Wing. *An Introduction to Transport Theory*. en. John Wiley & Sons, 1962.
- [16] G. Velarde, C. Ahnert, and J. M. Aragonés. “Analysis of the Eigenvalue Equations in k , λ , γ , and α Applied to Some Fast- and Thermal-Neutron Systems”. In: *Nuclear Science and Engineering* 66.3 (1978), pp. 284–294.
- [17] H. A. Abderrahim et al. “MYRRHA: A multipurpose accelerator driven system for research & development”. In: *Nuclear Instruments and Methods in Physics Research Section A: Accelerators, Spectrometers, Detectors and Associated Equipment* 463.3 (2001), pp. 487–494.
- [18] R. S. Modak and Anurag Gupta. “A scheme for the evaluation of dominant time-eigenvalues of a nuclear reactor”. In: *Annals of Nuclear Energy* 34.3 (2007), pp. 213–221. ISSN: 0306-4549. DOI: 10.1016/j.anucene.2006.12.009.
- [19] U. Hanebutte and P. N. Brown. *ARDRA, Scalable Parallel Code System to Perform Neutron and Radiation Transport Calculations*. Tech. rep. UCRL-TB-132078. Lawrence Livermore National Laboratory, 1999.
- [20] R. E. Alcouffe et al. *PARTISN: A Time-Dependent, Parallel Neutral Particle Transport Code System*. Tech. rep. LA-UR-05-3925. Los Alamos National Laboratory, 2005.
- [21] K. M. Case, G. Placzek, and F. Hoffmann. *Introduction to the Theory of Neutron Diffusion*. Tech. rep. Los Alamos National Laboratory, 1953.
- [22] R. S. Modak and A. Gupta. “A simple scheme for the direct evaluation of time-eigenvalues of neutron transport equation”. In: *Annals of Nuclear Energy* 30.2 (2003), pp. 211–222.
- [23] Jeffrey Willert, H. Park, and D. A. Knoll. “A comparison of acceleration methods for solving the neutron transport k-eigenvalue problem”. In: *Journal of Computational Physics* 274 (2014), pp. 681–694. ISSN: 0021-9991.
- [24] J. S. Warsa et al. “Krylov subspace iterations for deterministic k-eigenvalue calculations”. In: *Nuclear Science and Engineering* 147.1 (2004), pp. 26–42.
- [25] R. A. Horn and C. R. Johnson. *Matrix Analysis*. en. Cambridge University Press, 2012. ISBN: 978-1-139-78888-5.
- [26] G. H. Golub and C. F. Van Loan. *Matrix Computations*. en. JHU Press, 2012. ISBN: 978-1-4214-0859-0.
- [27] R. S. Modak, D. C. Sahni, and S. D. Paranjape. “Evaluation of higher K-eigenvalues of the neutron transport equation by Sn-method”. In: *Annals of Nuclear Energy* 22.6 (1995), pp. 359–366.
- [28] T. Yamamoto and Y. Miyoshi. “Reliable Method for Fission Source Convergence of Monte Carlo Criticality Calculation with Wielandt’s Method”. In: *Journal of Nuclear Science and Technology* 41.2 (2004), pp. 99–107.

- [29] I. C. F. Ipsen. "Computing an Eigenvector with Inverse Iteration". In: *SIAM Review* 39.2 (1997), pp. 254–291. ISSN: 0036-1445.
- [30] E. P. Wigner. "Mathematical problems of nuclear reactor theory". en. In: *Proceedings of Symposia in Applied Mathematics*. Ed. by G. Birkhoff and E. Wigner. Vol. 11. Providence, Rhode Island: American Mathematical Society, 1961, pp. 89–104.
- [31] R. S. Varga. *Matrix Iterative Analysis*. en. Springer Science & Business Media, 2009.
- [32] R. A. Horn and C. R. Johnson. *Topics in Matrix Analysis*. en. Cambridge University Press, 1994.
- [33] J. Ortega. *Numerical Analysis*. Classics in Applied Mathematics. Society for Industrial and Applied Mathematics, 1990.
- [34] A. M. Ostrowski. *Solution of Equations and Systems of Equations: Pure and Applied Mathematics: A Series of Monographs and Textbooks*. en. Elsevier, 2016.
- [35] P. N. Brown. "A Linear Algebraic Development of Diffusion Synthetic Acceleration for Three-Dimensional Transport Equations". In: *SIAM Journal on Numerical Analysis* 32.1 (1995), pp. 179–214.
- [36] P. N. Brown. *On the Probability of Initiation for Neutron Transport Calculations*. Tech. rep. LLNL-JRNL-401245. Lawrence Livermore National Laboratory, 2008.
- [37] P. N. Brown. *Probability of Initiation for Neutron Transport*. Tech. rep. LLNL-JRNL-522136. Lawrence Livermore National Laboratory, 2012.
- [38] B. G Carlson, K. D Lathrop, et al. *Transport theory: the method of discrete ordinates*. Los Alamos Scientific Laboratory of the University of California, 1965.
- [39] A. Greenbaum. *Iterative Methods for Solving Linear Systems*. en. SIAM, 1997. ISBN: 978-0-89871-396-1.
- [40] A. Sood, R. A. Forster, and D. K. Parsons. "Analytical Benchmark Test Set for Criticality Code Verification". In: *Progress in Nuclear Energy* 42.1 (2003), pp. 55–106.
- [41] B. R. Betzler. "Calculating Alpha Eigenvalues and Eigenfunctions with a Markov Transition Rate Matrix Monte Carlo Method". PhD thesis. University of Michigan, 2014.
- [42] B. Davison and J. B. Sykes. *Neutron transport theory*. Clarendon Press, 1957.
- [43] D. E. Kornreich and B. D. Ganapol. "The Green's Function Method for Nuclear Engineering Applications". In: *Nuclear Science and Engineering* 126.3 (1997), pp. 293–313.
- [44] J. D. Bess. *International Criticality Safety Benchmark Evaluation Project (ICSBEP)-ICSBEP 2015 Handbook*. Tech. rep. Organisation for Economic Co-Operation and Development, 2015.
- [45] E. E. Lewis et al. "Benchmark Specification for Deterministic 2-D/3-D MOX Fuel Assembly Transport Calculations Without Spatial Homogenization (C5G7 MOX)". In: *NEA/NSC* 280 (2001).

- [46] C. Cavarec et al. “The OECD/NEA Benchmark Calculations of Power Distributions Within Assemblies”. In: *Electricité de France* (1994).
- [47] R. Buck and E. Lent. “COG: A New, High-Resolution Code for Modeling Radiation Transport”. In: *Energy & Technology Review* (1993), p. 9.
- [48] D. G. Anderson. “Iterative Procedures for Nonlinear Integral Equations”. In: *Journal of the ACM (JACM)* 12.4 (1965), pp. 547–560.
- [49] H. Walker and P. Ni. “Anderson Acceleration for Fixed-Point Iterations”. In: *SIAM Journal on Numerical Analysis* 49.4 (2011), pp. 1715–1735. ISSN: 0036-1429.
- [50] A. Toth and C. Kelley. “Convergence Analysis for Anderson Acceleration”. In: *SIAM Journal on Numerical Analysis* 53.2 (2015), pp. 805–819. ISSN: 0036-1429.
- [51] MATLAB. *Version 9.6 (R2019a)*. Natick, Massachusetts: The MathWorks Inc., 2019.
- [52] M. Mokhtar-Kharroubi. *Mathematical Topics in Neutron Transport Theory: New Aspects*. Vol. 46. World Scientific, 1997.